

Minimizing Response Times of Automotive Dataflows on Multicore^{*}

Glenn A. Elliott[†], Namhoon Kim[†], Jeremy P. Erickson[†], Cong Liu[‡], and James H. Anderson[†]

[†]Dept. of Computer Science, University of North Carolina at Chapel Hill

[‡]Dept. of Computer Science, University of Texas at Dallas

Abstract

Dataflow software architectures are prevalent in prototypes of advanced automotive systems, for both driver-assisted and autonomous driving. Safety constraints of these systems necessitate real-time performance guarantees. Automotive prototypes often ensure such constraints through over-provisioning and dedicated hardware; however, a commercially viable system must utilize as few low-cost multicore processors as possible to meet size, weight, and power constraints. In short, these platforms must do more with less. To this end, we develop cache-aware and overhead-cognizant scheduling techniques that lessen guaranteed response times without unnecessarily constraining platform utilization. We implement these techniques in PGM^{RT}, a portable middleware framework for managing real-time dataflow applications on multicore platforms. The efficacy of our techniques is demonstrated through overhead-aware schedulability experiments and runtime observations. Results for our test platform show that cache-aware clustered scheduling outperforms naïve partitioned and global approaches in terms of schedulability and end-to-end response times of dataflows.

1 Introduction

Graph-based software architectures, often referred to as *dataflow* architectures, are common to software applications that process continual streams of data or events. In such architectures, vertices represent sequential code segments that operate upon data, and edges express the flow of data among vertices. The flexibility offered by such an architecture’s inherent modularity promotes code reuse and parallel development. Also, these architectures naturally support concurrency, since parallelism can be explicitly described by the graph structure. These characteristics have made dataflow architectures popular in multimedia technologies [13, 24] and the emerging field of computational photography [2, 27]. Dataflow architectures are also prevalent in the sensor-processing components in prototypes of advanced automotive systems, for both driver-assisted and autonomous driving (e.g., [20, 25, 26]). While many domains with dataflow architectures have timing requirements, the automotive case is set apart since timing violations may result in loss of life or property.

In addition to timing requirements, an automotive platform has size, weight, and power (SWaP) and manufacturing cost constraints. Such constraints are largely ignored in many existing prototypes of advanced automotive sys-

tems, which typically rely on over-provisioning and dedicated hardware to support real-time dataflow computations [20, 25, 26]. If advanced automotive features are to be commercially viable, then such computations must instead be consolidated onto as few low-cost processors as possible. However, consolidation only bolsters the need for efficient real-time scheduling techniques since more computations compete for fewer available processors.

Real-time dataflows. A number of methods for modeling the real-time behavior of dataflow applications have been developed for multiprocessor and distributed systems [4, 12, 15, 23]. Typically, such applications are modeled as directed acyclic graphs (DAGs), with nodes denoting tasks and edges denoting producer/consumer relationships. The predominant approach has been to map such a DAG onto a set of connected, but independently scheduled, processors. Under this *partitioned* approach, each task (DAG node) is statically assigned to a single processor. As with traditional partitioned multiprocessor scheduling, this method may suffer from utilization loss due to bin-packing problems.

More recently, Liu and Anderson explored dataflow applications on *globally* scheduled multiprocessors, wherein DAG tasks share a single run queue, and thus may migrate among processors [18]. Liu et al. showed that task response times are bounded under global earliest-deadline-first (G-EDF) scheduling, *without* utilization loss. Liu et al. extended these results to apply in *distributed* systems comprised of globally scheduled multicore machines [19]; these results can also be applied to a *single* cluster-scheduled multicore system (where groups of processors share a run queue). However, solutions optimized for shared-memory communication have not been investigated.

A similar DAG-based model has been used to analyze the hard real-time scheduling under G-EDF of tasks with parallelism within jobs [14, 17, 21, 22].

Sporadic task systems and minimizing response-time bounds. Devi et al. were the first to demonstrate that deadline-tardiness bounds (i.e., response-time bounds) can be derived for ordinary sporadic tasks scheduled by G-EDF, without utilization loss [6]. However, Bastoni et al. showed that algorithms like G-EDF may incur high runtime overheads and suffer from heavy cache-affinity loss [3]. As a result of these factors, real-time schedulability is reduced and the response-time bounds of schedulable task sets increase. Clustered schedulers, such as clustered EDF (C-EDF), can balance utilization loss against high overheads, striking a middle ground between partitioned and global scheduling.

Recently, Erickson et al. showed that “G-EDF-like” (GEL) schedulers, such as the global fair-lateness (G-FL)

^{*}Work supported by NSF grants CNS 1016954, CNS 1115284, CNS 1218693, and CNS 1239135, with additional support from General Motors.

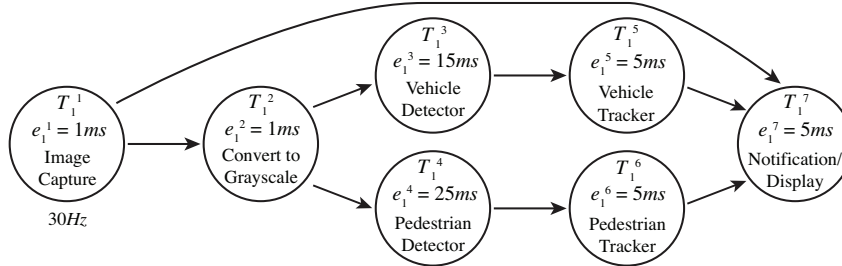


Figure 1: Vehicle and pedestrian detection and tracking component, expressed as a DAG. e_i^j denotes the execution time of task T_i^j .

scheduler, have provably smaller response-time bounds than G-EDF [9]. Under GEL schedulers, priority points (PPs) distinct from deadlines are defined to minimize worst-case response times. A GEL scheduler uses these PPs as pseudo-deadlines. Erickson et al. also showed that *job splitting* may further minimize bounds on response times [8]. Here, the scheduling priority of a job decreases as the job consumes discrete chunks of execution budget, effectively splitting each “real” job into a sequence of sub-jobs. Clustered variants of GEL schedulers can also be created by using the GEL scheduler for each cluster of processors.

Contributions. Future advanced automotive systems need computing platforms that support efficient real-time scheduling of dataflow applications on highly-utilized multicore processors. With this firmly in mind, we consider the problem of scheduling sporadic DAGs on multicore platforms with the goals of: (i) minimizing bounds on end-to-end latency; (ii) maximizing system utilization; (iii) improving analytical schedulability and observed performance; and (iv) providing a real-time software platform from which we may draw practical conclusions and facilitate future research. We meet (i) and (ii) by extending Liu et al.’s dataflow analysis and integrating it with Erickson et al.’s techniques to lessen DAG end-to-end response-time bounds. We avoid the high overheads of global scheduling through the use of the clustered fair-lateness (C-FL) scheduler. We also use job splitting to further reduce response times. We address (iii) through a cache-aware heuristic to assign tasks to clusters that promotes cache reuse and reduces communication costs. To meet (iv), we created portable real-time dataflow scheduling middleware called PGM^{RT}, which we run atop LITMUS^{RT}, a Linux-based real-time operating system jointly developed by UNC and MPI.¹ Using this implementation, we gathered overhead measurements, which we then integrated into overhead-aware schedulability experiments. We also conducted experiments in which observed end-to-end DAG response times were recorded under various configurations of PGM^{RT} to determine which configurations offer the best real-time behaviors while maximizing system utilization.

Organization. In the rest of the paper, we first provide needed background and review relevant prior work (Secs. 2–4). We then present a heuristic for mapping DAG tasks to clusters to promote efficient cache reuse (Sec. 5), discuss the implementation of PGM^{RT} (Sec. 6), present our experimental results (Sec. 7), and conclude (Sec. 8).

2 Background

We begin with additional motivation behind the graph-based scheduling of automotive applications. Fig. 1 depicts a hypothetical vehicle and pedestrian detection and tracking component of an advanced automotive system. A video camera feeds the source of the graph with video frames at 30Hz. T_1^1 converts the raw camera data into the common YUV color image format. T_1^1 hands the image to T_1^7 for display. It also passes the data to T_1^2 for computer vision processing. Vision algorithms often operate only on grayscale images, so T_1^2 strips the color components (U and V) from the image to produce a more compact grayscale image. T_1^2 then sends the grayscale image to T_1^3 and T_1^4 for vehicle and pedestrian detection, respectively. Although vehicle and pedestrian detectors may use similar algorithms, T_1^3 requires less execution time because it limits its search to the immediate road area before the vehicle. Information on detected vehicles and pedestrians is passed to T_1^5 and T_1^6 , respectively, for tracking. Here, detected objects are correlated with historical data to produce an estimated trajectory and speed for each object. This data is sent to T_1^7 , where the relevant information is overlaid on top of the original color image.

In this paper, we explore the use of C-FL scheduling in safety-critical applications like the one above. This may seem like an odd choice since EDF-like global and clustered schedulers, like C-FL, are commonly associated with “soft real-time” systems (i.e., those generally regarded as non-safety-critical) because in the absence of severe utilization constraints, analysis “only” provides bounds on deadline tardiness. However, C-FL is a viable choice in this domain for several reasons. First, C-FL still provides provable bounds on end-to-end latency for DAGs—timing properties can be guaranteed. Second, a survey of automotive studies on driver reactions places an *alert* driver’s reaction time around 700ms [11]. Some automotive software components may only have to react to events within this relatively lax time window in order to ensure safe operation. Finally, C-FL enables a high degree of system utilization. This is important in light of SWaP concerns. This last reason motivates our departure from partitioned fixed-priority scheduling, as prescribed by the AUTOSAR automotive standard [1], which suffers from well-known utilization constraints. We hope this work may be informative to future automotive standards.

3 System Model

In this section, we present the implicit-deadline sporadic DAG task model, which is our focus herein. Such a task

¹All source code is available at www.litmus-rt.org.

system is comprised of a set $\tau = \{T_1, T_2, \dots, T_n\}$ of n DAGs. Each DAG is a set $T_i = \{T_i^1, T_i^2, \dots, T_i^{z_i}\}$ of z_i tasks, with producer/consumer relationships. Each task releases a (potentially infinite) series of jobs $T_i^{j,1}, T_i^{j,2}, \dots$. An example DAG T_1 is depicted in Fig. 2. Each edge is directed from a *producer* task that produces data to a *consumer* task that consumes that data. A particular task T_i^j 's producers, $prod(T_i^j)$, are those on edges for which T_i^j is the consumer, and its consumers, $cons(T_i^j)$, are those on edges for which T_i^j is the producer. The maximum number of bytes that a job of T_i^j can produce for T_i^ℓ to consume is denoted as $b_i^{j \rightarrow \ell}$. Each job must wait to begin execution until one job from each of its producers has completed, so that the necessary input data is available. For example, in Fig. 2, for any k , $T_1^{4,k}$ needs input data from each of $T_1^{2,k}$ and $T_1^{3,k}$, so it must wait until those jobs complete.

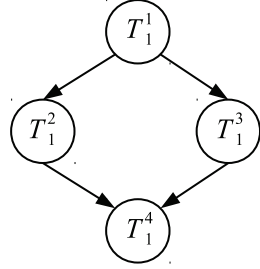


Figure 2: Precedence constraints within a DAG.

To simplify analysis, each DAG T_i has exactly one *source task* T_i^1 , which only has outgoing edges, and one *sink task* $T_i^{z_i}$, which has only incoming edges. Multi-source/sink DAGs may be supported with the addition of singular “virtual” sources and sinks that connect multiple sources and sinks, respectively. The *depth* of a task T_i^j is the number of edges on the longest path between T_i^1 and T_i^j , and the *height* of a DAG is the depth of its sink task. For example, the depth of T_1^4 in Fig. 2 is two, and T_1^4 is the sink task so the depth of T_1 is two. Also, each DAG has a common minimum separation time p_i for all of its tasks. Each job of any task in T_i has a deadline p_i time units after it is released. Each task T_i^j also has a parameter e_i^j , which denotes the worst-case execution time (WCET) for any of its jobs. This parameter *does not* include the cost of consuming data from $prod(T_i^j)$ —we account for this later in analysis. We assume that τ is scheduled on an identical multiprocessor.

Prior work [10, 18, 19] considered the more general *processing graph method (PGM)* to describe DAGs, where DAG nodes may have different periods. The implicit-deadline sporadic DAG model above is a restricted case of PGM DAGs. Our restricted model is sufficient to schedule the automotive workloads we consider. Further, the end-to-end latency bounds we show in Sec. 4 are tighter than would otherwise be possible using the more generalized analysis [18, 19]. However, the techniques herein can be applied to DAGs with nodes of different periods, so we present end-to-end latency bounds for such DAGs in [7].

4 Determining End-to-End Latency

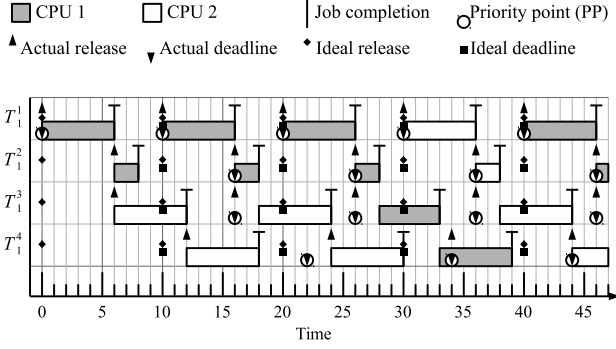
We now discuss how to apply results from [19] on PGM-based systems to analyze the end-to-end response time (or latency) of a DAG T_i . In [19], job release times and deadlines are computed on-the-fly such that tasks $T_i^j \in T_i$ behave

as independent sporadic tasks. Here, we present the ideas behind this technique and describe how it can be applied in our context.

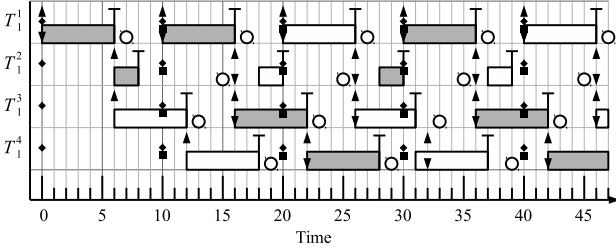
The analysis from [19] is general enough to apply to clustered algorithms wherein an intra-cluster scheduler is used from a broad class of *window-constrained* [16] global scheduling algorithms. Under a window-constrained global algorithm, all jobs share a single run queue, and each job is prioritized on the basis of a *priority point (PP)* that can move during execution, but that must remain within a constant distance of the job’s deadline. The released but unfinished jobs with the earliest PPs are scheduled for execution. The most well-known window-constrained algorithm is G-EDF, which uses the deadline of each job as its PP. However, Erickson et al. [9] demonstrated that allowing PPs set *earlier* than deadlines can result in better response-time bounds. The G-FL scheduler, mentioned in Sec. 1, functions in this way. Erickson et al. [8] also showed that response time bounds can be further improved by simulating a G-FL schedule of a task system with more frequent releases of smaller jobs. This method is referred to as *job splitting*. Unlike G-EDF and basic G-FL, G-FL with job splitting moves the PP of a job during execution. However, it does so in a way that maintains the window-constrained property. As noted above, clustered variants of these global algorithms can be obtained by using the global algorithm to schedule the tasks within each cluster. For the simple examples provided in this section, there is only one cluster, so G-EDF and G-FL are identical to C-EDF and C-FL, respectively, their clustered counterparts.

In a DAG T_i , the source task T_i^1 is assumed to follow the implicit-deadline sporadic task model: its releases are separated by at least p_i time units, and each job’s deadline is p_i time units after its release. We define for each job an *ideal release* and an *ideal deadline* that are identical to the release time and deadline of the corresponding job from the source task. We also define for each job $T_i^{j,k}$ an *actual release* that is sometimes later than its ideal release, and a corresponding *actual deadline* p_i units later. The source task is a special case in that its actual and ideal releases are identical, and thus its actual and ideal deadlines are identical. Scheduler decisions are always based on PPs derived from actual deadlines rather than ideal ones.

The primary purpose of delaying the actual release is to model the fact that a job cannot run before its producers have completed. Because G-EDF is the simplest window-constrained algorithm, we show in Fig. 3(a) the G-EDF scheduling of a DAG with the same structure as the DAG from Fig. 2 (ignoring overheads for simplicity). Observe that the actual releases of $T_1^{2,1}$ and $T_1^{3,1}$ are at time 6, when $T_1^{1,1}$ completes. Actual releases and deadlines must follow the sporadic task model. For example, consider time 33 in Fig. 3(a), when $T_1^{3,3}$ finishes early. Because all producers of $T_1^{4,3}$ are now complete, $T_1^{4,3}$ commences execution at time 33. However, because T_1^4 ’s last actual release was at time 24, the actual release of $T_1^{4,3}$ is not until time 34, and its actual deadline is at time 44. This is to ensure that the deadline used by the scheduler follows the sporadic task model. Prior response-time analysis [9] remains correct when jobs may



(a) System scheduled under G-EDF.



(b) System scheduled under G-FL.

Figure 3: Example schedules of the DAG depicted in Fig. 2 with $m = 2$, $p_1 = 10$, $e_1^1 = 6$, $e_1^2 = 2$, $e_1^3 = 6$, and $e_1^4 = 6$.

execute before their actual release times, as long as their actual deadlines follow the sporadic task model. Thus, if a job’s ideal release precedes its actual release, and all of its precedence constraints are satisfied, then it may commence execution if it has sufficient priority, as at time 33 in Fig. 3(b).

If the tasks in τ can be assigned onto clusters of CPUs such that no individual cluster is overutilized, then because *actual* deadlines follow the sporadic task model, any scheduler using a window-constrained scheduling algorithm within each cluster can ensure that no job $T_i^{j,k}$ completes more than some per-task constant R_i^j units (i.e., the response time bound) after its *actual* release, as shown in [16].

Liu et al. [19] demonstrated that this property can be used to provide a bound relative to each job’s *ideal* release, by showing that actual and ideal releases only differ by a bounded amount. The following theorem is similar to Thm. 3 in [19], but is much less pessimistic. (The improvements are described in an online appendix [7].)

Theorem 1. *Suppose that the tasks in τ can be assigned onto clusters of CPUs such that no individual cluster is overutilized. If Θ is the set of all tasks along the worst-case path² from T_i^1 to T_i^j , including both T_i^1 and T_i^j , then any job $T_i^{j,k}$ completes within*

$$\sum_{T_i^\ell \in \Theta} R_i^\ell$$

units of its ideal release.

We consider the end-to-end latency for an entire graph, rather than for a single job. However, by our definition of ideal releases, $T_i^{z_i}$ has the same ideal release as T_i^1 . There-

²That is, the path that maximizes the given sum.

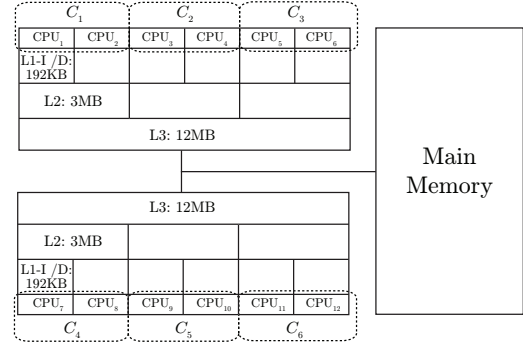


Figure 4: Example memory hierarchy. L2 clustering depicted.

fore, the latency of the graph is simply the bound provided by Thm. 1 with $j = z_i$.

Although the analysis in [19] was shown to be correct whenever a window-constrained scheduling algorithm is used within each cluster, it was only experimentally evaluated using C-EDF (and it was not evaluated based on a real scheduler implementation). As mentioned above, C-FL can provide superior response-time bounds by using PPs that are earlier than deadlines. C-FL biases scheduling priority towards tasks with larger e_i^j values. Recall that, because there is only one cluster in the example we are considering, G-FL is identical to C-FL. An example of the operation of G-FL is depicted in Fig. 3(b). Observe that, in comparison with the G-EDF schedule in Fig. 3(a), $T_1^{4,2}$ finishes at time 28 instead of time 30, $T_1^{4,3}$ finishes at time 37 instead of time 39, and so on. Thus, using G-FL or C-FL can reduce the end-to-end latency of a graph, as the theoretical bounds in [9] indicate. Although not pictured due to space constraints, job splitting can further reduce the latency of each graph. In this paper, we explore the use of both techniques.

5 Assigning Tasks to Clusters

We now examine the problem of assigning DAG tasks to processor clusters, and present an assignment heuristic designed to promote efficient cache sharing among DAG tasks. We also develop a method for determining overheads pertaining to the data passed between tasks.

In a shared-memory system, node output data is written directly to memory—there is no explicit message passing of data among nodes. Data may reside anywhere within the system’s memory hierarchy, from the private L1 cache of a processor to main memory. The cost of reading this data depends upon (i) the location of data within the memory hierarchy, and (ii) the processor from which the read is made. Reads become more costly as the distance between the data and the reader increases. For example, the cost of reading data from a processor’s own L1 cache is cheap, while reading data from an L3 cache is more expensive.

Consider the memory hierarchy of a dual-socket twelve-core system depicted in Fig. 4. Here, there are private per-CPU 192KB L1s for data (L1-D) and instructions (L1-I), pair-wise shared 3MB L2s, per-socket 12MB L3s, and finally, main memory. For simplicity, let us assume the caches are coherent, inclusive, fully associative, and follow a least-

recently-used (LRU) eviction policy.³ Suppose processors that share a common L2 are cluster-scheduled, as depicted in Fig. 4, and we wish to map the DAG depicted in Fig. 2 to this system. Further suppose that T_1^1 produces 128KB and 1MB of data for T_1^2 and T_1^3 , respectively, and T_1^2 and T_1^3 produce 128KB and 1MB of data respectively for T_1^4 . *Worst-fit decreasing* is a commonly studied partitioning heuristic, in which tasks are allocated to clusters in order of decreasing utilization, and each task is allocated to the cluster with the largest available capacity. Under such a heuristic, each task would be put in a separate cluster: T_1^1 in C_1 , T_1^2 in C_2 , T_1^3 in C_3 , and T_1^4 in C_4 . With this assignment, the read costs of T_1^2 and T_1^3 can be no less than reads from the L3 shared by C_1 , C_2 , and C_3 , as this is their closest common cache. Costs are greater for T_1^4 since C_4 has no common cache with C_2 or C_3 . A far more cache-efficient strategy is to put all tasks in C_1 , since all the written data (2.25MB) can fit within C_1 's 3MB L2 cache. Thus, the end-to-end latency of this graph may be less since each task executes for a shorter duration.

This illustrates that a cache-efficient partitioning heuristic for mapping nodes to clusters should be cognizant of the system's memory hierarchy and associated costs. Ultimately, this heuristic should place related nodes in the same or closest adjacent cluster, as long as schedulability is maintained. *This might not actually enhance schedulability* if conservative assumptions are made with respect to caches in timing analysis, but *runtime performance may still be positively impacted, which increases safety margins*.

5.1 Cache-Aware Task Assignment

In this section, we present a cache-aware task assignment heuristic, which is shown in Fig. 5. This heuristic was designed assuming the system of m processors consists of m/c clusters, each containing c processors. The heuristic reverts to the worst-fit decreasing heuristic after all clusters have total utilization exceeding an *aggressiveness factor* h . Since system overheads are charged later in schedulability analysis, the aggressiveness factor prevents loading a cluster to the degree that even small overheads lead to overutilization while other clusters remain underutilized.

We keep track of the following quantities. \mathcal{T} is the set of unassigned tasks from all DAGs, initially $\mathcal{T} = \bigcup_{T_i \in \tau} T_i$. $C = \{C_0, C_1, \dots, C_{m/c}\}$ is the set of all clusters. $a(T_i^j)$ for each T_i^j is the cluster to which T_i^j is assigned, initially *Nil*, indicating that it has not been assigned to a cluster.

We also utilize several functions. $cost(T_i^j)$ is the cost of reading all data produced for T_i^j by its producers, according to the cluster assignments of each $T_i^\ell \in prod(T_i^j)$ and T_i^j . If some $a(T_i^\ell)$ or $a(T_i^j)$ is *Nil*, then the tasks are assumed to be partitioned the farthest apart with respect to the memory hierarchy. $w(T_i^j) \triangleq (e_i^j + cost(T_i^j))/p_i$ is the approximated utilization of T_i^j after accounting for communication overheads. $u(C_k) \triangleq \sum_{T_i^k \in C_k} w(T_i^k)$ is the total utilization of a cluster, including communication overheads. Finally, $min(C)$ is the set of clusters with minimum $u(C_k)$.

³We address the practicality of these assumptions later in this paper.

```

PICKCLUSTER( $T_i^j$ : task,  $Q$ : list of clusters)
1  $X :=$  from  $Q$ , select clusters that minimize  $w(T_i^j)$ 
2  $X :=$  from  $X$ , select clusters that minimize:
    $\sum_{T_i^\ell \in cons(T_i^j)} w(T_i^\ell)$ 
3  $X :=$  from  $X$ , select clusters that places  $T_i^j$  closest to
   other tasks of the same graph
4 return first cluster in  $min(X)$ 

CACHEAWAREPARTITION
1 Sort  $\mathcal{T}$  by  $w(T_i^j)$  in decreasing order
2 for each  $T_i^j$  in the first  $(m - m/c)$  ordered tasks  $\in \mathcal{T}$ 
3    $a(T_i^j) :=$  PICKCLUSTER( $T_i^j, min(C)$ )
4 for each remaining  $T_i^j \in \mathcal{T}$ 
5    $Q := \{q \mid (q \in C) \wedge (u(q) + w(T_i^j) \leq h)\}$ 
6   if  $Q \neq \emptyset$ 
7      $a(T_i^j) :=$  PICKCLUSTER( $T_i^j, Q$ )
8   else
9      $a(T_i^j) :=$  PICKCLUSTER( $T_i^j, min(C)$ )

```

Figure 5: Cache-aware task assignment heuristic.

Algorithm description. We first describe PICKCLUSTER, which is used to select the best cluster for a particular task T_i^j . It accepts a parameter Q , a list of candidate clusters. In line 1, it first attempts to select the cluster that will result in the smallest value of $w(T_i^j)$. If there is a tie, then line 2 will continue to select the cluster that minimizes the cost of any consumers that are already assigned. If there is still a tie, then line 3 will select the cluster that places T_i^j closest to other tasks in T_i , even if those tasks are neither producers nor consumers of T_i^j . Finally, if there is still a tie, the cluster with minimum utilization is selected in line 4.

We now describe CACHEAWAREPARTITION, which performs the actual partitioning. The first part of our heuristic is based on some of the details from the response-time analysis in [9]. That analysis considers the number of tasks that may execute while a single processor is left idle. Ultimately, the $c - 1$ tasks of greatest utilization within a cluster have the most significant impact on response-time bounds. A cluster with a disproportionate number of high-utilization tasks may result in larger response-time bounds in comparison to clusters with lighter-utilization tasks, even if these clusters are equally loaded. We want to avoid this problem. Thus, we spread the first $(m/c) \cdot (c - 1) = m - m/c$ tasks as evenly as possible across clusters by using the worst-fit decreasing heuristic. This is done in lines 1–3. Ties are broken using PICKCLUSTER. For each remaining task (see line 4), we select in line 5 the set of all clusters for which adding T_i^j will not cause the cluster's utilization to exceed the aggressiveness factor h . If there are such clusters, then line 7 selects the best cluster using PICKCLUSTER. If not, then the algorithm reverts to a worst-fit heuristic (line 9), using PICKCLUSTER to break ties.

5.2 Assessing Data Passing Costs

The performance of CACHEAWAREPARTITION hinges on the function $cost(T_i^j)$ used to estimate the cost of passing data between tasks. We now describe a method for estimating $cost(T_i^j)$ that assesses the costs associated with passing data between tasks on a multicore platform with a complex

memory hierarchy.

The value of $cost(T_i^j)$ is obtained from careful measurements of cache behavior. We use an experimental method modeled after the “synthetic method” described in [5] that is used to assess cache preemption and migration delays. A non-preemptive instrumented process records the time taken to read a prescribed amount of sequential data from a “hot” cache. The process suspends for a short duration, resumes on a random processor, and rereads said data from the now “cold” cache. A cost is determined by subtracting the hot measurement from the cold. We classify this measurement according to the closest shared cache between the read-issuing processors. Measurements are classified as “memory” if there is no shared cache between them. After many thousands of measurements, we derive a lookup table indexed by closest common cache and data size. We collect two datasets using this method: (i) an “idle” dataset where the instrumented process runs alone, and (ii) a “polluter” dataset where “cold” measurements are taken in the presence of cache-trashing processes that introduce contention for both caches and memory bus.

These two datasets actually yield two variants of the $cost(T_i^j)$ function that provide lower and upper bounds of actual communication overhead. The lower bounds we obtain are based upon certain ideal assumptions (see below) regarding cache behavior. This is acceptable, because our main intent is to produce task assignments that improve runtime performance and hence increase safety margins, rather than to determine precise overhead costs. Indeed, rigorous analysis of cache behavior for the purpose of precise timing analysis is still an unresolved issue in the context of multi-core platforms. In the experiments presented in Sec. 7, we present schedulability results for the two extremes of “idle” and “polluter” overheads. If adequate timing analysis tools were available for multicore platforms, they would likely yield schedulability results between these two extremes.

The $cost(T_i^j)$ function *cannot* be derived by simply summing individual costs between each T_i^j and $T_i^\ell \in prod(T_i^j)$ due to cache sharing. We illustrate this with an example.

Example. Consider the memory hierarchy from Fig. 4. For simplicity, assume that caches are inclusive, fully associative, use an LRU eviction policy, and that no cache interference occurs due to instruction caching or operations from other processors. Suppose we wish to compute $cost(T_1^3)$ for the subgraph depicted in Fig. 6. Here, an L1-D cache is shared between T_1^2 and T_1^3 . Likewise, an L3 is shared between T_1^1 and T_1^3 . We will now walk through a worst-case sequence of operations that maximizes $cost(T_1^3)$.

Step 1: T_1^2 writes 1024KB of data for T_1^3 . The L1-D is only 192KB in size, so 192KB of this data is stored in the L1-D, while the remaining 832KB spills to the L2.

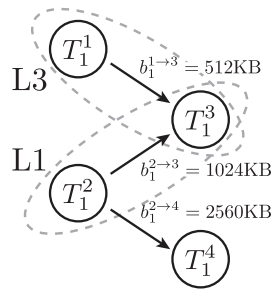


Figure 6: Subgraph with data passed between nodes.

Step 2: T_1^1 writes 512KB of data for T_1^3 . Although T_1^1 executes on a remote processor, a copy of this data resides in the L3 due to inclusivity.

Step 3: T_1^2 writes 2560KB of data for T_1^4 . This causes evictions on two levels. First, all of T_1^3 's data in the L1-D spills to the L2 after the first 192KB of T_1^4 's data is written. The L1-D continues to spill as remaining data is written. Ultimately, 2368KB of T_1^4 's data spills to the L2. The L2 must maintain a copy of the L1 (both instruction and data caches) due to inclusivity, so the L2 can only store 2688KB of spilled data. T_1^3 's data from Step 1 is evicted first according to the LRU policy, so 768KB of T_1^3 's data is spilled from the L2 to the L3, and 256KB of it remains in the L2.

Step 4: T_1^3 reads the 512KB of data from T_1^1 . This L3-read triggers 192KB of data from Step 3 to spill from the L1-D to the L2, which in turn triggers 192KB of T_1^3 's data from Step 1 to spill from the L2 to the L3. T_1^3 's remaining 64KB of data in the L2 is self-evicted as T_1^3 reads the rest of the data from T_1^1 .

Step 5: T_1^3 reads the 1024KB of data from T_1^2 . All 1024KB of data from Step 1 resides in the L3 due to spills. All of T_1^3 's data is read from the L3, so we charge T_1^3 for 1536KB of data read from the L3, according to the overhead dataset.

Our general algorithm to compute $cost(T_i^j)$ is outlined as follows. First, we assume all $T_i^\ell \in prod(T_i^j)$ collectively write data for T_i^j prior to data for any $T_i^k \in cons(T_i^\ell)$, and we model evictions to track the location of T_i^j 's data. Next, we assume that T_i^j reads the most distant data first, and we continue to track the location of T_i^j 's remaining data by modeling self-evictions. We sum overhead costs according to the location of data as it is read by T_i^j .

A remark on optimism. We have made optimistic assumptions in computing $cost(T_i^j)$: full associativity, LRU, no instruction caching, etc. Since $cost(T_i^j)$ conservatively estimates best-case conditions in the “idle” case, it can provide a lower bound on overhead costs. However, this optimism is of no consequence under our “polluter” dataset, where all costs are equivalent: every read of a new cache line results in a cache miss at all levels. Thus, $cost(T_i^j)$ can provide both an upper and lower bound on overheads, according to the dataset. Deeply involved timing analysis techniques are necessary to provide tighter bounds.

6 Implementation

PGM^{RT} is a portable lightweight middleware layer we developed to manage the coordinated execution of dataflow applications. We describe the subset of PGM^{RT} necessary to support the automotive workloads that we have discussed. However, PGM^{RT} supports the full PGM specification; please see the online version of this paper for a full description of PGM^{RT}'s API and capabilities [7].

Graphs, nodes, and edges. Each graph is identified by a unique name and path, similar to a UNIX named pipe. Applications use PGM^{RT}'s API to create new graphs described by nodes and edges. Real-time tasks, as unique threads of execution within the same address space or separate pro-

cesses, use PGM^{RT}'s API to access information about a named graph and claim/bind to a node and its edges.

Precedence constraints. As described in Sec. 4, non-source nodes have two types of precedence constraints: job and producer constraints. Job constraints are satisfied in PGM^{RT} since a single thread binds to each node—jobs are naturally serialized by this thread.

Predecessor constraints are tracked by *tokens*. A producer generates one token on each outbound edge upon job completion. A consumer's producer constraints are satisfied when there is at least one token on each of its incoming edges. The consumer blocks (suspends execution) whenever the requisite tokens are unavailable. When the needed tokens are available, the consumer consumes one token from each of its incoming edges and the task is ready to execute.

Token production/consumption is realized through increment/decrement operations on per-edge token counters, similar to counting semaphores. Although these tokens do not transmit data explicitly, tokens can coordinate data sharing in application-level logic. Since consumers may suspend execution, producers must have a mechanism to signal consumers of new tokens. This is achieved using a monitor synchronization primitive, specifically, a POSIX (pthread) condition variable, one per consumer.⁴ A consumer blocks on its condition variable if it does not have its requisite tokens. A producer signals the condition variable whenever it is the last producer to satisfy all of its consumer's producer constraints.

Real-time concerns. PGM^{RT} described as above can be used with general-purpose schedulers. However, additional enhancements are required to ensure deterministic real-time behavior. These relate to deterministic token signaling and proper deadline assignment.

The preemption of a consumer while it is signaling a sequence of consumers may leave processors in remote clusters idle. To avoid this, producers are non-preemptive during the signaling process. In the LITMUS^{RT}-based version of PGM^{RT} used in the experiments in Sec. 7, we use LITMUS^{RT}'s capabilities to quickly enter and exit these non-preemptive code sections. For a portable alternative, interrupts may be disabled from userspace (e.g., `sti/cli` instructions on x86 processors). These short durations of non-preemption must be accounted for in real-time analysis, since they may momentarily delay higher priority work from being scheduled.

Recall from Sec. 4 that a job's ideal (actual) deadline is computed as p_i time units after its ideal (actual) release. The ideal release time of a job can be tracked with a high-resolution timer. However, the actual release time depends upon token arrival, so the actual deadline must be computed on-the-fly. In our LITMUS^{RT}-based implementation, immediately before a consumer blocks for tokens, it sets a "token-wait" flag in memory shared by userspace and the kernel. The kernel checks this flag whenever a real-time task is awoken from a sleeping state. If set, and the current time is later than the ideal release time, the kernel automatically com-

putes the actual release and deadline for the job and clears the flag. Otherwise, the ideal and actual deadlines coincide. Observe that this computation requires the current time to approximate the arrival time of the last token—this is ensured by the producer's non-preemption discussed earlier. For a portable approach, producers may set the deadline of a consumer directly prior to signaling, but this comes at the cost of system call overheads and requires support from the operating system.

7 Experimental Results

In this section, we evaluate PGM^{RT} via an overhead-aware schedulability study and a case-study of observed end-to-end latencies.

7.1 Schedulability Experiments

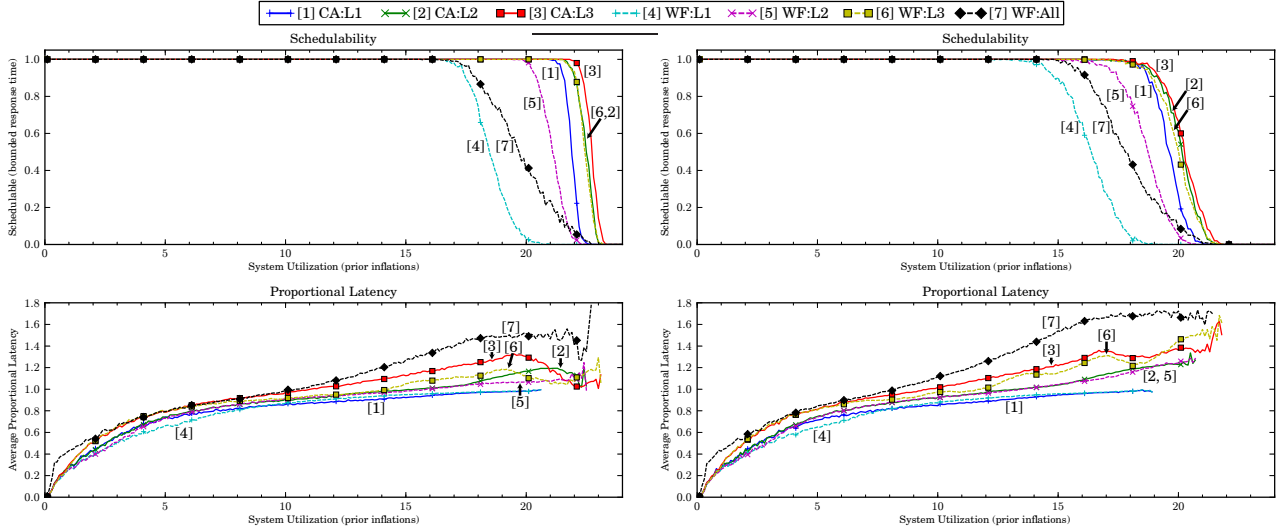
We evaluate C-FL cluster scheduling, job splitting, and our cache-aware cluster assignment techniques through overhead-aware schedulability experiments. We randomly generated DAGs of varying characteristics and tested them for schedulability using the methods described in [8]. We now describe the experimental process we used.

Overheads. Our implementation of PGM^{RT} on LITMUS^{RT} was run on a four-socket (24-core) Intel Xeon L7455 running at 2.13GHz. Each socket has the same memory hierarchy as that in Fig. 4. Every core has a private 8-way set-associative 192KB L1-data and L1-instruction cache. Core pairs share a 12-way set-associative 3MB L2 cache. Finally, the cores on each socket share a 12-way set-associative 12MB L3 cache. We measured worst-case runtime overheads and preemption/migration delays in the manner described in [5]. We also measured data-passing overheads, as described in Sec. 5.

We made several changes to the overhead-accounting techniques for C-FL as described in [8] to support DAGs under PGM^{RT}. First, we account for non-preemptivity during consumer signaling, as this can delay higher priority work from being scheduled. Second, we account for the system calls made by producers to wake consumers. Finally, we only charge for release-timer overheads of graph source tasks; non-source nodes do not use release timers.

Experimental setup. Random DAGs for schedulability experiments were generated according to several parameters in a multistep process. Task utilizations were generated using three uniform and three bimodal distributions. The ranges of the uniform distributions were [0.001, 0.1] (*light*), [0.1, 0.4] (*medium*), and [0.5, 0.9] (*heavy*). The bimodal distributions randomly selected from two uniform distributions with ranges [0.001, 0.5] and [0.5, 0.9] with respective probabilities of 8/9 and 1/9 (*bimo-light*), 6/9 and 3/9 (*bimo-medium*), and 4/8 and 5/9 (*bimo-heavy*). Task periods were generating using three uniform distributions with ranges [3ms, 33ms] (*uni-short*), [10ms, 100ms] (*uni-moderate*), [50ms, 250ms] (*uni-long*). The number of DAGs in a task set were selected uniformly in the range [1,12]. The height of a DAG was determined by a "height-factor." The height-factor was generated using four uniform distributions, with ranges of

⁴On LITMUS^{RT}, PGM^{RT} uses a low-overhead implementation of a monitor that combines spinlocks with Linux's "fast userspace mutex" interface and LITMUS^{RT}'s special support for non-preemptive code sections.



(a) Without polluter overheads.

(b) With polluter overheads.

Figure 7: Schedulability of pipeline DAGs with *uni-long* periods, *uni-medium* task utilizations, and *medium-weight* edges.

[1/3, 1/2] (*short-height*), [1/2,3/4] (*medium-height*), [3/4, 1] (*tall-height*) [1,1] (*pipeline*). DAG height is computed as $\lceil \text{height-factor} \cdot \# \text{ of DAG nodes} \rceil$. A uniform distribution of range [1,3] controlled the number of consumers for each non-sink task. The amount of data passed from producer to consumer, or “edge working set size” (EWSS), was controlled by three uniform and three bimodal distributions. The uniform distributions were [1KB, 64KB] (*light-weight*), [256KB, 1024KB] (*medium-weight*), and [2MB, 8MB] (*heavy-weight*). The bimodal distributions randomly selected from two uniform distributions with ranges [64KB, 256KB] and [2MB, 8MB] with respective probabilities of 8/9 and 1/9 (*bimo-light-weight*), 6/9 and 3/9 (*bimo-medium-weight*), and 4/8 and 5/9 (*bimo-heavy-weight*). Tasks were generated by selecting a utilization and period. Tasks were added to a task set until a specified system utilization was reached. After selecting the number of DAGs to generate, tasks were assigned to a random DAG, with a constraint ensuring that each DAG had at least one node. A height-factor was then selected for each DAG and its height determined. After selecting a random source and sink for each DAG, a random number of consumers was selected for each non-sink task. We then selected the amount of data transmitted on each edge. The “working set size” of each task (used to compute preemption/migration overheads) was computed as the sum of a task’s in-bound EWSS. Finally, the period of each non-source task was adjusted to match that of its source node—we scaled execution time to maintain utilization.

A unique combination of the above distributions defined a set of experiment settings. For each 0.1 increment in the system utilization range (0,24], we generated 1,000 task sets. Schedulability under C-FL for each task set was checked under a combination of the following conditions: (i) according to cluster configuration, where the L1s, L2s, L3s, and main memory defined clusters of size one, two, six, and 24, respectively; (ii) task cluster assignment heuristics of worst-fit (WF) in decreasing task utilization and our cache-aware (CA) method (with an aggressiveness factor 75% of cluster

capacity); and (iii) cache overheads under idle and polluter conditions. We used a university compute cluster to test the schedulability of over 800 billion task sets.

For each schedulable task set, we computed the end-to-end latency of each DAG according to Eq. (1) from Sec. 4, with $T_i^j = T_i^{z_i}$, when scheduled with job splitting. The extent of splitting was determined from overhead data (which limits the extent of splitting) using a procedure from [8]. A *proportional end-to-end latency* metric was computed by dividing the computed end-to-end latency by $p_i \cdot (\text{height}(T_i) + 1)$.

Results. We present a selection of results from our experiments that illustrate the general trends observed across all data. All schedulability results are available in [7]. Fig. 7 shows results for pipelined shaped DAGs with “uni-long” periods, “uni-medium” task utilizations, and “medium-weight” edges. The top (bottom) of Fig. 7(a) and Fig. 7(b) depict schedulability (proportional end-to-end latency under job splitting) results under idle and cache-polluter overheads, respectively.

Obs. 1. Cache-aware assignment improves schedulability.

In the top inset of Fig. 7(a), compare CA and WF cluster assignment for L1 clustering (lines 1 and 4, respectively). Observe that under CA:L1, 50% of task sets with a utilization of about 22.0 were schedulable. In comparison, under WF:L1, only 50% of task sets with a utilization of about 18.5 were schedulable. Moreover, no task sets with a utilization of 22.0 were schedule under WF:L1. CA cluster assignment outperforms WF cluster assignment for L2 and L3 clustering as well, although the gap in performance is smaller. For example, CA:L3 (line 3) offers only slightly better schedulability than WF:L3 (line 6).

As expected, schedulability across all methods under cache-polluter overheads is worse, as depicted in the top inset of Fig. 7(b). However, at no point does WF cluster assignment outperform CA cluster assignment for the same cluster configuration. This may come as a surprise since no parti-

tioning scheme can reduce the cache-related overheads incurred under the cache-polluter dataset (see end of Sec. 5). However, the CA heuristic also assigns tasks according to an approximated utilization ($w(T_i^j)$) that includes cache-related costs. Thus, the CA heuristic is able to make better task assignments, even if it does not reduce incurred overheads.

Obs. 2. Cache-aware cluster assignment is resistant to bin-packing utilization loss.

Cluster configuration strongly affects schedulability under WF cluster assignment. This is observed by comparing WF:L1 (line 4), WF:L2 (line 5), and WF:L3 (line 6) within the top insets of Fig. 7. WF:L3 outperforms WF:L2 by a wide margin, and WF:L2 similarly outperforms WF:L1. In contrast, compare CA:L1 (line 1), CA:L2 (line 2), and CA:L3 (line 3) within the top insets of Fig. 7. The differences in schedulability are much less.

Obs. 3. Computed proportional end-to-end latency is less for smaller clusters.

L1 clustering gave the smallest overall proportional latencies, as shown by lines 1 and 4 in both bottom insets of Fig. 7. This is expected since deadlines are never missed under partitioned EDF scheduling if no cluster is overutilized. However, we also observe that proportional latency is very small (no more than about 1.2) under CA and WF cluster assignment under L2 clustering (lines 2 and 5, respectively). Proportional latency is greater under L3 clustering (lines 3 and 6), but not as great as under global scheduling (line 7) in either bottom inset of Fig. 7.

Obs. 4. There are trade-offs between schedulability and proportional end-to-end latency.

Schedulability is best under CA:L3 in Fig. 7. However, besides global scheduling (line 7), CA:L3 has worst proportional end-to-end latency (line 3). The converse is true for smaller clusters. These results suggest that the system designer is faced with three interesting choices: (i) minimize end-to-end latency by using the smallest cluster configuration where their application is schedulable; or (ii) increase safety margins in provisioned task execution time and use larger clusters to maintain schedulability; or (iii) decrease processor speed (effectively increasing system utilization) and use larger clusters to maintain schedulability. Choices (ii) and (iii) are extremely attractive in an automotive setting. Choice (ii) increases safety, while choice (iii) may reduce SWaP and manufacturing costs.

7.2 Runtime Evaluation

We now describe our runtime evaluation of PGM^{RT}. We implemented a PGM^{RT} application that executes a DAG on LITMUS^{RT}. Upon invocation, a node performs a repeated summation over all input data from producers, and then writes output for all consumers. The invocation executes for at least a specified length of time, but will execute for longer durations under poor cache performance.

Experimental setup. We generated task sets composed of several DAGs according to two experimental parameters: DAG shape and the amount of data passed between nodes. DAG shape was pipelined or rectangular. In a pipelined

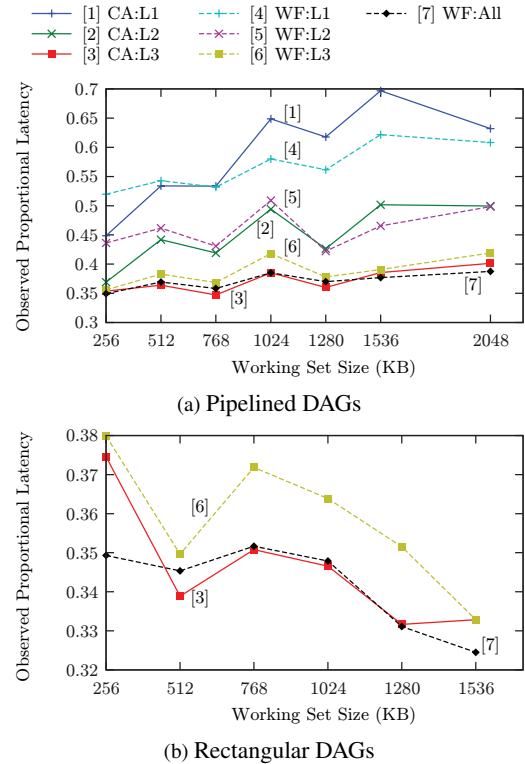


Figure 8: Avg. 99th percentile of observed proportional latencies.

DAG, every interior node has only one producer and one consumer. Rectangular DAGs are made of several pipelined sub-DAGs, joined by a source and sink. The amount of data passed between a producer and consumer was tested at points of [256KB, 512KB, 768KB, 1024KB, 1280KB, 1536KB, 2048KB]. We generated five task sets (trials) for each combination of DAG shape and amount of data passed. Each task set was deemed schedulable, according to our overhead-aware analysis under polluter overheads, for our 24-core evaluation platform. We assigned tasks to clusters using both the cache-aware and worst-fit decreasing heuristics. Each task set was executed for 30 seconds (both with and without job splitting) and we measured the observed end-to-end latency. Only the top-performing approaches for pipelined DAGs were tested on rectangular DAGs.

Results. We present the proportional end-to-end latencies observed in our experiments for pipelined DAGs and rectangular DAGs made of three pipelines. We omit results for job splitting because it provided little improvement due to low split factors. Fig. 8 depicts our results for task sets with a total utilization of 13.0 (prior to overhead accounting). The x -axis is EWSS. The y -axis is observed proportional latencies. The 99th percentile of observed proportional latencies (99% of observed latencies are less than a given y -value), averaged across the five trials, is plotted. We make the following observations.

Obs. 5. Observed end-to-end latencies are better for larger clusters.

In Fig. 8(a), we see that performance is largely dictated by cluster configuration rather than the cluster assignment method. For example, the observations for WF:L2 (line 5)

and CA:L2 (line 2) are relatively similar. The same trend holds for L1 and L3 clustering. We also note that L3 clustering performs well, completing the positive results from schedulability experiments for L3 clustering. Finally, we observe that global scheduling performs surprisingly well (line 7), considering that analytical results suggested that global scheduling would perform poorly.

Obs. 6. Cache-aware methods may yield smaller latencies.

The cache-aware heuristic outperforms the worst-fit heuristic for smaller EWSSs. However, there appears to be a trend where worst-fit performs better for larger EWSSs. In Fig. 8(a), observe the intersections between CA:L1 (line 1) and WF:L1 (line 4) at 768KB, and CA:L2 (line 2) and WF:L2 (line 5) at 1280KB. CA:L3 (line 3) and WF:L3 (line 6) do not intersect in Fig. 8(a), but do in Fig. 8(b) at 1536KB. The cache-aware heuristic sacrifices load balancing across clusters for a chance at cache efficiency. However, as cache utilization grows, actualized gains become more difficult to realize.

We conclude with the observation that cache-aware clustered scheduling methods strongly affect schedulability and end-to-end latency bounds. On our experiments, we see that these methods maximize schedulability and are competitive in analytical and observed latency. This suggests that future automotive standards should consider clustered deadline-oriented schedulers to maximize resource utilization.

8 Conclusion

In this paper, we have presented solutions to problems of scheduling real-time dataflow applications on multicore processors. We explored dataflow applications in advanced automotive systems, and discussed how best to meet SWaP and manufacturing costs constraints, while providing timing guarantees for safe operation and responsiveness. We derived analytical bounds on the end-to-end latency of such applications. We also developed a high-level model of cache behavior, and the overheads thereof, to drive a cache-aware heuristic we use to map dataflow computations to processors. We also presented PGM^{RT}, a portable middleware for managing real-time dataflow applications. Using overheads obtained through PGM^{RT} running on LITMUS^{RT}, we performed overhead-aware schedulability experiments. The results validate our approach, and demonstrate that cache-aware techniques, coupled with clustered processor scheduling, can yield better timing properties than naïve partitioned or global scheduling. We also presented results from runtime experiments that bolster the benefits of our techniques.

In future work, we would like to extend support to accelerator coprocessors (e.g., GPUs and FPGAs), and also perform a case study with real-world automotive applications.

Acknowledgement: We thank Dr. Shige Wang of General Motors for his helpful comments on drafts of this paper.

References

- [1] AUTOSAR Release 4.1, Specification of Operating System. <http://www.autosar.org>, 2013.
- [2] A. Adams, D. E. Jacobs, J. Dolson, M. Tico, K. Pulli, E. Talvala, B. Ajdin, D. Vaquero, H. Lensch, M. Horowitz, et al. The Frankencamera: an experimental platform for computational photography. *ACM Trans. on Graphics*, 2010.
- [3] A. Bastoni, B. Brandenburg, and J. Anderson. An empirical comparison of global, partitioned, and clustered multiprocessor edf schedulers. In *31st RTSS*, 2010.
- [4] R. Bettati and J. Liu. End-to-end scheduling to meet deadlines in distributed systems. In *12th ICDCS*, 1992.
- [5] B. Brandenburg. *Scheduling and Locking in Multiprocessor Real-Time Operating Systems*. PhD thesis, Univ. of North Carolina at Chapel Hill, 2011.
- [6] U. Devi and J. Anderson. Tardiness bounds for global EDF scheduling on a multiprocessor. In *26th RTSS*, 2005.
- [7] G. Elliott, N. Kim, J. Erickson, C. Liu, and J. Anderson. Appendix to minimizing response times of automotive dataflows on multicore. <http://cs.unc.edu/~anderson/papers.html>, February 2014.
- [8] J. Erickson and J. Anderson. Reducing tardiness under global scheduling by splitting jobs. In *25th ECRTS*, 2013.
- [9] J. Erickson, J. Anderson, and B. Ward. Fair lateness scheduling: reducing maximum lateness in G-EDF-like scheduling. *Real-Time Sys.*, 50(1), 2014.
- [10] S. Goddard. *On the Management of Latency in the Synthesis of Real-Time Signal Processing Systems from Processing Graphs*. PhD thesis, Univ. of North Carolina, 1998.
- [11] M. Green. “How long does it take to stop?” Methodological analysis of driver perception-brake times. *Transportation Human Factors*, 2(3), 2000.
- [12] C. Hsueh and K. Lin. Scheduling real-time systems with end-to-end timing constraints using the distributed pinwheel model. *IEEE Trans. on Computers*, 50(1), 2001.
- [13] Khronos Group Inc. *OpenMAX IL API Specification*, 2005.
- [14] K. Lakshmanan, S. Kato, and R. Rajkumar. Scheduling parallel real-time tasks on multi-core processors. In *31st RTSS*, 2010.
- [15] E. Lee and G. Messerschmitt. Synchronous data flow. *IEEE Transactions on Computers*, 75(9), 1987.
- [16] H. Leontyev and J. Anderson. Generalized tardiness bounds for global multiprocessor scheduling. In *28th RTSS*, 2007.
- [17] J. Li, K. Agrawal, C. Lu, and C. Gill. Analysis of global EDF for parallel tasks. In *25th ECRTS*, pages 3–13, 2013.
- [18] C. Liu and J. Anderson. Supporting soft real-time DAG-based systems on multiprocessors with no utilization loss. In *31st RTSS*, 2010.
- [19] C. Liu and J. Anderson. Supporting graph-based real-time applications in distributed systems. In *17th RTCSA*, 2011.
- [20] I. Miller, M. Campbell, D. Huttenlocher, F. Kline, A. Nathan, S. Lupashin, J. Catlin, B. Schimpf, P. Moran, N. Zych, et al. Team Cornell’s skynet: Robust perception and planning in an urban environment. *Journal of Field Robotics*, 25(8), 2008.
- [21] A. Saifullah, K. Agrawal, C. Lu, and C. Gill. Multi-core real-time scheduling for generalized parallel task models. In *32nd RTSS*, 2011.
- [22] A. Saifullah, D. Ferry, K. Agrawal, C. Lu, and C. Gill. Real-time scheduling of parallel tasks under a general dag model. Technical Report WUCSE-2012-14, Washington University, St. Louis, USA, 2012.
- [23] L. Sha and S. Sathaye. A systematic approach to designing distributed real-time systems. *Computer*, 26(9), 1993.
- [24] W. Taymans, S. Baker, A. Wingo, R. Bultje, and S. Kost. *GStreamer Application Development Manual (1.2.2)*, 2013.
- [25] C. Urmson, C. Baker, J. Dolan, P. Rybski, B. Salesky, W. Whittaker, D. Ferguson, and M. Darms. Autonomous driving in traffic: Boss and the urban challenge. *AI Mag.*, 30(2), 2009.
- [26] J. Wei, J. Snider, J. Kim, J. Dolan, R. Rajkumar, and B. Litkouhi. Towards a viable autonomous driving research platform. In *Intelligent Vehicles Symposium*, 2013.

A End-to-End Response Time Details

In this appendix, we present theorems and proofs in support of those presented in Sec. 4.

Theorem 2. *Suppose that the tasks in τ can be assigned onto clusters of CPUs such that no individual cluster is overutilized. If Θ is the set of all tasks along the worst-case path from T_i^1 to T_i^j , including both T_i^1 and T_i^j , then any job $T_i^{j,k}$ completes within*

$$\sum_{T_i^\ell \in \Theta} R_i^\ell$$

units of its ideal release.

Proof. We denote the ideal release of $T_i^{j,k}$ as $r_i^{j,k}$ and the actual release of $T_i^{j,k}$ as $d(T_i^{j,k})$.

The theorem can be proved by induction on task depth. As the base case, we consider the source task $T_i^{1,k}$. By our definition of actual releases, $r(T_i^{1,k}) = r_i^{1,k}$. Therefore, by the definition of R_i^j , $T_i^{1,k}$ completes within R_i^j units of $r(T_i^{1,k}) = r_i^{1,k}$, and the theorem holds.

For the induction step, assume that for any $T_i^{q,v}$, where T_i^q is a producer of T_i^j and θ is the set of all tasks along the worst-case path from T_i^1 to T_i^q , including both T_i^1 and T_i^q , and

$$t_f(T_i^{q,v}) - r_i^{q,v} \leq \sum_{T_i^\ell \in \theta} R_i^\ell. \quad (1)$$

We want to prove that

$$t_f(T_i^{j,k}) - r_i^{j,k} \leq \sum_{T_i^\ell \in \Theta} R_i^\ell. \quad (2)$$

We consider three cases.

Case 1: $r(T_i^{j,k}) = r_i^{j,k}$. In this case, the lemma follows by the definition of R_i^j .

Case 2: $r(T_i^{j,k}) = t_f(T_i^{q,v})$ for one of $T_i^{j,k}$'s producers $T_i^{q,v}$. We have

$$\begin{aligned} & t_f(T_i^{j,k}) - r_i^{j,k} \\ &= \{\text{Rearranging}\} \\ & t_f(T_i^{j,k}) - r(T_i^{j,k}) + r(T_i^{j,k}) - r_i^{j,k} \\ &\leq \{\text{By the definition of } R_i^j\} \\ & R_i^j + r(T_i^{j,k}) - r_i^{j,k} \\ &= \{\text{By the case we are considering}\} \\ & R_i^j + t_f(T_i^{q,v}) - r_i^{q,v} \\ &= \{\text{Because } T_i^{q,v} \text{ is a producer of } T_i^{j,k}\} \\ & R_i^j + t_f(T_i^{q,v}) - r_i^{q,v} \\ &\leq \{\text{By (1)}\} \end{aligned}$$

$$\begin{aligned} & R_i^j + \sum_{T_i^\ell \in \theta} R_i^\ell \\ &\leq \{\text{By the definitions of } \theta \text{ and } \Theta\} \\ & \sum_{T_i^\ell \in \Theta} R_i^\ell. \end{aligned}$$

Case 3: $k > 1$ and $r(T_i^{j,k}) = r(T_i^{j,k-1}) + p_i$. We denote as $T_i^{j,w}$ the last job of T_i^j released before $T_i^{j,k}$ such that either $r(T_i^{j,w}) = r_i^{j,w}$ or, for some producer $T_i^{q,v}$ of $T_i^{j,k}$, $r(T_i^{j,w}) = t_f(T_i^{q,v})$. Such a job must exist because $T_i^{j,1}$ must satisfy this condition. By the definition of $T_i^{j,w}$, we have

$$r(T_i^{j,k}) = r(T_i^{j,w}) + (k - w) \cdot p_i. \quad (3)$$

Furthermore, because $T_i^{j,k}$ and $T_i^{j,w}$ are from the same task, and because ideal releases follow the sporadic task model,

$$r_i^{j,k} \geq r_i^{j,w} + (k - w) \cdot p_i. \quad (4)$$

We have

$$\begin{aligned} & t_f(T_i^{j,k}) - r_i^{j,k} \\ &= \{\text{Rearranging}\} \\ & t_f(T_i^{j,k}) - r(T_i^{j,k}) + r(T_i^{j,k}) - r_i^{j,k} \\ &\leq \{\text{By the definition of } R_i^j\} \\ & R_i^j + r(T_i^{j,k}) - r_i^{j,k} \\ &\leq \{\text{By (3) and (4)}\} \\ & R_i^j + r(T_i^{j,w}) + (k - w) \cdot p_i - r_i^{j,w} - (k - w) \cdot p_i \\ &= \{\text{Rearranging}\} \\ & R_i^j + r(T_i^{j,w}) - r_i^{j,w}. \end{aligned} \quad (5)$$

We now consider two subcases, based on the value of $r(T_i^{j,w})$.

Case 3.1: $r(T_i^{j,w}) = r_i^{j,w}$. In this case, we have

$$\begin{aligned} & t_f(T_i^{j,k}) - r_i^{j,k} \\ &= \{\text{By (5)}\} \\ & R_i^j + r(T_i^{j,w}) - r_i^{j,w} \\ &= \{\text{By the case we are considering}\} \\ & R_i^j + r_i^{j,w} - r_i^{j,w} \\ &= \{\text{Rearranging}\} \\ & R_i^j \\ &\leq \sum_{T_i^\ell \in \Theta} R_i^\ell. \end{aligned}$$

Case 3.2: $r(T_i^{j,w}) = t_f(T_i^{q,v})$ for some producer $T_i^{q,v}$ of $T_i^{j,w}$. In this case, we have

$$\begin{aligned} & t_f(T_i^{j,k}) - r_i^{j,k} \\ &= \{\text{By (5)}\} \end{aligned}$$

$$\begin{aligned}
& R_i^j + r(T_i^{j,w}) - r_i^{j,w} \\
&= \{\text{By the case we are considering}\} \\
& R_i^j + t_f(T_i^{q,v}) - r_i^{q,w} \\
&= \{\text{Because } T_i^{q,v} \text{ is a producer of } T_i^{j,w}\} \\
& R_i^j + t_f(T_i^{q,v}) - r_i^{q,v} \\
&\leq \{\text{By (1)}\} \\
& R_i^j + \sum_{T_i^\ell \in \theta} R_i^\ell \\
&\leq \{\text{By the definitions of } \theta \text{ and } \Theta\} \\
& \sum_{T_i^\ell \in \Theta} R_i^\ell.
\end{aligned}$$

□

B End-to-End Response Time Bounds for DAGs with Different Periods

In this appendix, we present theorems and proofs for end-to-end response-time bounds for sporadic DAGs graphs where nodes may have different periods. Although nodes may have different periods, we assume that the source and sink node share a common period (the meaning of an end-to-end response time bound is ambiguous, otherwise).

B.1 Additional Notation

We adapt analysis for rate-based DAGs for analysis of sporadic DAGs. We require additional notation to describe rate-based a DAG. Unless stated otherwise, the same notation and graph restrictions from Sec. 3 are assumed.

A *DAG-based RB task system* is comprised of a set $\tau^{RB} = \{T_1, T_2, \dots, T_n\}$ of n independent DAG-based RB tasks. Each RB task T_i^j is specified by four parameters: $(x_i^j, y_i^j, d_i^j, e_i^j)$. The pair (x_i^j, y_i^j) represents the maximum execution rate of T_i^j : x_i^j is the maximum number of invocations of the task in any interval $[t \cdot y_i^j, (t+1) \cdot y_i^j)$ ($t \geq 0$) of length y_i^j ; such an invocation is called a *job* of the task. x_i^j and y_i^j are assumed to be non-negative integers. Additionally, d_i^j is the task's relative deadline. The *utilization* of each RB task T_i^j in T_i , denoted u_i^j , is $e_i^j \cdot \frac{x_i^j}{y_i^j}$. The *utilization of the task system* τ^{RB} is $U_{sum}(\tau^{RB}) = \sum_{T_i \in \tau^{RB}} \sum_{T_i^j \in T_i} u_i^j$. We denote the depth of a node in a DAG (as defined in Sec. 3) with the parameter K_i^j .

The release time of the k^{th} job of T_i^j is at time $r^{RB}(T_i^{j,k})$ and has a deadline at time $d^{RB}(T_i^{j,k})$. For any job $T_i^{j,k}$, $d^{RB}(T_i^{j,k}) = r^{RB}(T_i^{j,k}) + d_i^j$. Because RB tasks may execute at different rates, and their job release times are not specifically defined (only maximum rates are specified). However, as shown in [10], job precedence constraints can be explicitly determined from PGM graph descriptions.

Finally, observe that a rate-base DAG is a sporadic DAG

iff $x_i^j = 1$ for all tasks. In this case, y_i^j becomes equivalent to p_i , the minimum separation time between a task's jobs under the sporadic task model.

B.2 Response Time Bounds

We now derive bounds for DAGs with nodes of different periods.

Theorem 3. [18] *In any G-EDF schedule for the sporadic task system τ on m processors, if $U_{sum}(\tau) \leq m$, then the response time of any job $T_i^{j,k}$, with respect to its delayed release $r(T_i^{j,k})$, is at most Δ_i^j , where Δ_i^j is an expression depending on system parameters specified in [18], i.e.,*

$$t_f(T_i^{j,k}) - r(T_i^{j,k}) \leq \Delta_i^j + y_i^j/x_i^j, \quad (6)$$

$$\text{where } \Delta_i^j = \frac{\sum_{m-1 \text{ largest } e_i} e_i - \min_{T_i \in \tau} e_i}{m - \sum_{m-2 \text{ largest } u_i} u_i}.$$

As discussed in Sec. 4, the above holds for any window-constrained scheduler, though the derivation for Δ_i^j may change. Theorem 3 only gives a response time bound for any job $T_i^{j,k}$ with respect to its delayed release, $r(T_i^{j,k})$. $T_i^{j,k}$ can have greater response time with respect to its original release, $r^{RB}(T_i^{j,k})$. Therefore, we must bound the actual response time any job $T_i^{j,k}$ may experience with respect to its original release. The following theorem [18] gives such a bound. Let $y_i^{max} = \max(y_i^1, y_i^2, \dots, y_i^{z_i})$.

Def. 1. Let λ_i^j denote the set of tasks that form the simple path with the largest weight connecting the source task of T_i and T_i^j . Any edge connecting nodes T_i^j and T_i^k has a weight $W_i^{j,k}$ equal to the response time bound of T_i^j w.r.t. its redefined release time. Let L_i^j denote the *number* of tasks in λ_i^j .

Theorem 4. [18] *In any G-EDF schedule for τ^{RB} on m processors, if $U_{sum}(\tau^{RB}) \leq m$, then the response time of any job $T_i^{j,k}$ of a task T_i^j , with respect to its original release, $r^{RB}(T_i^{j,k})$, is:*

$$\begin{aligned}
& t_f(T_i^{j,k}) - r^{RB}(T_i^{j,k}) \\
& \leq \sum_{T_i^\ell \in \lambda_i^j} \Delta_i^\ell + 3 \cdot L_i^k \cdot y_i^{max} + y_i^j/x_i^j, \quad (7)
\end{aligned}$$

where Δ_i^ℓ denotes the response time bound of T_i^ℓ w.r.t. its redefined release time.

Def. 2. The end-to-end response time bound of a DAG T_i is given by $\max_k \left(f(T_i^{z_i,k}) - r^{RB}(T_i^{1,k}) \right)$, where $f(T_i^{z_i,k})$

denotes the completion time of $T_i^{z_i,k}$ (i.e., the k^{th} job of the sink task of T_i). This end-to-end response time bound represents the maximum duration from the release time of any job $T_i^{1,k}$ to the completion of the corresponding job of $T_i^{z_i,k}$. Since we assume that source and sink share a common period, any job $T_i^{z_i,k}$ is triggered (transitively speaking) due to the completion of job $T_i^{1,k}$.

Theorem 5. In any window-constrained schedule for τ on m processors, if $U_{sum}(\tau) \leq m$, then the end-to-end response time of any DAG T_i , denoted R_i , is at most

$$\sum_{T_i^\ell \in \lambda_i^{z_i}} \Delta_i^\ell + 4 \cdot L_i^{z_i} \cdot y_i^{max}, \quad (8)$$

where Δ_i^ℓ denotes the response time bound of T_i^ℓ w.r.t. its redefined release time.

Proof. This theorem directly follows from Theorem 4.

$$\begin{aligned} R_i &= \max_k \left(f(T_i^{z_i, k}) - r^{RB}(T_i^{1, k}) \right) \\ &\leq \max_k \left(f(T_i^{z_i, k}) - r^{RB}(T_i^{z_i, k}) \right) + (L_i^{z_i} - 1) \cdot y_i^{max} \\ &\quad \{ \text{By Theorem 4} \} \\ &= \left(\sum_{T_i^\ell \in \lambda_i^{z_i}} \Delta_i^\ell + 3 \cdot L_i^{z_i} \cdot y_i^{max} + y_i^{z_i} / x_i^{z_i} \right) \\ &\quad + ((L_i^{z_i} - 1) \cdot y_i^{max}) \\ &\quad \{ \text{Apply } x_i^{z_i} = 1, \text{ expand, and rearrange} \} \\ &= \sum_{T_i^\ell \in \lambda_i^{z_i}} \Delta_i^\ell + 3 \cdot L_i^{z_i} \cdot y_i^{max} + L_i^{z_i} \cdot y_i^{max} \\ &\quad + (y_i^{z_i} - y_i^{max}) \\ &\leq \sum_{T_i^\ell \in \lambda_i^{z_i}} \Delta_i^\ell + 4 \cdot L_i^{z_i} \cdot y_i^{max}. \end{aligned}$$

□

C PGM^{RT} Implementation Details

We provide additional details on the implementation of PGM^{RT} in this appendix—namely, the available interprocess communication mechanisms and the PGM^{RT} API. An overview of PGM^{RT}'s basic features can be found in Sec. 6.

C.1 IPC Mechanisms

Consumers block (suspend execution) whenever they lack the requisite tokens. Producers must have a mechanism to signal consumers of new tokens. The appropriate underlying interprocess communication (IPC) mechanism depends upon how tokens are used: tokens may be *event-signaling* or *data-passing*. Regardless of the underlying IPC, nodes produce and consume tokens using a common API.

With event-signaling tokens, token production and consumption is realized through increment/decrement operations on per-edge token counters, similar to counting semaphores. Although these tokens do not transmit data implicitly, tokens can coordinate data sharing in application-level logic. For example, a token may signal the availability of new data in an out-of-band queue (i.e., a data structure outside the purview of PGM^{RT}) shared between two nodes. Signaling is achieved via a monitor synchronization primi-

tive; specifically, a POSIX (pthread) condition variable, one per consumer. A consumer blocks on its condition variable if it does not have requisite tokens on every edge. A producer signals the condition variable whenever it is the last producer to satisfy all of its consumer's token constraints.

The use of pthread condition variables has the drawback in that threads that utilize the synchronization primitive must first acquire a pthread mutex. This suspension-based mutex can be problematic in a real-time setting. First, it can introduce heavy overheads, due to context switching, with respect to very short critical sections in PGM^{RT}. Such overheads may be pessimistically accounted for in real-time analysis. Second, suspensions are difficult to model under some methods of real-time analysis (e.g., “suspension-oblivious” analysis [5]). Finally, an operating system may offer little or no support for real-time priority inheritance for pthread mutexes. As an alternative to pthread-based monitor, PGM^{RT} also offers a FIFO-ordered spinlock-based monitor built upon Linux's “fast userspace mutex.” Its use can eliminate costly context switches and problematic suspensions. Furthermore, the duration of priority inversions are bounded since spinning tasks wait non-preemptively. On non-LITMUS^{RT} platforms, non-preemptive waiting is achieved by disabling CPU interrupts from the userspace (e.g., `sti/cli/pushf/popf` instructions on x86 processors). On LITMUS^{RT}, PGM^{RT} utilizes LITMUS^{RT}'s special support for non-preemptive code sections.

With data-passing tokens, each byte-sized token is interpreted as a byte of data. Byte-ordering is preserved through FIFO-ordered token consumption. PGM^{RT} supports data-passing through either named pipes (FIFOs), message queues (MQs), and stream sockets (e.g., TCP)—all IPCs are POSIX-standard. We classify these mechanisms collectively as IPC channels. One channel is created for each edge. Consumers block on the set of channels, represented as a list of file descriptors, from each inbound edge using `select()`.⁵ The operating system wakes the consumer whenever data arrives on a previously empty channel. Consumers `read()/recv()` tokens from the channel once tokens are available on all edges. Under PGM^{RT}, all read/write operations are non-blocking in order to avoid excessive thread suspensions. Under non-blocking writes, producers continually write data from within a loop until all data has been written. Consumers similarly loop while reading. As a fallback, consumers suspend through `select()` if inbound data is exhausted before the requisite number of bytes have been read. Due to the general lack of introspective capabilities with the above IPC mechanisms (specifically, the inability to query the IPC channel regarding the amount of available data), PGM consumer thresholds greater than the number of tokens consumed per node invocation are not easily supported. However, PGM^{RT} offers a solution to this problem that we discuss next.

The use of `select()` for data-passing tokens can introduce additional thread suspensions since `select()` wakes a blocked thread when data becomes available on any *one*

⁵The use of `select()` with MQs is not strictly POSIX-compliant, but such use is commonly supported.

channel. Thus, a consumer waiting for data on all inbound edges must loop on `select()` until data arrives on all inbound edges.⁶ To avoid this, PGM^{RT} offers “fast” variants of FIFO- and MQ-based channels, where the underlying channel IPC is *wrapped* with event-signaling tokens. Here, the availability of data is tracked by event-signaling tokens, with each token corresponding to one byte of data. As with plain event-signaling tokens, consumers block on a monitor, and are awoken by the last producer to satisfy all token constraints. Producers only transmit event-signaling tokens after they have written the produced data to the associated channel. Thus, consumers using the fast channels avoid repeated suspensions while looping on `select()`. Moreover, support for PGM consumer thresholds greater than the number of tokens consumed per node invocation is made trivial by event-signaling token counters. Thus, the fast channel variants also support PGM’s consumer thresholds. There is one limitation to using event-signaling tokens in this context: a reliance upon shared memory. As a result, PGM^{RT} does not offer a fast variant of stream socket channels, since producers and consumers connected by these channels are expected to reside on different computers in a distributed system.

C.2 The PGM^{RT} API

Regardless of the underlying IPC mechanism, PGM^{RT} provides a unified API (in the C language) for the creation of graphs, nodes, and edges, and the production and consumption of tokens and the passing of data.

Graph management. The PGM^{RT} runtime is initialized by a call to `pgm_init()`. Graphs are created by `pgm_init_graph()`. Mirroring the design pattern used by named FIFOs and POSIX message queues, graphs are uniquely identified by a path and name. `pgm_init_node()` is called to add a named node to a given graph. Similarly, `pgm_init_edge()` is also used to add a named edge, connecting two nodes within the same graph. The token constraints and edge type (i.e., event-signaling or specified type of a data-passing edge) are provided to `pgm_init_edge()` by the user.

All graph meta-data (e.g., graph structure, nodes, token constraints, edge types, etc.) are stored in a memory-mapped file. Graphs that have a common path share the same file. Because the meta-data file is memory-mapped, different processes can coordinate, delegating different nodes of the same graph to different processes. That is, a single graph may be executed by multiple processes. Processes and threads claim exclusive ownership over a node by calling `pgm_claim_node()`. If the particular node claimed is unimportant, then `pgm_claim_any_node()` may be called to claim a single available node. A claimed node cannot be claimed by any other process or thread until the owner has released the node with a call to `pgm_release_node()`. PGM^{RT} provides many APIs for querying the properties of graphs, nodes, and edges. This includes APIs for obtaining the inbound or outbound degree of

⁶Operating system modifications to support an “all-or-nothing” variant of `select()` could be used to address this issue.

a node, lists of node predecessors or successors, lists of inbound or outbound edges, edge token constraints, and edge type.

Graph execution. It is expected that one thread of execution claims one node from a graph. Threads wait for tokens to arrive for a specified node by calling `pgm_wait()`. The calling thread will block until all token constraints have been satisfied. Once `pgm_wait()` returns, data received through data-passing edges is available in per-edge data buffers. A consumer can obtain a pointer to each buffer by calling `pgm_get_edge_buf_c()`, which returns a `void*`. The buffer is appropriately sized (in terms of bytes) to match the number tokens the consumer consumes on each invocation. For data-passing edges, producers write data to per-edge data buffers. A producer can obtain a pointer to each buffer by calling `pgm_get_edge_buf_p()`, which also returns a `void*`. This buffer is also appropriately sized to match the number of tokens the producer produces on each invocation. Producers may write to these buffers as necessary during their execution. A thread calls `pgm_complete()` to signal the completion of a node invocation. At this point, `pgm_complete()` pushes (writes) any data stored in data-passing edge buffers over the associated data-passing IPC. `pgm_complete()` also generates the appropriate tokens for event-signaling edges, and wakes up any consumers for which the producer was the first to satisfy the consumer’s token constraints across all of the consumer’s inbound edges.

More on edge buffers. Edge buffer pointers remain unchanged unless the user explicitly assigns a new buffer. That is, buffers are reused each node invocation. Thus, a thread does *not* need to call `pgm_get_edge_buf_c()` or `pgm_get_edge_buf_p()` each time it consumes or produces data. However, a thread can allocate additional appropriately sized buffers by calling `pgm_malloc_edge_buf_c()` or `pgm_malloc_edge_buf_p()` for consumer and producer buffers, respectively. Buffers allocated by `pgm_malloc_edge_buf_c()` and `pgm_malloc_edge_buf_p()` are initially in an unassigned state in that they are not currently used by a particular edge. These buffers can be later assigned to an edge by calling `pgm_swap_edge_buf_c()` or `pgm_swap_edge_buf_p()`, to swap an unassigned buffer with the current consumer or producer buffer, respectively. These functions return the previously assigned buffer, which is now in an unassigned state. Buffers may also be swapped between edges by calling `pgm_swap_edge_bufs()`. This function is particularly useful when a thread needs to pass consumed data directly to one of its own consumers since this avoids memory copies. A thread is responsible for freeing the memory any unassigned buffers by calling `pgm_free()` when the buffer is no longer needed.

Graph termination. The termination of graph execution is realized by calling `pgm_terminate()` from each graph source node. The command to terminate is automatically propagated from node to node. However, PGM^{RT} only propagates the termination command to a node after that node has exhausted all tokens that it

can feasibly consume (any remaining tokens are discarded). A thread is notified of termination by the return code of `pgm_wait()`. Upon termination, a thread is responsible for freeing any unassigned buffers and calling `pgm_release_node()`. A graph is completely destroyed with a call to `pgm_destroy_graph()`. Finally, the entire PGM^{RT} runtime is torn down with a call to `pgm_destroy()`.

Real-time OS integration. Although PGM^{RT} has been explicitly designed with techniques that are friendly to real-time scheduling and analysis (e.g., non-preemption and non-blocking reads and writes), PGM^{RT} does not directly manage real-time priorities, since the mechanisms for controlling priorities may change from scheduler to scheduler and operating system to operating system. Thus, it is the responsibility of the thread to establish its scheduling priority.⁷ Under a fixed-priority scheduler, such as POSIX's SCHED_FIFO, a thread's priority is set during initialization. However, under LITMUS^{RT} with deadline-based scheduling, additional coordination is necessary. Here, a thread notifies LITMUS^{RT} that it is about to wait for tokens immediately before calling `pgm_wait()`. Based on this notification, LITMUS^{RT} assigns the appropriate priority (deadline) if and when the thread wakes from a suspension. This thread notifies LITMUS^{RT} that it has acquired all of its tokens immediately after `pgm_wait()` returns, preventing LITMUS^{RT} from reassessing the thread's priority in the future.

This completes our description of PGM^{RT} and its API. The code for PGM^{RT} may be found at www.github.com/GElliott/pgm or www.litmus-rt.org.

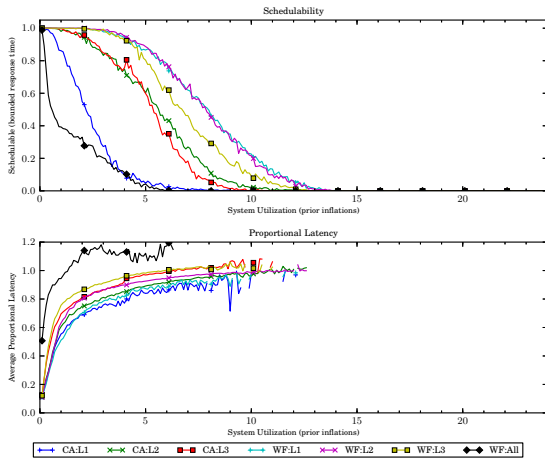
⁷Because PGM^{RT} is not strictly bound to a real-time operating system, it can also be used under a general (non-real-time) operating system scheduler.

D Extended Schedulability Experiment

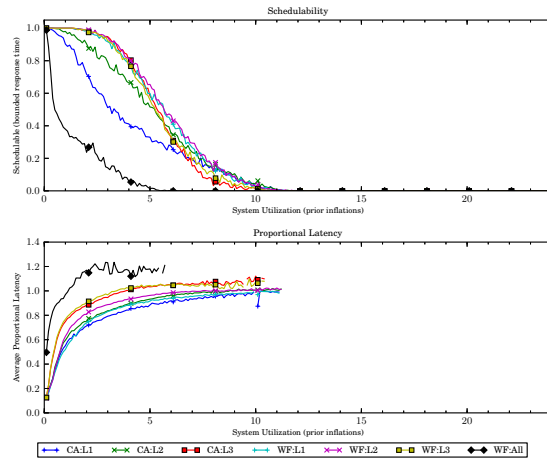
In this appendix, we present all schedulability results for the experiments described in Sec. 7. The left-hand column in the following pages show schedulability and proportional end-to-end latencies for experiments where non-cache-polluter overheads are assumed. The corresponding right-hand column depicts results for the same schedulability experiment parameters, but under cache-polluter overheads. Cache polluter overheads have little effect on schedulability in experiments with light and medium per-task utilizations and small edge working set sizes (EWSSs). Fig. 30 illustrates one such case. Cache polluter overheads have a stronger effect in experiments with heavy per-task utilizations or large EWSSs. Fig. 339 depicts an example of this scenario.

In general, the most interesting results are those of experiments with bimodal distributions for EWSSs. Not only do cache polluter overheads generally have a stronger effect, but interesting differences among cluster configurations emerge. This can be observed in Fig. 259b, where per-task utilizations are heavy and EWSSs are bimodal. Here, cache-aware L1 and L2 clustering generally offers better schedulability for task sets with utilizations less than 17.0. However, cache-aware L3 clustering can still schedule about 30% of task sets with utilizations of 20.0, whereas cache-aware L1 and L2 clustering can schedule no more than 5% of task sets with this utilization.

Finally, we found that graph depth had little effect on *proportional* end-to-end latency.

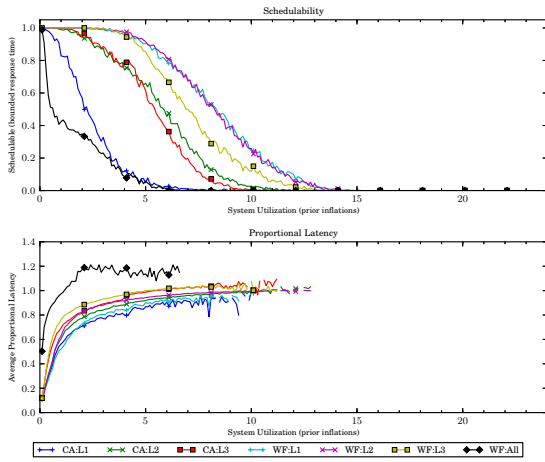


(a) Without polluter overheads.

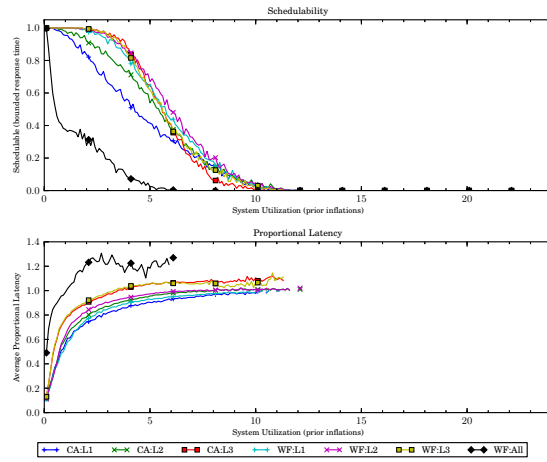


(b) With polluter overheads.

Figure 9: Results for *uni-light* per-task utilization, *uni-short* period, *light-weight* EWSS, and *uni-short* height factor.

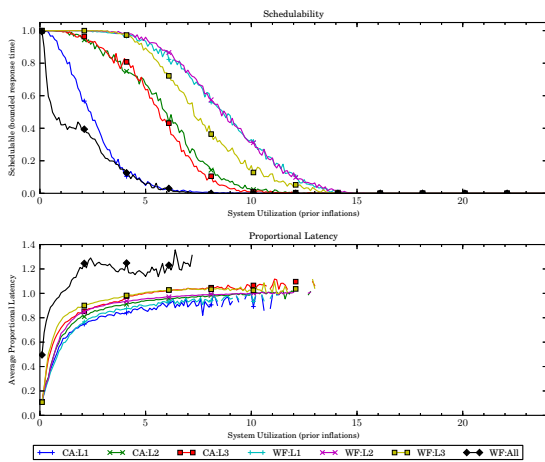


(a) Without polluter overheads.

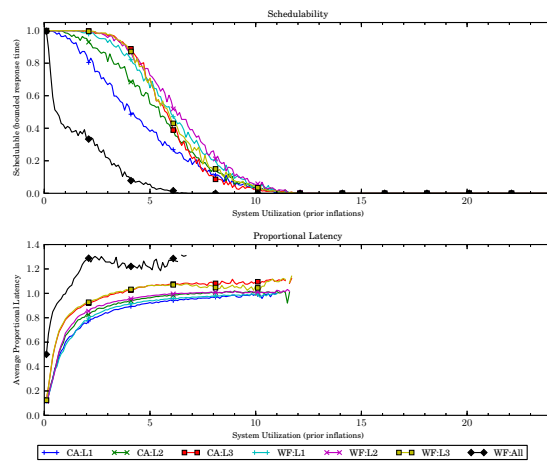


(b) With polluter overheads.

Figure 10: Results for *uni-light* per-task utilization, *uni-short* period, *light-weight* EWSS, and *uni-medium* height factor.

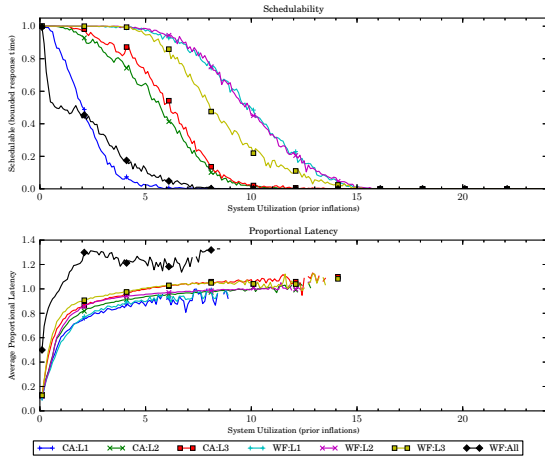


(a) Without polluter overheads.

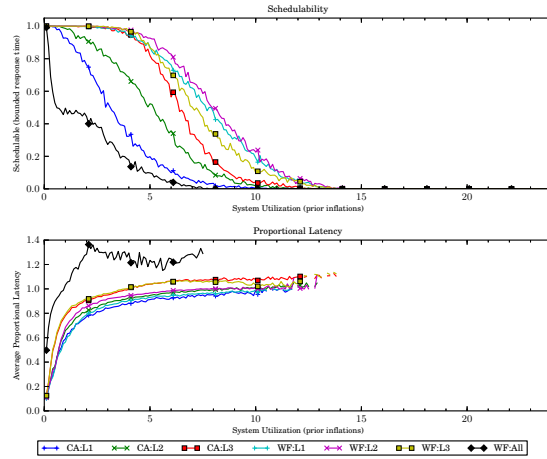


(b) With polluter overheads.

Figure 11: Results for *uni-light* per-task utilization, *uni-short* period, *light-weight* EWSS, and *uni-tall* height factor.

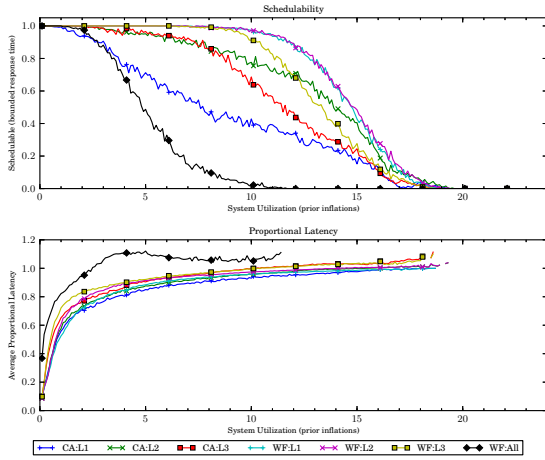


(a) Without polluter overheads.

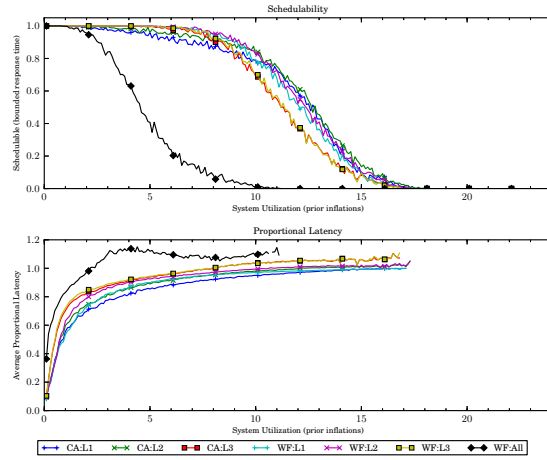


(b) With polluter overheads.

Figure 12: Results for *uni-light* per-task utilization, *uni-short* period, *light-weight* EWSS, and *pipeline* height factor.

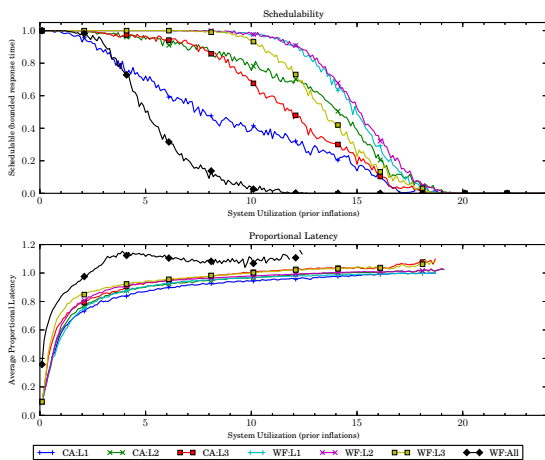


(a) Without polluter overheads.

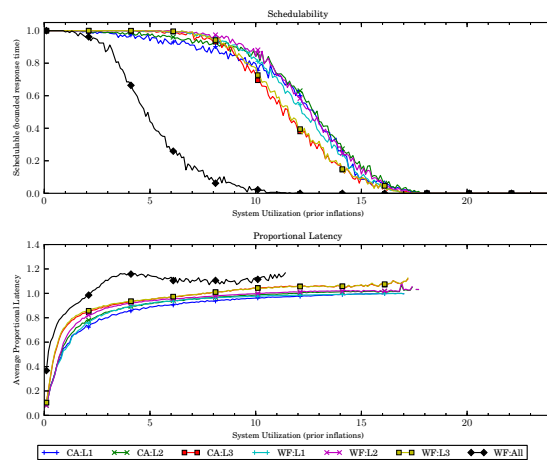


(b) With polluter overheads.

Figure 13: Results for *uni-light* per-task utilization, *uni-moderate* period, *light-weight* EWSS, and *uni-short* height factor.

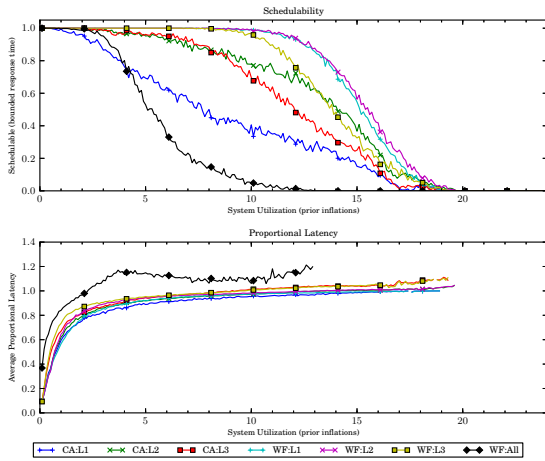


(a) Without polluter overheads.

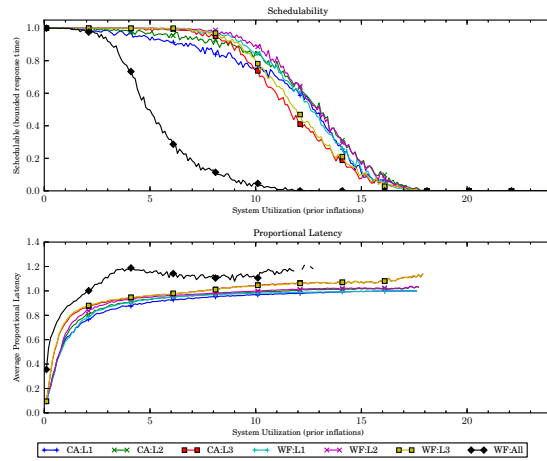


(b) With polluter overheads.

Figure 14: Results for *uni-light* per-task utilization, *uni-moderate* period, *light-weight* EWSS, and *uni-medium* height factor.

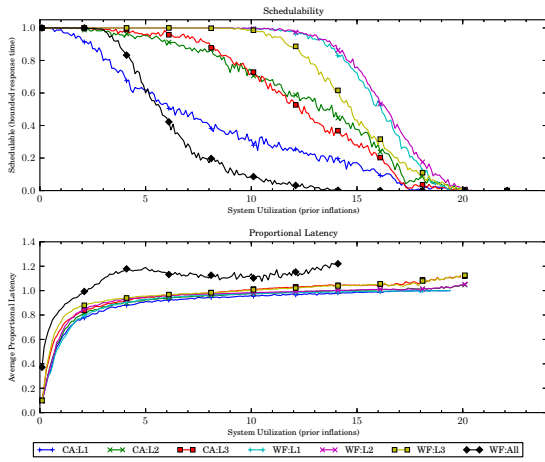


(a) Without polluter overheads.

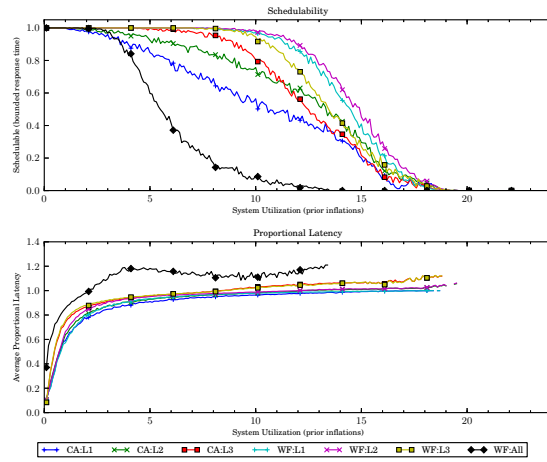


(b) With polluter overheads.

Figure 15: Results for *uni-light* per-task utilization, *uni-moderate* period, *light-weight* EWSS, and *uni-tall* height factor.

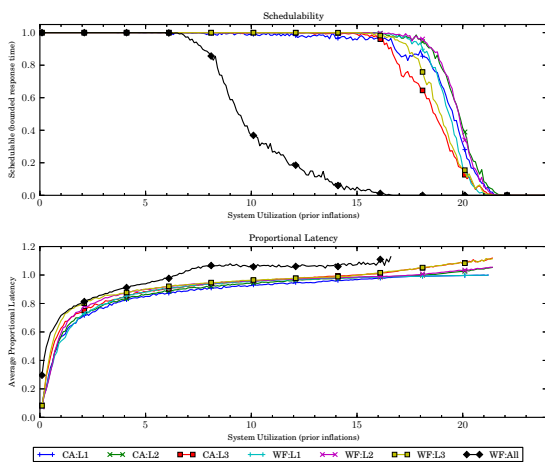


(a) Without polluter overheads.

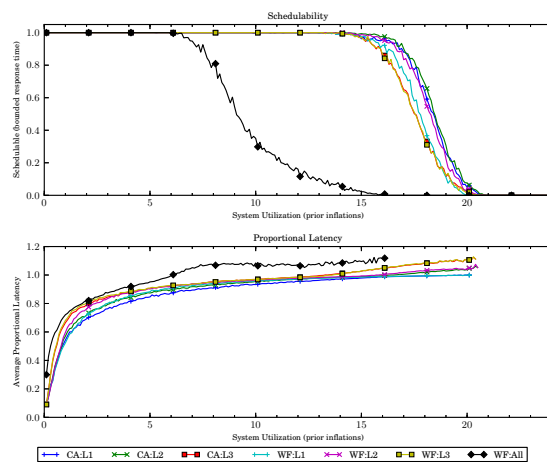


(b) With polluter overheads.

Figure 16: Results for *uni-light* per-task utilization, *uni-moderate* period, *light-weight* EWSS, and *pipeline* height factor.

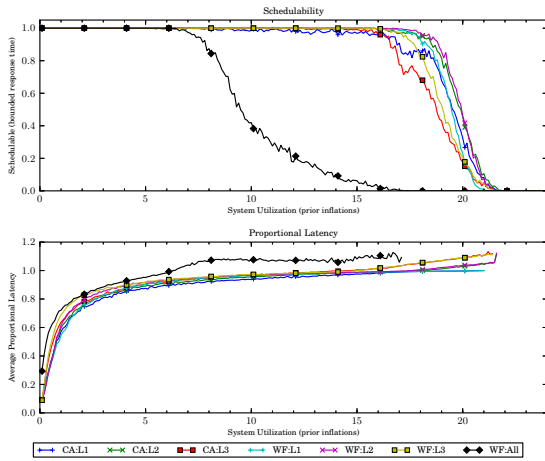


(a) Without polluter overheads.

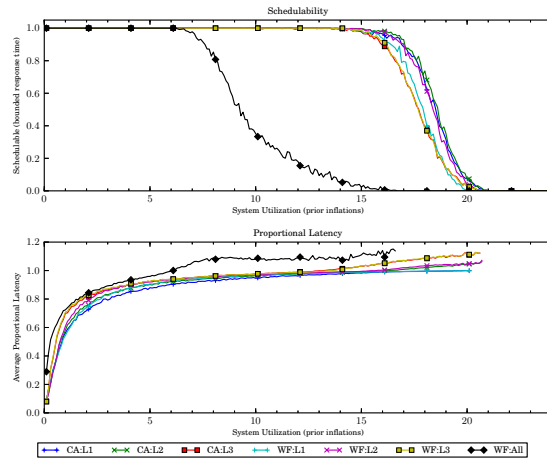


(b) With polluter overheads.

Figure 17: Results for *uni-light* per-task utilization, *uni-long* period, *light-weight* EWSS, and *uni-short* height factor.

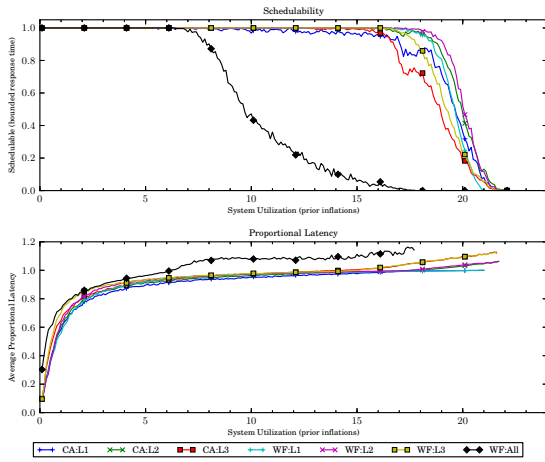


(a) Without polluter overheads.

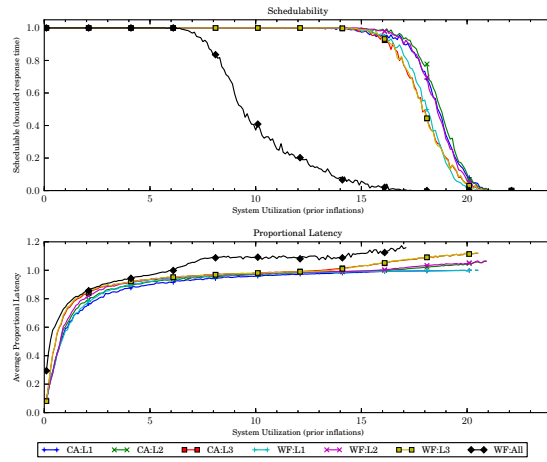


(b) With polluter overheads.

Figure 18: Results for *uni-light* per-task utilization, *uni-long* period, *light-weight* EWSS, and *uni-medium* height factor.

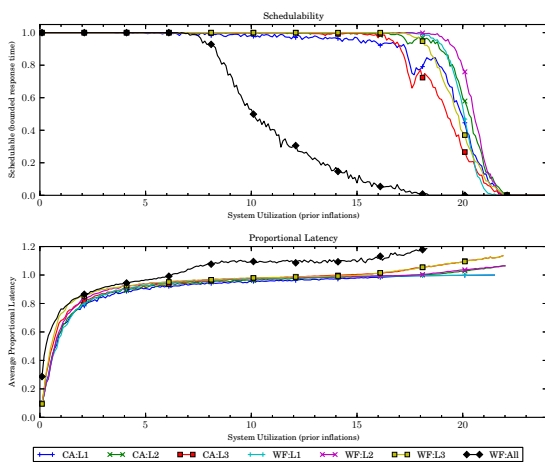


(a) Without polluter overheads.

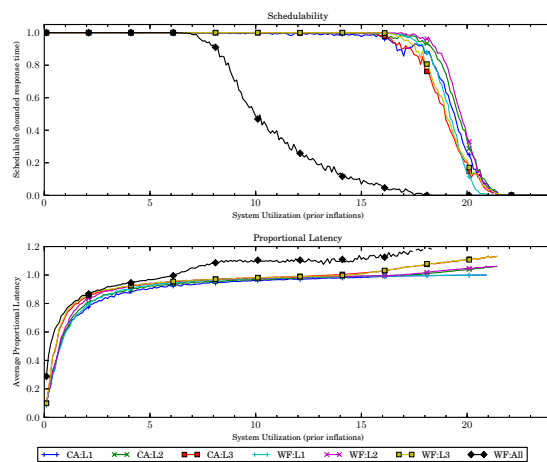


(b) With polluter overheads.

Figure 19: Results for *uni-light* per-task utilization, *uni-long* period, *light-weight* EWSS, and *uni-tall* height factor.

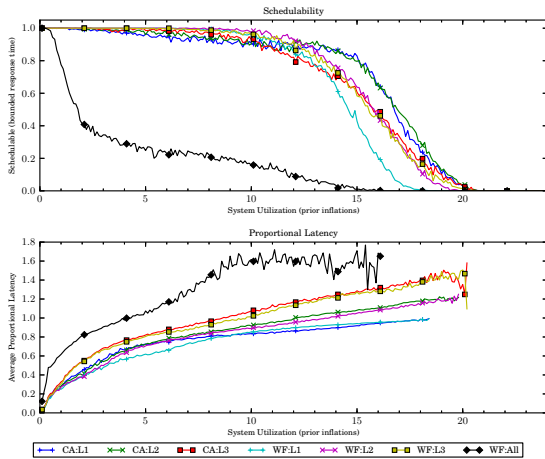


(a) Without polluter overheads.

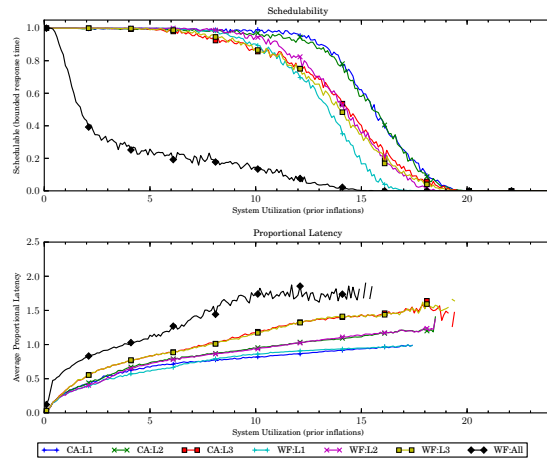


(b) With polluter overheads.

Figure 20: Results for *uni-light* per-task utilization, *uni-long* period, *light-weight* EWSS, and *pipeline* height factor.

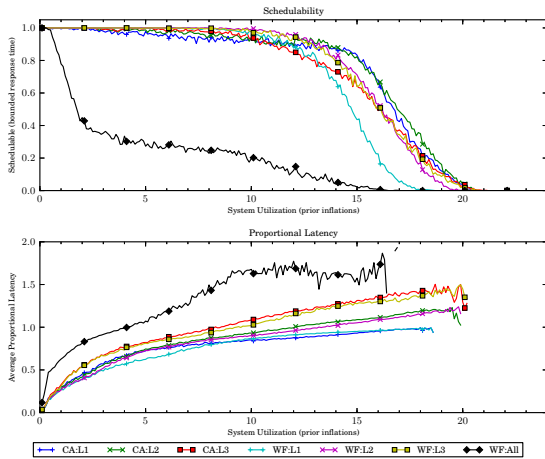


(a) Without polluter overheads.

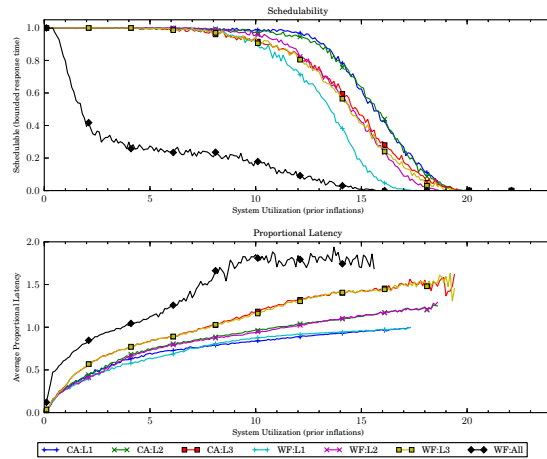


(b) With polluter overheads.

Figure 21: Results for *uni-medium* per-task utilization, *uni-short* period, *light-weight* EWSS, and *uni-short* height factor.

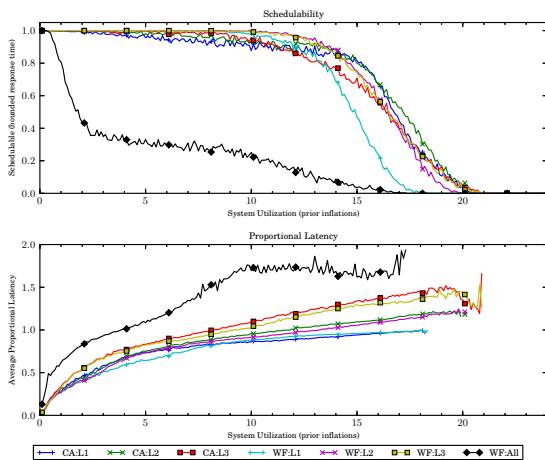


(a) Without polluter overheads.

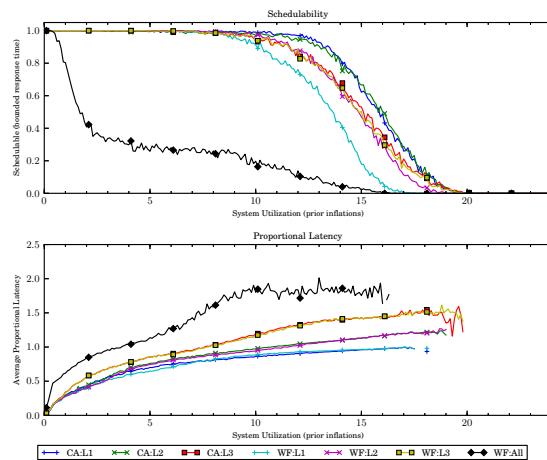


(b) With polluter overheads.

Figure 22: Results for *uni-medium* per-task utilization, *uni-short* period, *light-weight* EWSS, and *uni-medium* height factor.

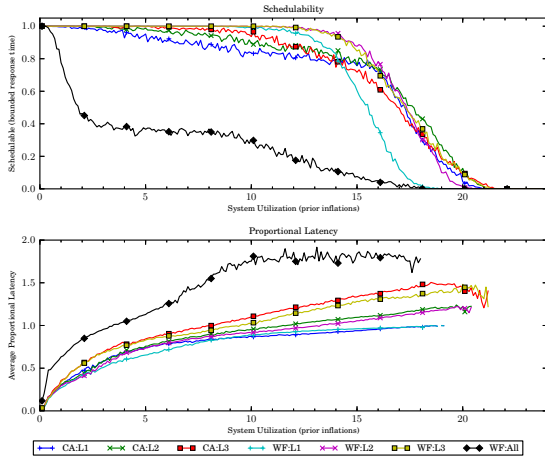


(a) Without polluter overheads.

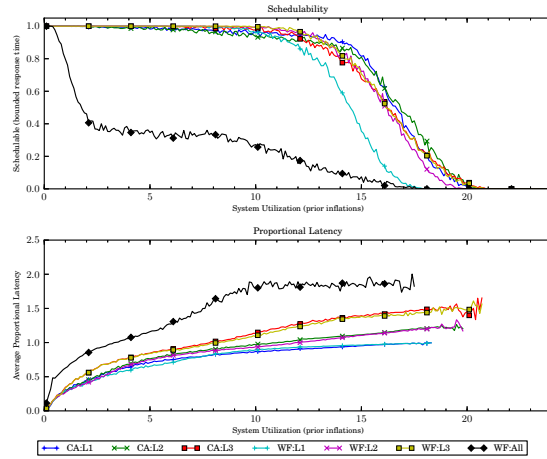


(b) With polluter overheads.

Figure 23: Results for *uni-medium* per-task utilization, *uni-short* period, *light-weight* EWSS, and *uni-tall* height factor.

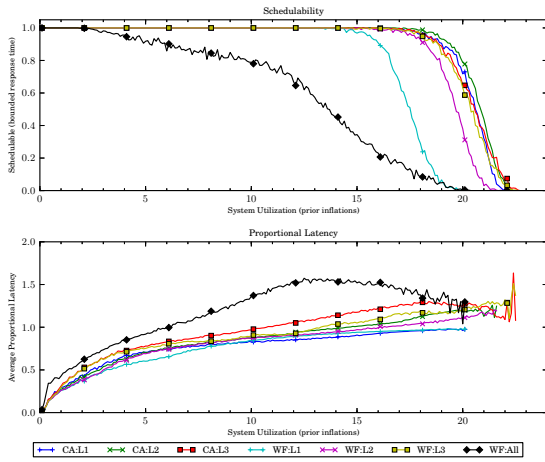


(a) Without polluter overheads.

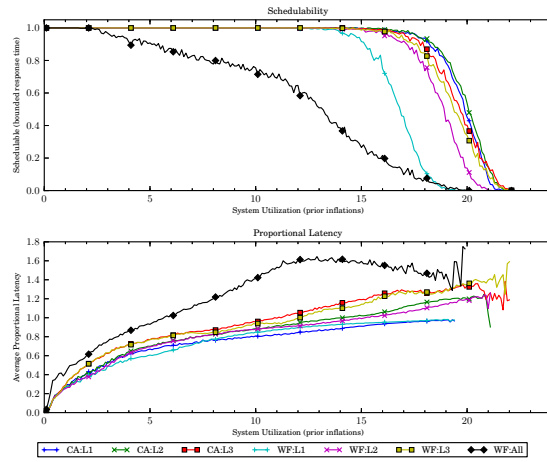


(b) With polluter overheads.

Figure 24: Results for *uni-medium* per-task utilization, *uni-short* period, *light-weight* EWSS, and *pipeline* height factor.

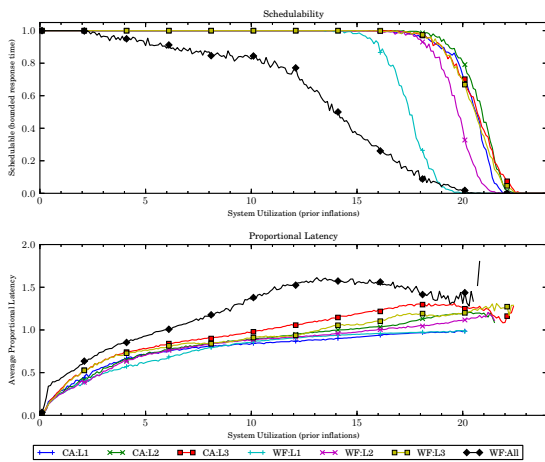


(a) Without polluter overheads.

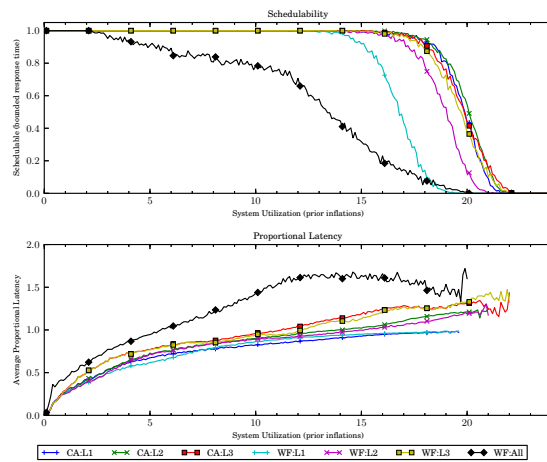


(b) With polluter overheads.

Figure 25: Results for *uni-medium* per-task utilization, *uni-moderate* period, *light-weight* EWSS, and *uni-short* height factor.

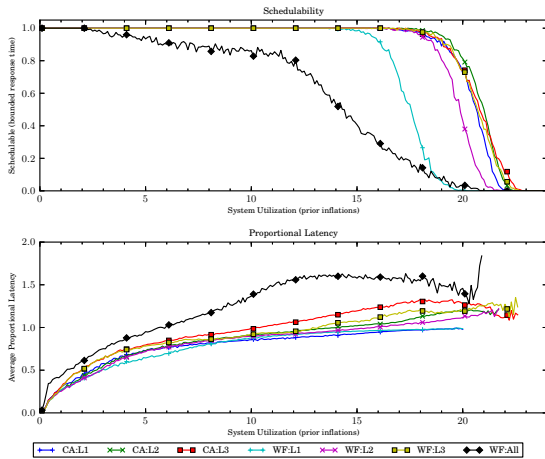


(a) Without polluter overheads.

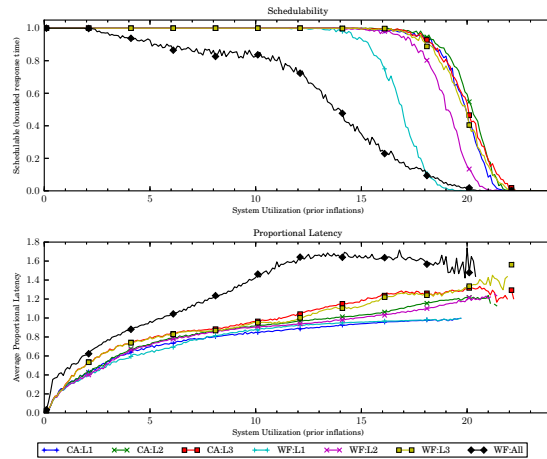


(b) With polluter overheads.

Figure 26: Results for *uni-medium* per-task utilization, *uni-moderate* period, *light-weight* EWSS, and *uni-medium* height factor.

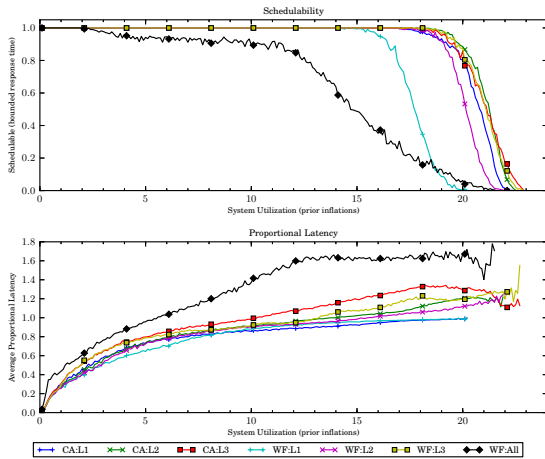


(a) Without polluter overheads.

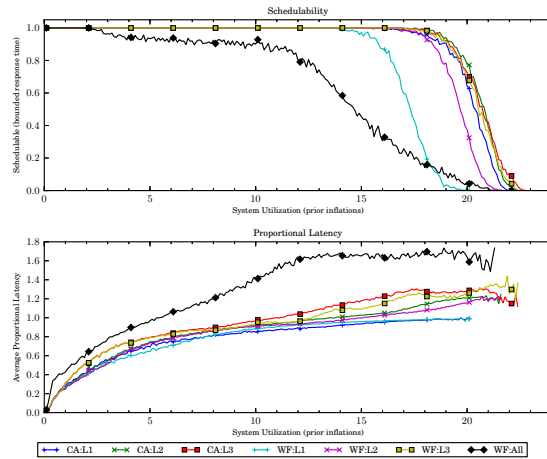


(b) With polluter overheads.

Figure 27: Results for *uni-medium* per-task utilization, *uni-moderate* period, *light-weight* EWSS, and *uni-tall* height factor.

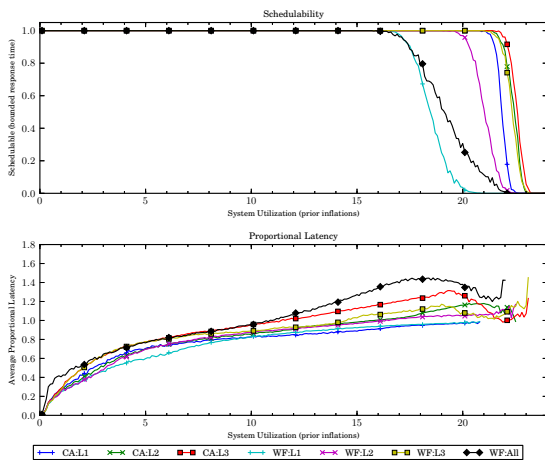


(a) Without polluter overheads.

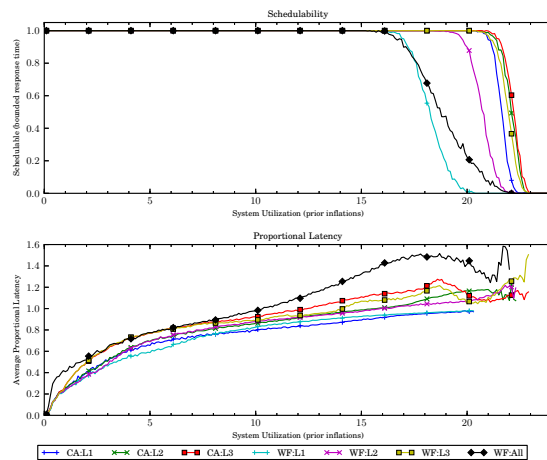


(b) With polluter overheads.

Figure 28: Results for *uni-medium* per-task utilization, *uni-moderate* period, *light-weight* EWSS, and *pipeline* height factor.

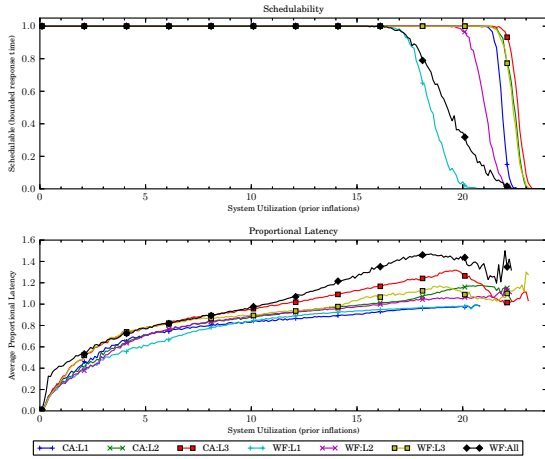


(a) Without polluter overheads.

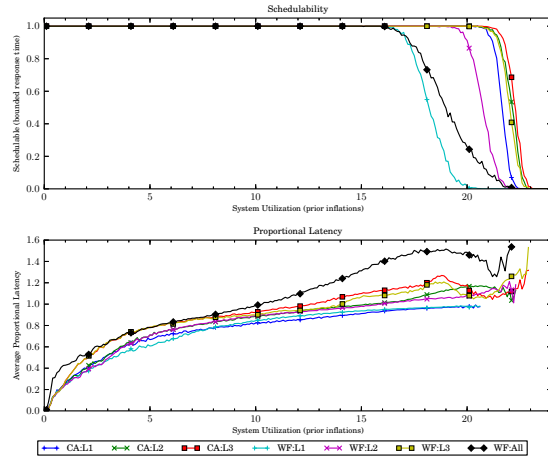


(b) With polluter overheads.

Figure 29: Results for *uni-medium* per-task utilization, *uni-long* period, *light-weight* EWSS, and *uni-short* height factor.

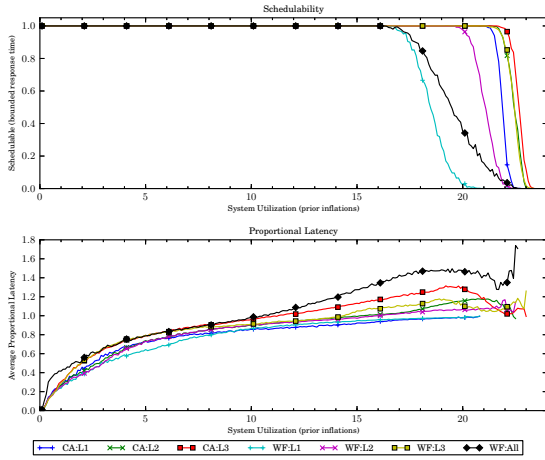


(a) Without polluter overheads.

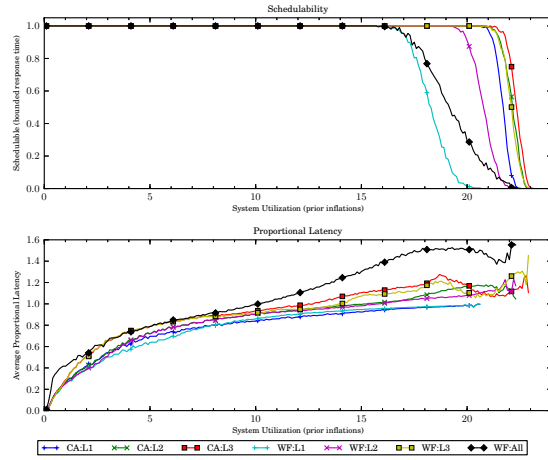


(b) With polluter overheads.

Figure 30: Results for *uni-medium* per-task utilization, *uni-long* period, *light-weight* EWSS, and *uni-medium* height factor.

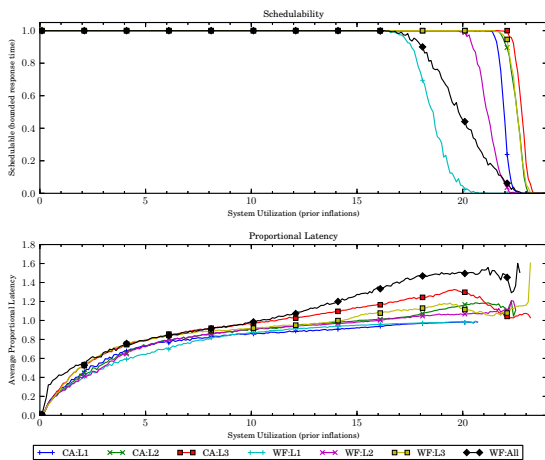


(a) Without polluter overheads.

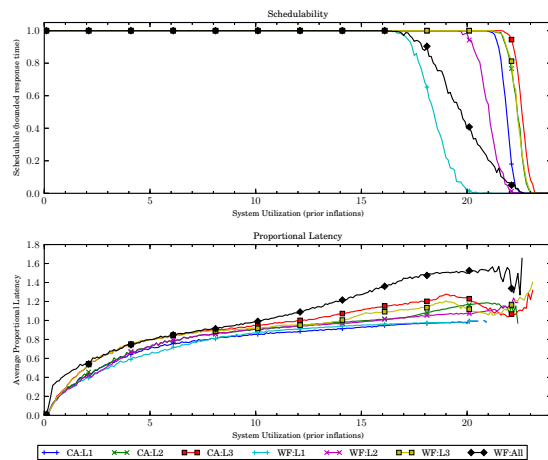


(b) With polluter overheads.

Figure 31: Results for *uni-medium* per-task utilization, *uni-long* period, *light-weight* EWSS, and *uni-tall* height factor.

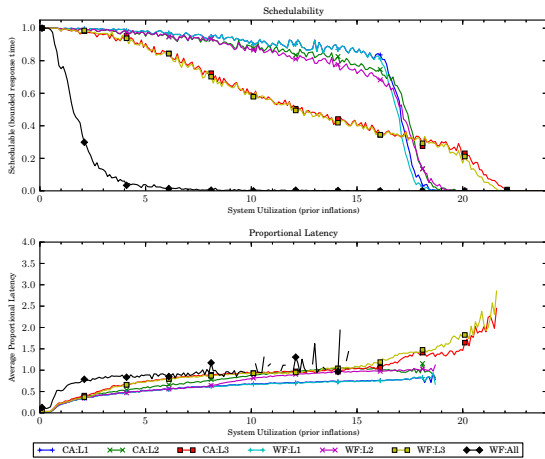


(a) Without polluter overheads.

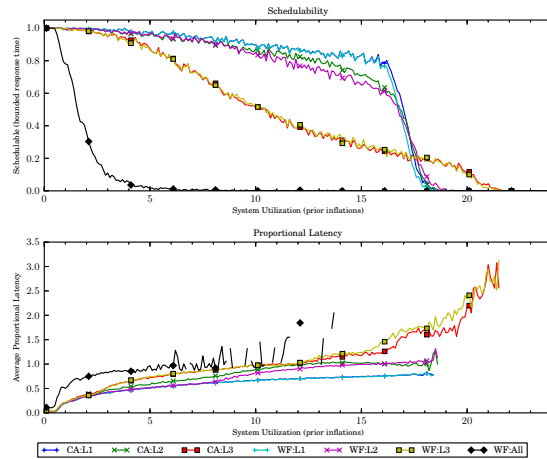


(b) With polluter overheads.

Figure 32: Results for *uni-medium* per-task utilization, *uni-long* period, *light-weight* EWSS, and *pipeline* height factor.

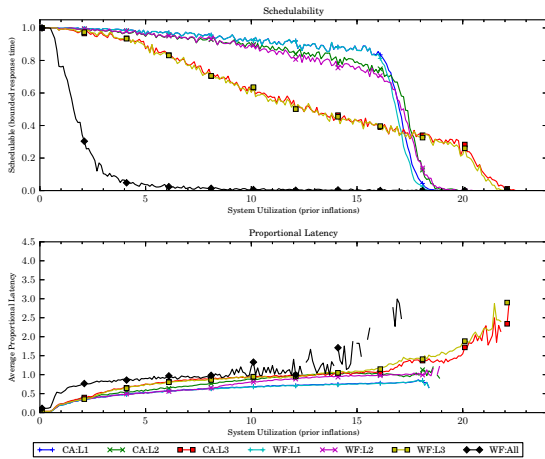


(a) Without polluter overheads.

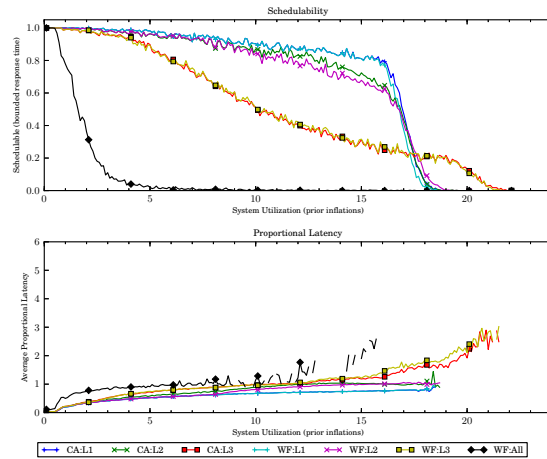


(b) With polluter overheads.

Figure 33: Results for *uni-heavy* per-task utilization, *uni-short* period, *light-weight* EWSS, and *uni-short* height factor.

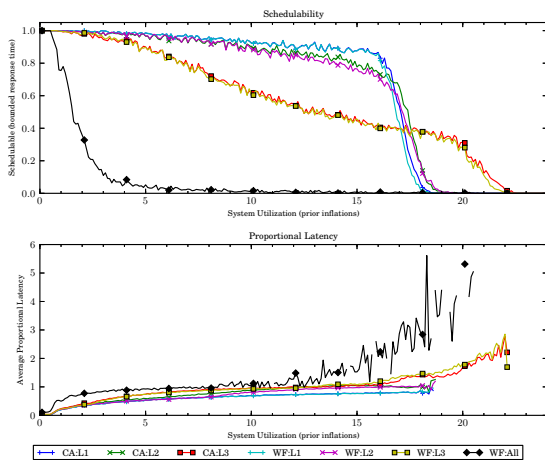


(a) Without polluter overheads.

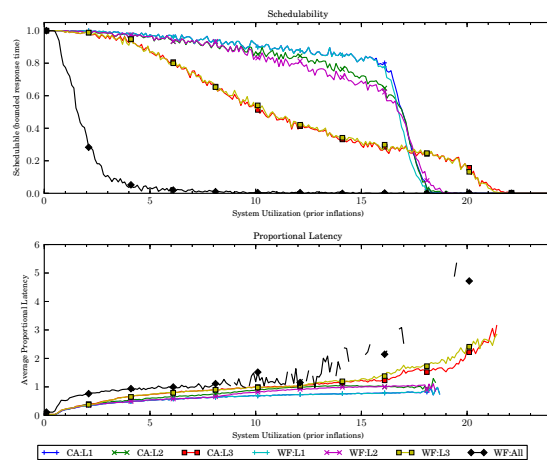


(b) With polluter overheads.

Figure 34: Results for *uni-heavy* per-task utilization, *uni-short* period, *light-weight* EWSS, and *uni-medium* height factor.

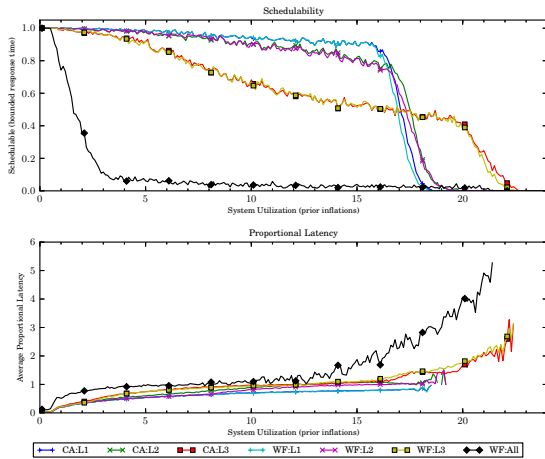


(a) Without polluter overheads.

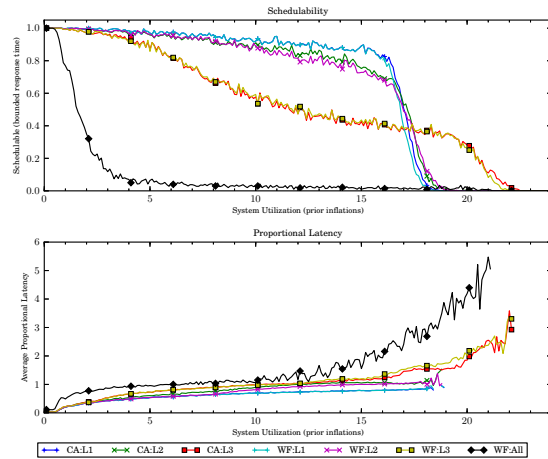


(b) With polluter overheads.

Figure 35: Results for *uni-heavy* per-task utilization, *uni-short* period, *light-weight* EWSS, and *uni-tall* height factor.

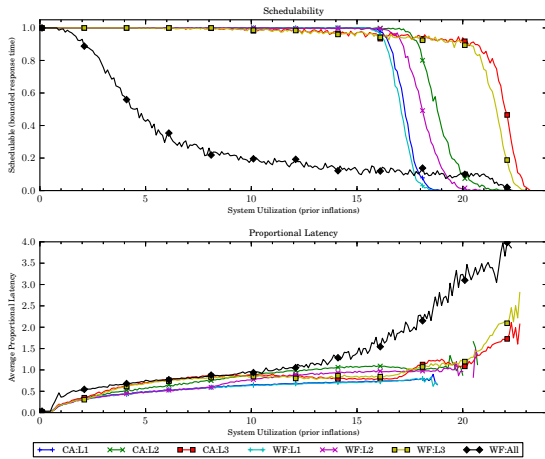


(a) Without polluter overheads.

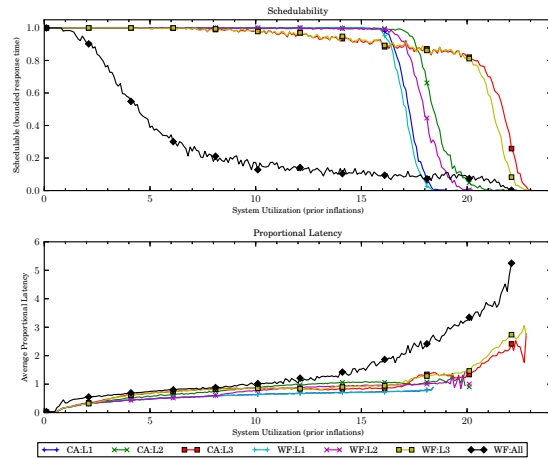


(b) With polluter overheads.

Figure 36: Results for *uni-heavy* per-task utilization, *uni-short* period, *light-weight* EWSS, and *pipeline* height factor.

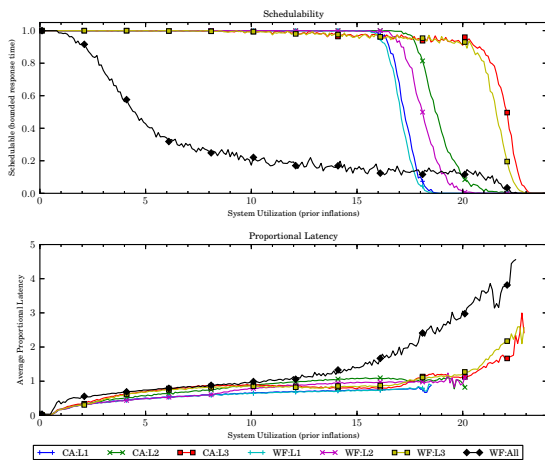


(a) Without polluter overheads.

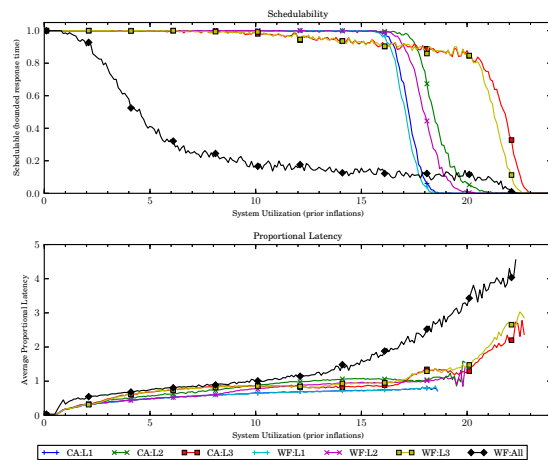


(b) With polluter overheads.

Figure 37: Results for *uni-heavy* per-task utilization, *uni-moderate* period, *light-weight* EWSS, and *uni-short* height factor.

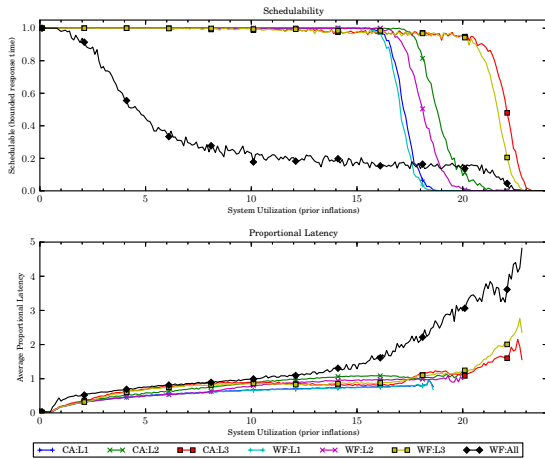


(a) Without polluter overheads.

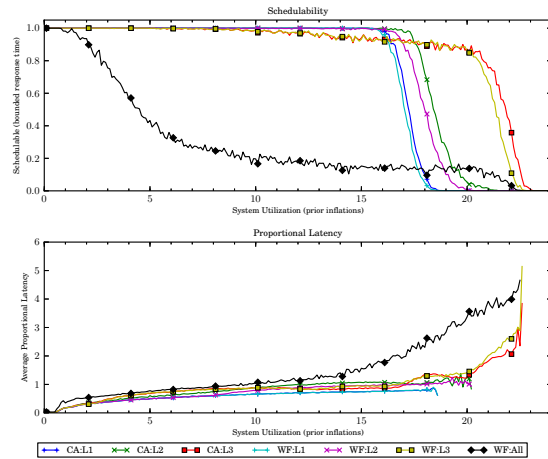


(b) With polluter overheads.

Figure 38: Results for *uni-heavy* per-task utilization, *uni-moderate* period, *light-weight* EWSS, and *uni-medium* height factor.

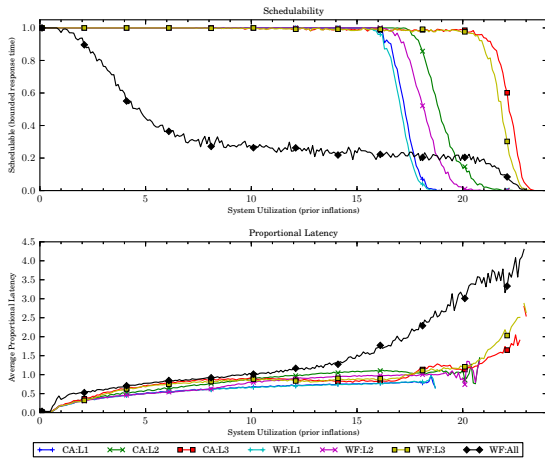


(a) Without polluter overheads.

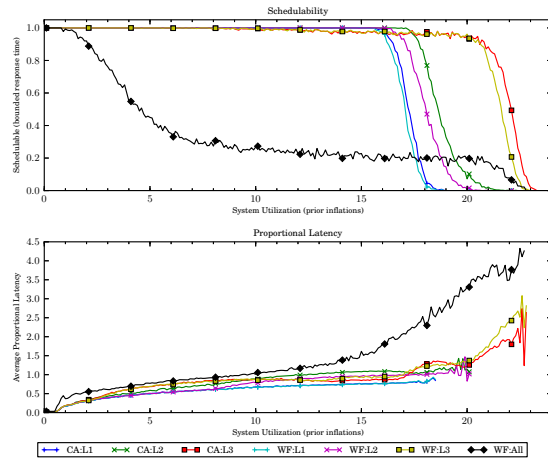


(b) With polluter overheads.

Figure 39: Results for *uni-heavy* per-task utilization, *uni-moderate* period, *light-weight* EWSS, and *uni-tall* height factor.

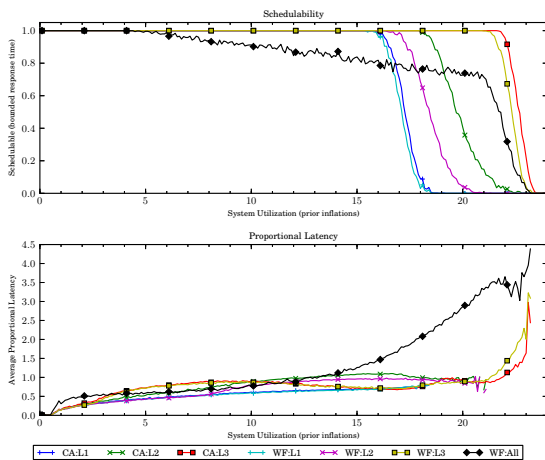


(a) Without polluter overheads.

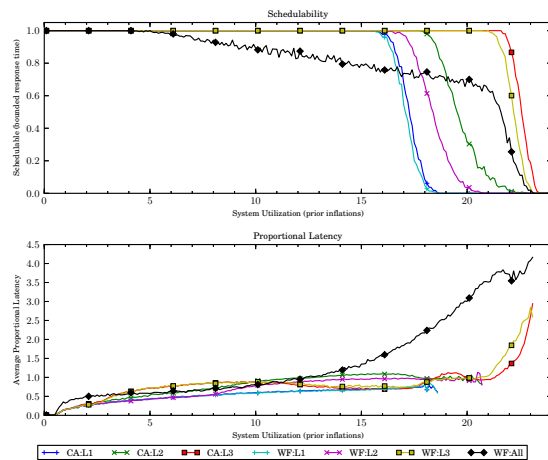


(b) With polluter overheads.

Figure 40: Results for *uni-heavy* per-task utilization, *uni-moderate* period, *light-weight* EWSS, and *pipeline* height factor.

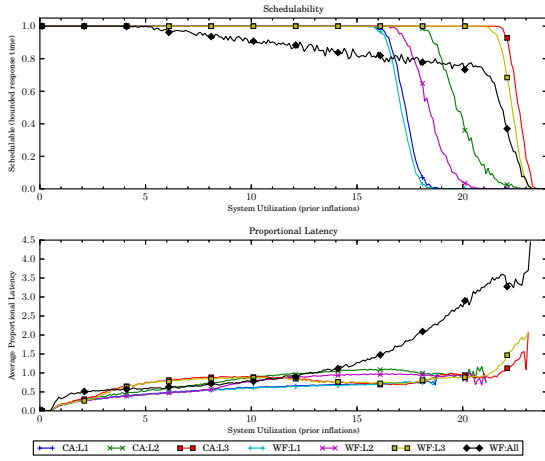


(a) Without polluter overheads.

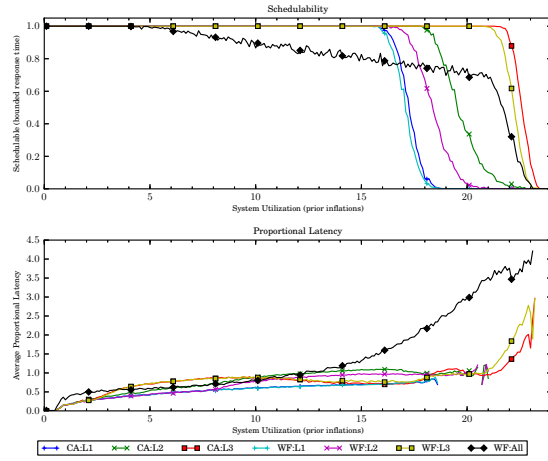


(b) With polluter overheads.

Figure 41: Results for *uni-heavy* per-task utilization, *uni-long* period, *light-weight* EWSS, and *uni-short* height factor.

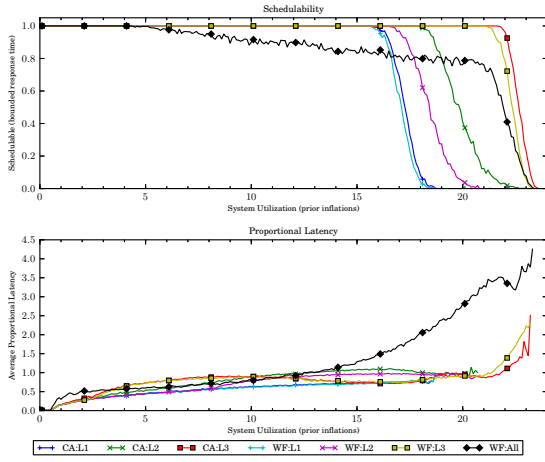


(a) Without polluter overheads.

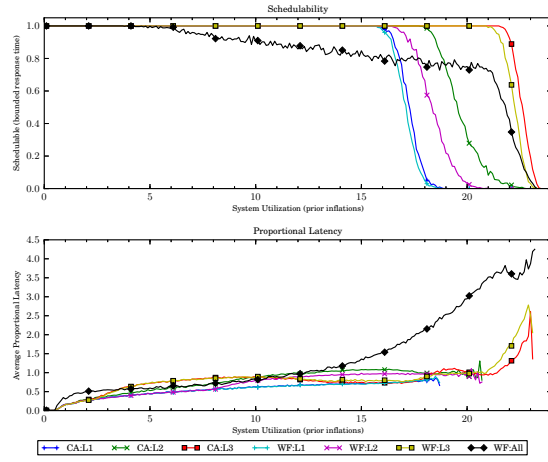


(b) With polluter overheads.

Figure 42: Results for *uni-heavy* per-task utilization, *uni-long* period, *light-weight* EWSS, and *uni-medium* height factor.

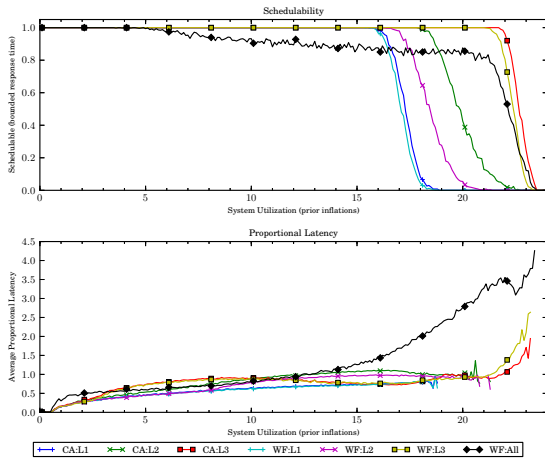


(a) Without polluter overheads.

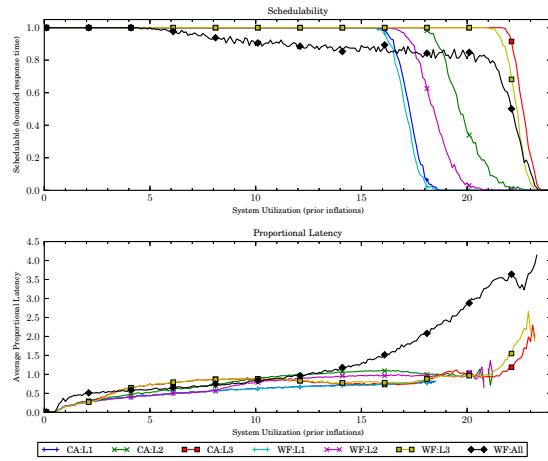


(b) With polluter overheads.

Figure 43: Results for *uni-heavy* per-task utilization, *uni-long* period, *light-weight* EWSS, and *uni-tall* height factor.

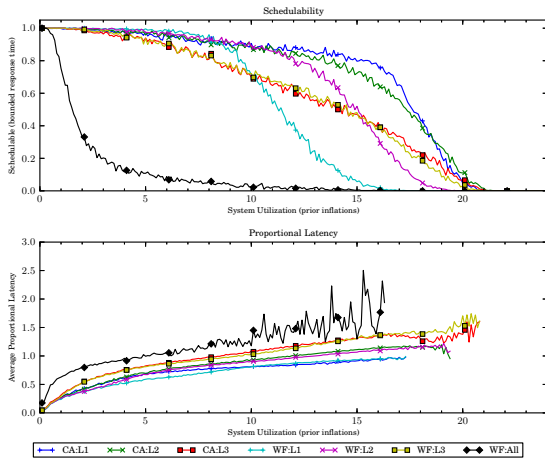


(a) Without polluter overheads.

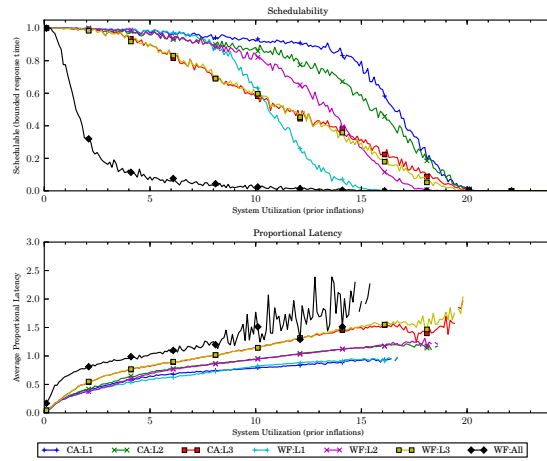


(b) With polluter overheads.

Figure 44: Results for *uni-heavy* per-task utilization, *uni-long* period, *light-weight* EWSS, and *pipeline* height factor.

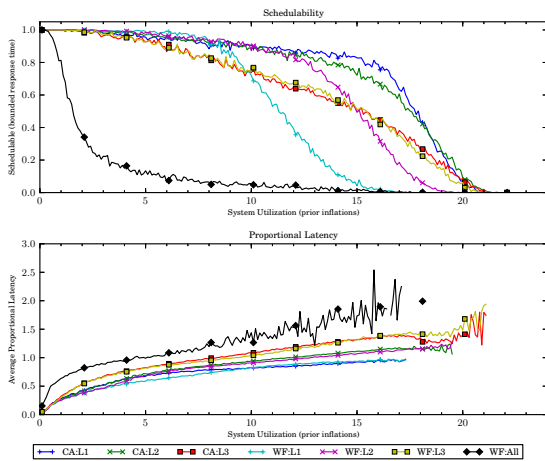


(a) Without polluter overheads.

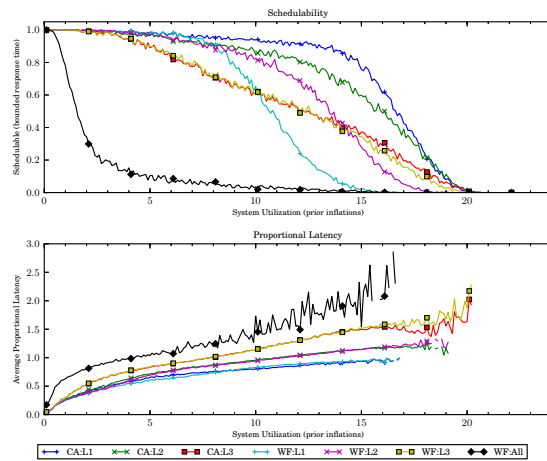


(b) With polluter overheads.

Figure 45: Results for *bimo-light* per-task utilization, *uni-short* period, *light-weight* EWSS, and *uni-short* height factor.

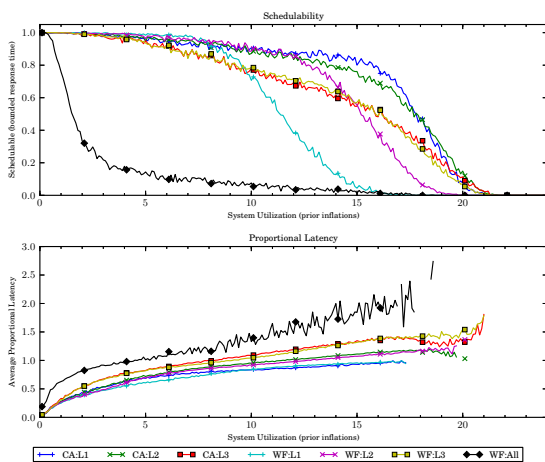


(a) Without polluter overheads.

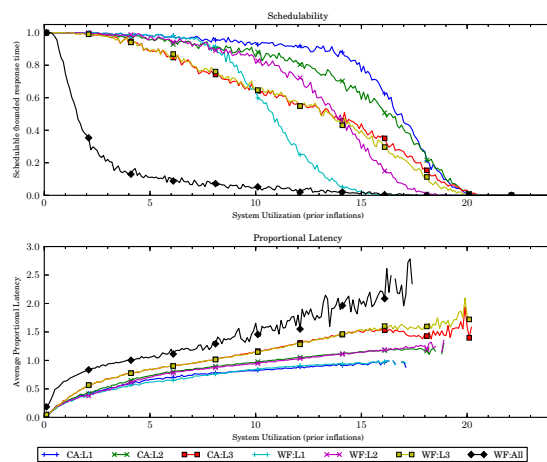


(b) With polluter overheads.

Figure 46: Results for *bimo-light* per-task utilization, *uni-short* period, *light-weight* EWSS, and *uni-medium* height factor.

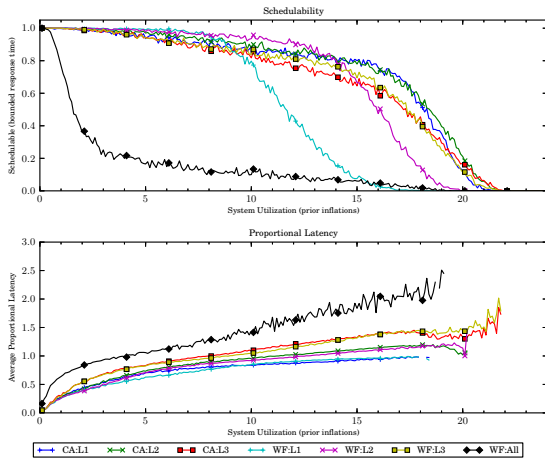


(a) Without polluter overheads.

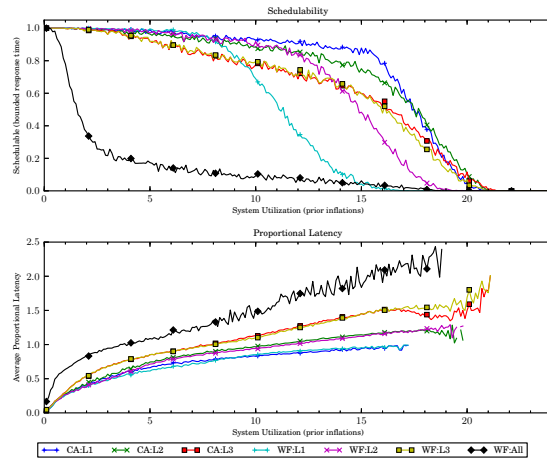


(b) With polluter overheads.

Figure 47: Results for *bimo-light* per-task utilization, *uni-short* period, *light-weight* EWSS, and *uni-tall* height factor.

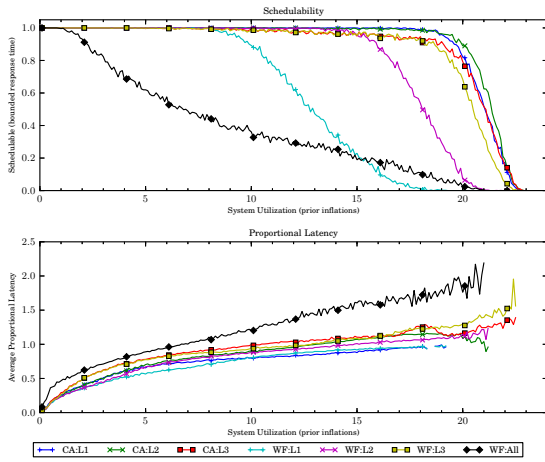


(a) Without polluter overheads.

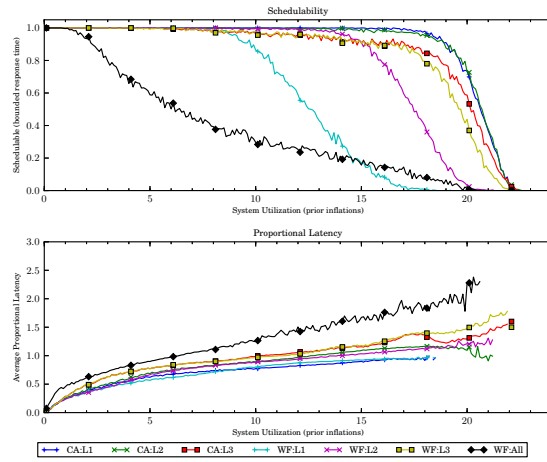


(b) With polluter overheads.

Figure 48: Results for *bimo-light* per-task utilization, *uni-short* period, *light-weight* EWSS, and *pipeline* height factor.

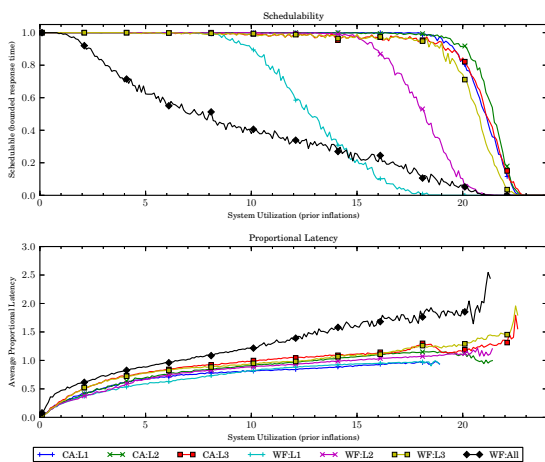


(a) Without polluter overheads.

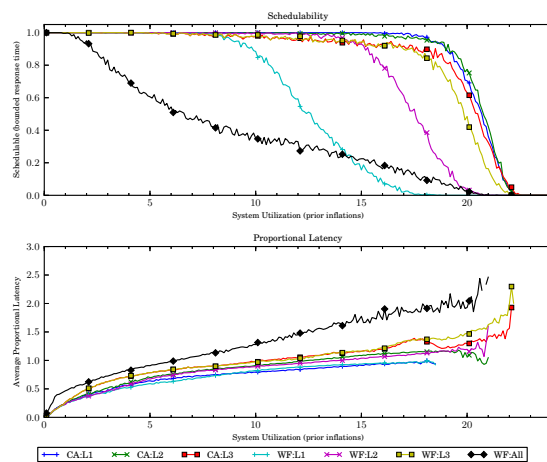


(b) With polluter overheads.

Figure 49: Results for *bimo-light* per-task utilization, *uni-moderate* period, *light-weight* EWSS, and *uni-short* height factor.

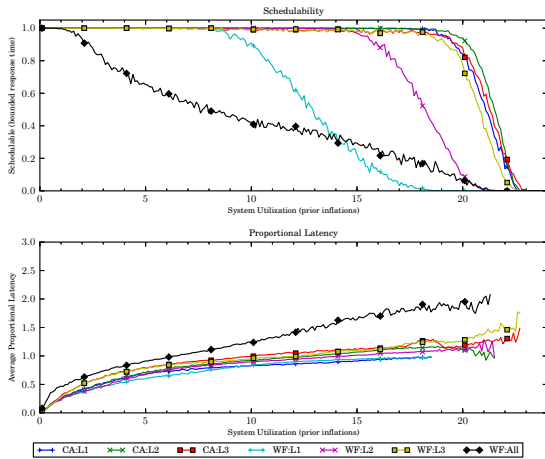


(a) Without polluter overheads.

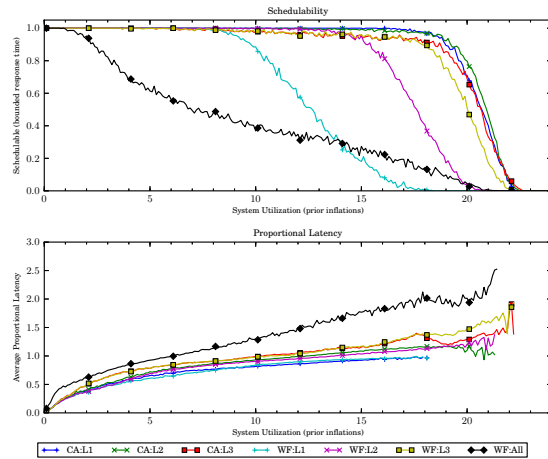


(b) With polluter overheads.

Figure 50: Results for *bimo-light* per-task utilization, *uni-moderate* period, *light-weight* EWSS, and *uni-medium* height factor.

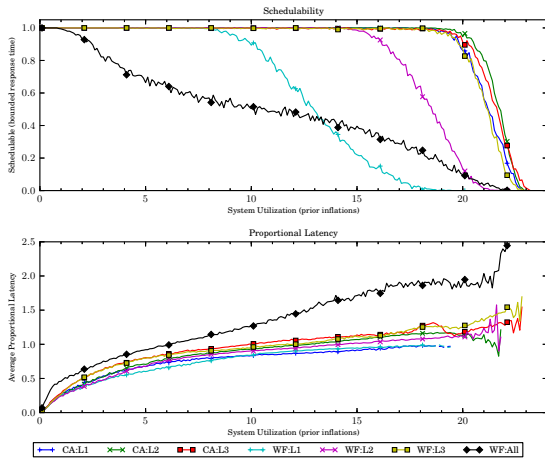


(a) Without polluter overheads.

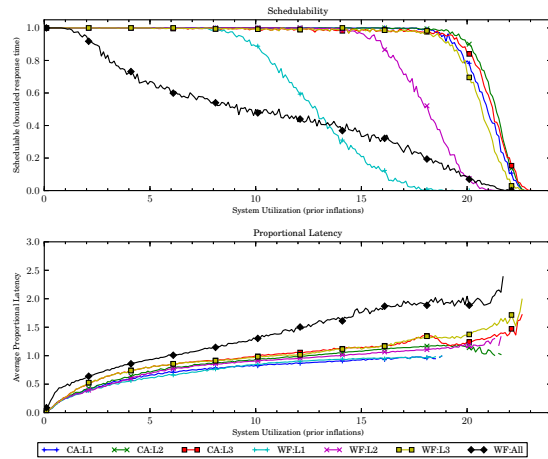


(b) With polluter overheads.

Figure 51: Results for *bimo-light* per-task utilization, *uni-moderate* period, *light-weight* EWSS, and *uni-tall* height factor.

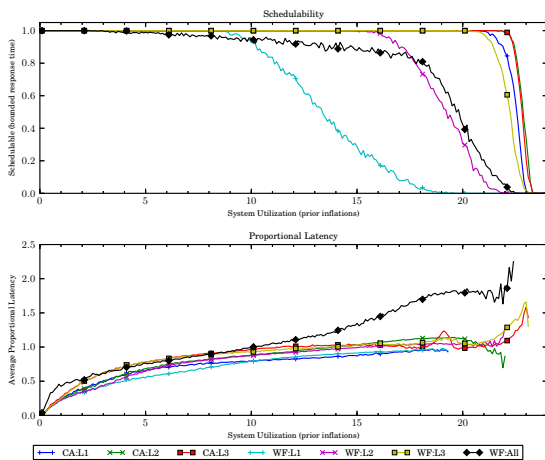


(a) Without polluter overheads.

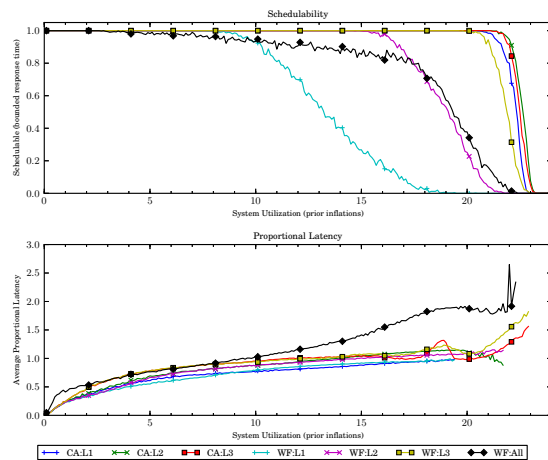


(b) With polluter overheads.

Figure 52: Results for *bimo-light* per-task utilization, *uni-moderate* period, *light-weight* EWSS, and *pipeline* height factor.

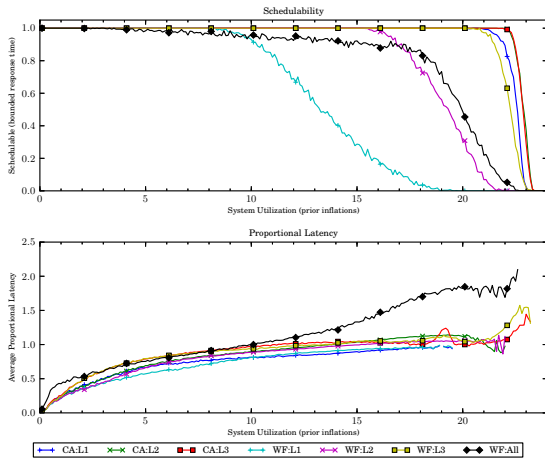


(a) Without polluter overheads.

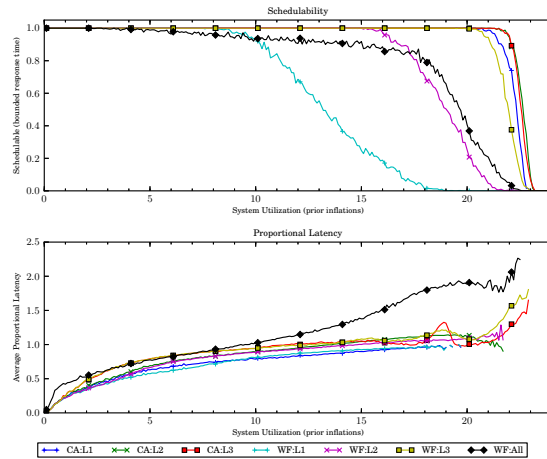


(b) With polluter overheads.

Figure 53: Results for *bimo-light* per-task utilization, *uni-long* period, *light-weight* EWSS, and *uni-short* height factor.

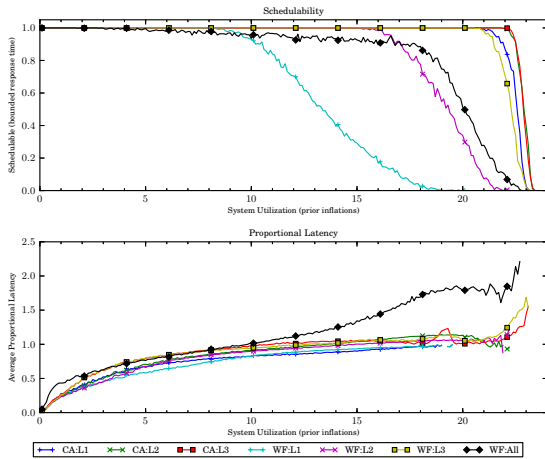


(a) Without polluter overheads.

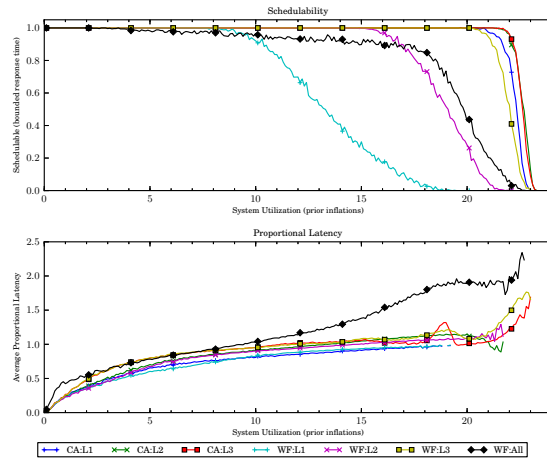


(b) With polluter overheads.

Figure 54: Results for *bimo-light* per-task utilization, *uni-long* period, *light-weight* EWSS, and *uni-medium* height factor.

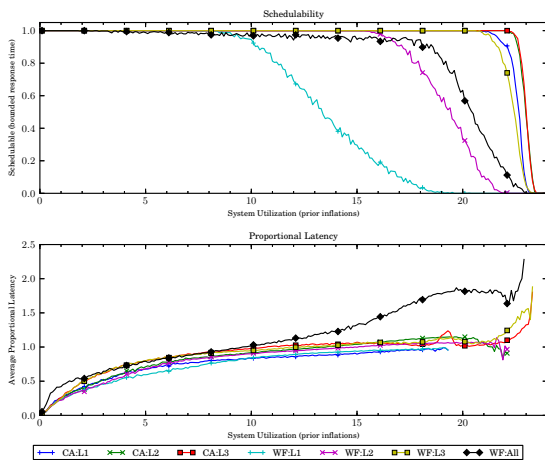


(a) Without polluter overheads.

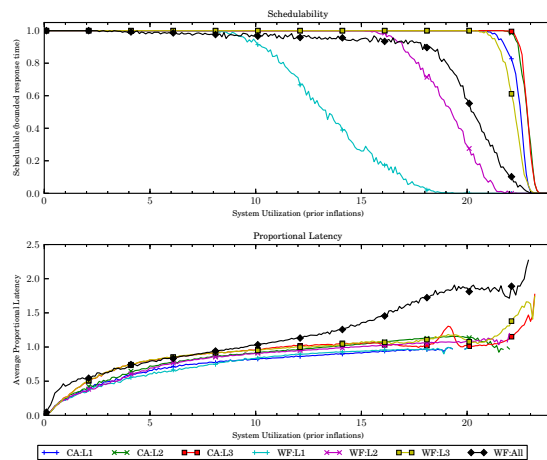


(b) With polluter overheads.

Figure 55: Results for *bimo-light* per-task utilization, *uni-long* period, *light-weight* EWSS, and *uni-tall* height factor.

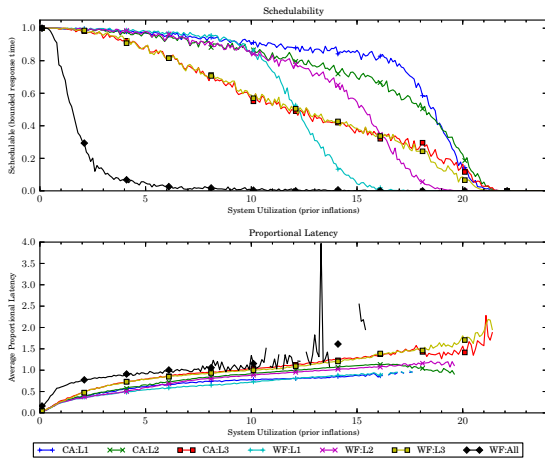


(a) Without polluter overheads.

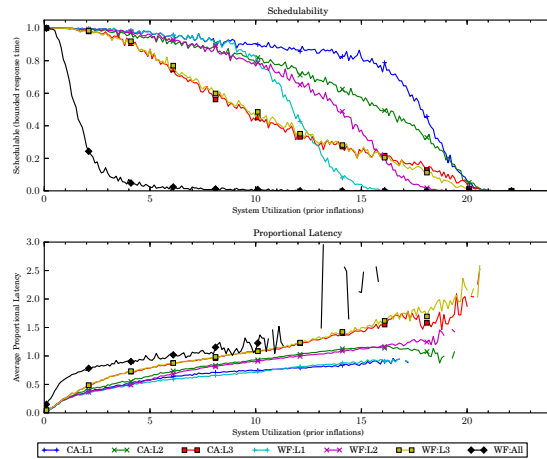


(b) With polluter overheads.

Figure 56: Results for *bimo-light* per-task utilization, *uni-long* period, *light-weight* EWSS, and *pipeline* height factor.

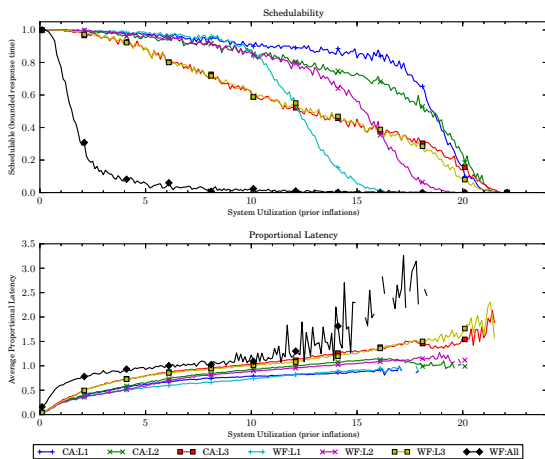


(a) Without polluter overheads.

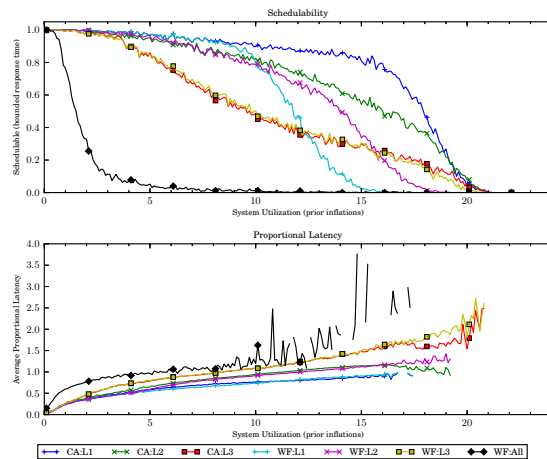


(b) With polluter overheads.

Figure 57: Results for *bimo-medium* per-task utilization, *uni-short* period, *light-weight* EWSS, and *uni-short* height factor.

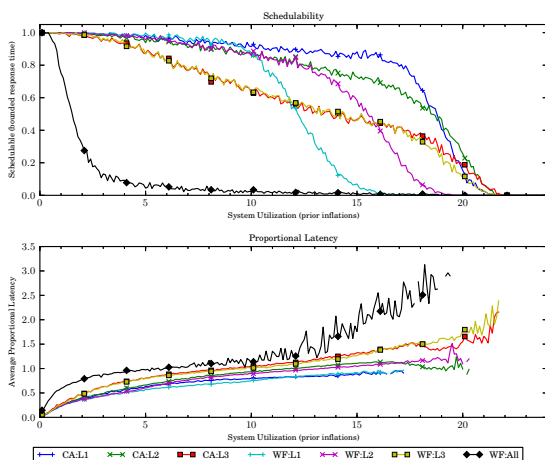


(a) Without polluter overheads.

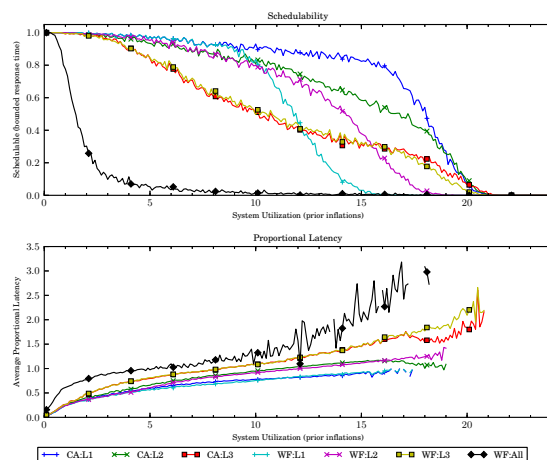


(b) With polluter overheads.

Figure 58: Results for *bimo-medium* per-task utilization, *uni-short* period, *light-weight* EWSS, and *uni-medium* height factor.

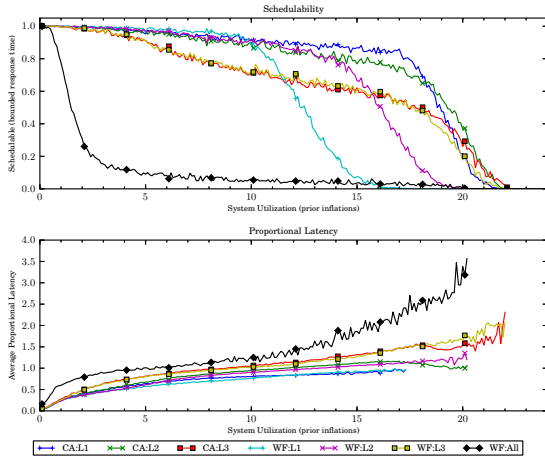


(a) Without polluter overheads.

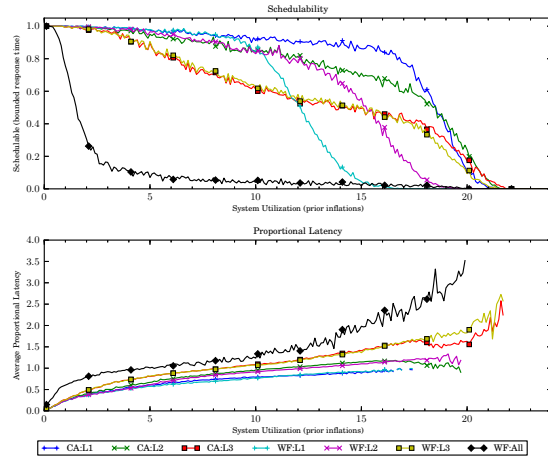


(b) With polluter overheads.

Figure 59: Results for *bimo-medium* per-task utilization, *uni-short* period, *light-weight* EWSS, and *uni-tall* height factor.

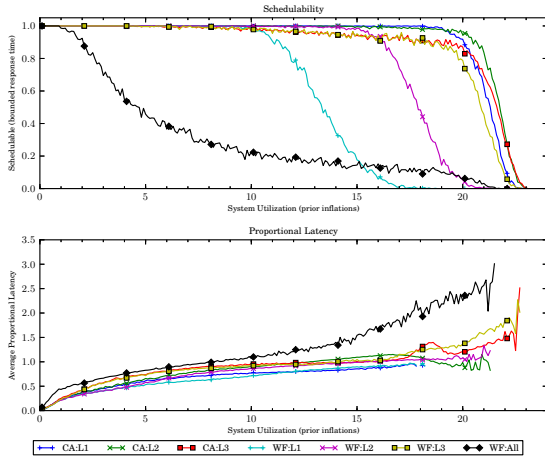


(a) Without polluter overheads.

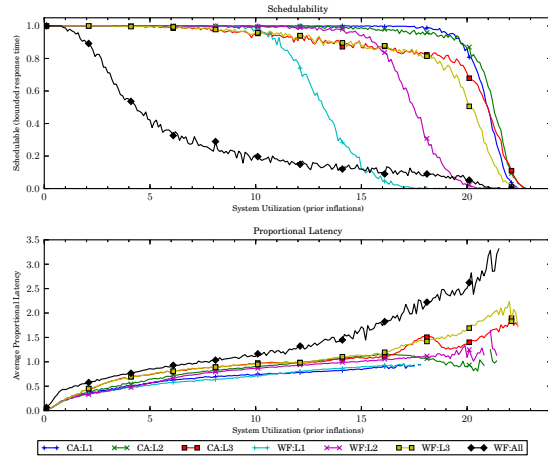


(b) With polluter overheads.

Figure 60: Results for *bimo-medium* per-task utilization, *uni-short* period, *light-weight* EWSS, and *pipeline* height factor.

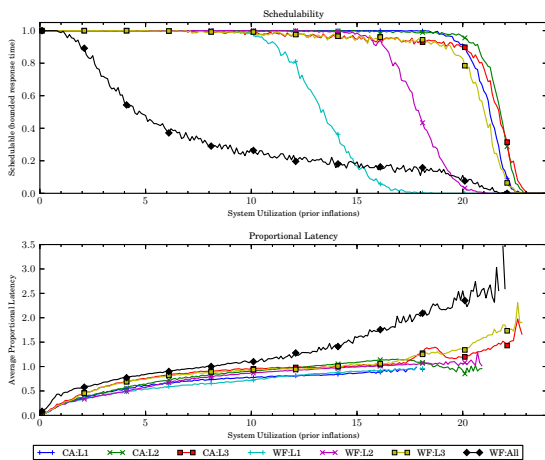


(a) Without polluter overheads.

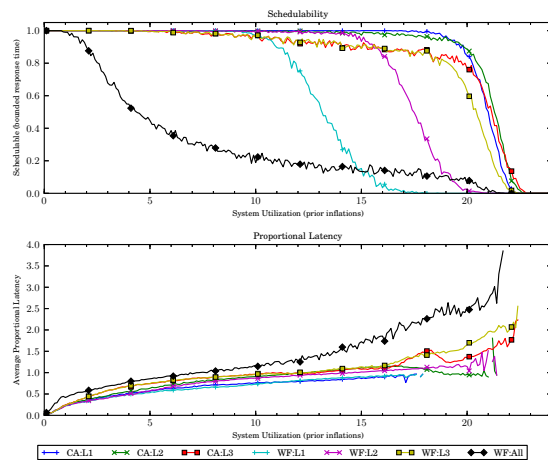


(b) With polluter overheads.

Figure 61: Results for *bimo-medium* per-task utilization, *uni-moderate* period, *light-weight* EWSS, and *uni-short* height factor.

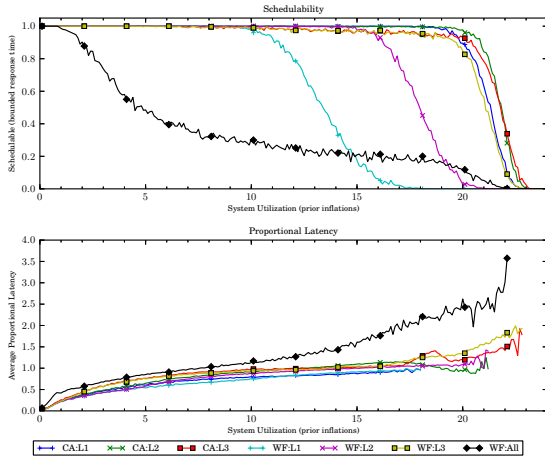


(a) Without polluter overheads.

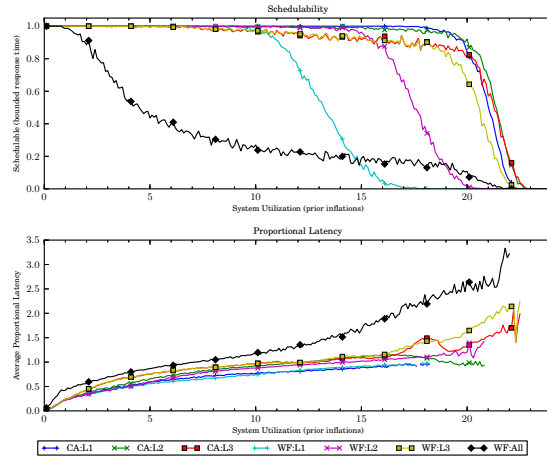


(b) With polluter overheads.

Figure 62: Results for *bimo-medium* per-task utilization, *uni-moderate* period, *light-weight* EWSS, and *uni-medium* height factor.

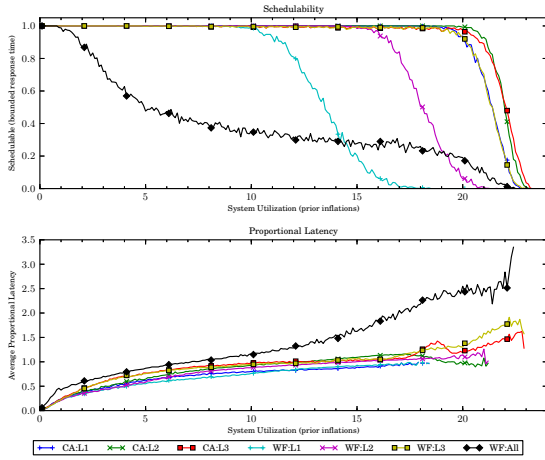


(a) Without polluter overheads.

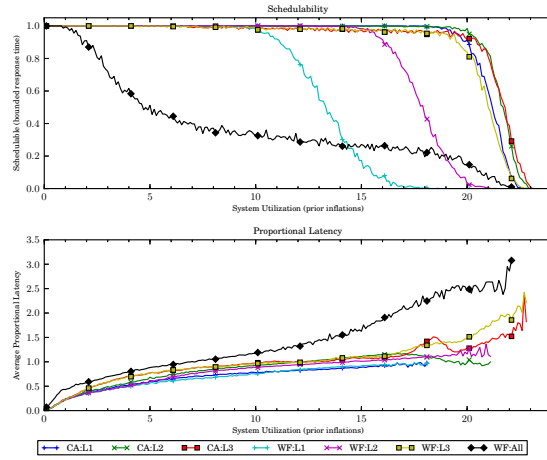


(b) With polluter overheads.

Figure 63: Results for *bimo-medium* per-task utilization, *uni-moderate* period, *light-weight* EWSS, and *uni-tall* height factor.

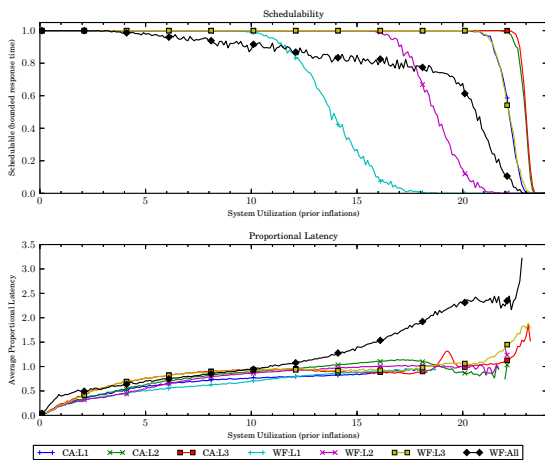


(a) Without polluter overheads.

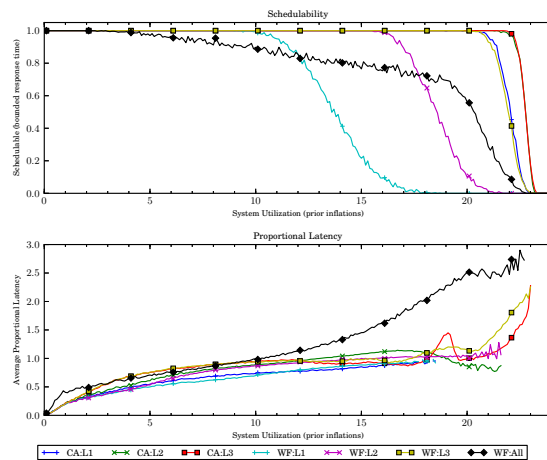


(b) With polluter overheads.

Figure 64: Results for *bimo-medium* per-task utilization, *uni-moderate* period, *light-weight* EWSS, and *pipeline* height factor.

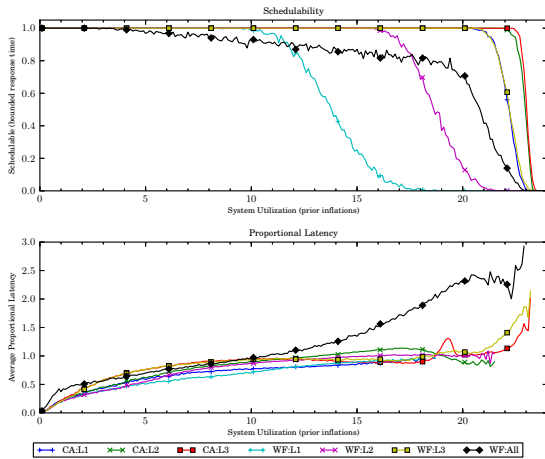


(a) Without polluter overheads.

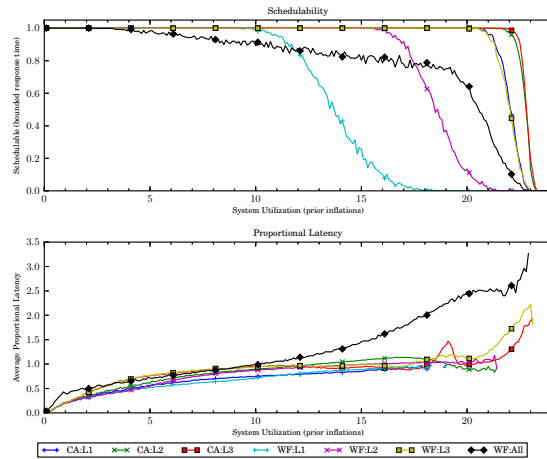


(b) With polluter overheads.

Figure 65: Results for *bimo-medium* per-task utilization, *uni-long* period, *light-weight* EWSS, and *uni-short* height factor.

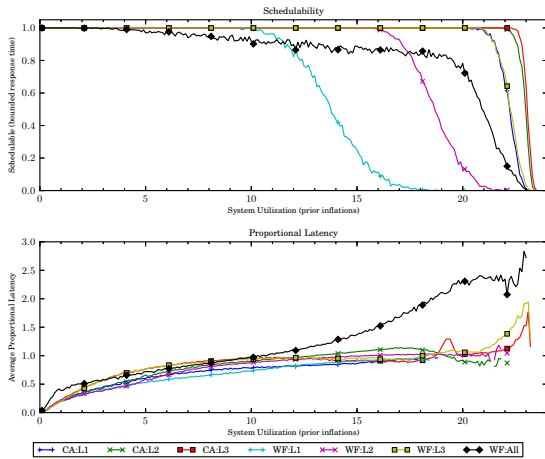


(a) Without polluter overheads.

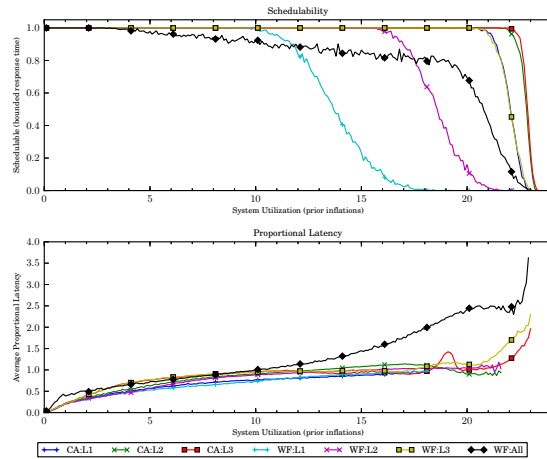


(b) With polluter overheads.

Figure 66: Results for *bimo-medium* per-task utilization, *uni-long* period, *light-weight* EWSS, and *uni-medium* height factor.

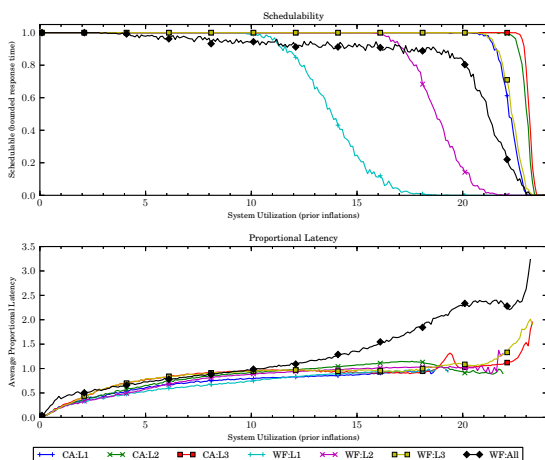


(a) Without polluter overheads.

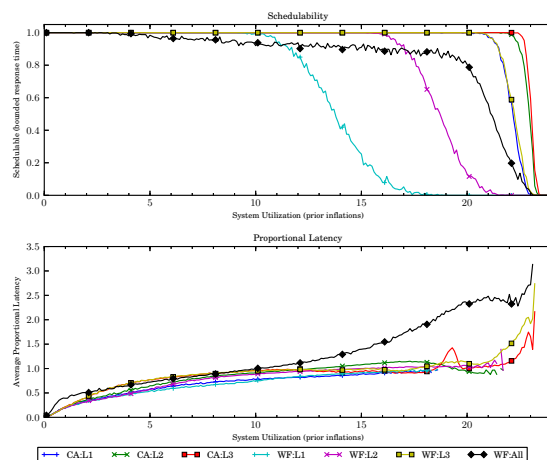


(b) With polluter overheads.

Figure 67: Results for *bimo-medium* per-task utilization, *uni-long* period, *light-weight* EWSS, and *uni-tall* height factor.

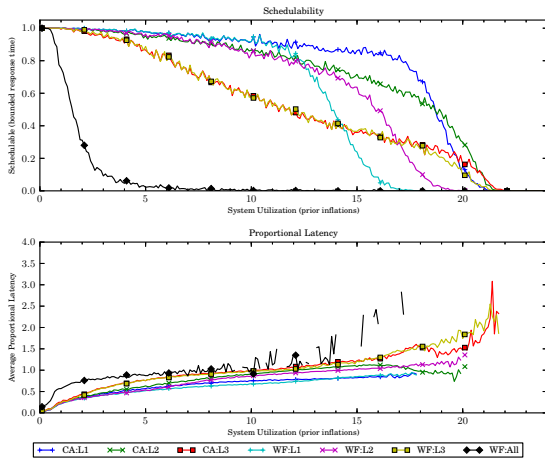


(a) Without polluter overheads.

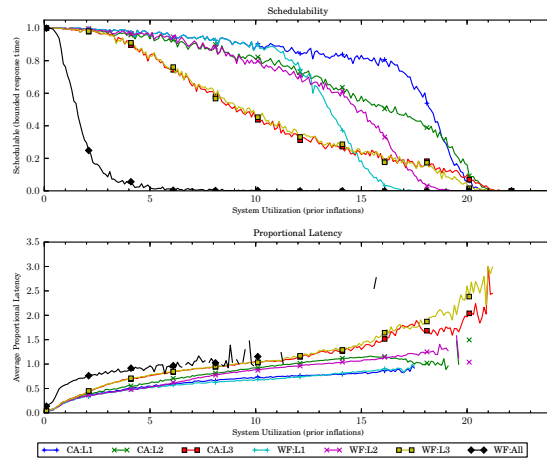


(b) With polluter overheads.

Figure 68: Results for *bimo-medium* per-task utilization, *uni-long* period, *light-weight* EWSS, and *pipeline* height factor.

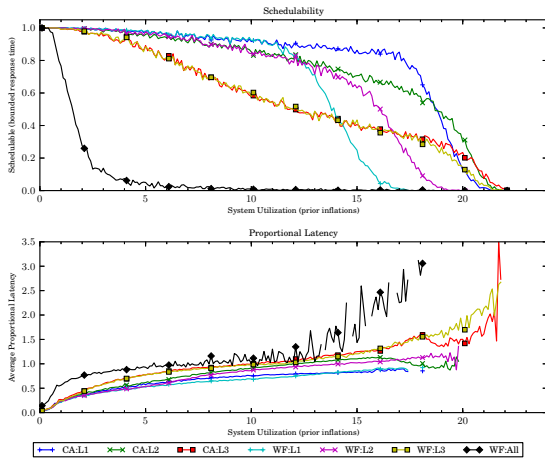


(a) Without polluter overheads.

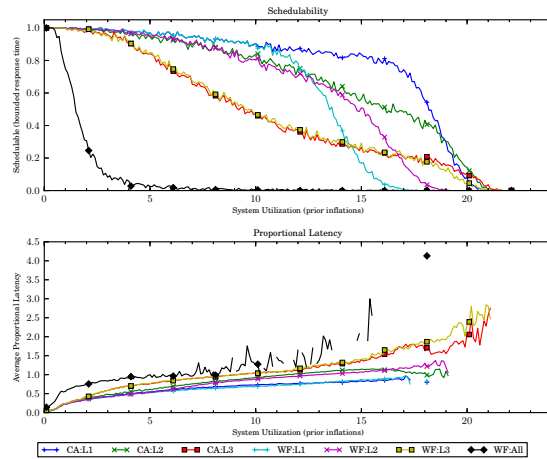


(b) With polluter overheads.

Figure 69: Results for *bimo-heavy* per-task utilization, *uni-short* period, *light-weight* EWSS, and *uni-short* height factor.

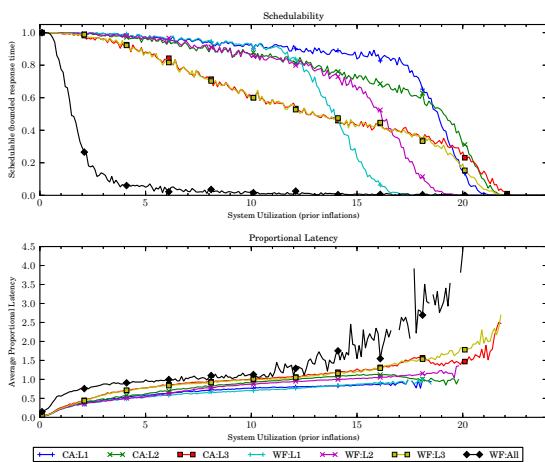


(a) Without polluter overheads.

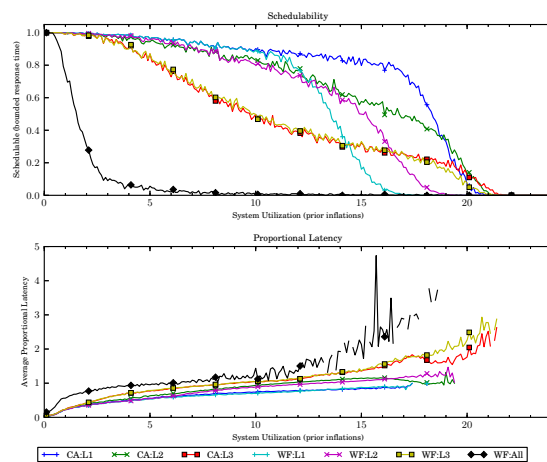


(b) With polluter overheads.

Figure 70: Results for *bimo-heavy* per-task utilization, *uni-short* period, *light-weight* EWSS, and *uni-medium* height factor.

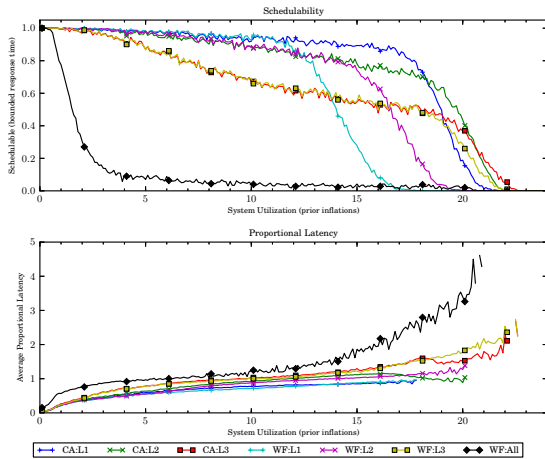


(a) Without polluter overheads.

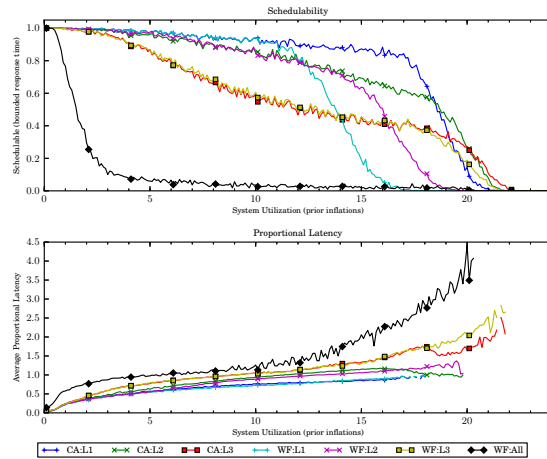


(b) With polluter overheads.

Figure 71: Results for *bimo-heavy* per-task utilization, *uni-short* period, *light-weight* EWSS, and *uni-tall* height factor.

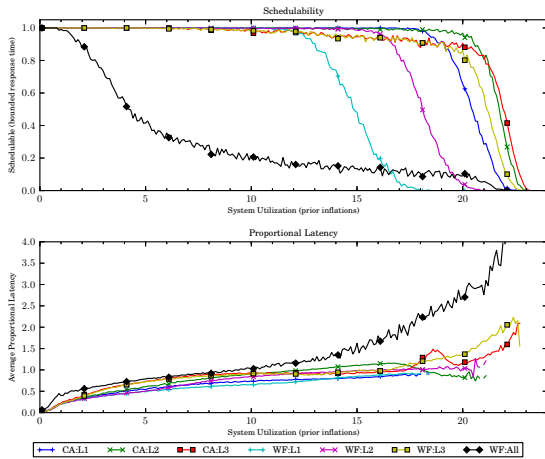


(a) Without polluter overheads.

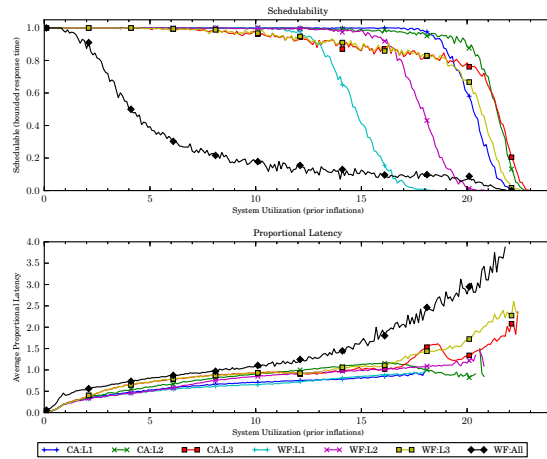


(b) With polluter overheads.

Figure 72: Results for *bimo-heavy* per-task utilization, *uni-short* period, *light-weight* EWSS, and *pipeline* height factor.

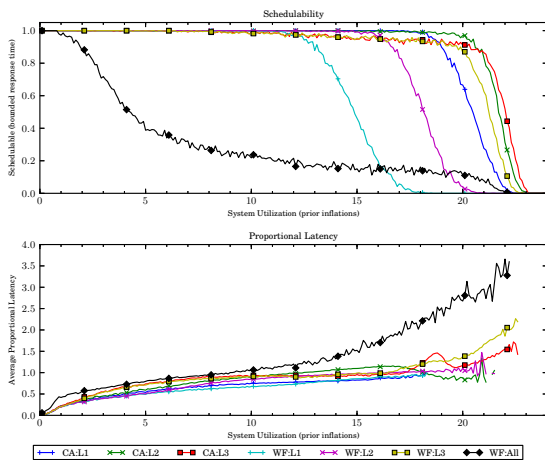


(a) Without polluter overheads.

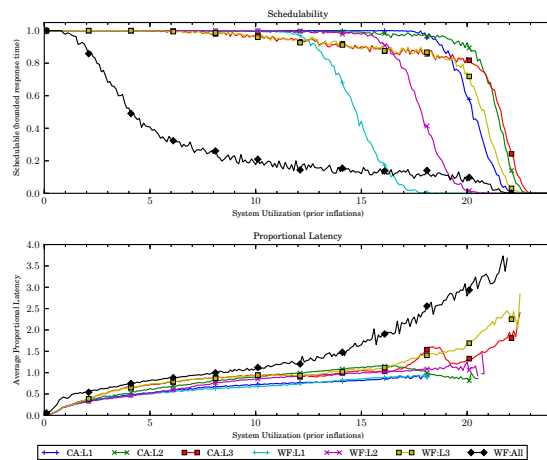


(b) With polluter overheads.

Figure 73: Results for *bimo-heavy* per-task utilization, *uni-moderate* period, *light-weight* EWSS, and *uni-short* height factor.

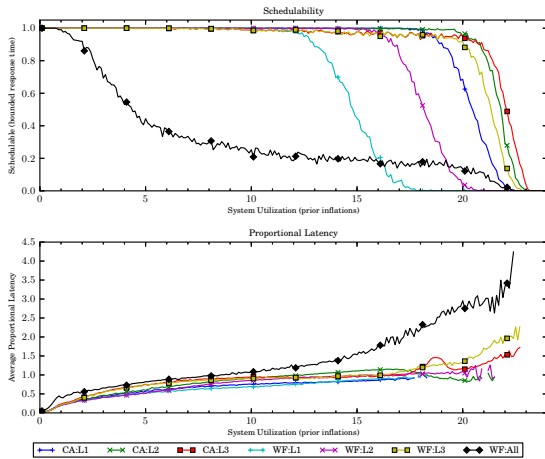


(a) Without polluter overheads.

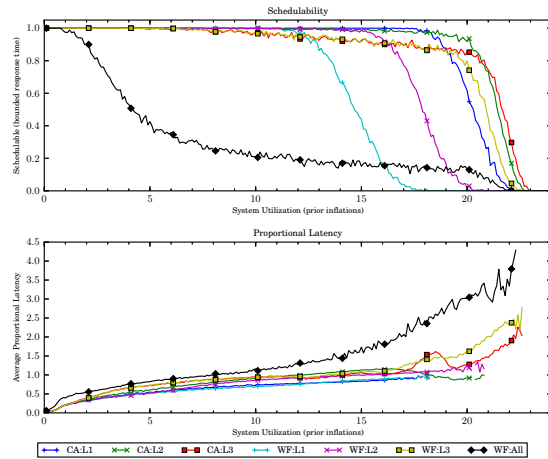


(b) With polluter overheads.

Figure 74: Results for *bimo-heavy* per-task utilization, *uni-moderate* period, *light-weight* EWSS, and *uni-medium* height factor.

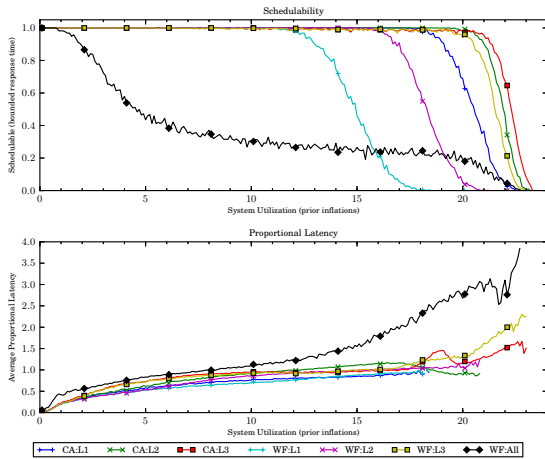


(a) Without polluter overheads.

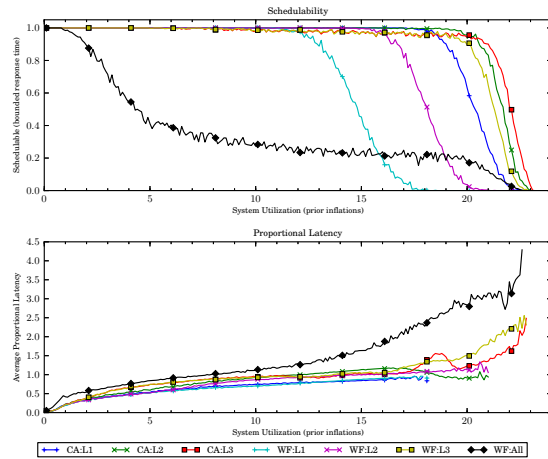


(b) With polluter overheads.

Figure 75: Results for *bimo-heavy* per-task utilization, *uni-moderate* period, *light-weight* EWSS, and *uni-tall* height factor.

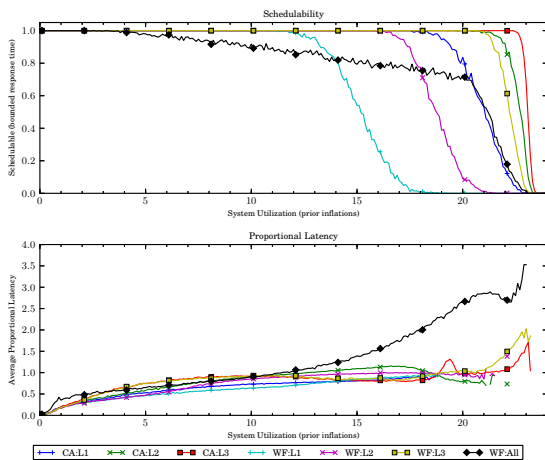


(a) Without polluter overheads.

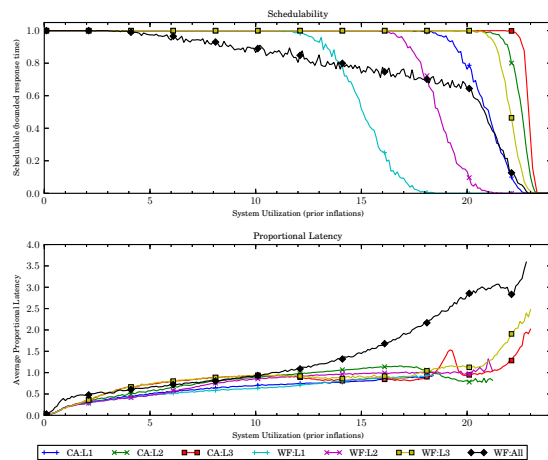


(b) With polluter overheads.

Figure 76: Results for *bimo-heavy* per-task utilization, *uni-moderate* period, *light-weight* EWSS, and *pipeline* height factor.

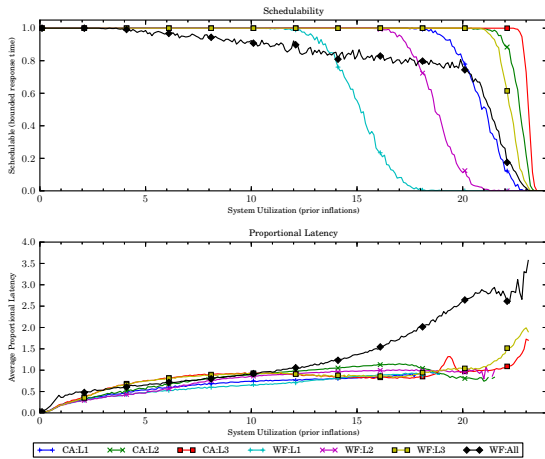


(a) Without polluter overheads.

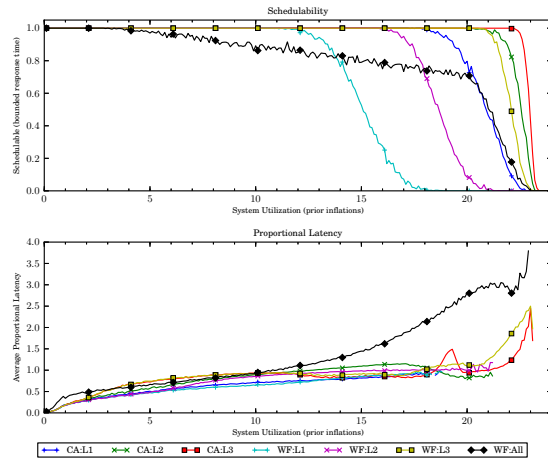


(b) With polluter overheads.

Figure 77: Results for *bimo-heavy* per-task utilization, *uni-long* period, *light-weight* EWSS, and *uni-short* height factor.

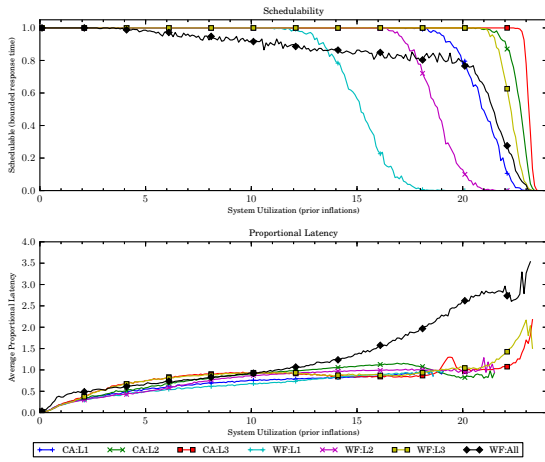


(a) Without polluter overheads.

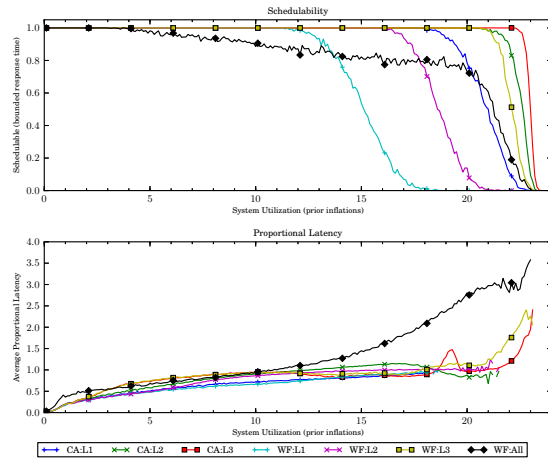


(b) With polluter overheads.

Figure 78: Results for *bimo-heavy* per-task utilization, *uni-long* period, *light-weight* EWSS, and *uni-medium* height factor.

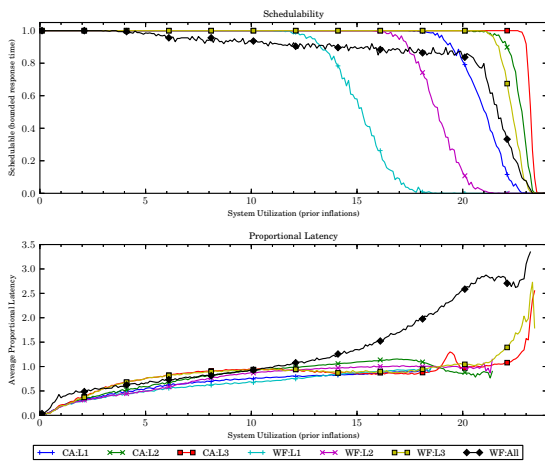


(a) Without polluter overheads.

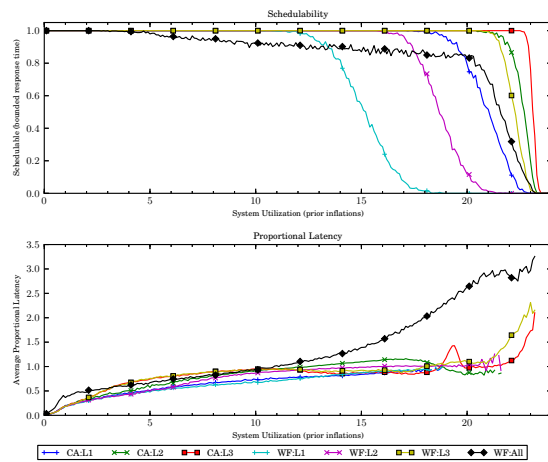


(b) With polluter overheads.

Figure 79: Results for *bimo-heavy* per-task utilization, *uni-long* period, *light-weight* EWSS, and *uni-tall* height factor.

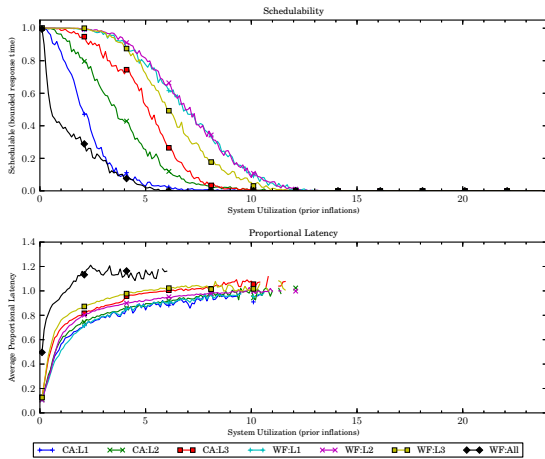


(a) Without polluter overheads.

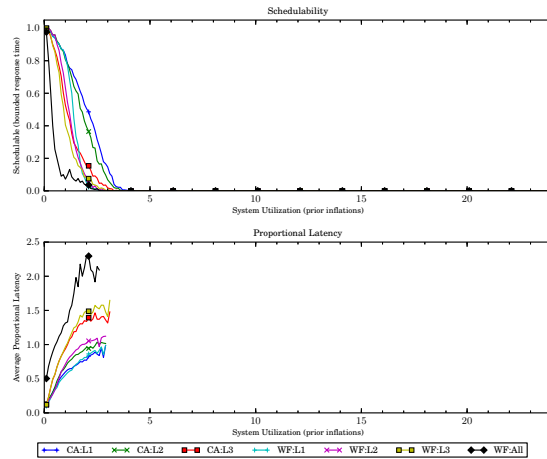


(b) With polluter overheads.

Figure 80: Results for *bimo-heavy* per-task utilization, *uni-long* period, *light-weight* EWSS, and *pipeline* height factor.

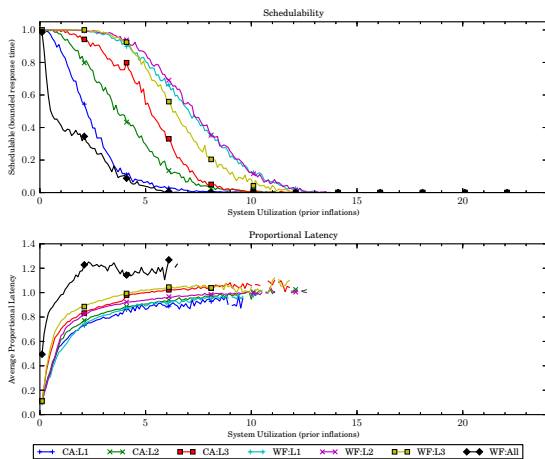


(a) Without polluter overheads.

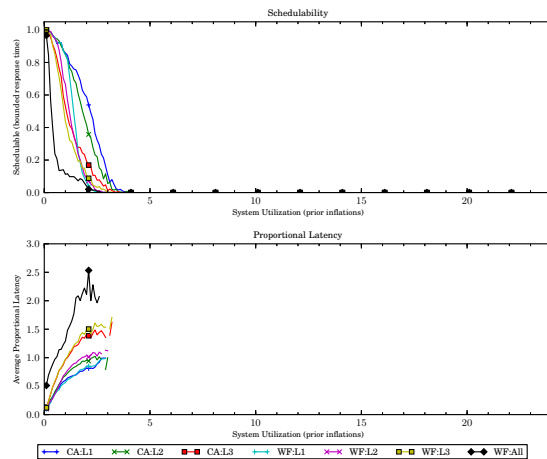


(b) With polluter overheads.

Figure 81: Results for *uni-light* per-task utilization, *uni-short* period, *medium-weight* EWSS, and *uni-short* height factor.

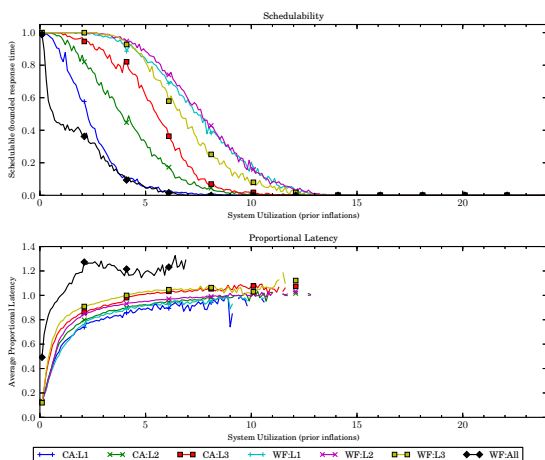


(a) Without polluter overheads.

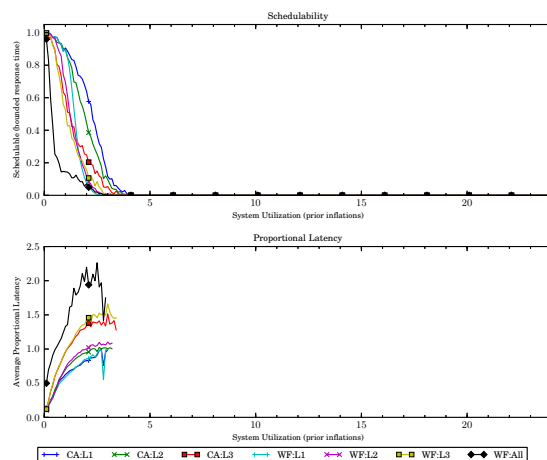


(b) With polluter overheads.

Figure 82: Results for *uni-light* per-task utilization, *uni-short* period, *medium-weight* EWSS, and *uni-medium* height factor.

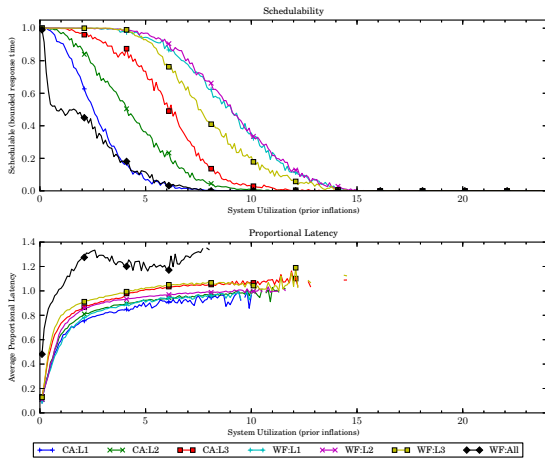


(a) Without polluter overheads.

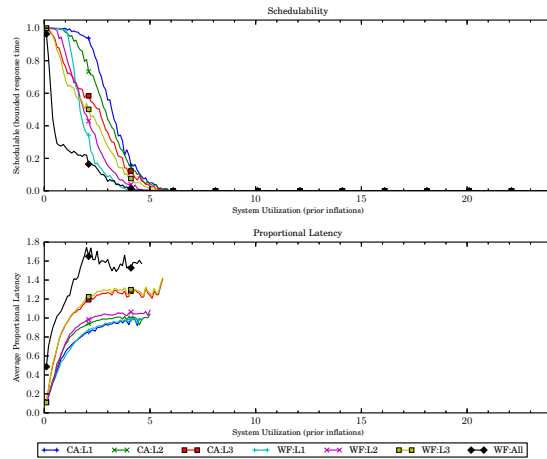


(b) With polluter overheads.

Figure 83: Results for *uni-light* per-task utilization, *uni-short* period, *medium-weight* EWSS, and *uni-tall* height factor.

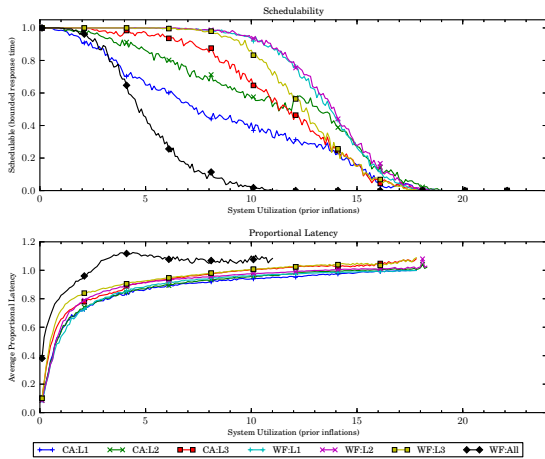


(a) Without polluter overheads.

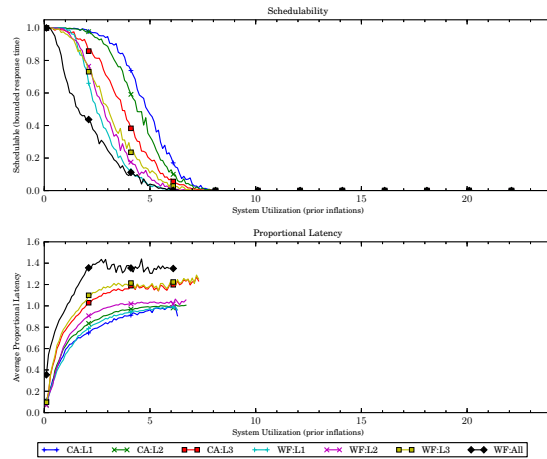


(b) With polluter overheads.

Figure 84: Results for *uni-light* per-task utilization, *uni-short* period, *medium-weight* EWSS, and *pipeline* height factor.

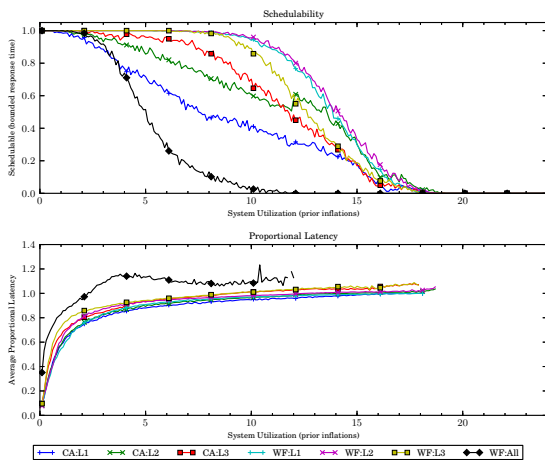


(a) Without polluter overheads.

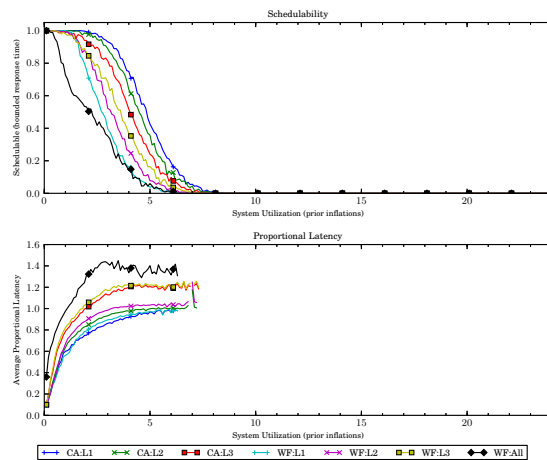


(b) With polluter overheads.

Figure 85: Results for *uni-light* per-task utilization, *uni-moderate* period, *medium-weight* EWSS, and *uni-short* height factor.

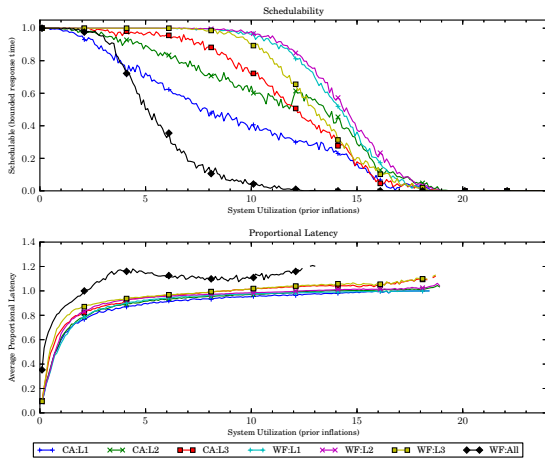


(a) Without polluter overheads.

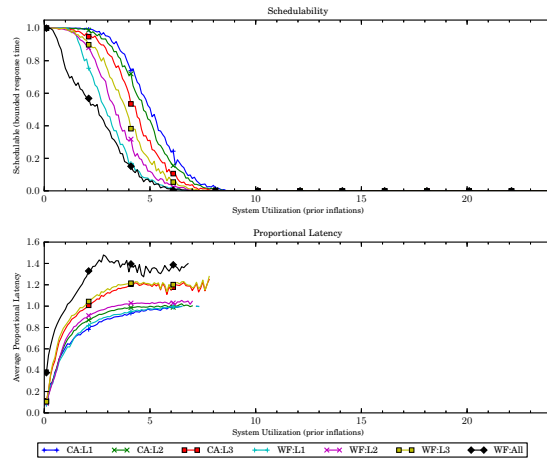


(b) With polluter overheads.

Figure 86: Results for *uni-light* per-task utilization, *uni-moderate* period, *medium-weight* EWSS, and *uni-medium* height factor.

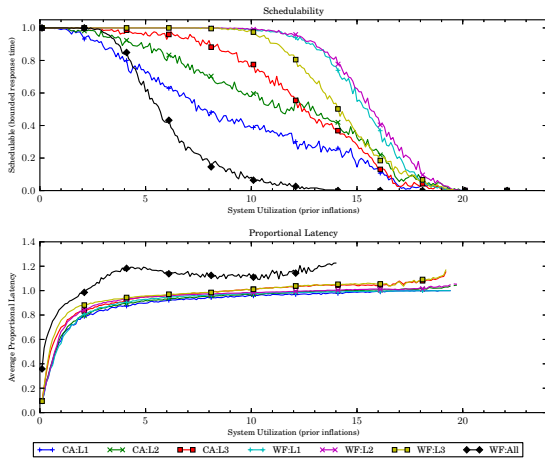


(a) Without polluter overheads.

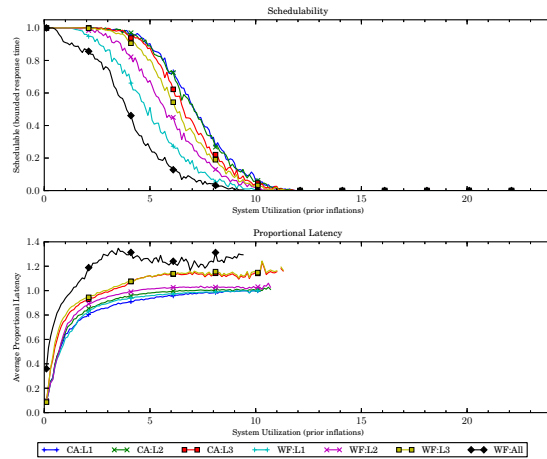


(b) With polluter overheads.

Figure 87: Results for *uni-light* per-task utilization, *uni-moderate* period, *medium-weight* EWSS, and *uni-tall* height factor.

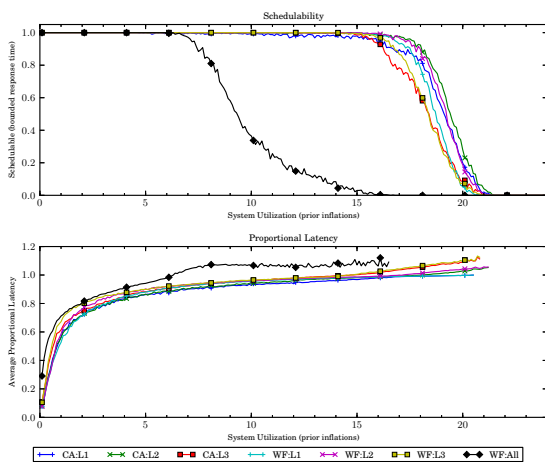


(a) Without polluter overheads.

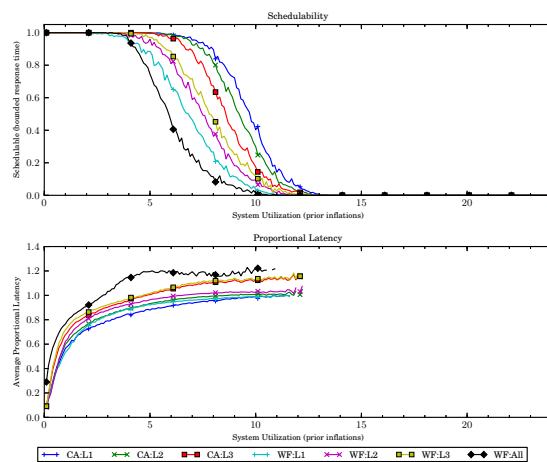


(b) With polluter overheads.

Figure 88: Results for *uni-light* per-task utilization, *uni-moderate* period, *medium-weight* EWSS, and *pipeline* height factor.

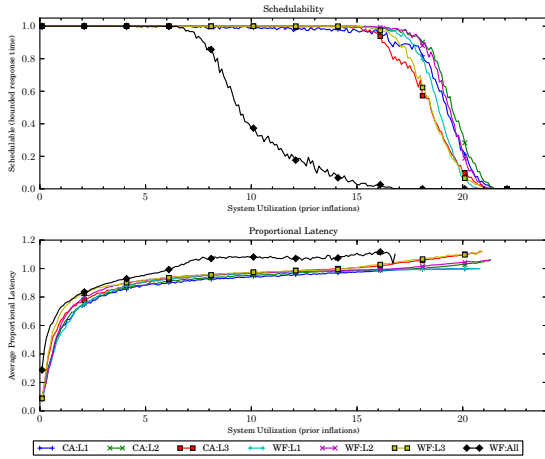


(a) Without polluter overheads.

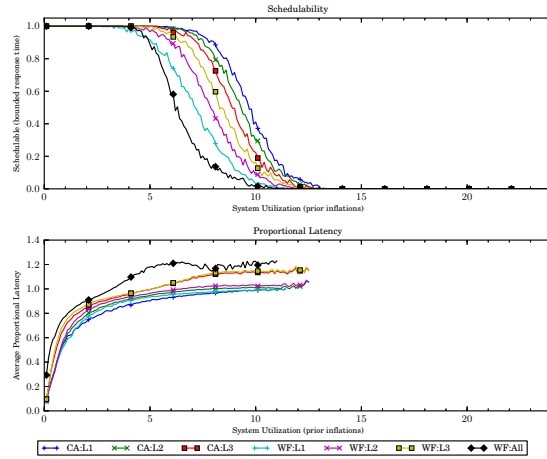


(b) With polluter overheads.

Figure 89: Results for *uni-light* per-task utilization, *uni-long* period, *medium-weight* EWSS, and *uni-short* height factor.

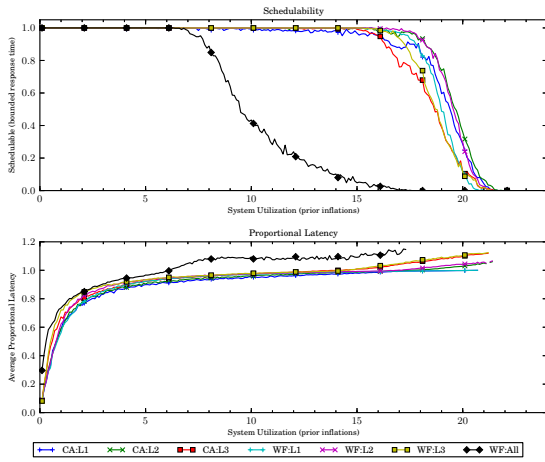


(a) Without polluter overheads.

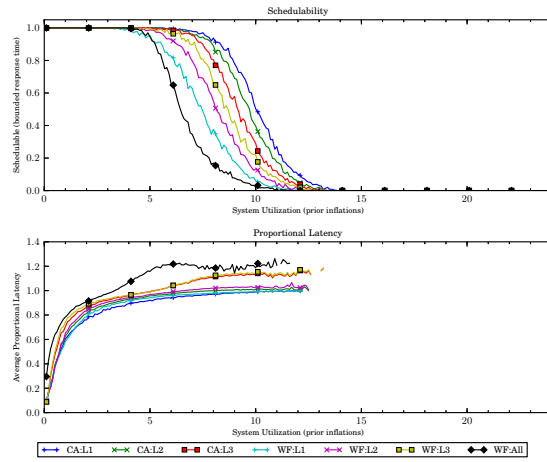


(b) With polluter overheads.

Figure 90: Results for *uni-light* per-task utilization, *uni-long* period, *medium-weight* EWSS, and *uni-medium* height factor.

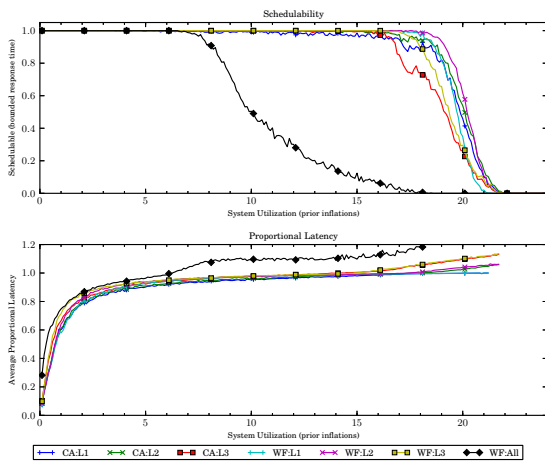


(a) Without polluter overheads.

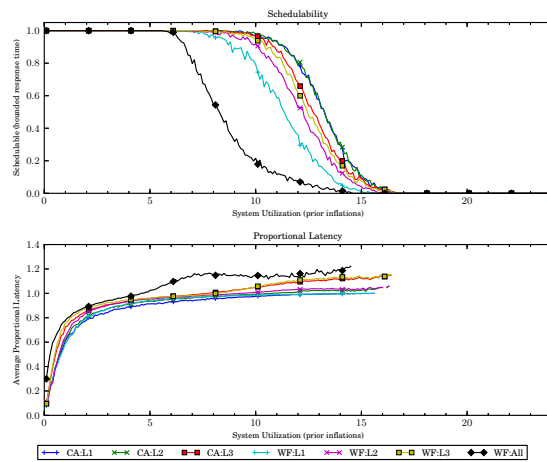


(b) With polluter overheads.

Figure 91: Results for *uni-light* per-task utilization, *uni-long* period, *medium-weight* EWSS, and *uni-tall* height factor.

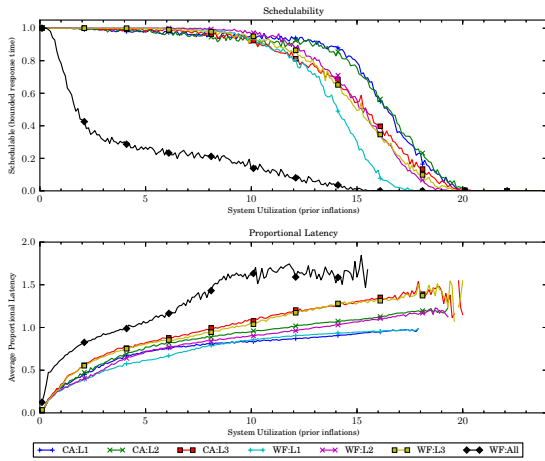


(a) Without polluter overheads.

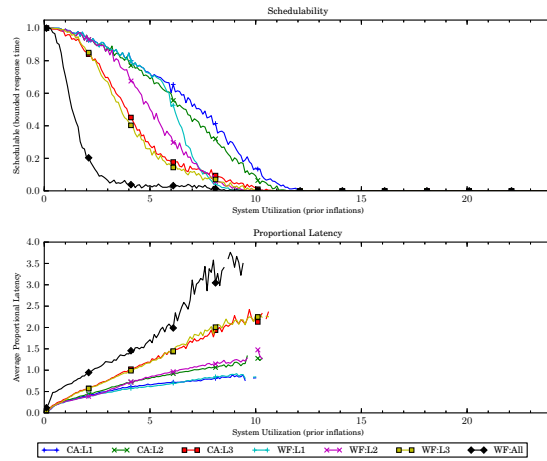


(b) With polluter overheads.

Figure 92: Results for *uni-light* per-task utilization, *uni-long* period, *medium-weight* EWSS, and *pipeline* height factor.

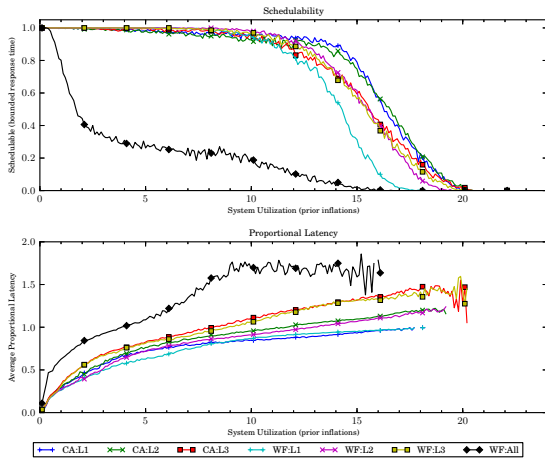


(a) Without polluter overheads.

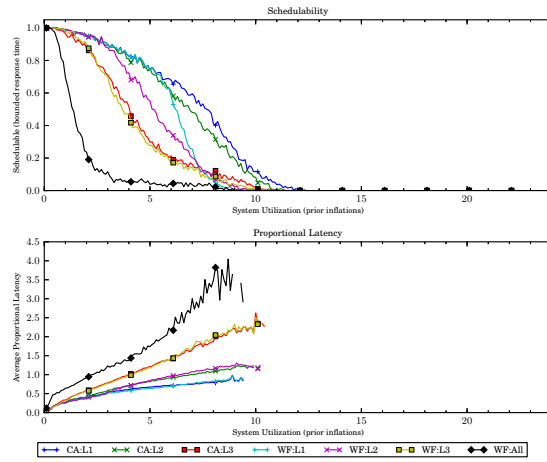


(b) With polluter overheads.

Figure 93: Results for *uni-medium* per-task utilization, *uni-short* period, *medium-weight* EWSS, and *uni-short* height factor.

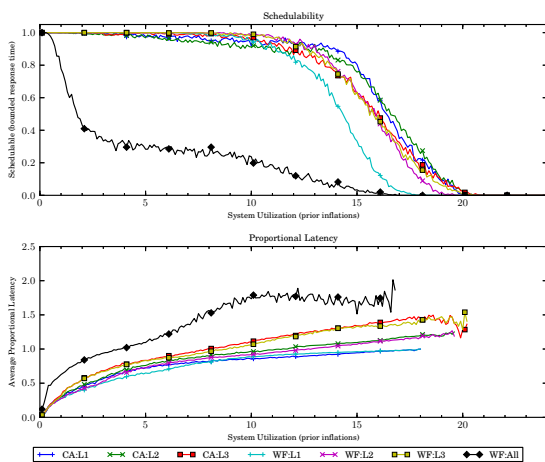


(a) Without polluter overheads.

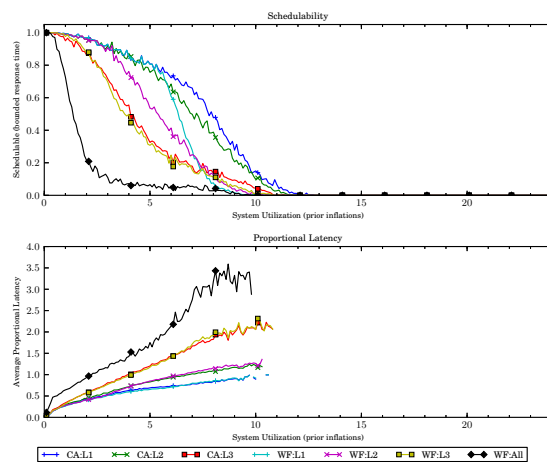


(b) With polluter overheads.

Figure 94: Results for *uni-medium* per-task utilization, *uni-short* period, *medium-weight* EWSS, and *uni-medium* height factor.

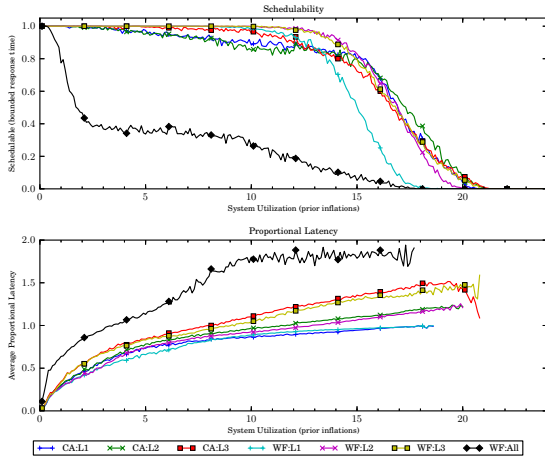


(a) Without polluter overheads.

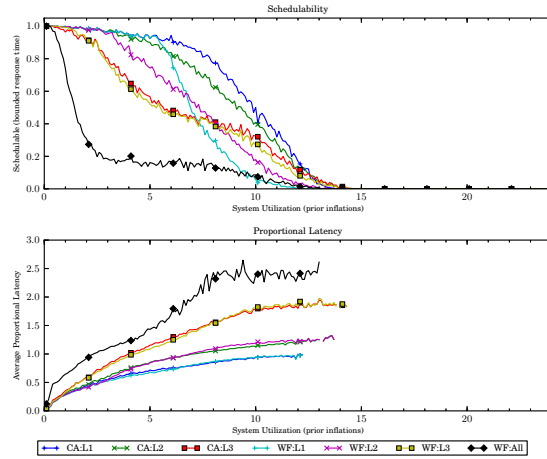


(b) With polluter overheads.

Figure 95: Results for *uni-medium* per-task utilization, *uni-short* period, *medium-weight* EWSS, and *uni-tall* height factor.

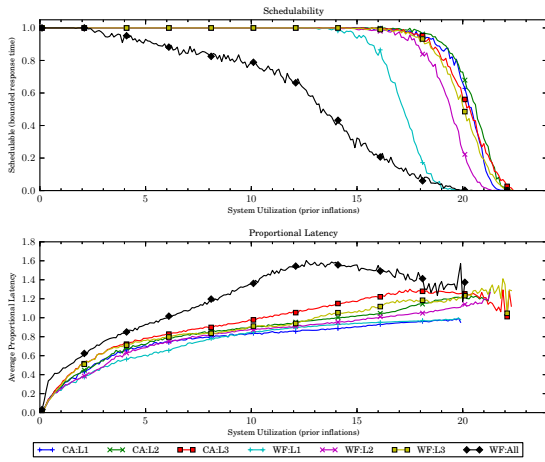


(a) Without polluter overheads.

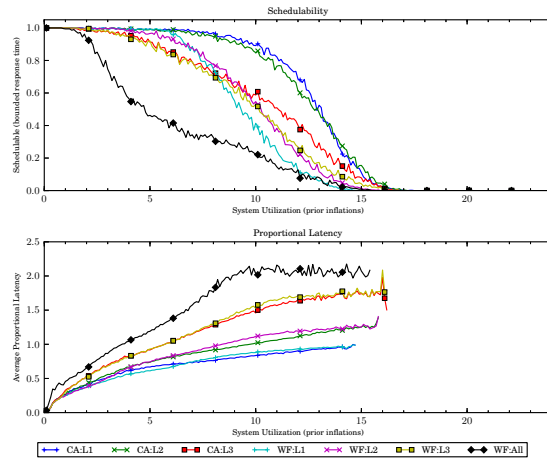


(b) With polluter overheads.

Figure 96: Results for *uni-medium* per-task utilization, *uni-short* period, *medium-weight* EWSS, and *pipeline* height factor.

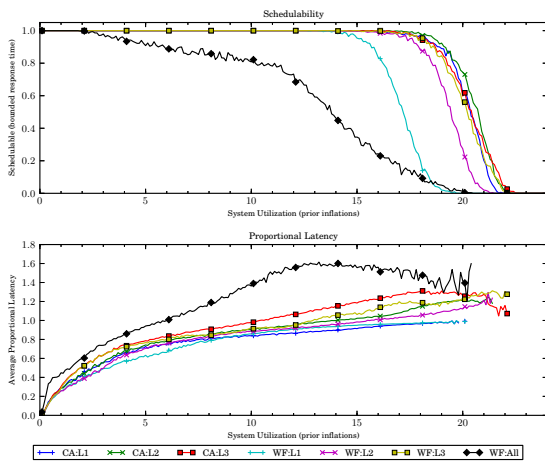


(a) Without polluter overheads.

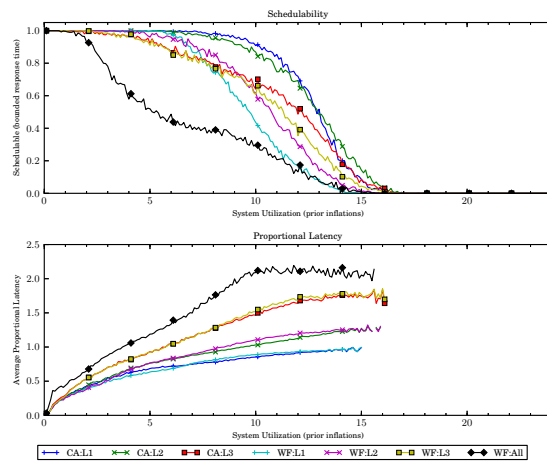


(b) With polluter overheads.

Figure 97: Results for *uni-medium* per-task utilization, *uni-moderate* period, *medium-weight* EWSS, and *uni-short* height factor.

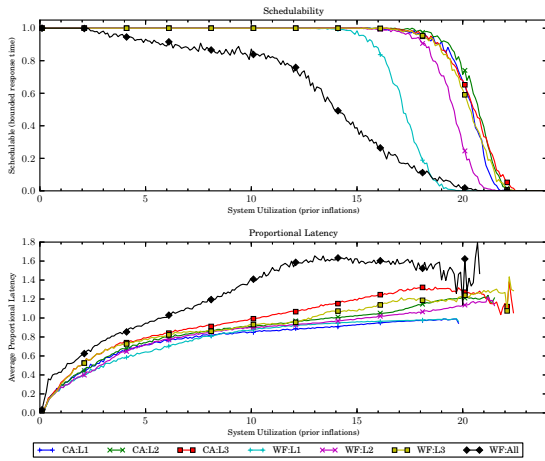


(a) Without polluter overheads.

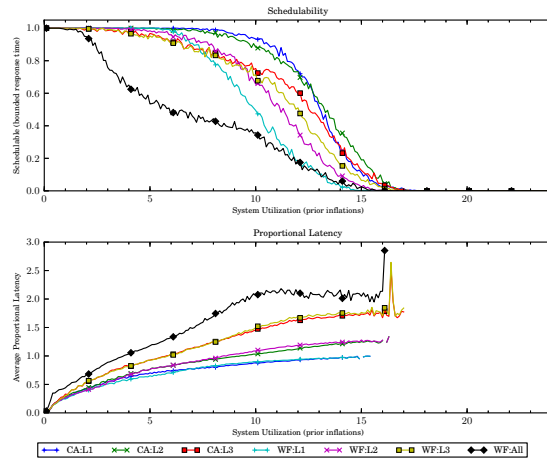


(b) With polluter overheads.

Figure 98: Results for *uni-medium* per-task utilization, *uni-moderate* period, *medium-weight* EWSS, and *uni-medium* height factor.

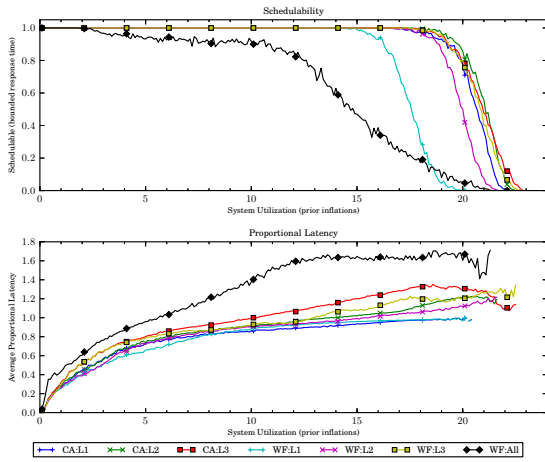


(a) Without polluter overheads.

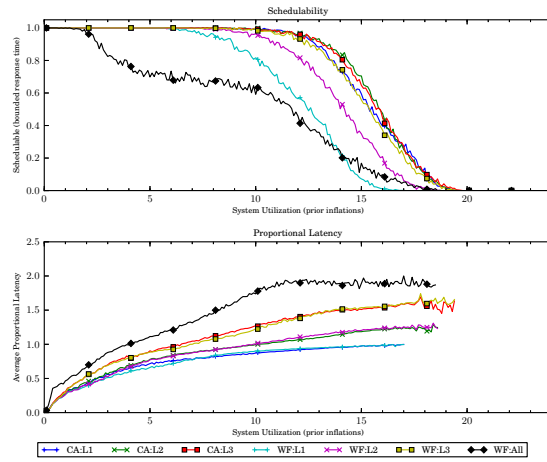


(b) With polluter overheads.

Figure 99: Results for *uni-medium* per-task utilization, *uni-moderate* period, *medium-weight* EWSS, and *uni-tall* height factor.

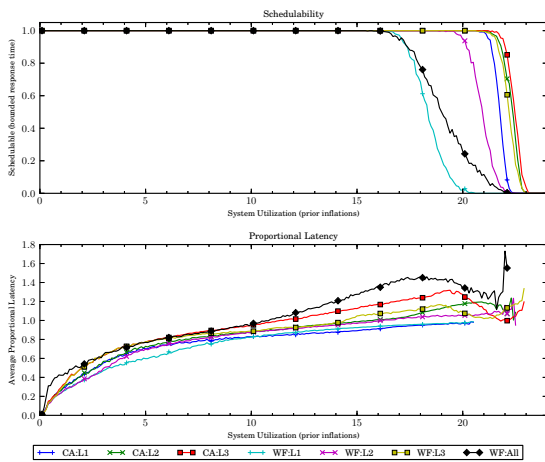


(a) Without polluter overheads.

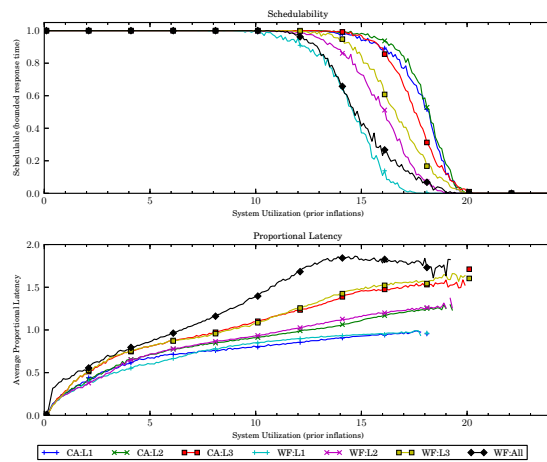


(b) With polluter overheads.

Figure 100: Results for *uni-medium* per-task utilization, *uni-moderate* period, *medium-weight* EWSS, and *pipeline* height factor.

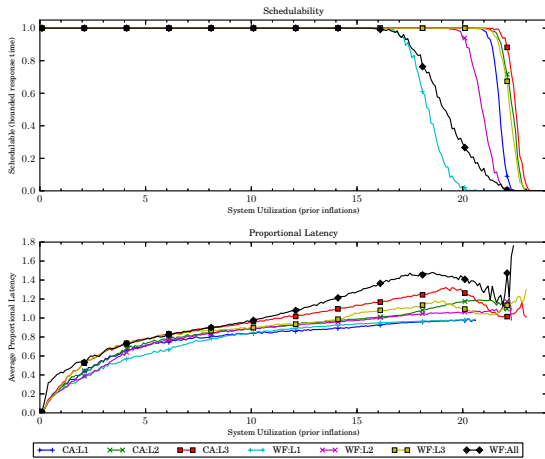


(a) Without polluter overheads.

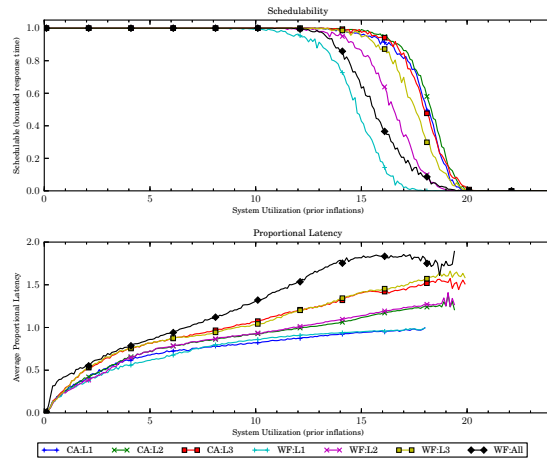


(b) With polluter overheads.

Figure 101: Results for *uni-medium* per-task utilization, *uni-long* period, *medium-weight* EWSS, and *uni-short* height factor.

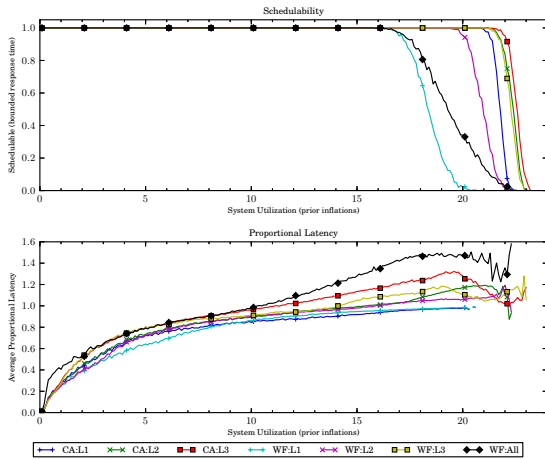


(a) Without polluter overheads.

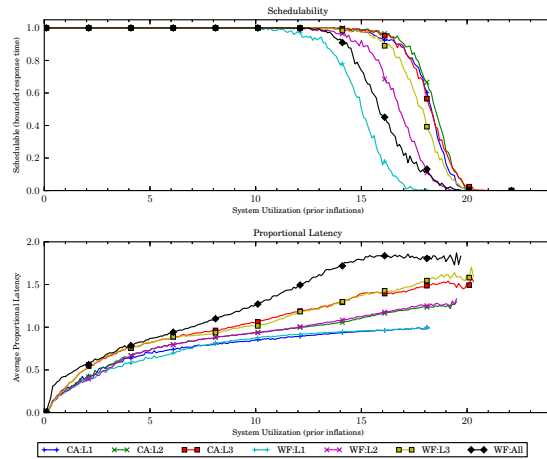


(b) With polluter overheads.

Figure 102: Results for *uni-medium* per-task utilization, *uni-long* period, *medium-weight* EWSS, and *uni-medium* height factor.

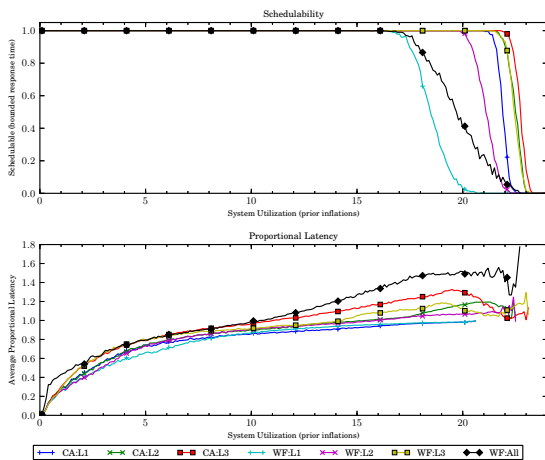


(a) Without polluter overheads.

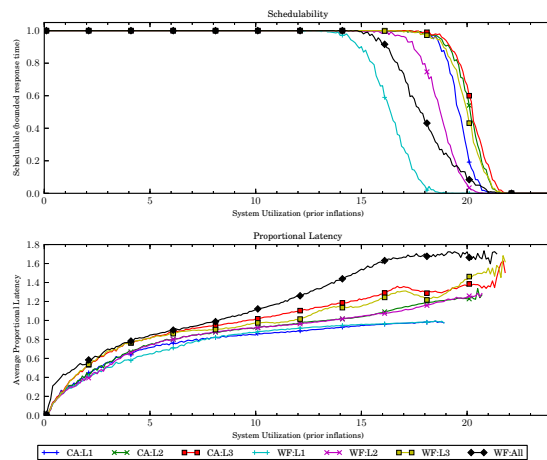


(b) With polluter overheads.

Figure 103: Results for *uni-medium* per-task utilization, *uni-long* period, *medium-weight* EWSS, and *uni-tall* height factor.

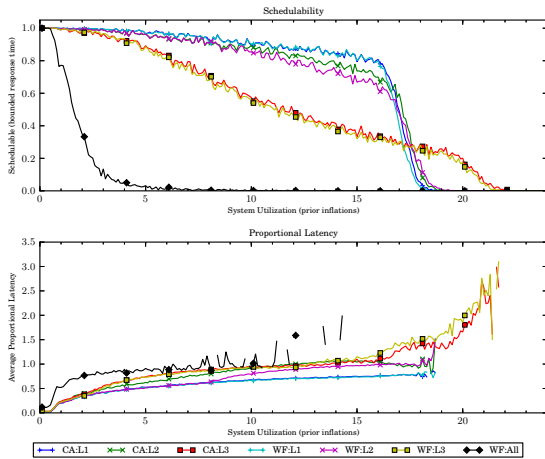


(a) Without polluter overheads.

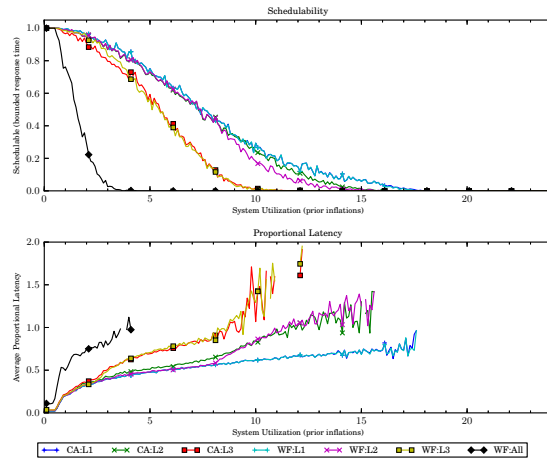


(b) With polluter overheads.

Figure 104: Results for *uni-medium* per-task utilization, *uni-long* period, *medium-weight* EWSS, and *pipeline* height factor.

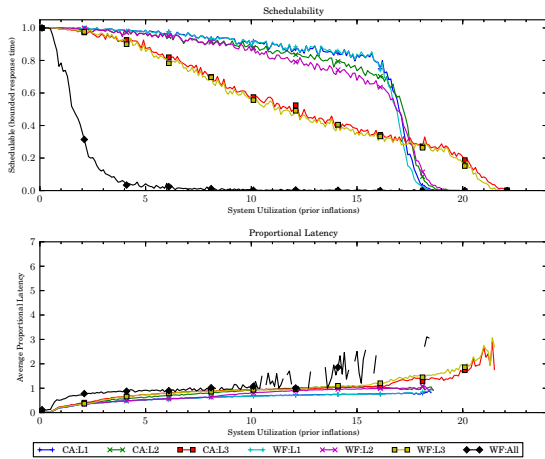


(a) Without polluter overheads.

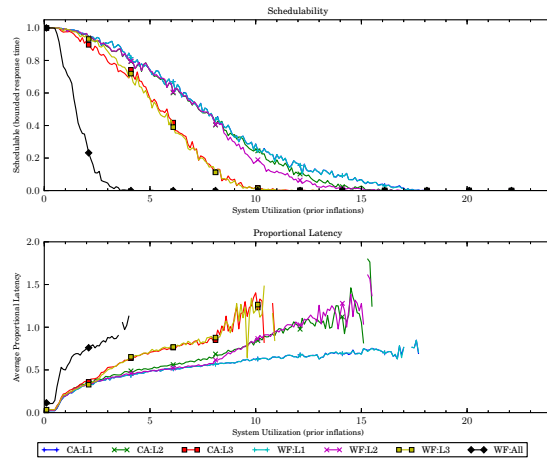


(b) With polluter overheads.

Figure 105: Results for *uni-heavy* per-task utilization, *uni-short* period, *medium-weight* EWSS, and *uni-short* height factor.

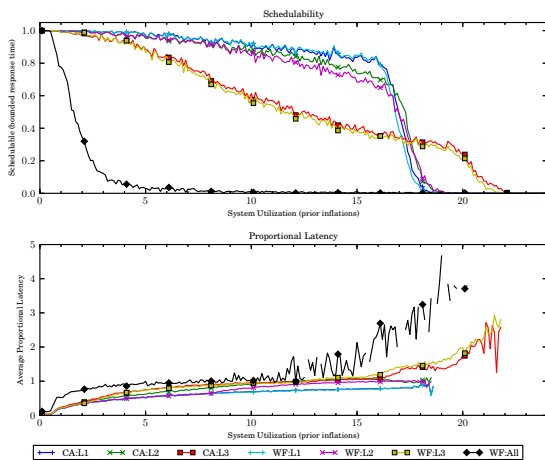


(a) Without polluter overheads.

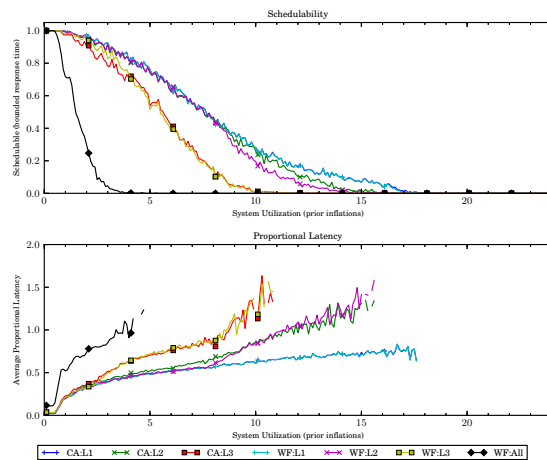


(b) With polluter overheads.

Figure 106: Results for *uni-heavy* per-task utilization, *uni-short* period, *medium-weight* EWSS, and *uni-medium* height factor.

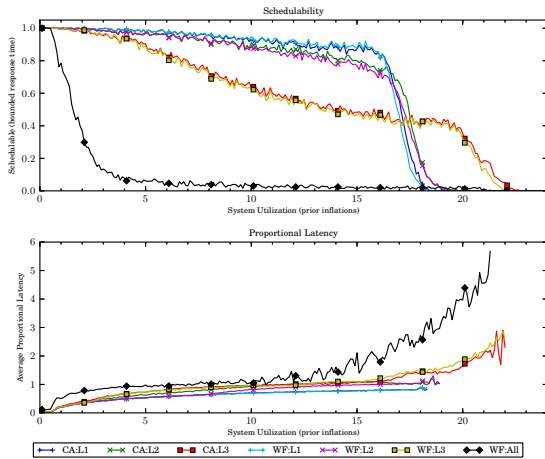


(a) Without polluter overheads.

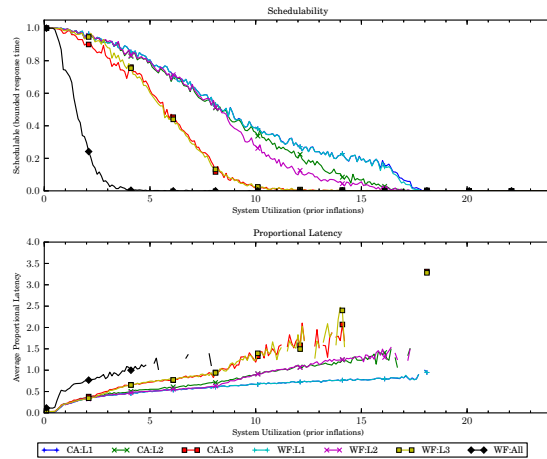


(b) With polluter overheads.

Figure 107: Results for *uni-heavy* per-task utilization, *uni-short* period, *medium-weight* EWSS, and *uni-tall* height factor.

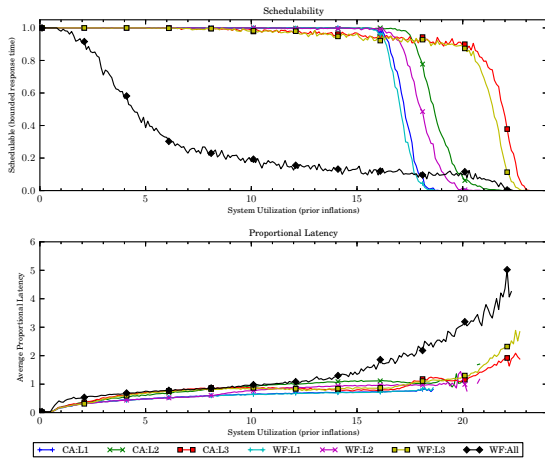


(a) Without polluter overheads.

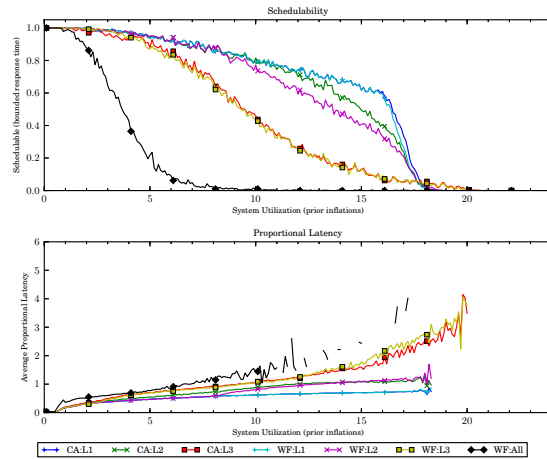


(b) With polluter overheads.

Figure 108: Results for *uni-heavy* per-task utilization, *uni-short* period, *medium-weight* EWSS, and *pipeline* height factor.

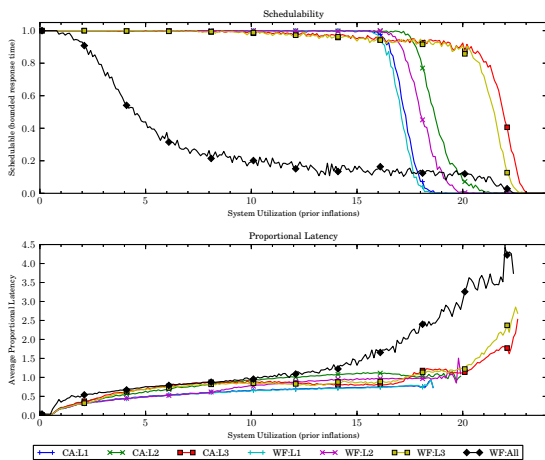


(a) Without polluter overheads.

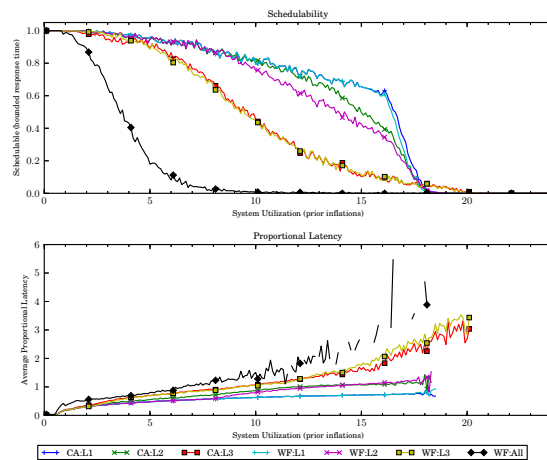


(b) With polluter overheads.

Figure 109: Results for *uni-heavy* per-task utilization, *uni-moderate* period, *medium-weight* EWSS, and *uni-short* height factor.

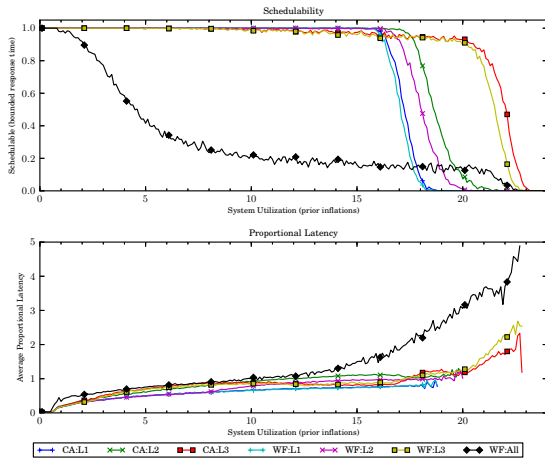


(a) Without polluter overheads.

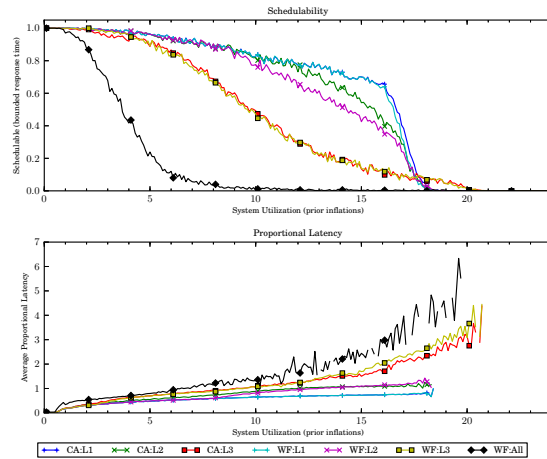


(b) With polluter overheads.

Figure 110: Results for *uni-heavy* per-task utilization, *uni-moderate* period, *medium-weight* EWSS, and *uni-medium* height factor.

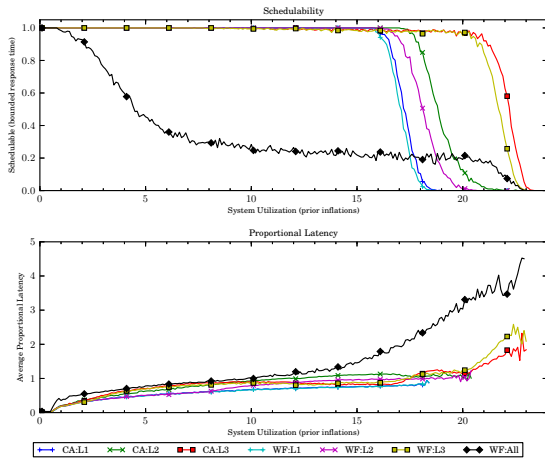


(a) Without polluter overheads.

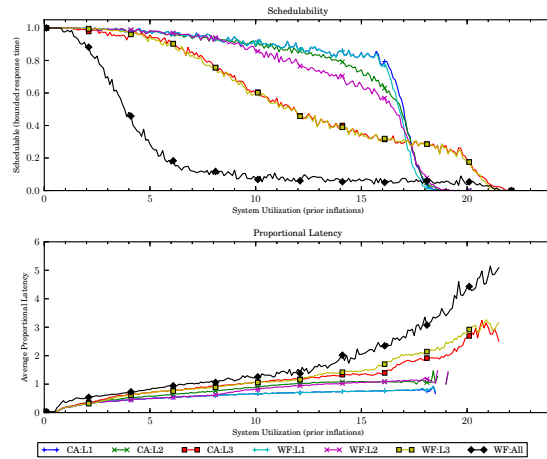


(b) With polluter overheads.

Figure 111: Results for *uni-heavy* per-task utilization, *uni-moderate* period, *medium-weight* EWSS, and *uni-tall* height factor.

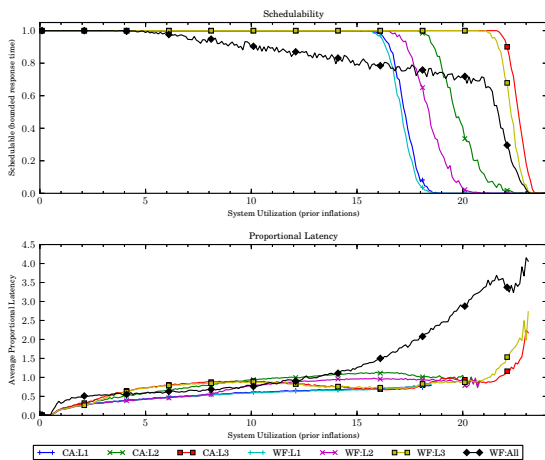


(a) Without polluter overheads.

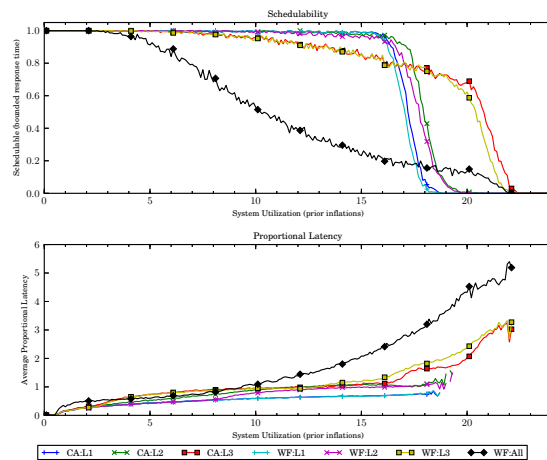


(b) With polluter overheads.

Figure 112: Results for *uni-heavy* per-task utilization, *uni-moderate* period, *medium-weight* EWSS, and *pipeline* height factor.

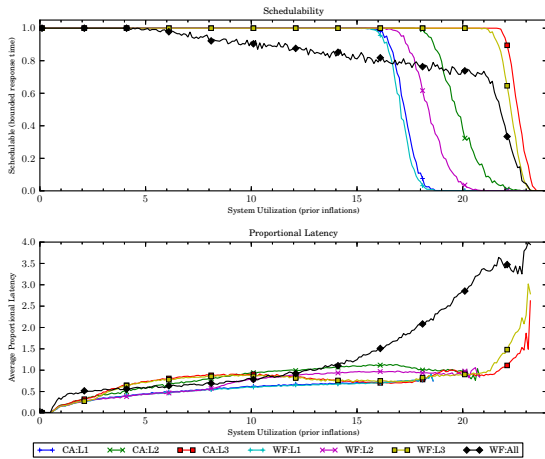


(a) Without polluter overheads.

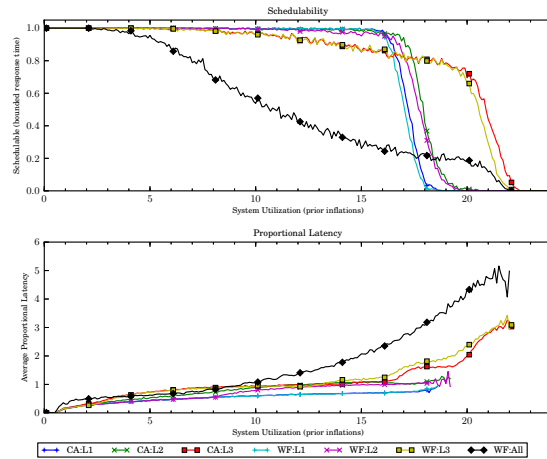


(b) With polluter overheads.

Figure 113: Results for *uni-heavy* per-task utilization, *uni-long* period, *medium-weight* EWSS, and *uni-short* height factor.

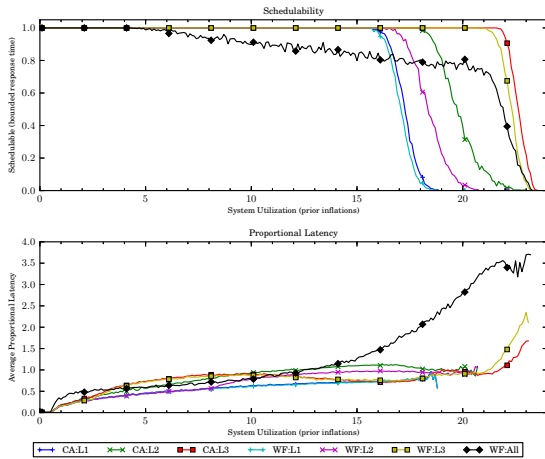


(a) Without polluter overheads.

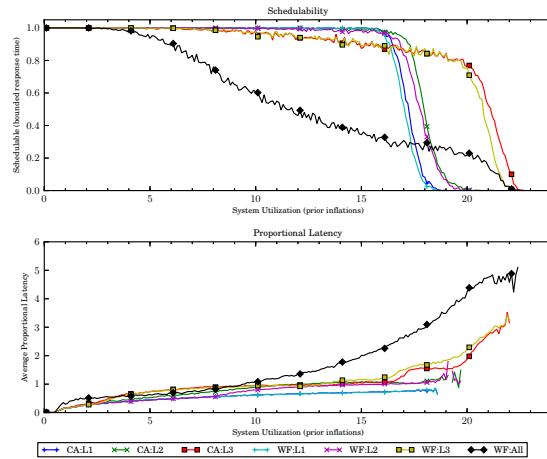


(b) With polluter overheads.

Figure 114: Results for *uni-heavy* per-task utilization, *uni-long* period, *medium-weight* EWSS, and *uni-medium* height factor.

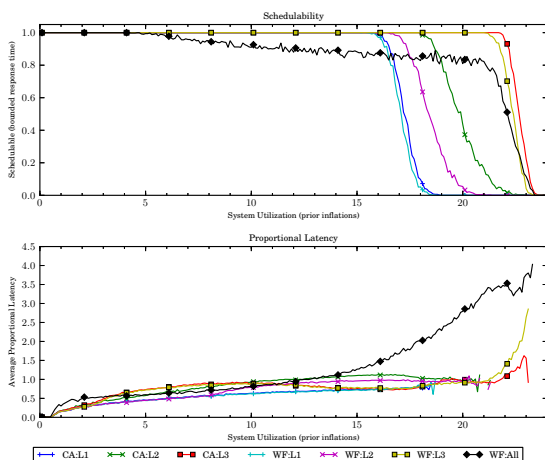


(a) Without polluter overheads.

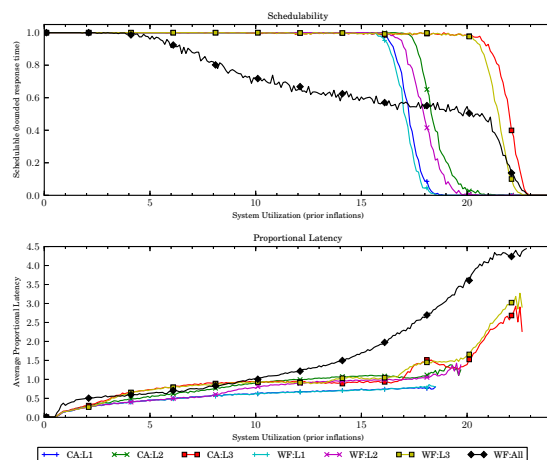


(b) With polluter overheads.

Figure 115: Results for *uni-heavy* per-task utilization, *uni-long* period, *medium-weight* EWSS, and *uni-tall* height factor.

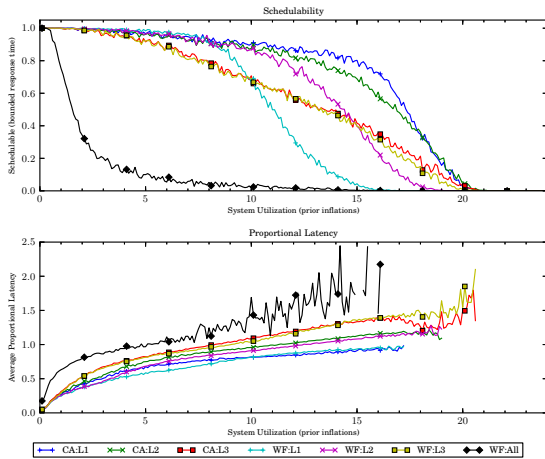


(a) Without polluter overheads.

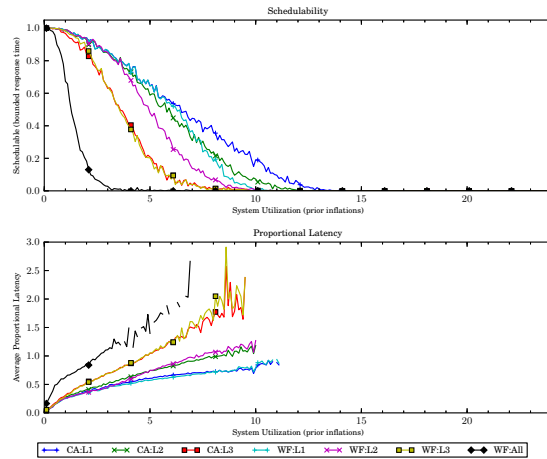


(b) With polluter overheads.

Figure 116: Results for *uni-heavy* per-task utilization, *uni-long* period, *medium-weight* EWSS, and *pipeline* height factor.

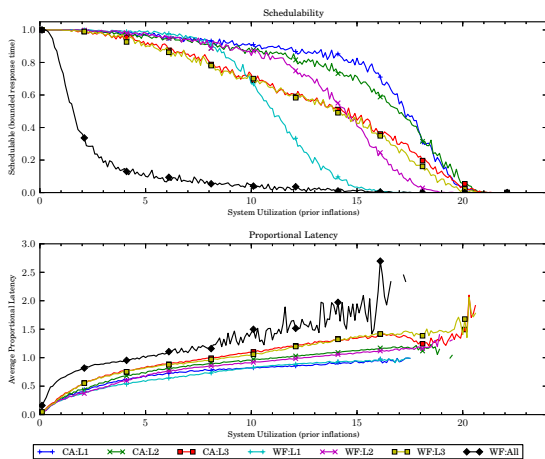


(a) Without polluter overheads.

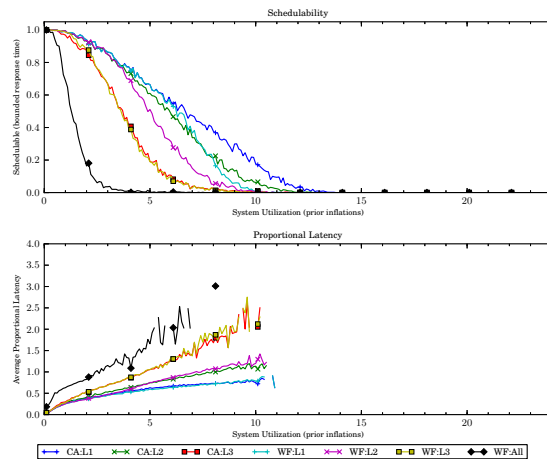


(b) With polluter overheads.

Figure 117: Results for *bimo-light* per-task utilization, *uni-short* period, *medium-weight* EWSS, and *uni-short* height factor.

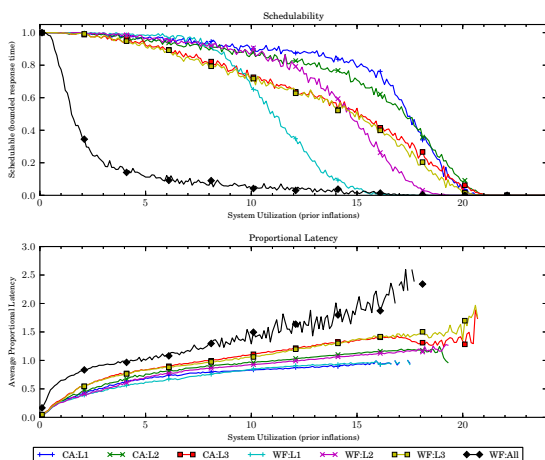


(a) Without polluter overheads.

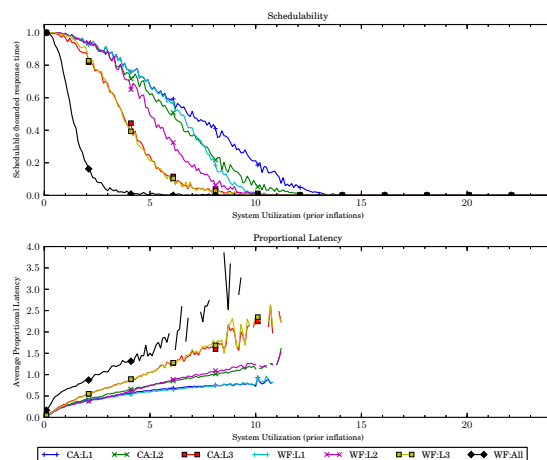


(b) With polluter overheads.

Figure 118: Results for *bimo-light* per-task utilization, *uni-short* period, *medium-weight* EWSS, and *uni-medium* height factor.

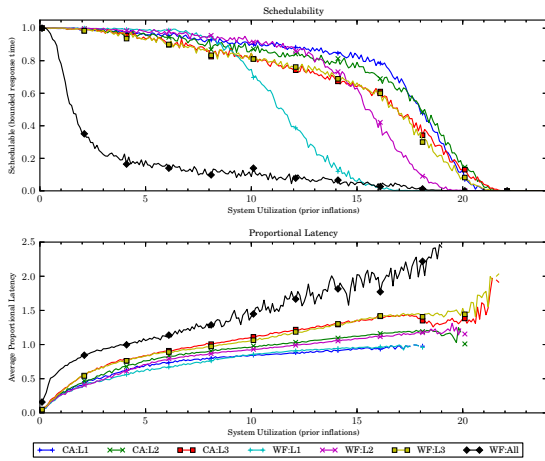


(a) Without polluter overheads.

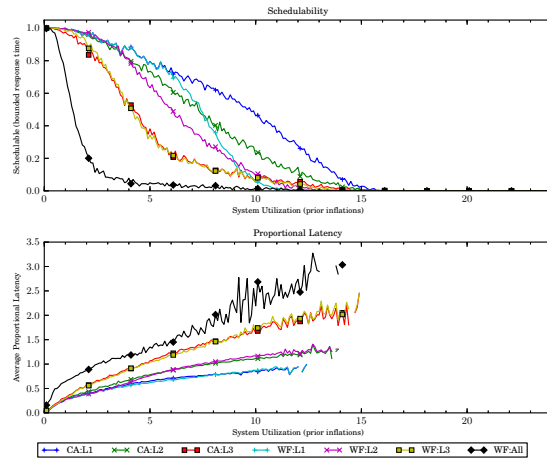


(b) With polluter overheads.

Figure 119: Results for *bimo-light* per-task utilization, *uni-short* period, *medium-weight* EWSS, and *uni-tall* height factor.

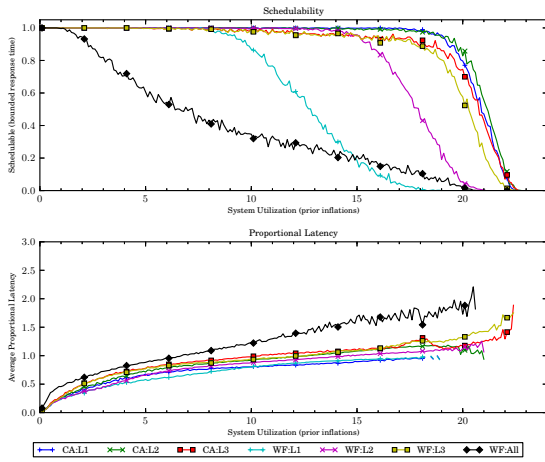


(a) Without polluter overheads.

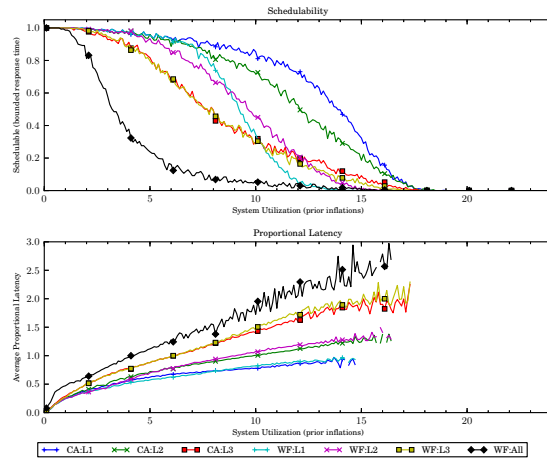


(b) With polluter overheads.

Figure 120: Results for *bimo-light* per-task utilization, *uni-short* period, *medium-weight* EWSS, and *pipeline* height factor.

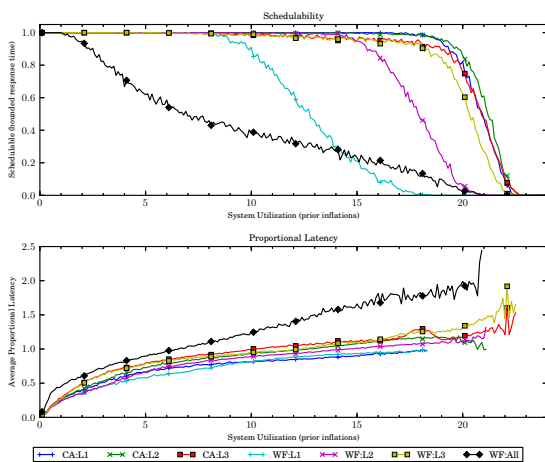


(a) Without polluter overheads.

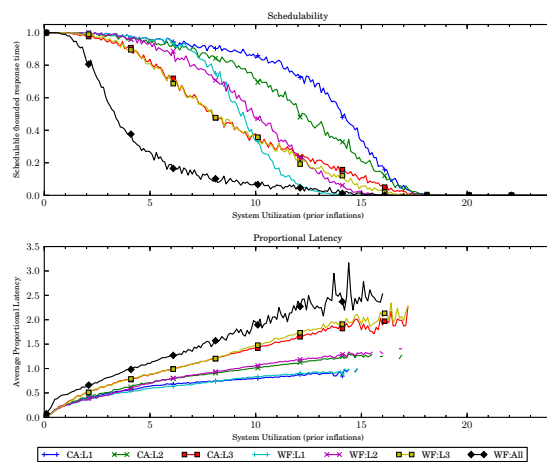


(b) With polluter overheads.

Figure 121: Results for *bimo-light* per-task utilization, *uni-moderate* period, *medium-weight* EWSS, and *uni-short* height factor.

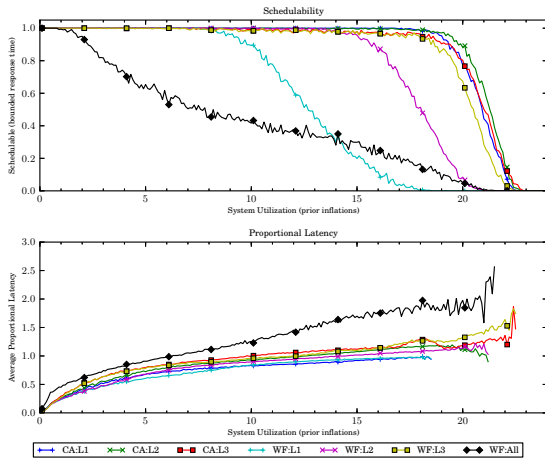


(a) Without polluter overheads.

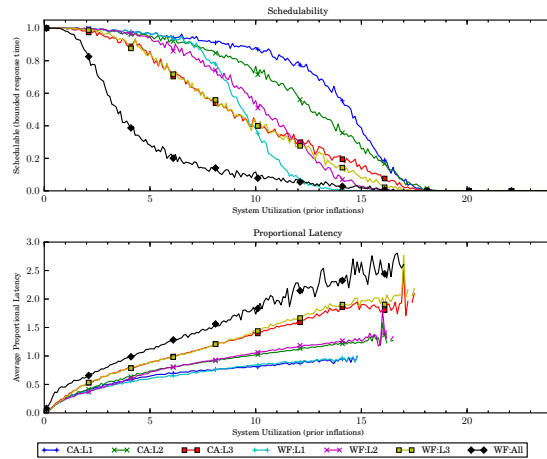


(b) With polluter overheads.

Figure 122: Results for *bimo-light* per-task utilization, *uni-moderate* period, *medium-weight* EWSS, and *uni-medium* height factor.

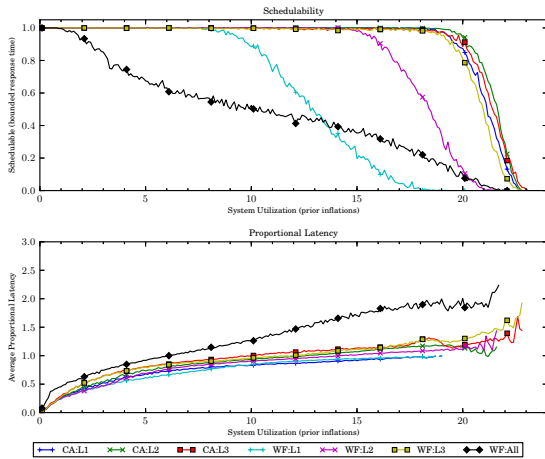


(a) Without polluter overheads.

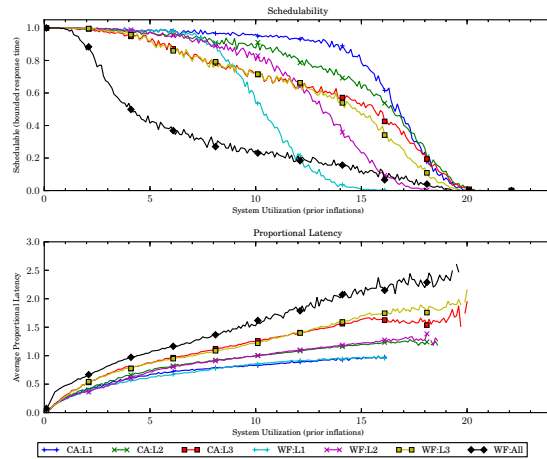


(b) With polluter overheads.

Figure 123: Results for *bimo-light* per-task utilization, *uni-moderate* period, *medium-weight* EWSS, and *uni-tall* height factor.

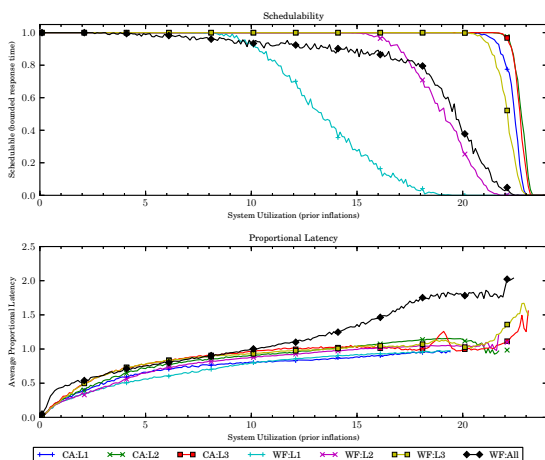


(a) Without polluter overheads.

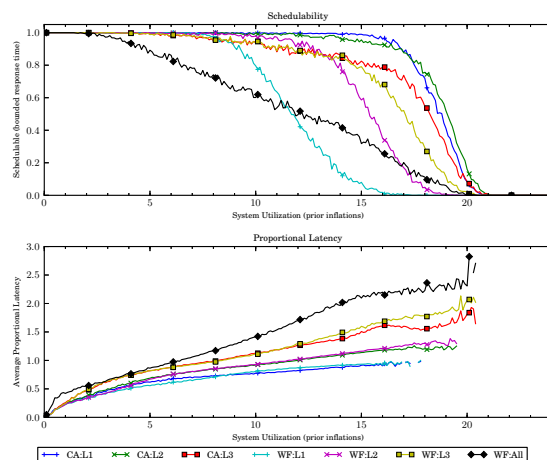


(b) With polluter overheads.

Figure 124: Results for *bimo-light* per-task utilization, *uni-moderate* period, *medium-weight* EWSS, and *pipeline* height factor.

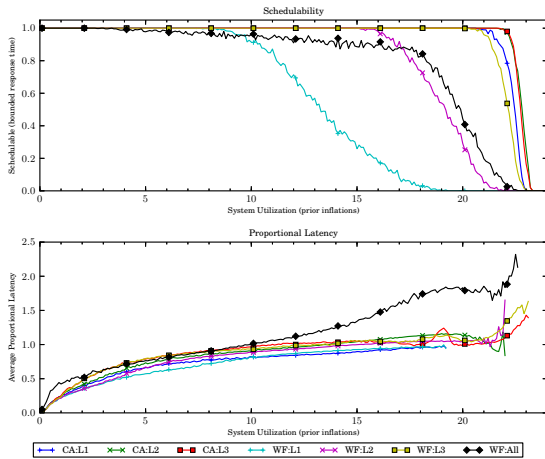


(a) Without polluter overheads.

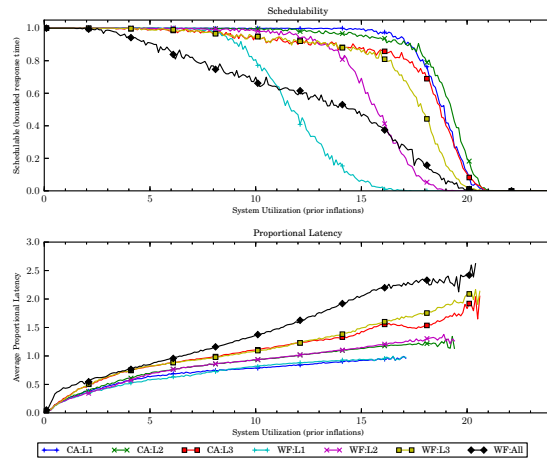


(b) With polluter overheads.

Figure 125: Results for *bimo-light* per-task utilization, *uni-long* period, *medium-weight* EWSS, and *uni-short* height factor.

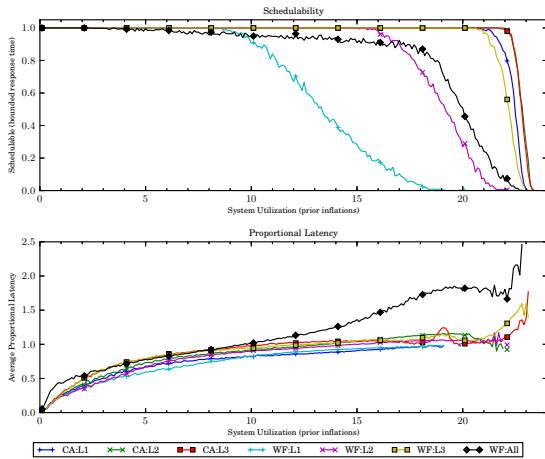


(a) Without polluter overheads.

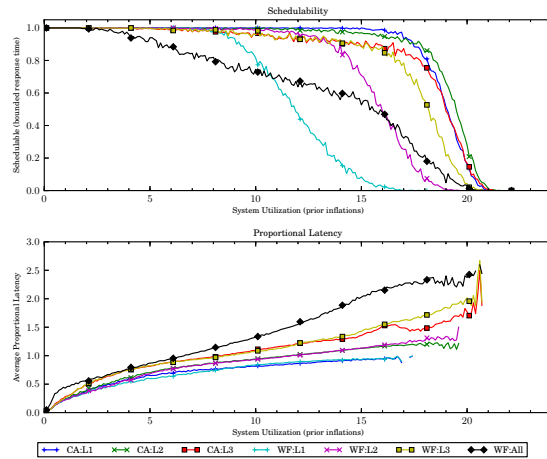


(b) With polluter overheads.

Figure 126: Results for *bimo-light* per-task utilization, *uni-long* period, *medium-weight* EWSS, and *uni-medium* height factor.

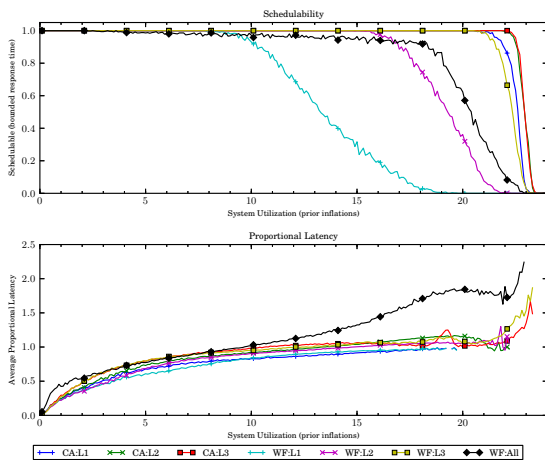


(a) Without polluter overheads.

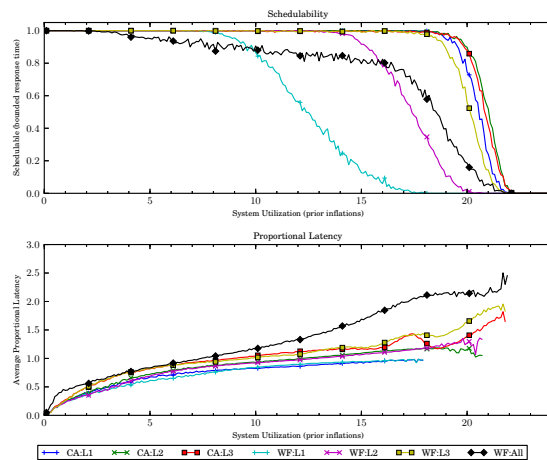


(b) With polluter overheads.

Figure 127: Results for *bimo-light* per-task utilization, *uni-long* period, *medium-weight* EWSS, and *uni-tall* height factor.

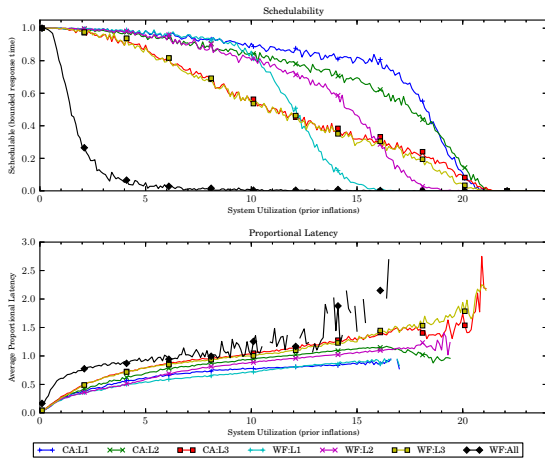


(a) Without polluter overheads.

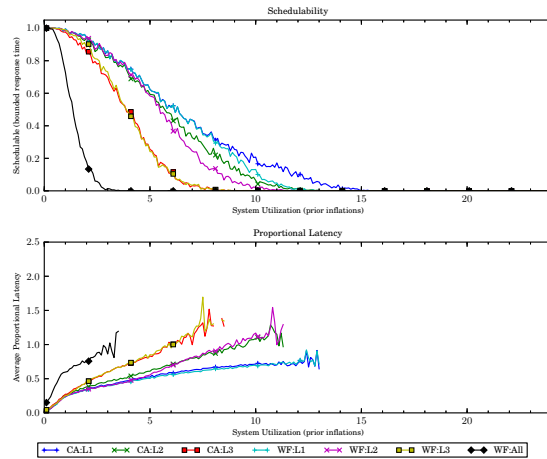


(b) With polluter overheads.

Figure 128: Results for *bimo-light* per-task utilization, *uni-long* period, *medium-weight* EWSS, and *pipeline* height factor.

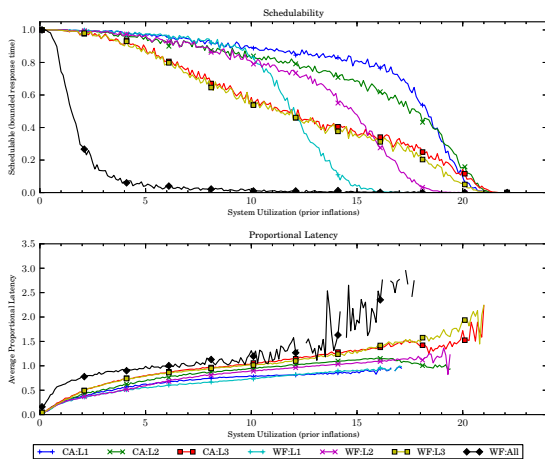


(a) Without polluter overheads.

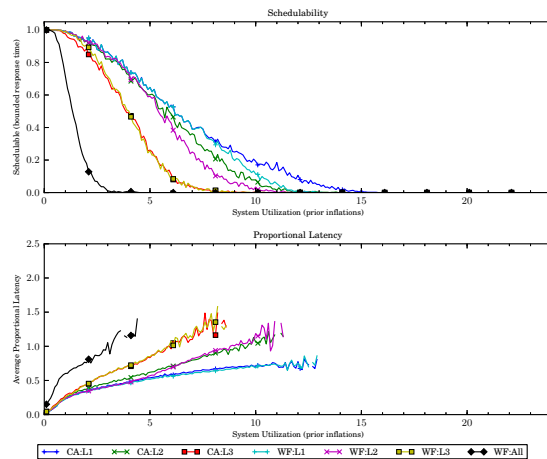


(b) With polluter overheads.

Figure 129: Results for *bimo-medium* per-task utilization, *uni-short* period, *medium-weight* EWSS, and *uni-short* height factor.

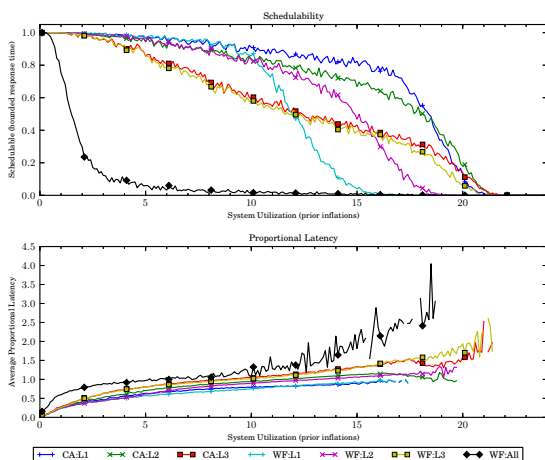


(a) Without polluter overheads.

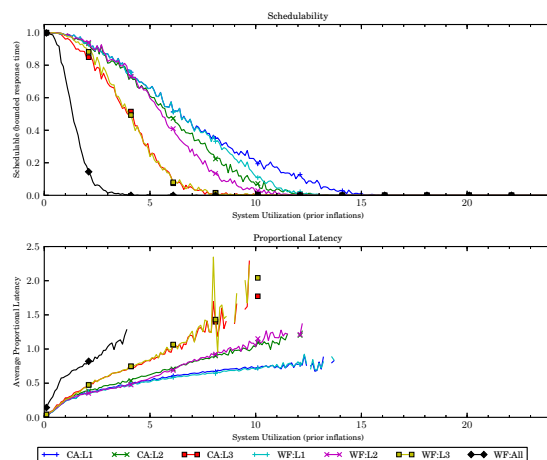


(b) With polluter overheads.

Figure 130: Results for *bimo-medium* per-task utilization, *uni-short* period, *medium-weight* EWSS, and *uni-medium* height factor.

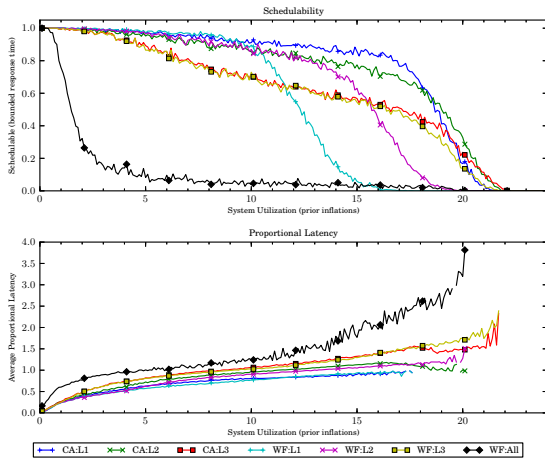


(a) Without polluter overheads.

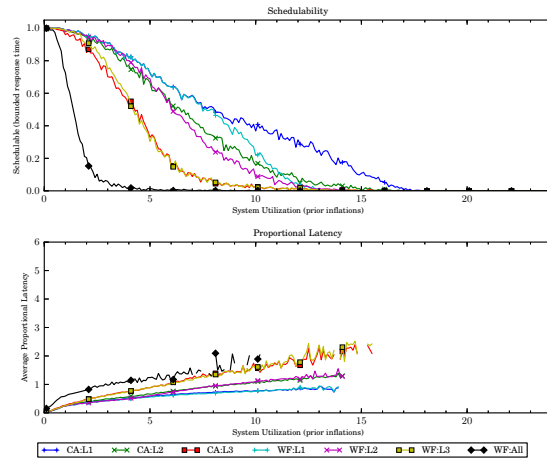


(b) With polluter overheads.

Figure 131: Results for *bimo-medium* per-task utilization, *uni-short* period, *medium-weight* EWSS, and *uni-tall* height factor.

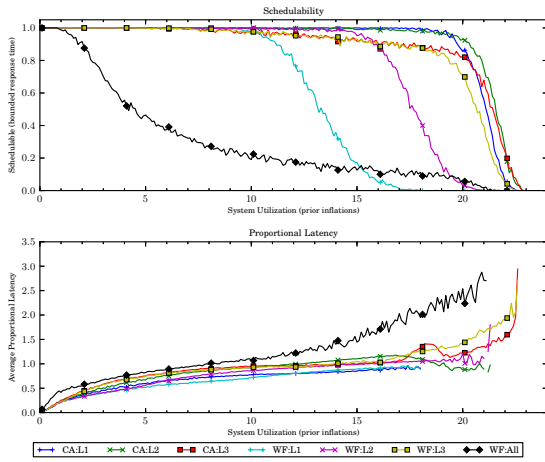


(a) Without polluter overheads.

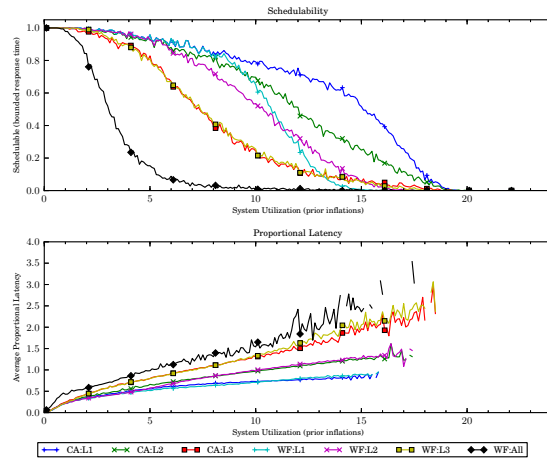


(b) With polluter overheads.

Figure 132: Results for *bimo-medium* per-task utilization, *uni-short* period, *medium-weight* EWSS, and *pipeline* height factor.

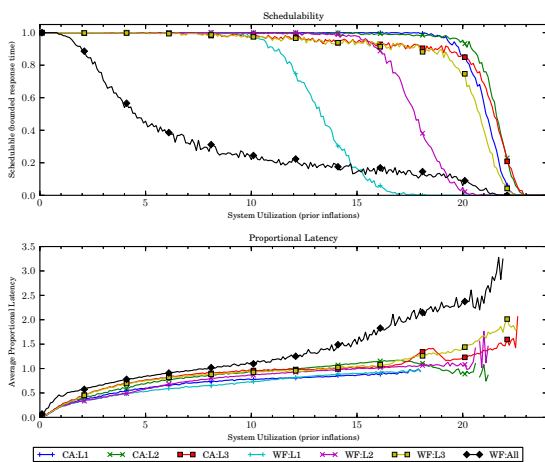


(a) Without polluter overheads.

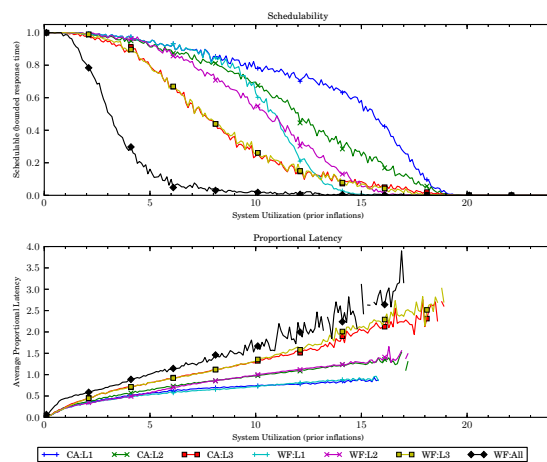


(b) With polluter overheads.

Figure 133: Results for *bimo-medium* per-task utilization, *uni-moderate* period, *medium-weight* EWSS, and *uni-short* height factor.

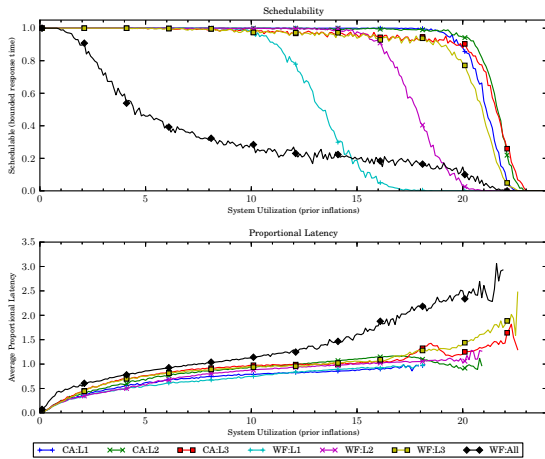


(a) Without polluter overheads.

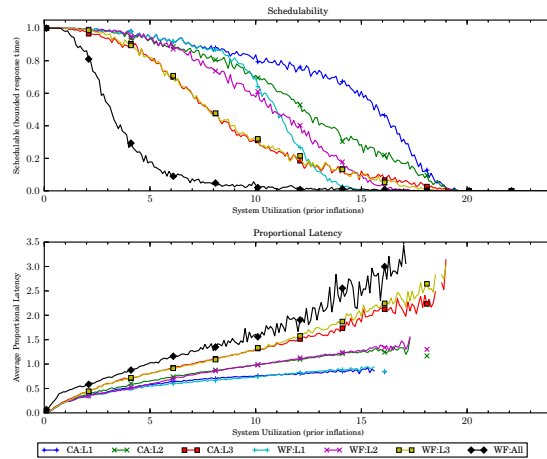


(b) With polluter overheads.

Figure 134: Results for *bimo-medium* per-task utilization, *uni-moderate* period, *medium-weight* EWSS, and *uni-medium* height factor.

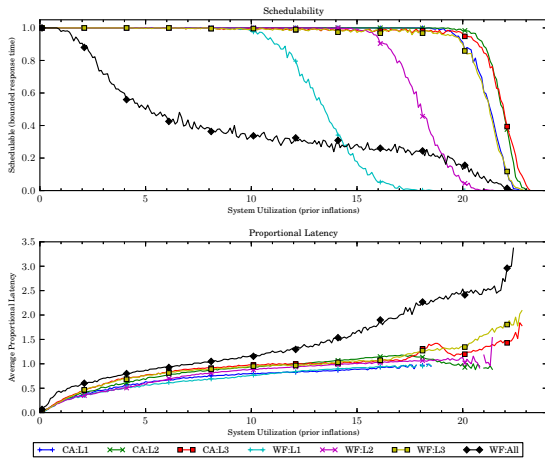


(a) Without polluter overheads.

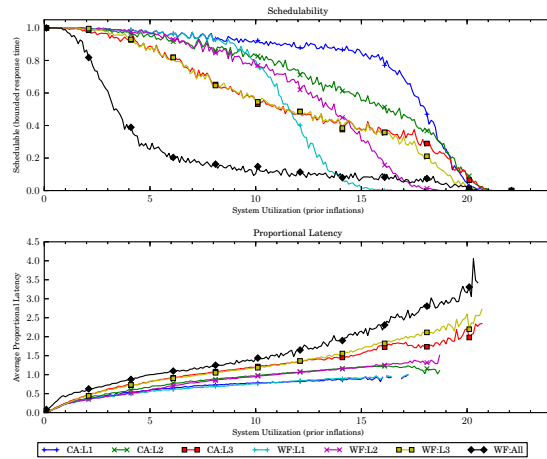


(b) With polluter overheads.

Figure 135: Results for *bimo-medium* per-task utilization, *uni-moderate* period, *medium-weight* EWSS, and *uni-tall* height factor.

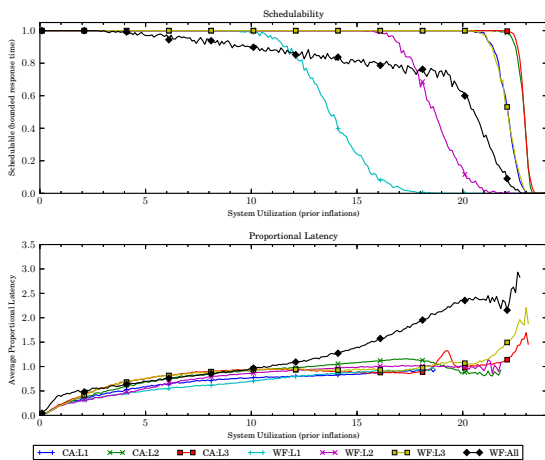


(a) Without polluter overheads.

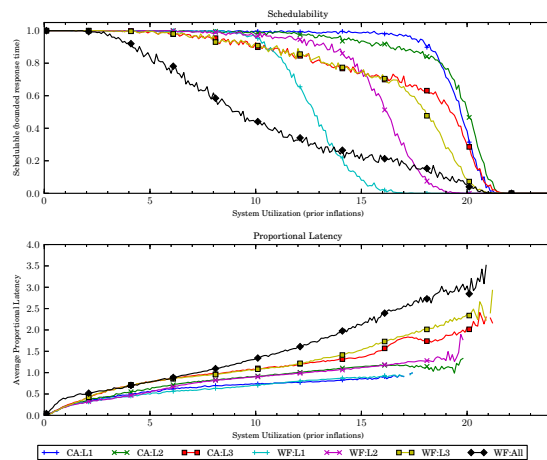


(b) With polluter overheads.

Figure 136: Results for *bimo-medium* per-task utilization, *uni-moderate* period, *medium-weight* EWSS, and *pipeline* height factor.

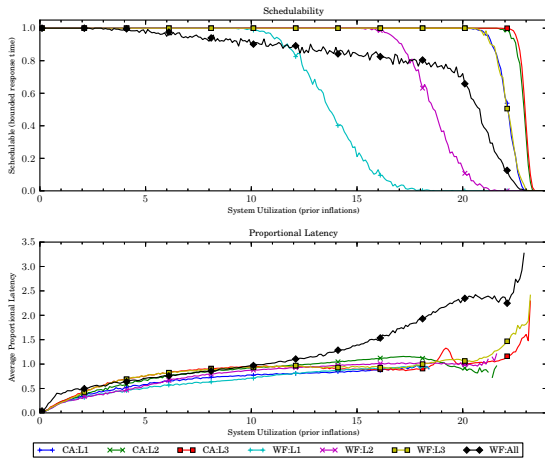


(a) Without polluter overheads.

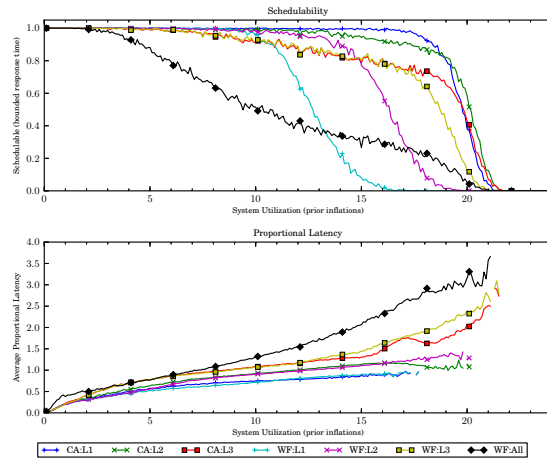


(b) With polluter overheads.

Figure 137: Results for *bimo-medium* per-task utilization, *uni-long* period, *medium-weight* EWSS, and *uni-short* height factor.

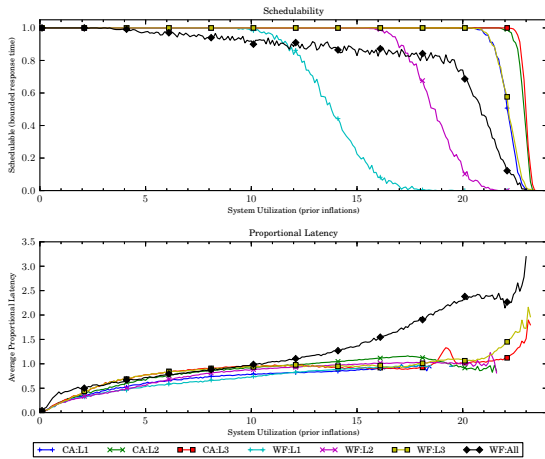


(a) Without polluter overheads.

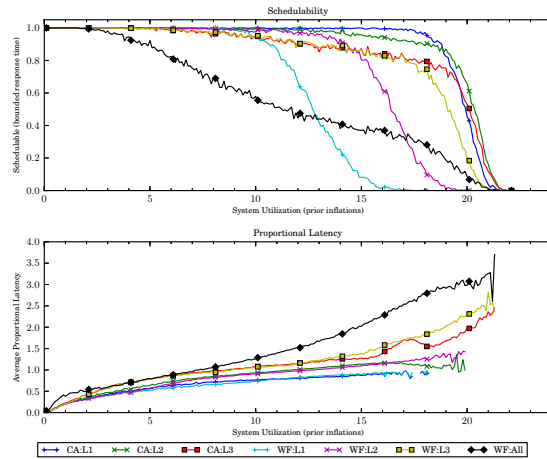


(b) With polluter overheads.

Figure 138: Results for *bimo-medium* per-task utilization, *uni-long* period, *medium-weight* EWSS, and *uni-medium* height factor.

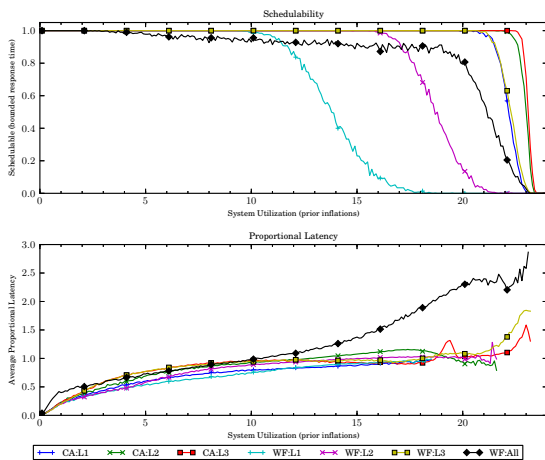


(a) Without polluter overheads.

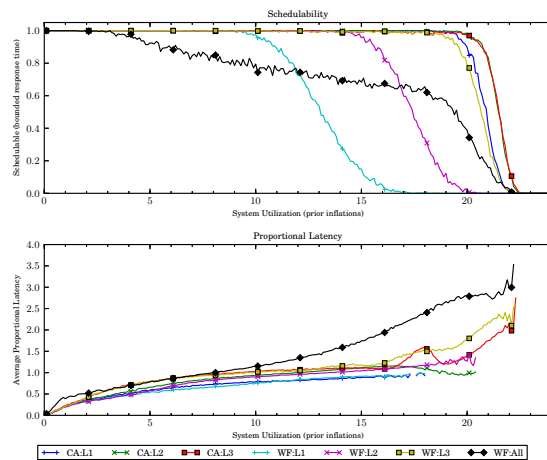


(b) With polluter overheads.

Figure 139: Results for *bimo-medium* per-task utilization, *uni-long* period, *medium-weight* EWSS, and *uni-tall* height factor.

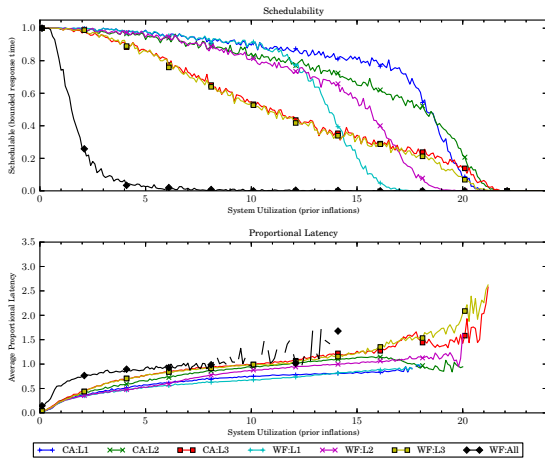


(a) Without polluter overheads.

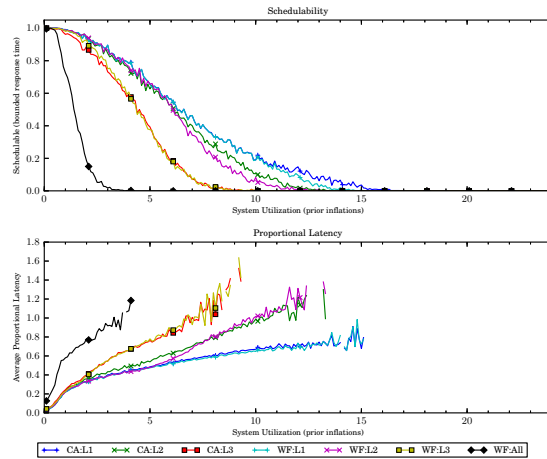


(b) With polluter overheads.

Figure 140: Results for *bimo-medium* per-task utilization, *uni-long* period, *medium-weight* EWSS, and *pipeline* height factor.

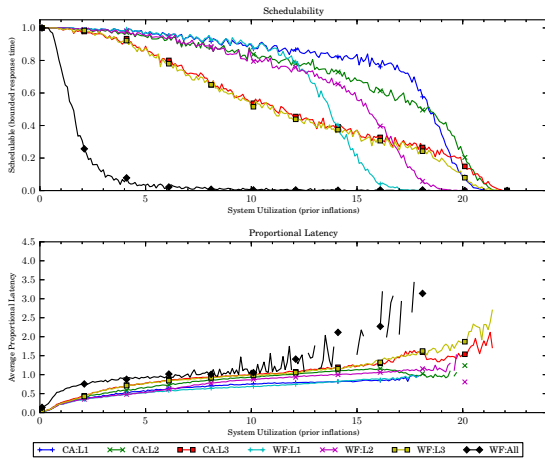


(a) Without polluter overheads.

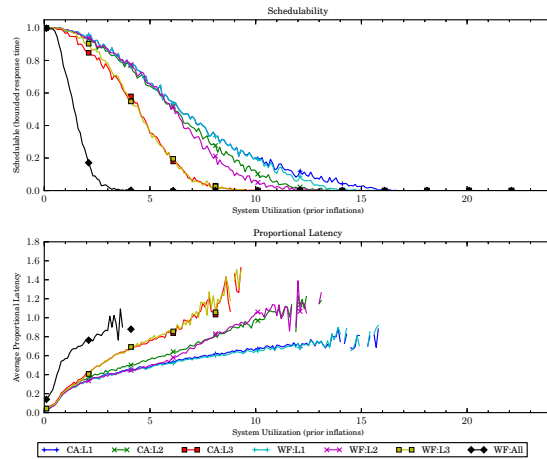


(b) With polluter overheads.

Figure 141: Results for *bimo-heavy* per-task utilization, *uni-short* period, *medium-weight* EWSS, and *uni-short* height factor.

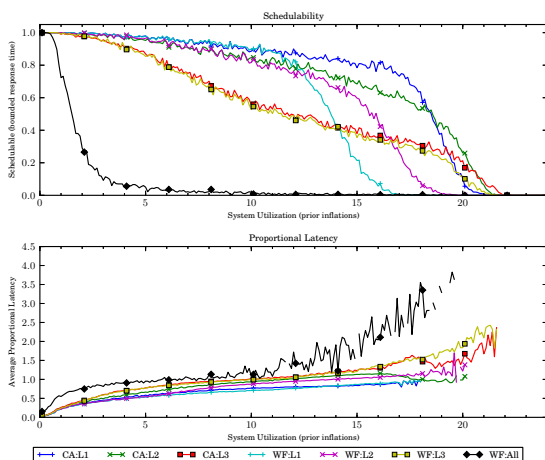


(a) Without polluter overheads.

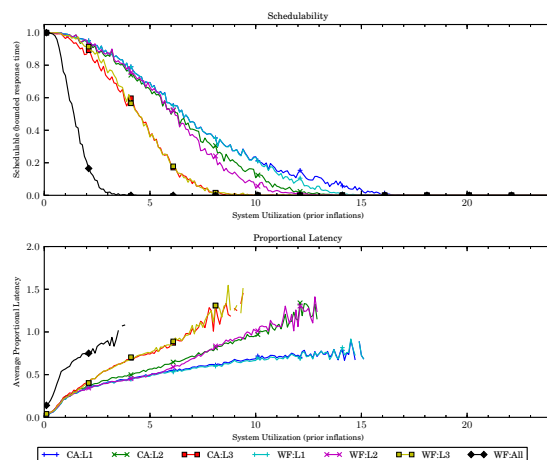


(b) With polluter overheads.

Figure 142: Results for *bimo-heavy* per-task utilization, *uni-short* period, *medium-weight* EWSS, and *uni-medium* height factor.

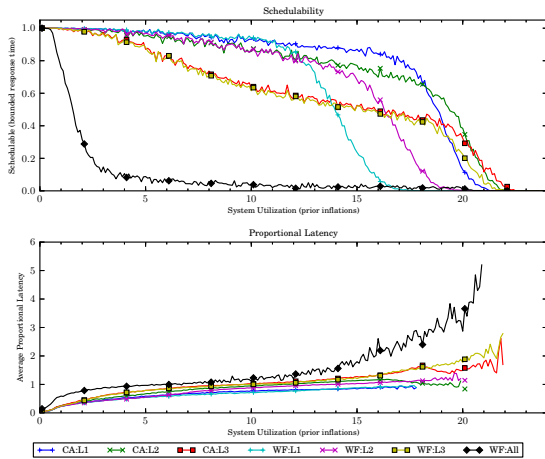


(a) Without polluter overheads.

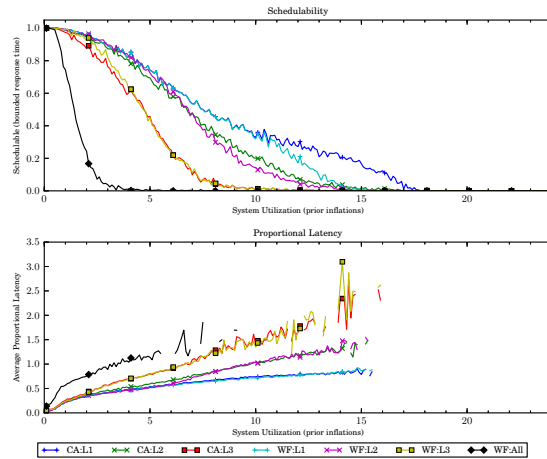


(b) With polluter overheads.

Figure 143: Results for *bimo-heavy* per-task utilization, *uni-short* period, *medium-weight* EWSS, and *uni-tall* height factor.

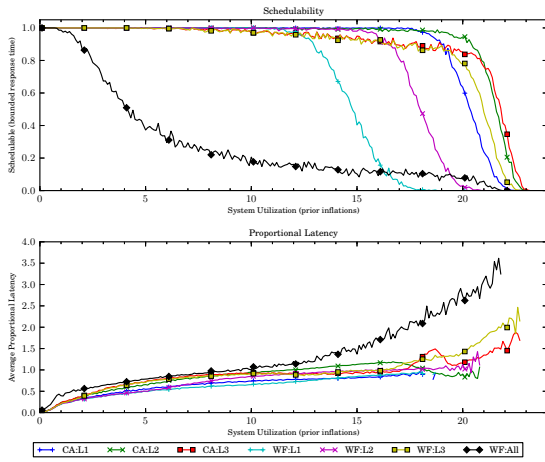


(a) Without polluter overheads.

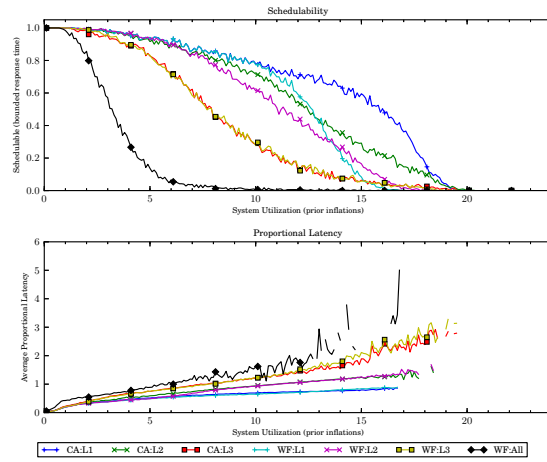


(b) With polluter overheads.

Figure 144: Results for *bimo-heavy* per-task utilization, *uni-short* period, *medium-weight* EWSS, and *pipeline* height factor.

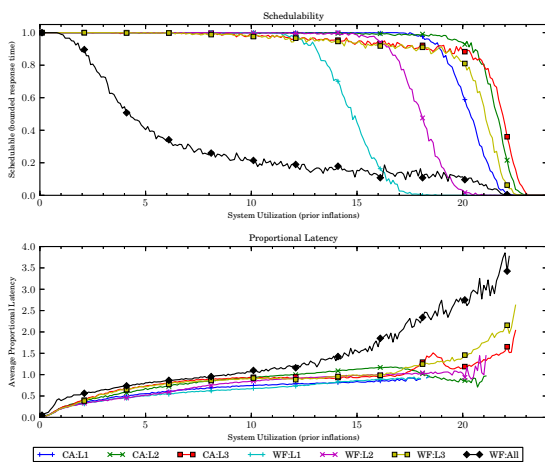


(a) Without polluter overheads.

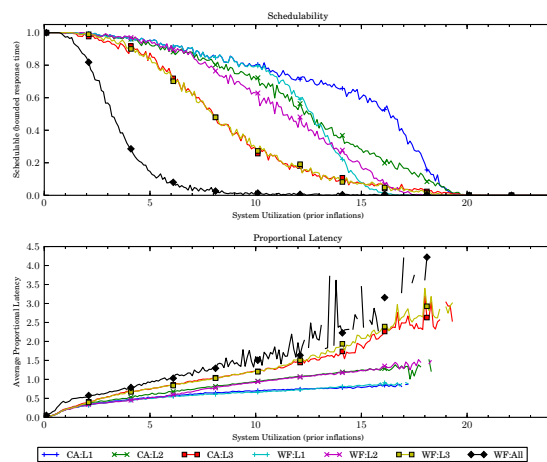


(b) With polluter overheads.

Figure 145: Results for *bimo-heavy* per-task utilization, *uni-moderate* period, *medium-weight* EWSS, and *uni-short* height factor.

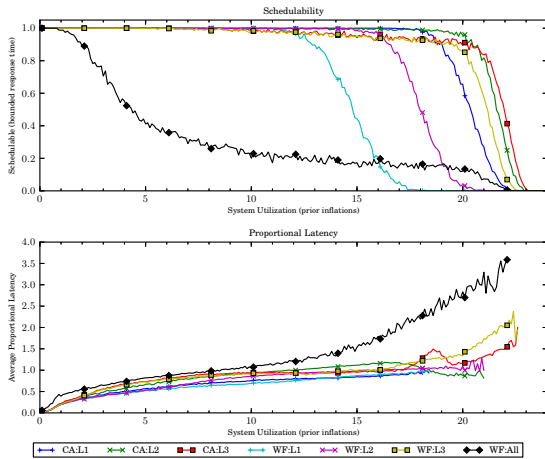


(a) Without polluter overheads.

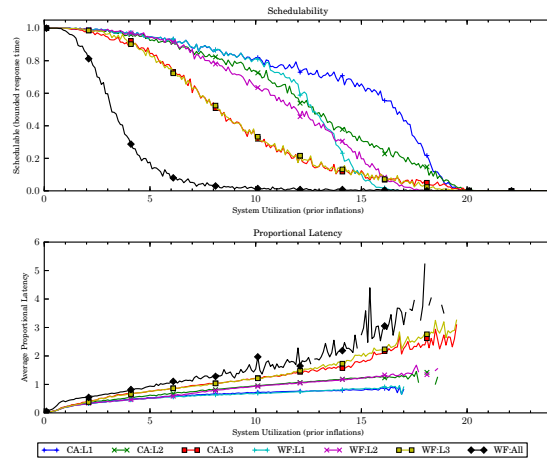


(b) With polluter overheads.

Figure 146: Results for *bimo-heavy* per-task utilization, *uni-moderate* period, *medium-weight* EWSS, and *uni-medium* height factor.

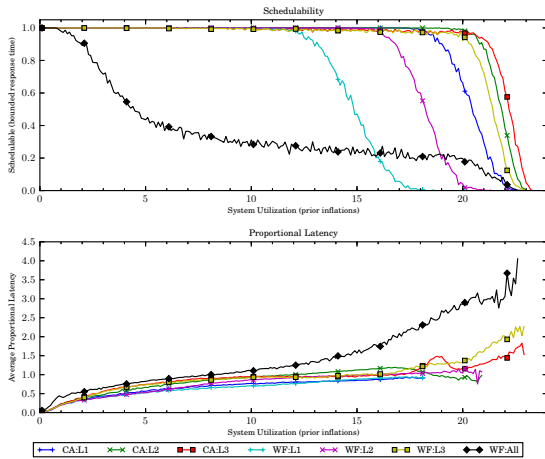


(a) Without polluter overheads.

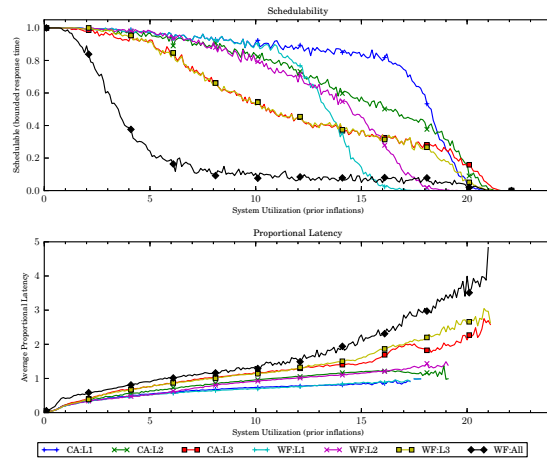


(b) With polluter overheads.

Figure 147: Results for *bimo-heavy* per-task utilization, *uni-moderate* period, *medium-weight* EWSS, and *uni-tall* height factor.

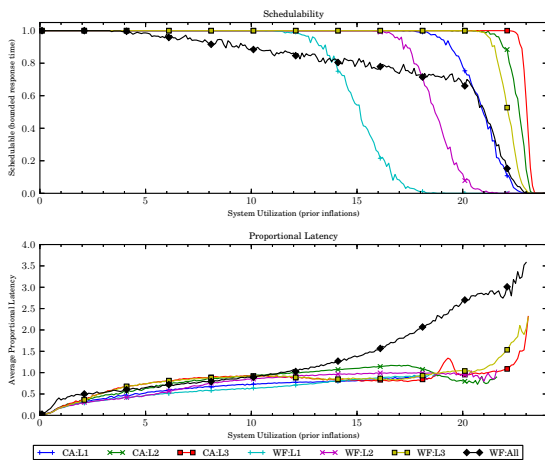


(a) Without polluter overheads.

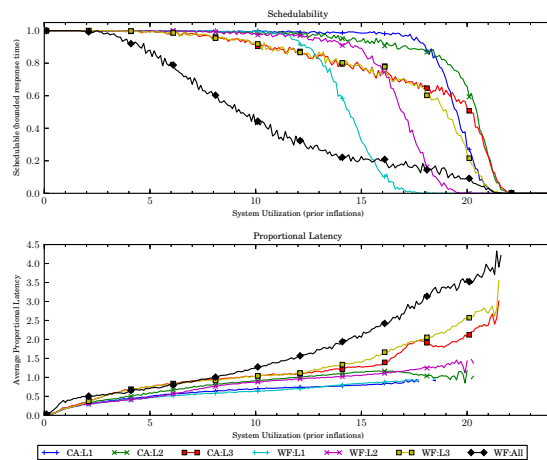


(b) With polluter overheads.

Figure 148: Results for *bimo-heavy* per-task utilization, *uni-moderate* period, *medium-weight* EWSS, and *pipeline* height factor.

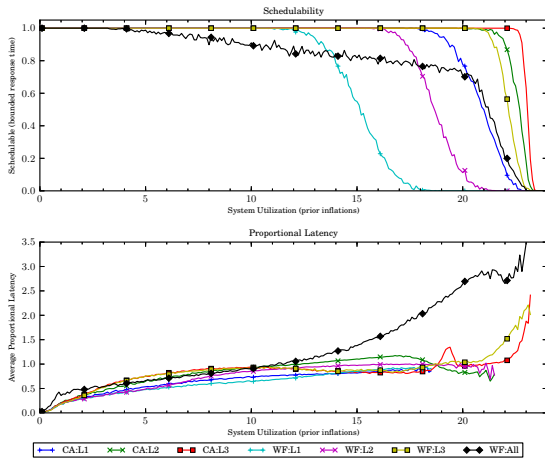


(a) Without polluter overheads.

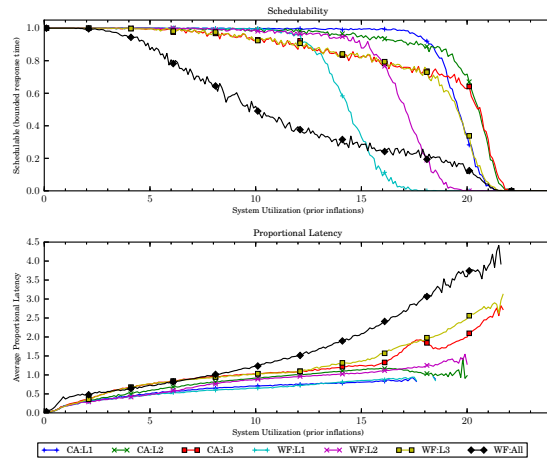


(b) With polluter overheads.

Figure 149: Results for *bimo-heavy* per-task utilization, *uni-long* period, *medium-weight* EWSS, and *uni-short* height factor.

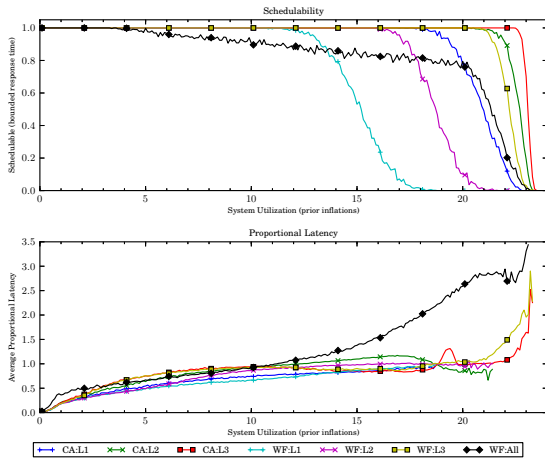


(a) Without polluter overheads.

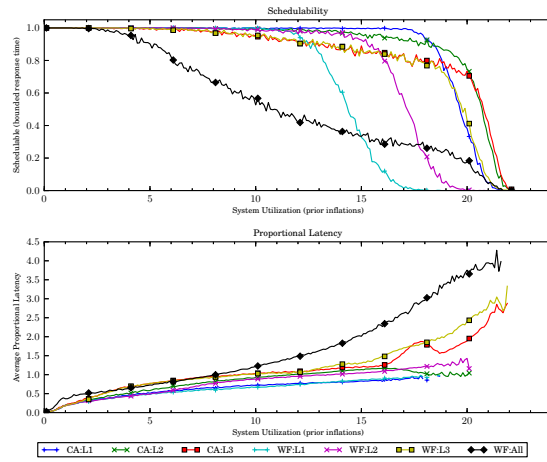


(b) With polluter overheads.

Figure 150: Results for *bimo-heavy* per-task utilization, *uni-long* period, *medium-weight* EWSS, and *uni-medium* height factor.

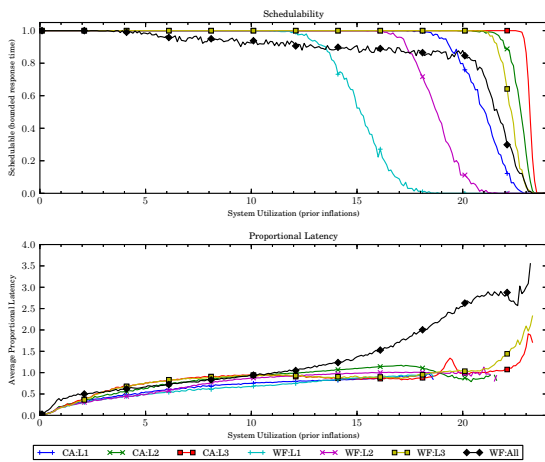


(a) Without polluter overheads.

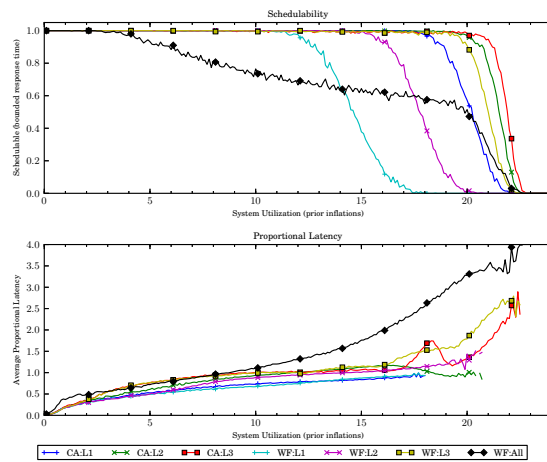


(b) With polluter overheads.

Figure 151: Results for *bimo-heavy* per-task utilization, *uni-long* period, *medium-weight* EWSS, and *uni-tall* height factor.

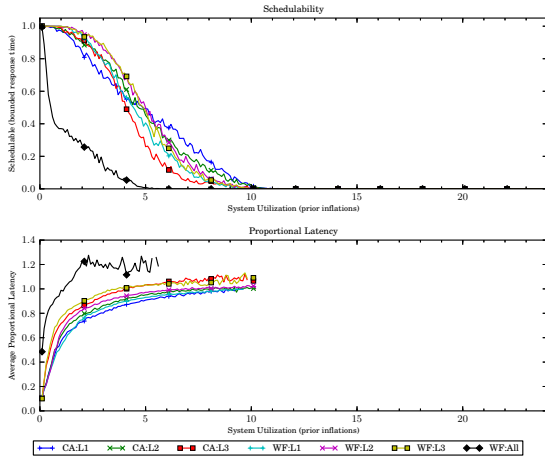


(a) Without polluter overheads.

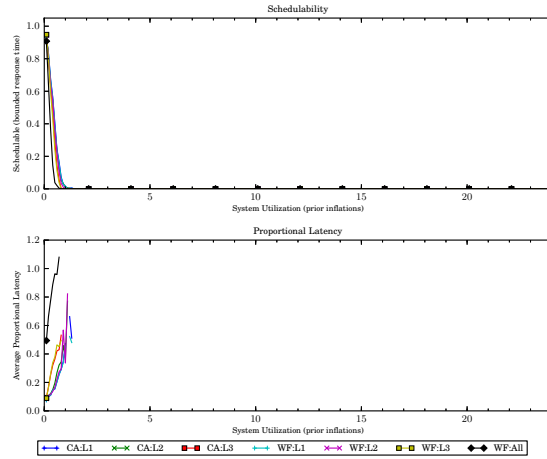


(b) With polluter overheads.

Figure 152: Results for *bimo-heavy* per-task utilization, *uni-long* period, *medium-weight* EWSS, and *pipeline* height factor.

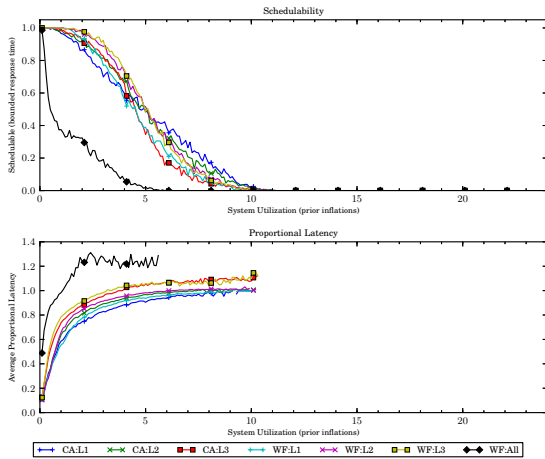


(a) Without polluter overheads.

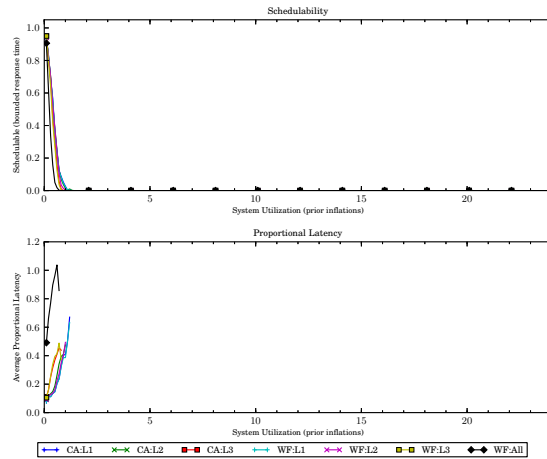


(b) With polluter overheads.

Figure 153: Results for *uni-light* per-task utilization, *uni-short* period, *heavy-weight* EWSS, and *uni-short* height factor.

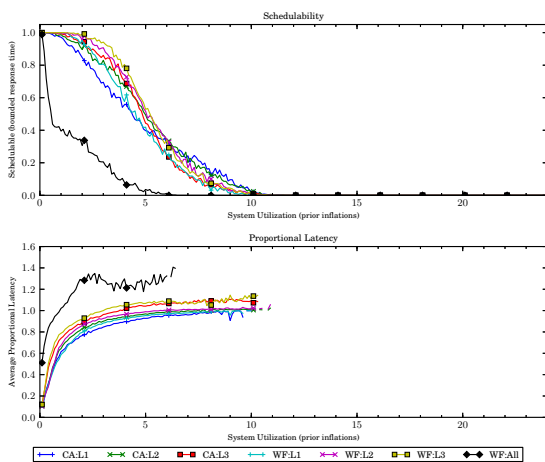


(a) Without polluter overheads.

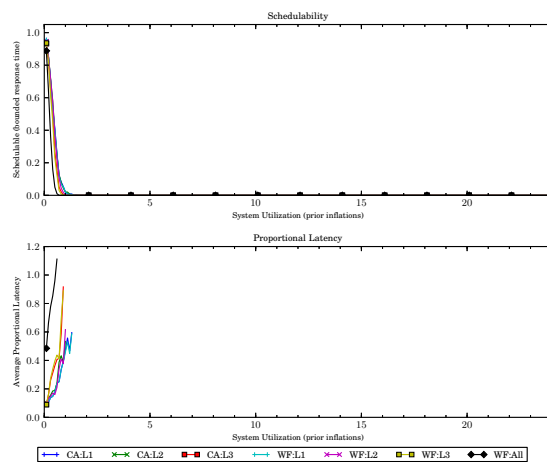


(b) With polluter overheads.

Figure 154: Results for *uni-light* per-task utilization, *uni-short* period, *heavy-weight* EWSS, and *uni-medium* height factor.

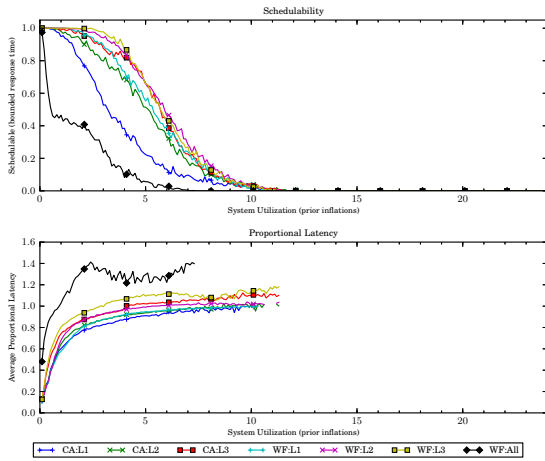


(a) Without polluter overheads.

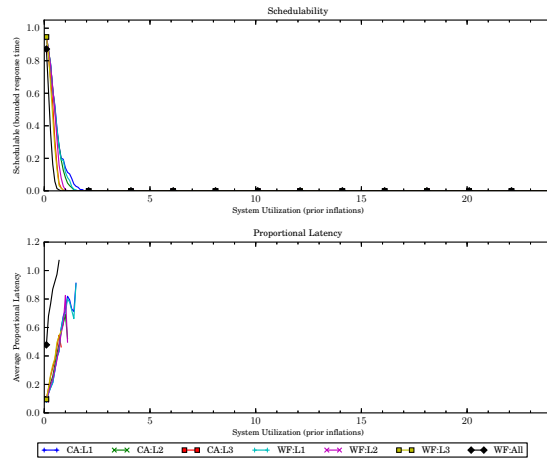


(b) With polluter overheads.

Figure 155: Results for *uni-light* per-task utilization, *uni-short* period, *heavy-weight* EWSS, and *uni-tall* height factor.

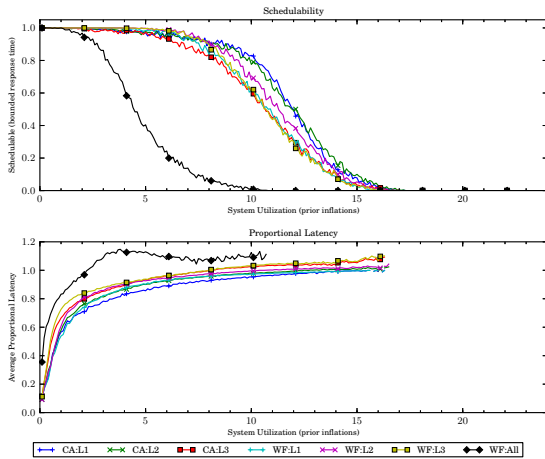


(a) Without polluter overheads.

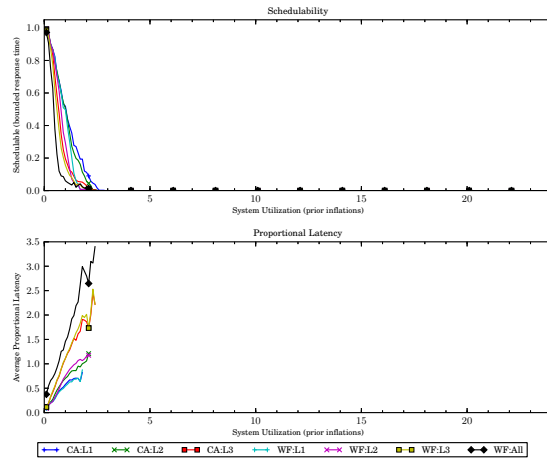


(b) With polluter overheads.

Figure 156: Results for *uni-light* per-task utilization, *uni-short* period, *heavy-weight* EWSS, and *pipeline* height factor.

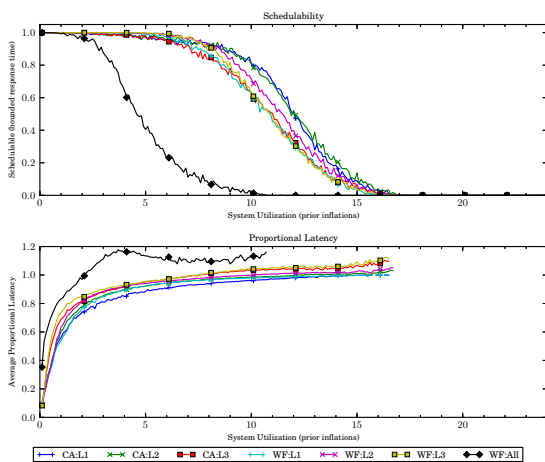


(a) Without polluter overheads.

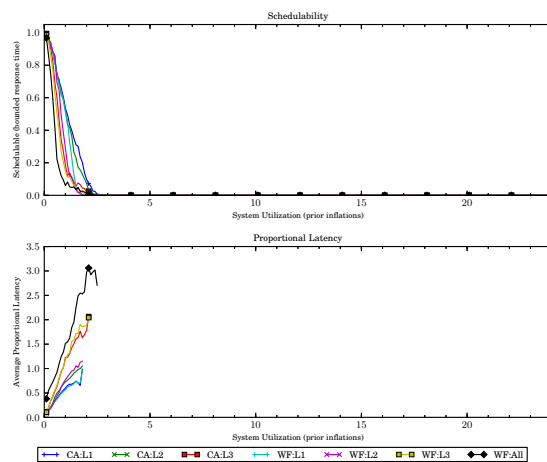


(b) With polluter overheads.

Figure 157: Results for *uni-light* per-task utilization, *uni-moderate* period, *heavy-weight* EWSS, and *uni-short* height factor.

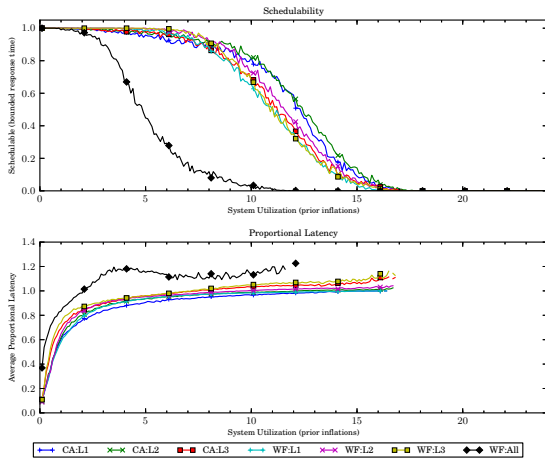


(a) Without polluter overheads.

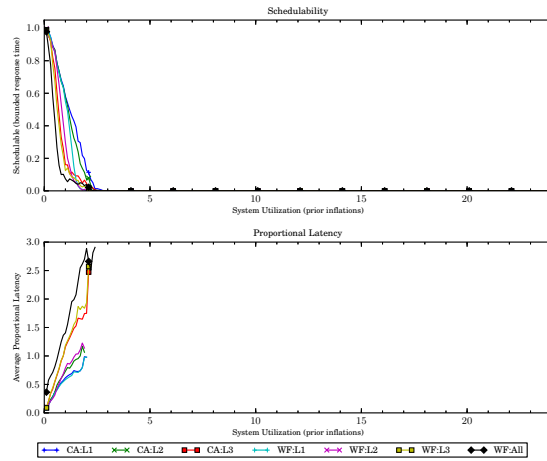


(b) With polluter overheads.

Figure 158: Results for *uni-light* per-task utilization, *uni-moderate* period, *heavy-weight* EWSS, and *uni-medium* height factor.

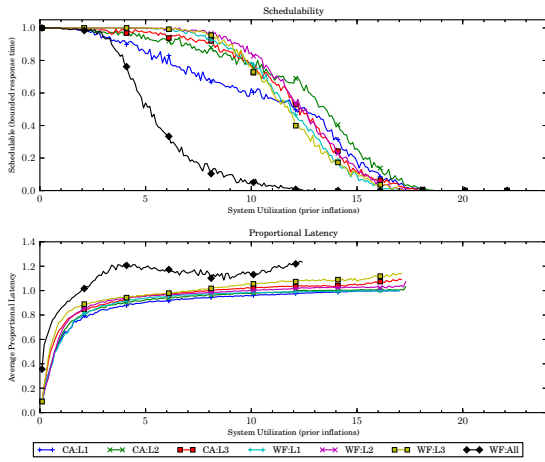


(a) Without polluter overheads.

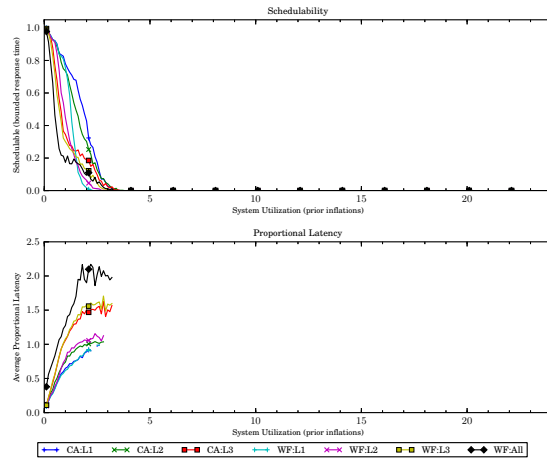


(b) With polluter overheads.

Figure 159: Results for *uni-light* per-task utilization, *uni-moderate* period, *heavy-weight* EWSS, and *uni-tall* height factor.

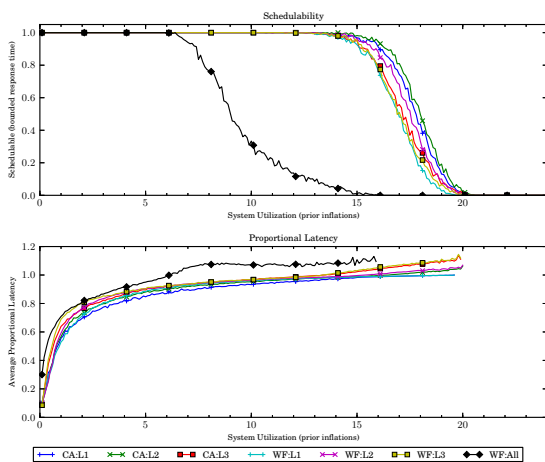


(a) Without polluter overheads.

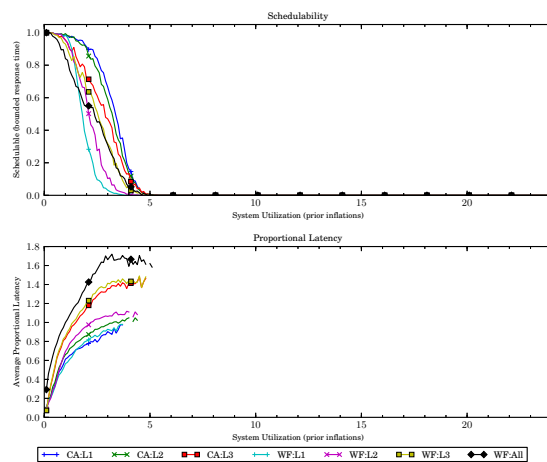


(b) With polluter overheads.

Figure 160: Results for *uni-light* per-task utilization, *uni-moderate* period, *heavy-weight* EWSS, and *pipeline* height factor.

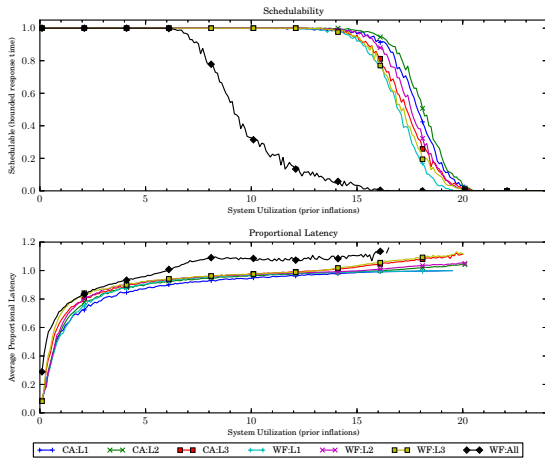


(a) Without polluter overheads.

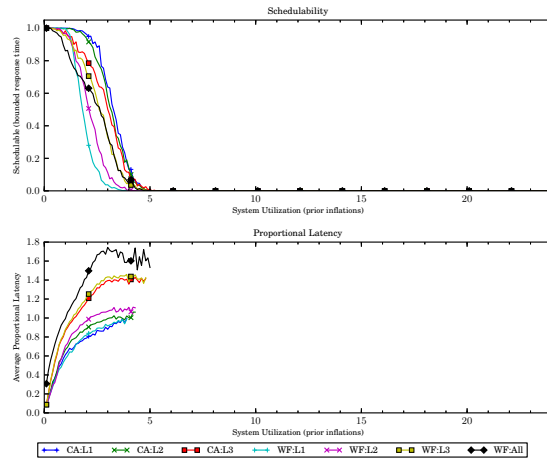


(b) With polluter overheads.

Figure 161: Results for *uni-light* per-task utilization, *uni-long* period, *heavy-weight* EWSS, and *uni-short* height factor.

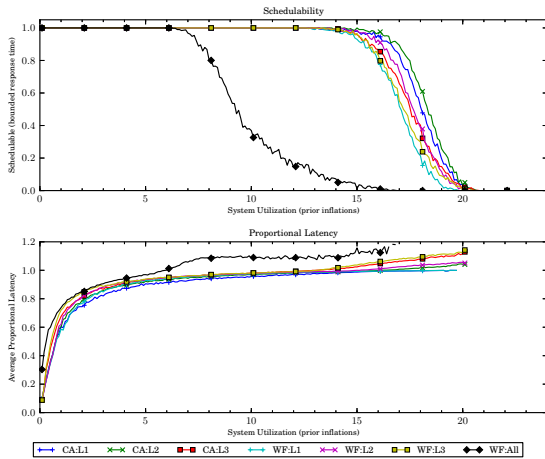


(a) Without polluter overheads.

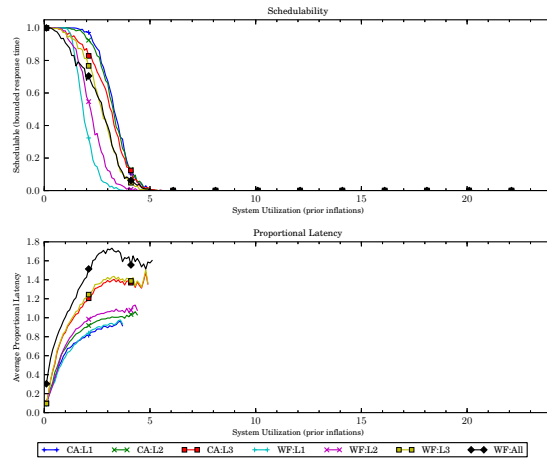


(b) With polluter overheads.

Figure 162: Results for *uni-light* per-task utilization, *uni-long* period, *heavy-weight* EWSS, and *uni-medium* height factor.

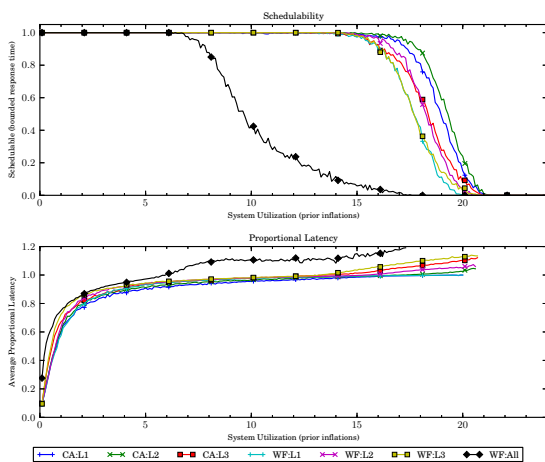


(a) Without polluter overheads.

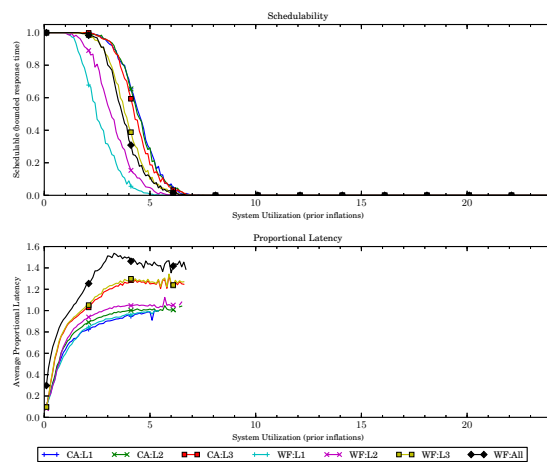


(b) With polluter overheads.

Figure 163: Results for *uni-light* per-task utilization, *uni-long* period, *heavy-weight* EWSS, and *uni-tall* height factor.

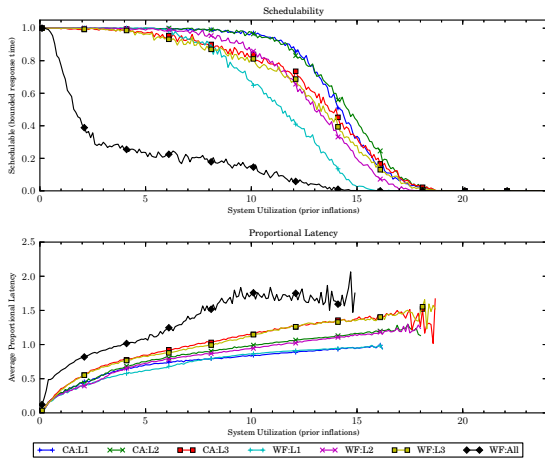


(a) Without polluter overheads.

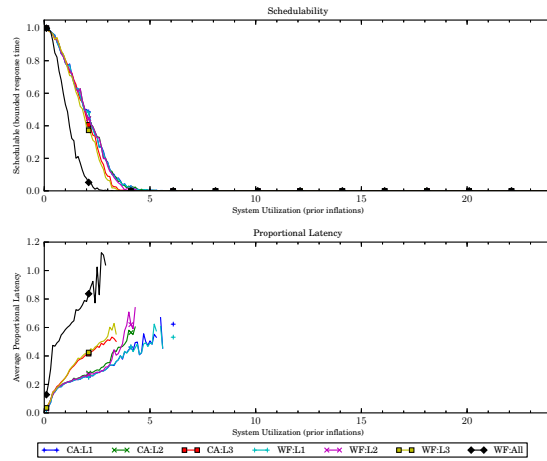


(b) With polluter overheads.

Figure 164: Results for *uni-light* per-task utilization, *uni-long* period, *heavy-weight* EWSS, and *pipeline* height factor.

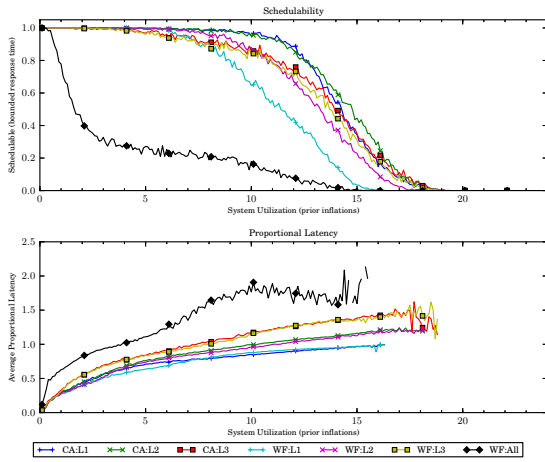


(a) Without polluter overheads.

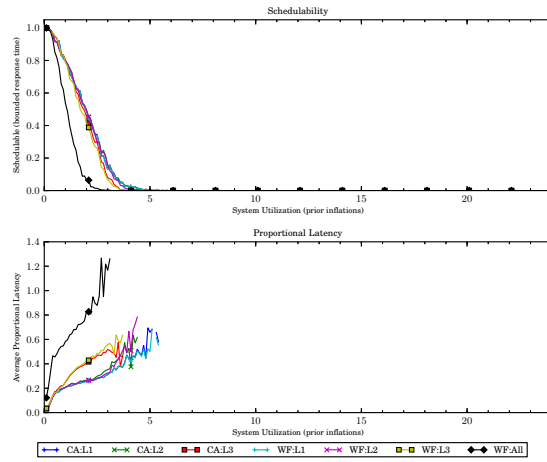


(b) With polluter overheads.

Figure 165: Results for *uni-medium* per-task utilization, *uni-short* period, *heavy-weight* EWSS, and *uni-short* height factor.

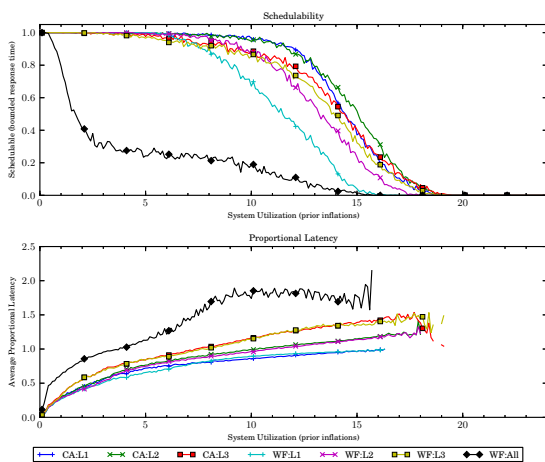


(a) Without polluter overheads.

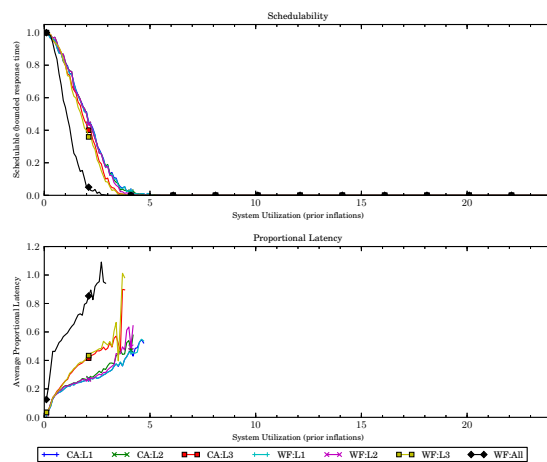


(b) With polluter overheads.

Figure 166: Results for *uni-medium* per-task utilization, *uni-short* period, *heavy-weight* EWSS, and *uni-medium* height factor.

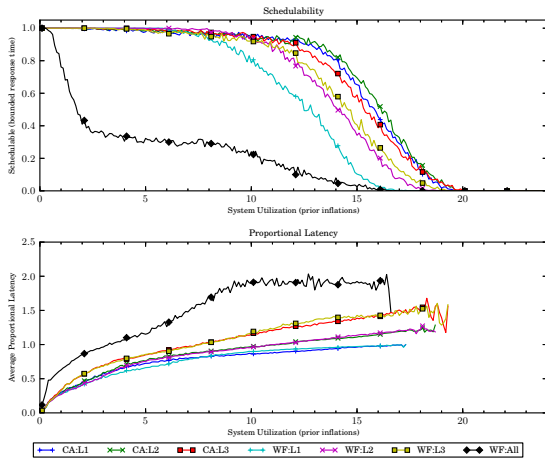


(a) Without polluter overheads.

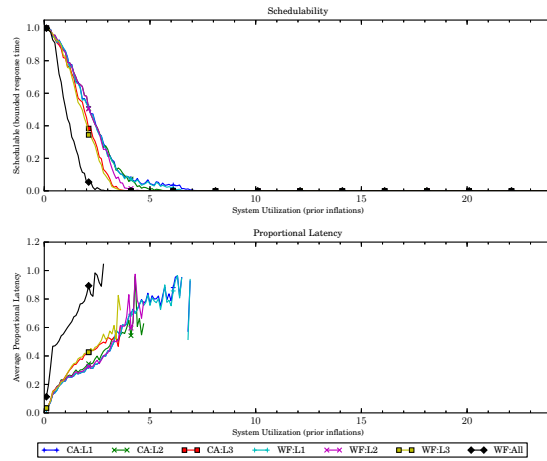


(b) With polluter overheads.

Figure 167: Results for *uni-medium* per-task utilization, *uni-short* period, *heavy-weight* EWSS, and *uni-tall* height factor.

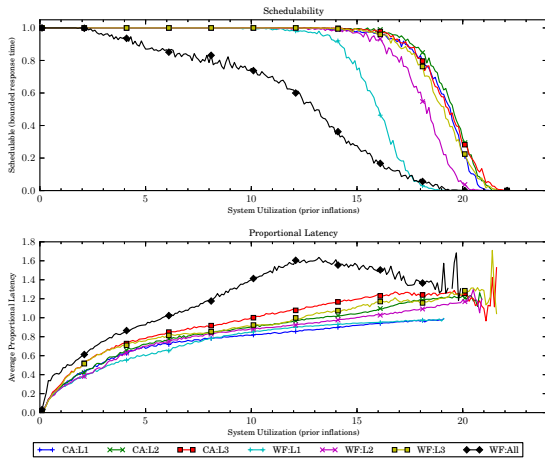


(a) Without polluter overheads.

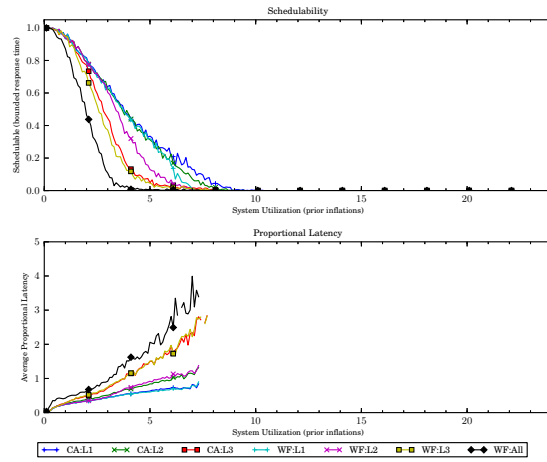


(b) With polluter overheads.

Figure 168: Results for *uni-medium* per-task utilization, *uni-short* period, *heavy-weight* EWSS, and *pipeline* height factor.

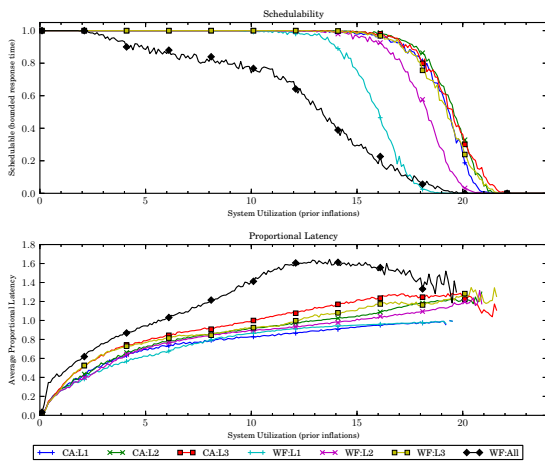


(a) Without polluter overheads.

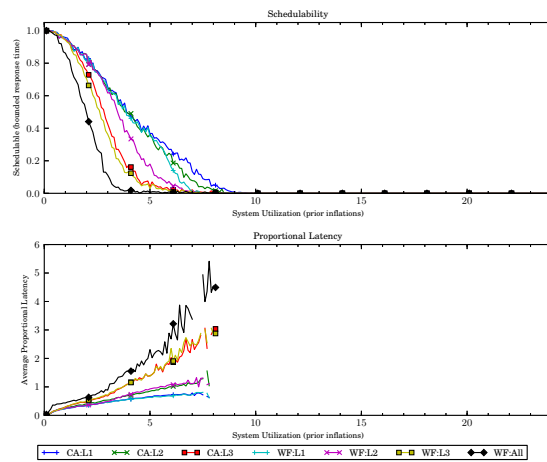


(b) With polluter overheads.

Figure 169: Results for *uni-medium* per-task utilization, *uni-moderate* period, *heavy-weight* EWSS, and *uni-short* height factor.

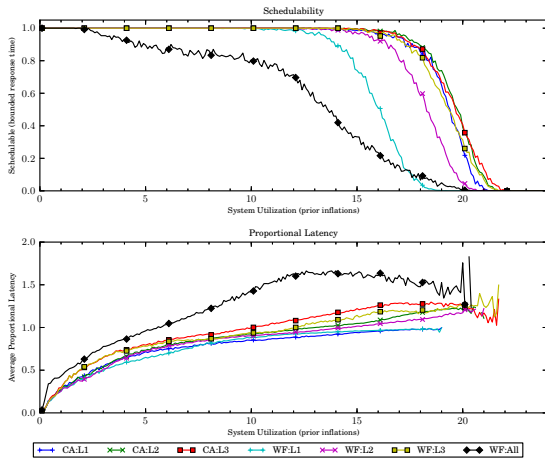


(a) Without polluter overheads.

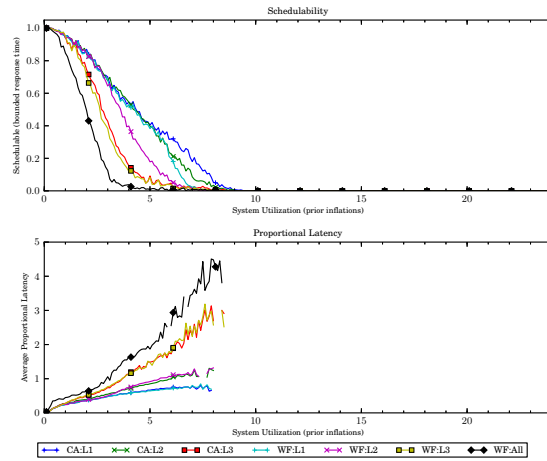


(b) With polluter overheads.

Figure 170: Results for *uni-medium* per-task utilization, *uni-moderate* period, *heavy-weight* EWSS, and *uni-medium* height factor.

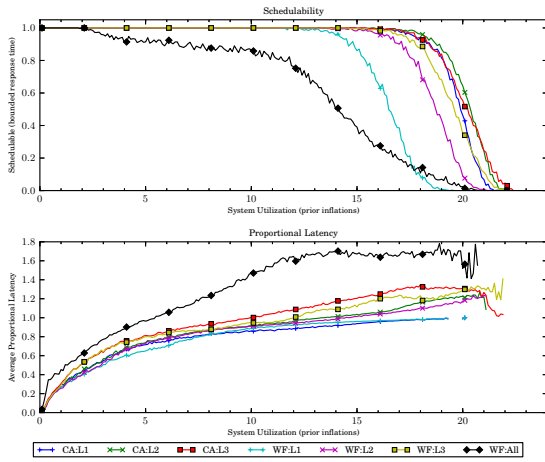


(a) Without polluter overheads.

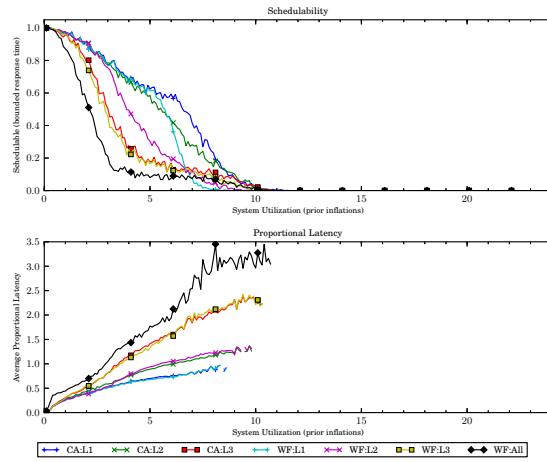


(b) With polluter overheads.

Figure 171: Results for *uni-medium* per-task utilization, *uni-moderate* period, *heavy-weight* EWSS, and *uni-tall* height factor.

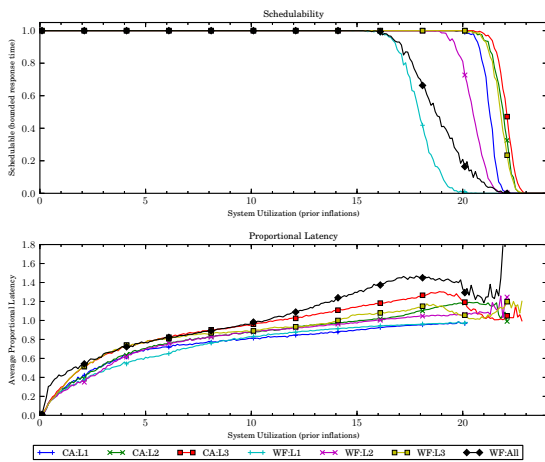


(a) Without polluter overheads.

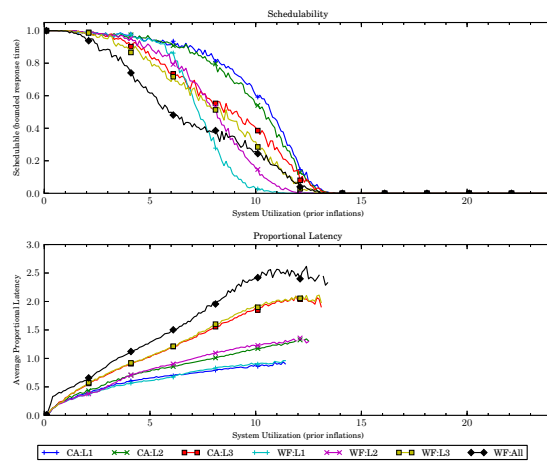


(b) With polluter overheads.

Figure 172: Results for *uni-medium* per-task utilization, *uni-moderate* period, *heavy-weight* EWSS, and *pipeline* height factor.

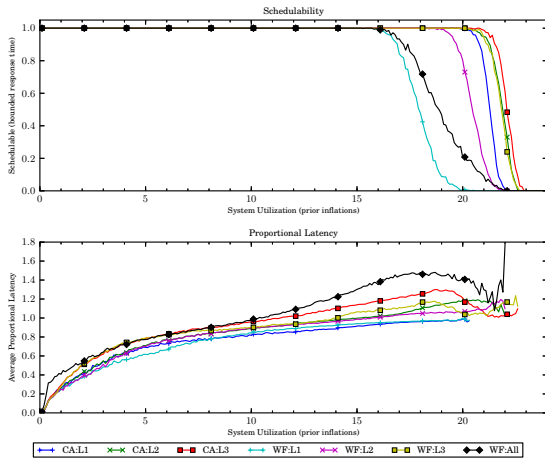


(a) Without polluter overheads.

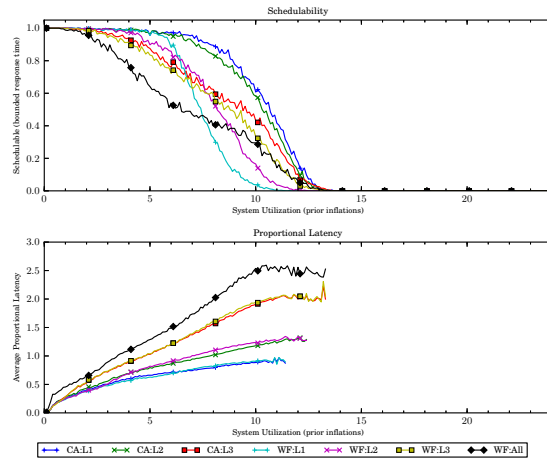


(b) With polluter overheads.

Figure 173: Results for *uni-medium* per-task utilization, *uni-long* period, *heavy-weight* EWSS, and *uni-short* height factor.

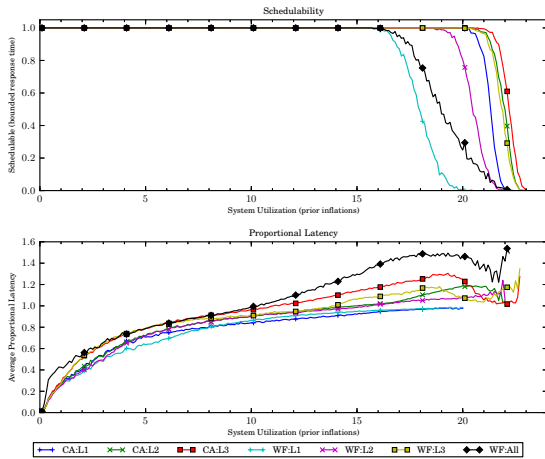


(a) Without polluter overheads.

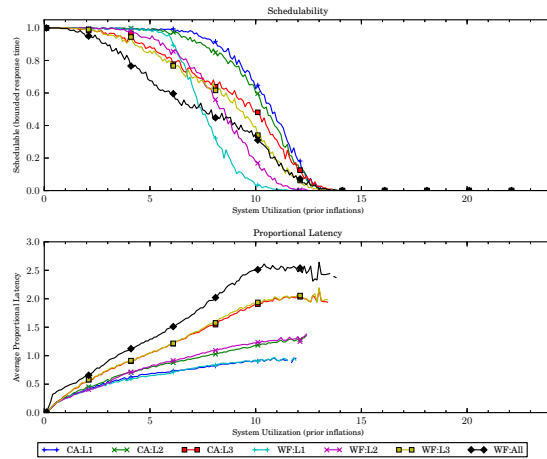


(b) With polluter overheads.

Figure 174: Results for *uni-medium* per-task utilization, *uni-long* period, *heavy-weight* EWSS, and *uni-medium* height factor.

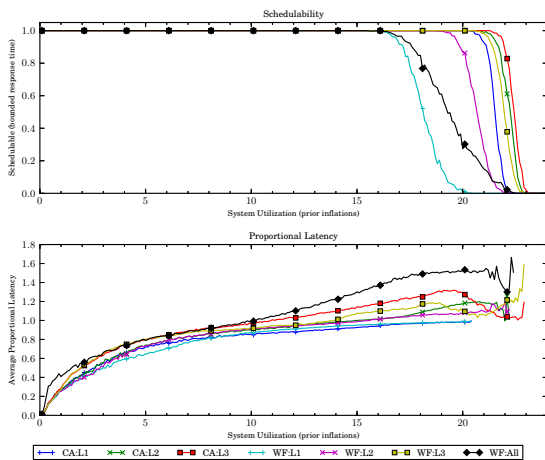


(a) Without polluter overheads.

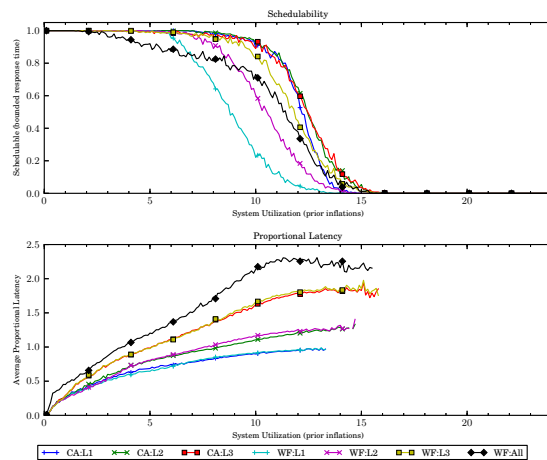


(b) With polluter overheads.

Figure 175: Results for *uni-medium* per-task utilization, *uni-long* period, *heavy-weight* EWSS, and *uni-tall* height factor.

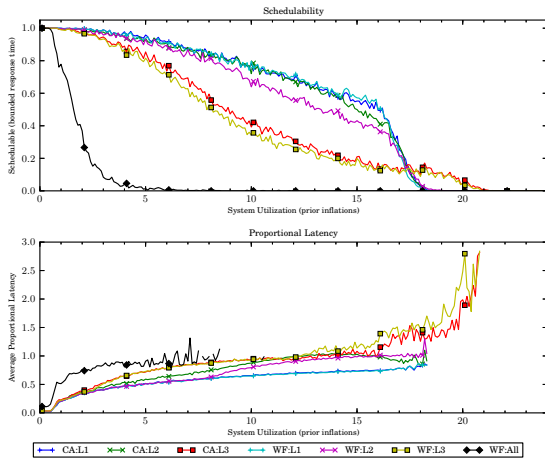


(a) Without polluter overheads.

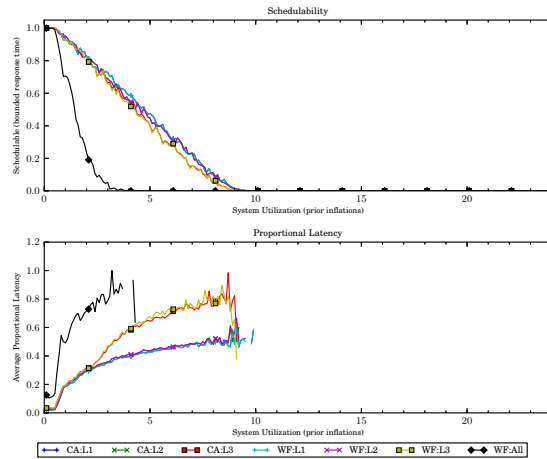


(b) With polluter overheads.

Figure 176: Results for *uni-medium* per-task utilization, *uni-long* period, *heavy-weight* EWSS, and *pipeline* height factor.

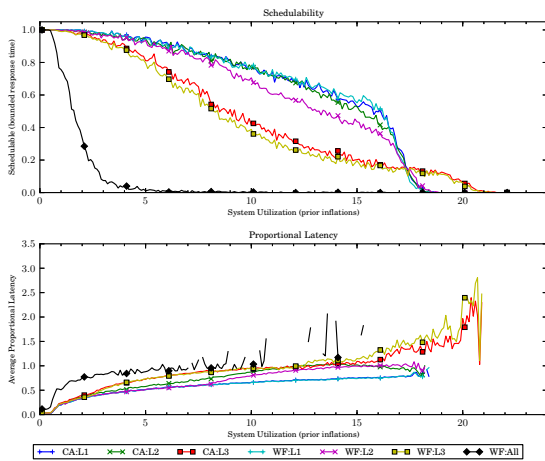


(a) Without polluter overheads.

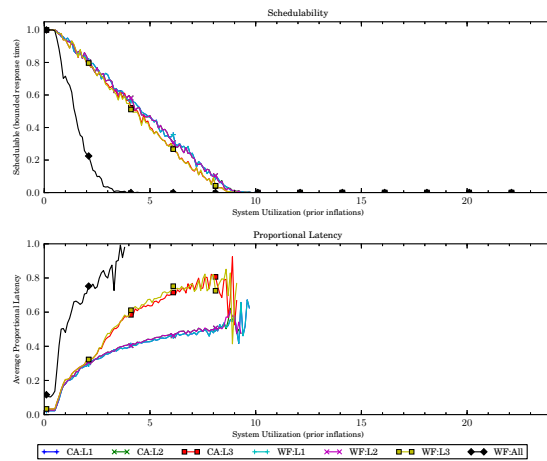


(b) With polluter overheads.

Figure 177: Results for *uni-heavy* per-task utilization, *uni-short* period, *heavy-weight* EWSS, and *uni-short* height factor.

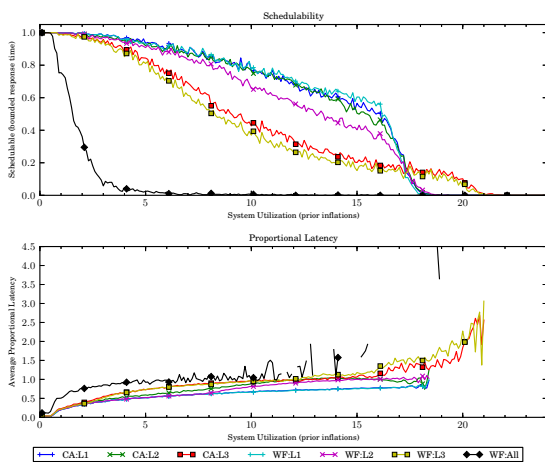


(a) Without polluter overheads.

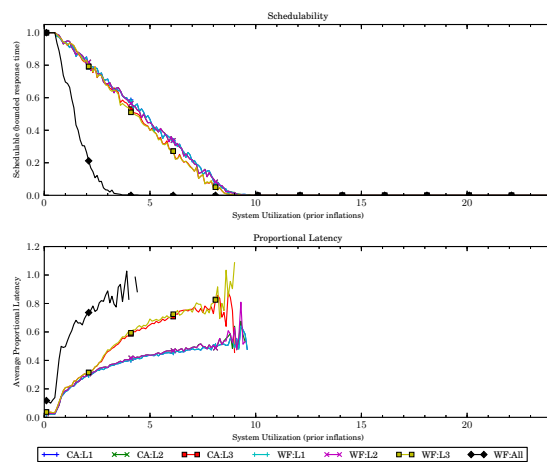


(b) With polluter overheads.

Figure 178: Results for *uni-heavy* per-task utilization, *uni-short* period, *heavy-weight* EWSS, and *uni-medium* height factor.

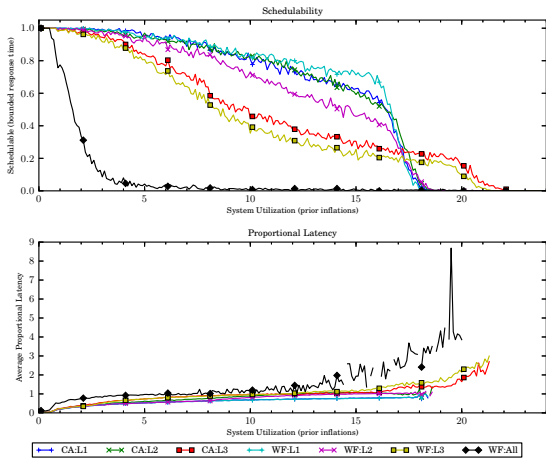


(a) Without polluter overheads.

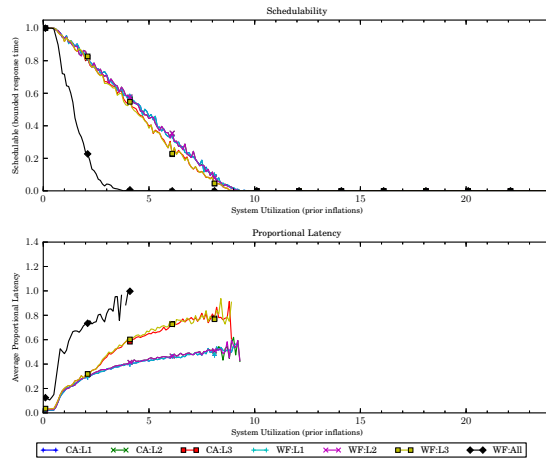


(b) With polluter overheads.

Figure 179: Results for *uni-heavy* per-task utilization, *uni-short* period, *heavy-weight* EWSS, and *uni-tall* height factor.

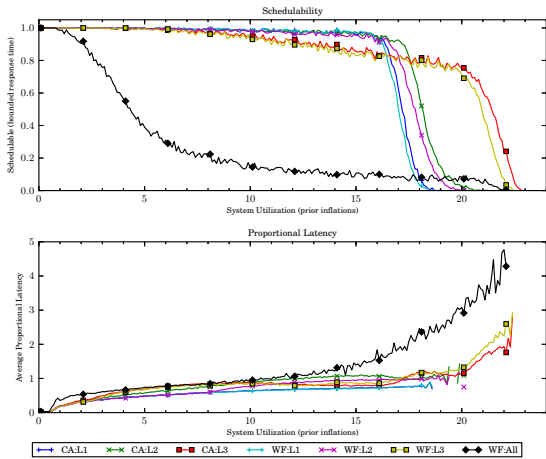


(a) Without polluter overheads.

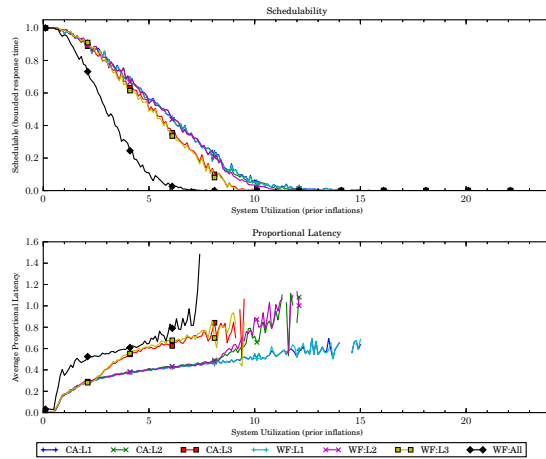


(b) With polluter overheads.

Figure 180: Results for *uni-heavy* per-task utilization, *uni-short* period, *heavy-weight* EWSS, and *pipeline* height factor.

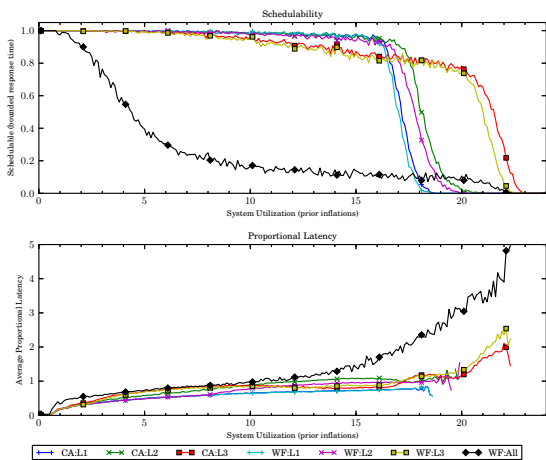


(a) Without polluter overheads.

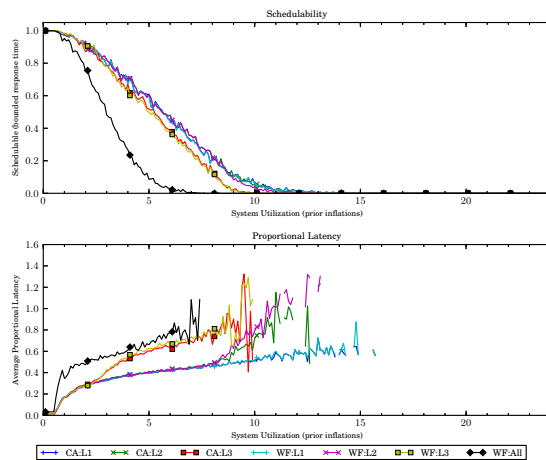


(b) With polluter overheads.

Figure 181: Results for *uni-heavy* per-task utilization, *uni-moderate* period, *heavy-weight* EWSS, and *uni-short* height factor.

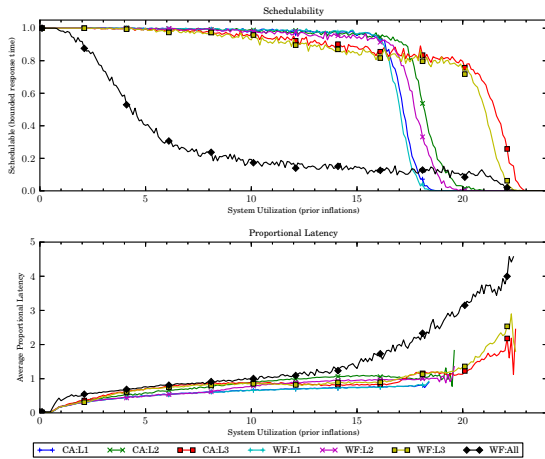


(a) Without polluter overheads.

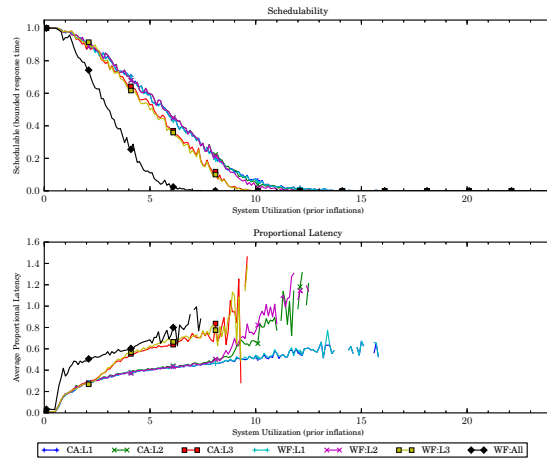


(b) With polluter overheads.

Figure 182: Results for *uni-heavy* per-task utilization, *uni-moderate* period, *heavy-weight* EWSS, and *uni-medium* height factor.

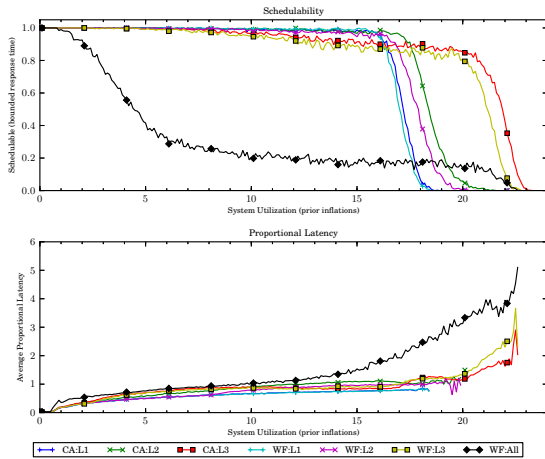


(a) Without polluter overheads.

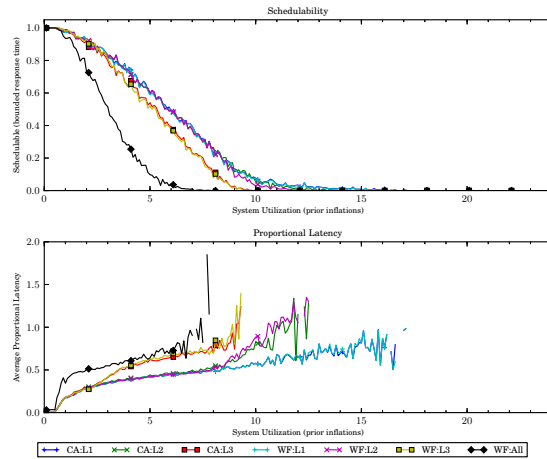


(b) With polluter overheads.

Figure 183: Results for *uni-heavy* per-task utilization, *uni-moderate* period, *heavy-weight* EWSS, and *uni-tall* height factor.

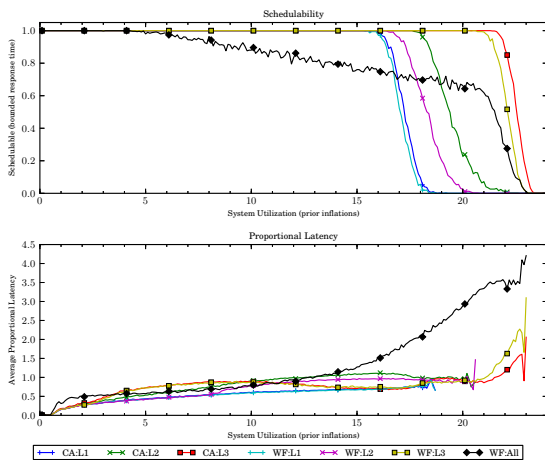


(a) Without polluter overheads.

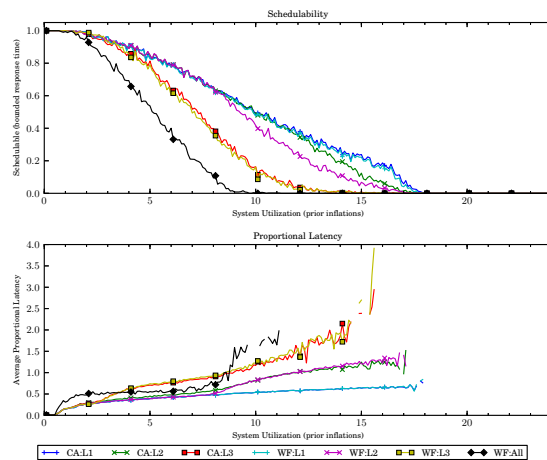


(b) With polluter overheads.

Figure 184: Results for *uni-heavy* per-task utilization, *uni-moderate* period, *heavy-weight* EWSS, and *pipeline* height factor.

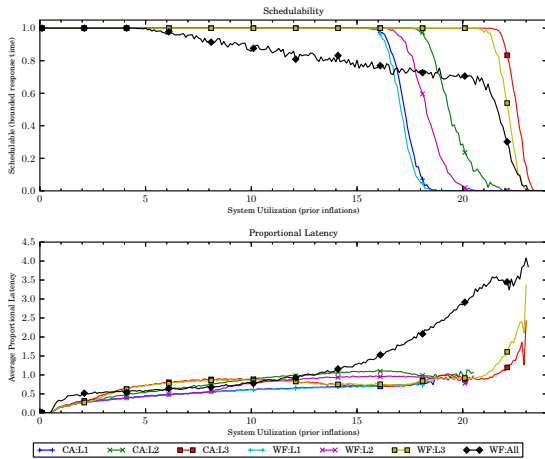


(a) Without polluter overheads.

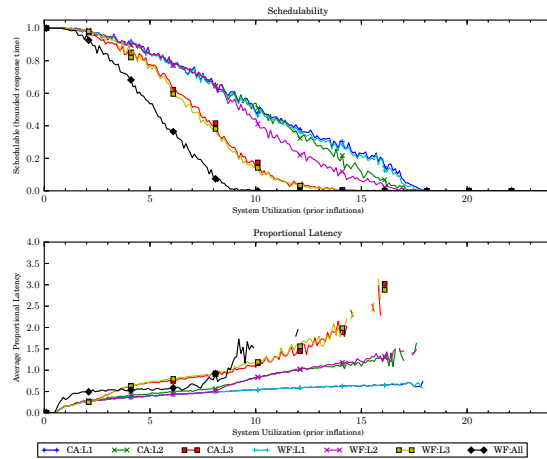


(b) With polluter overheads.

Figure 185: Results for *uni-heavy* per-task utilization, *uni-long* period, *heavy-weight* EWSS, and *uni-short* height factor.

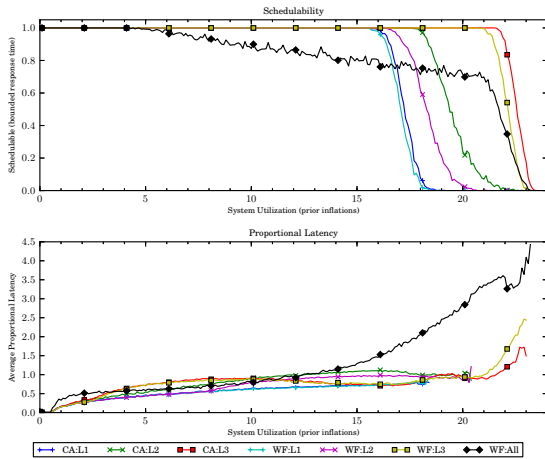


(a) Without polluter overheads.

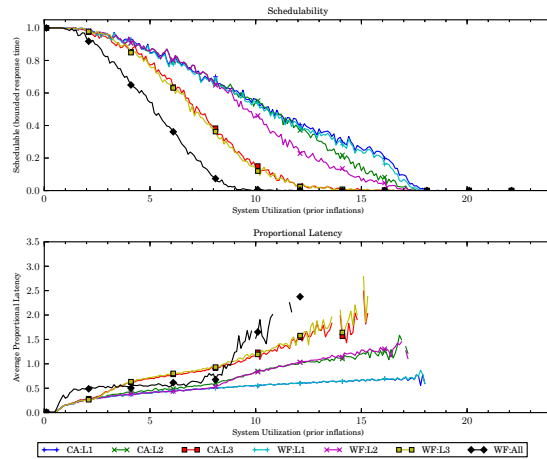


(b) With polluter overheads.

Figure 186: Results for *uni-heavy* per-task utilization, *uni-long* period, *heavy-weight* EWSS, and *uni-medium* height factor.

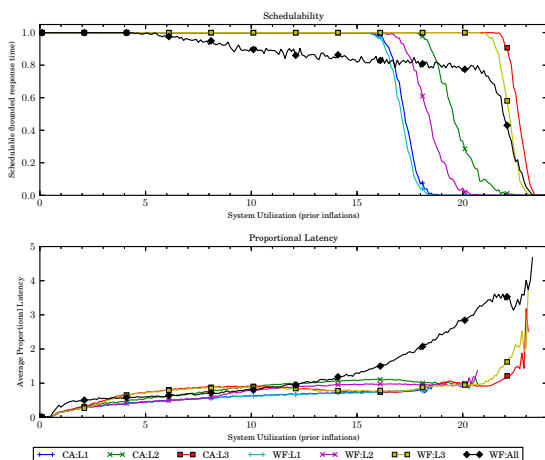


(a) Without polluter overheads.

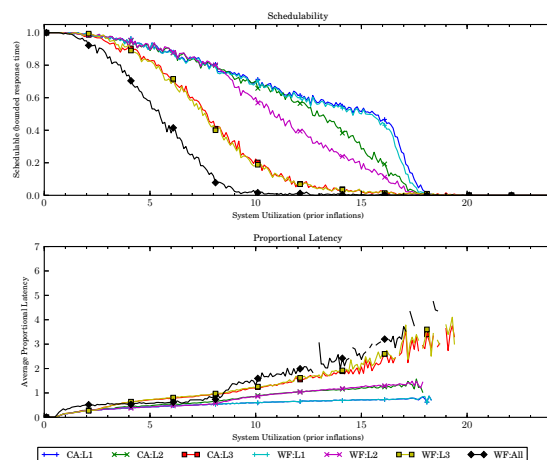


(b) With polluter overheads.

Figure 187: Results for *uni-heavy* per-task utilization, *uni-long* period, *heavy-weight* EWSS, and *uni-tall* height factor.

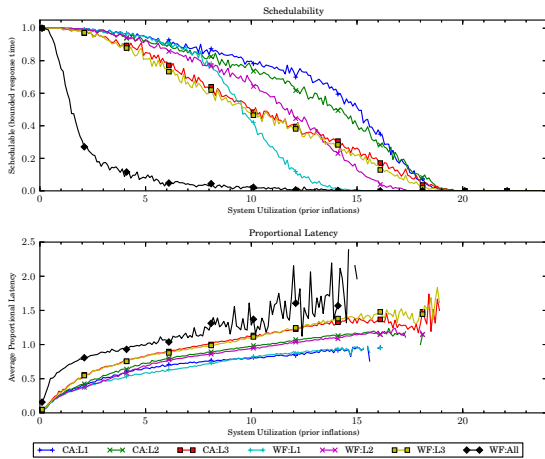


(a) Without polluter overheads.

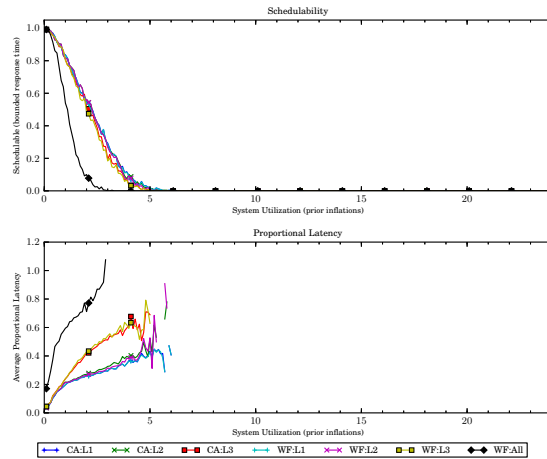


(b) With polluter overheads.

Figure 188: Results for *uni-heavy* per-task utilization, *uni-long* period, *heavy-weight* EWSS, and *pipeline* height factor.

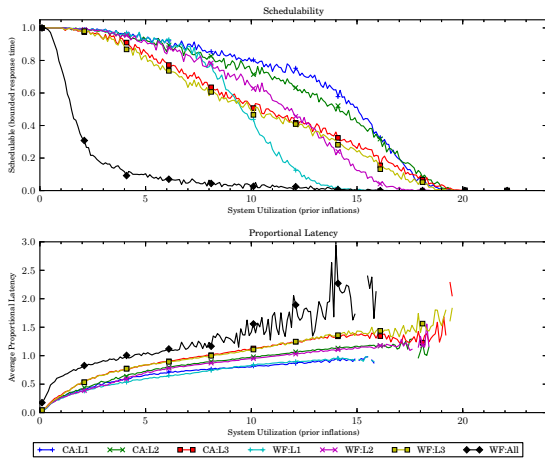


(a) Without polluter overheads.

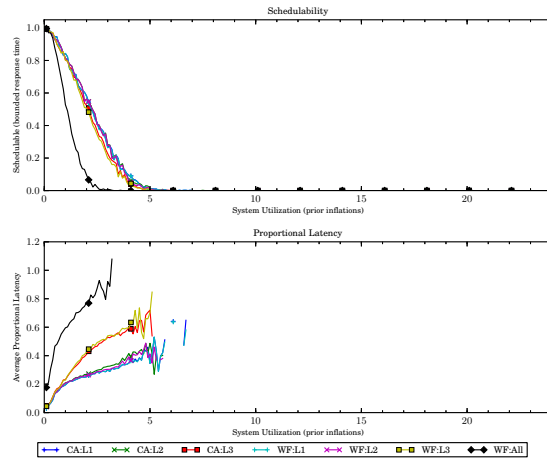


(b) With polluter overheads.

Figure 189: Results for *bimo-light* per-task utilization, *uni-short* period, *heavy-weight* EWSS, and *uni-short* height factor.

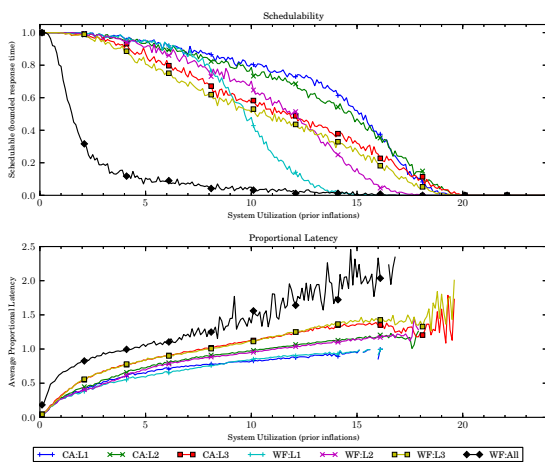


(a) Without polluter overheads.

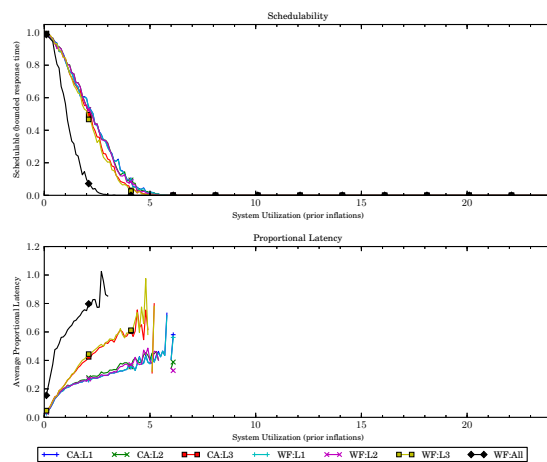


(b) With polluter overheads.

Figure 190: Results for *bimo-light* per-task utilization, *uni-short* period, *heavy-weight* EWSS, and *uni-medium* height factor.

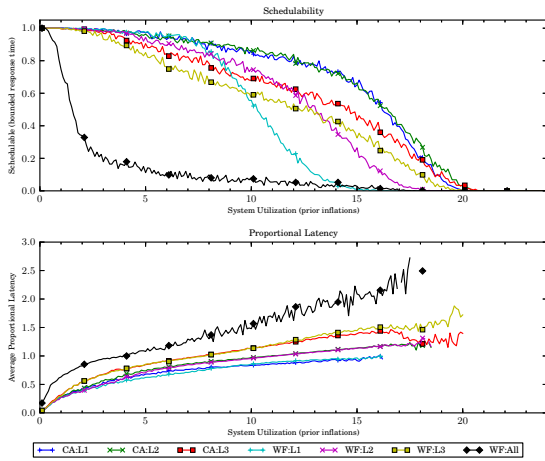


(a) Without polluter overheads.

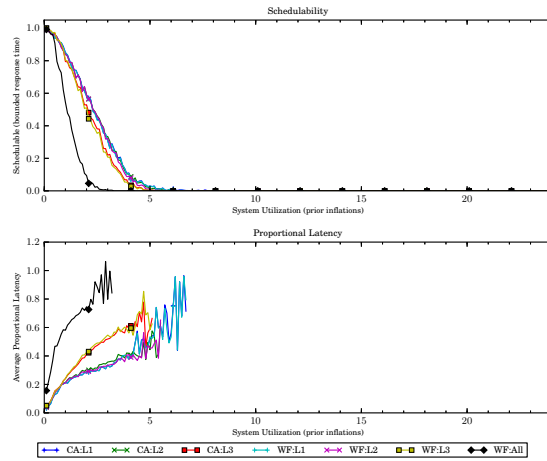


(b) With polluter overheads.

Figure 191: Results for *bimo-light* per-task utilization, *uni-short* period, *heavy-weight* EWSS, and *uni-tall* height factor.

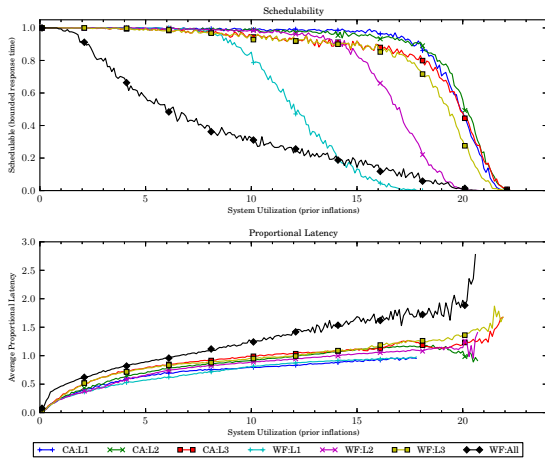


(a) Without polluter overheads.

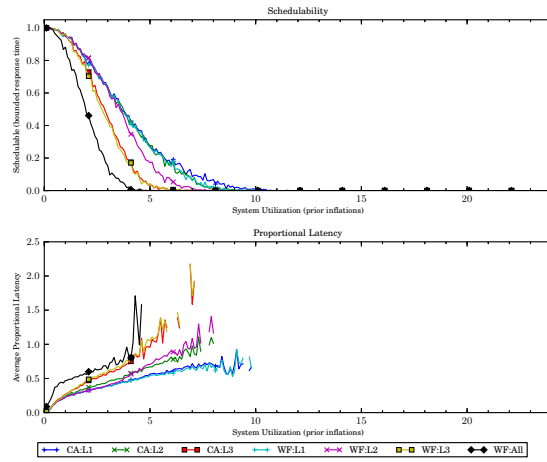


(b) With polluter overheads.

Figure 192: Results for *bimo-light* per-task utilization, *uni-short* period, *heavy-weight* EWSS, and *pipeline* height factor.

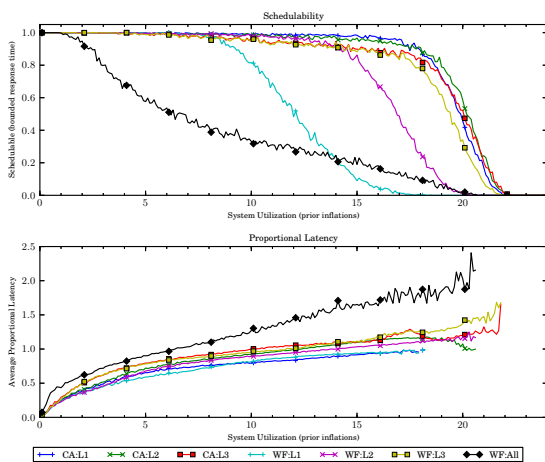


(a) Without polluter overheads.

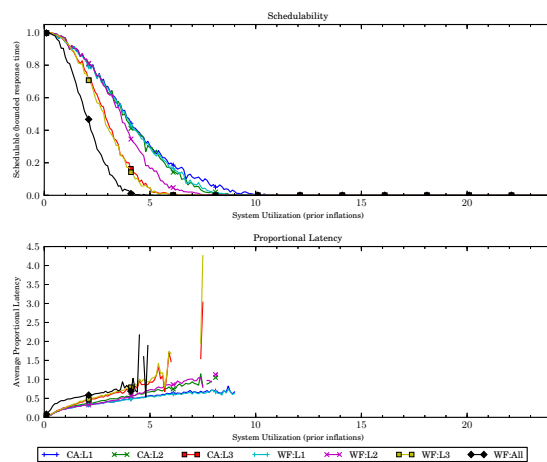


(b) With polluter overheads.

Figure 193: Results for *bimo-light* per-task utilization, *uni-moderate* period, *heavy-weight* EWSS, and *uni-short* height factor.

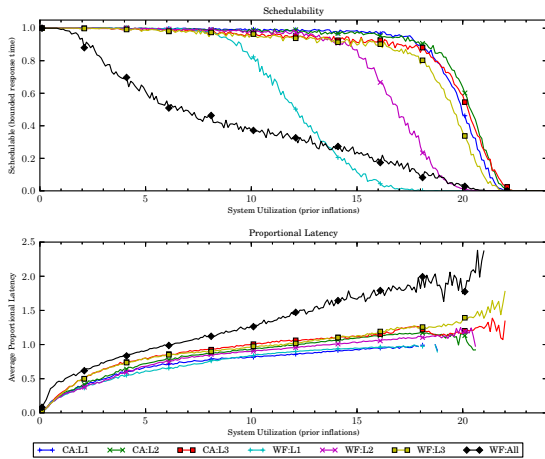


(a) Without polluter overheads.

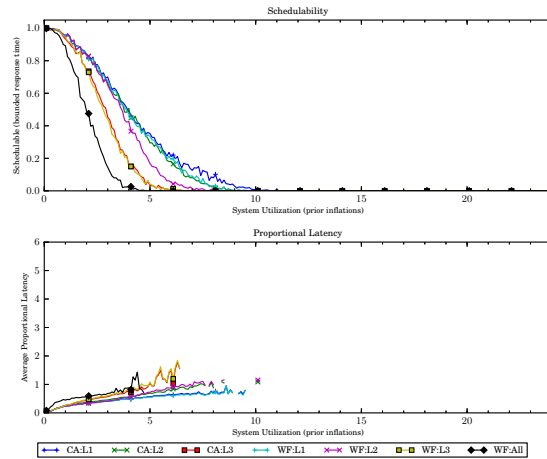


(b) With polluter overheads.

Figure 194: Results for *bimo-light* per-task utilization, *uni-moderate* period, *heavy-weight* EWSS, and *uni-medium* height factor.

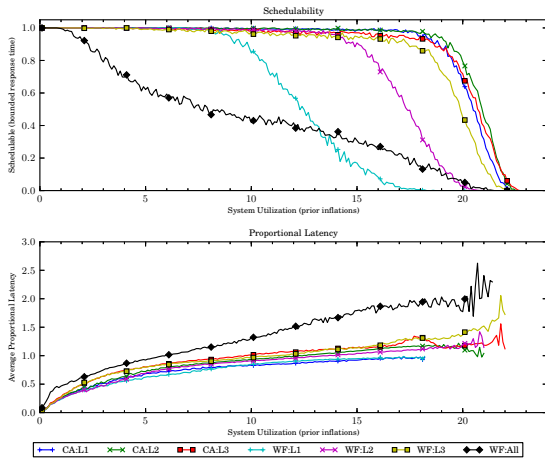


(a) Without polluter overheads.

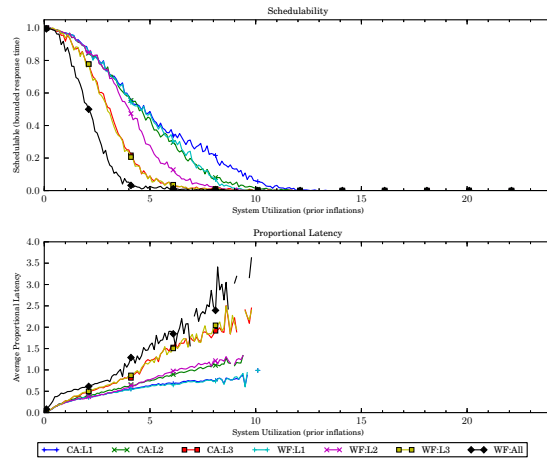


(b) With polluter overheads.

Figure 195: Results for *bimo-light* per-task utilization, *uni-moderate* period, *heavy-weight* EWSS, and *uni-tall* height factor.

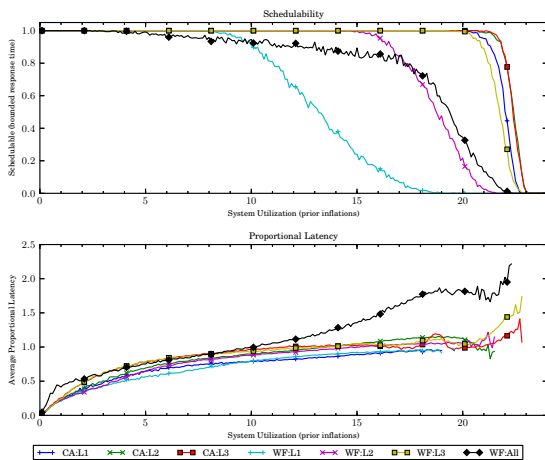


(a) Without polluter overheads.

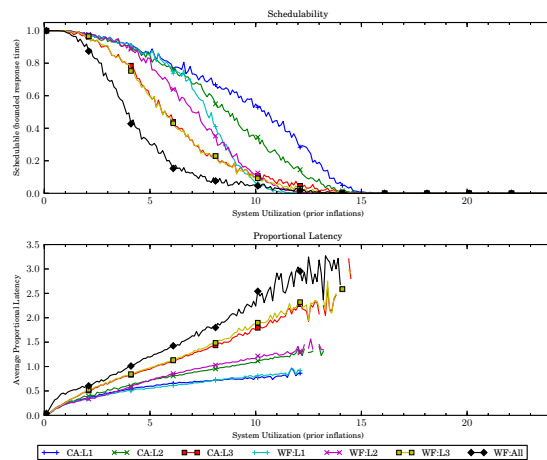


(b) With polluter overheads.

Figure 196: Results for *bimo-light* per-task utilization, *uni-moderate* period, *heavy-weight* EWSS, and *pipeline* height factor.

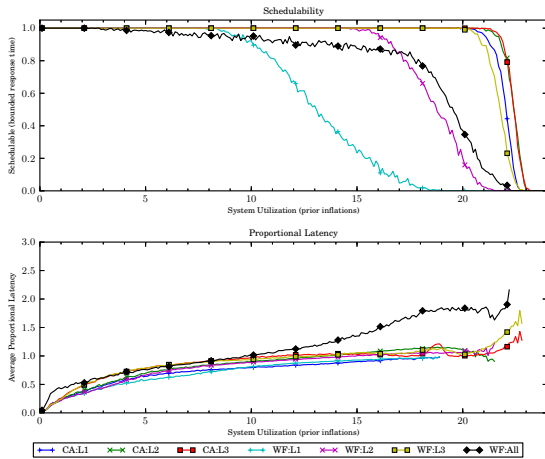


(a) Without polluter overheads.

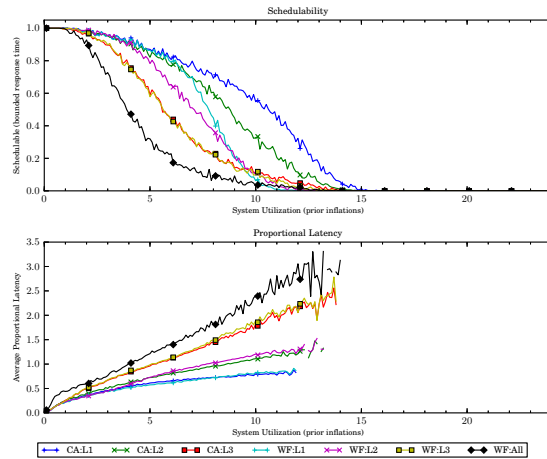


(b) With polluter overheads.

Figure 197: Results for *bimo-light* per-task utilization, *uni-long* period, *heavy-weight* EWSS, and *uni-short* height factor.

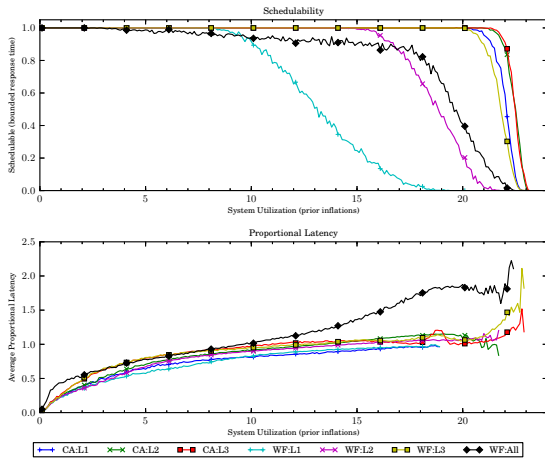


(a) Without polluter overheads.

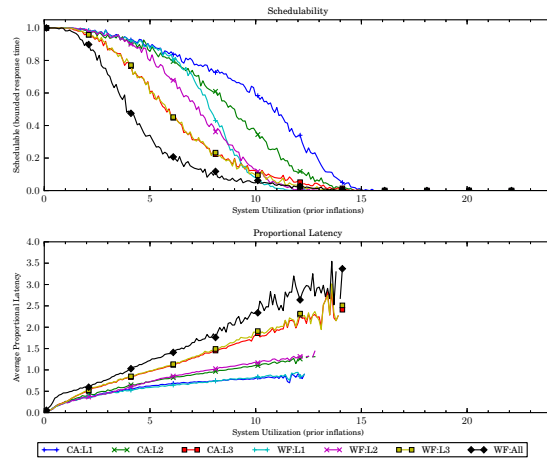


(b) With polluter overheads.

Figure 198: Results for *bimo-light* per-task utilization, *uni-long* period, *heavy-weight* EWSS, and *uni-medium* height factor.

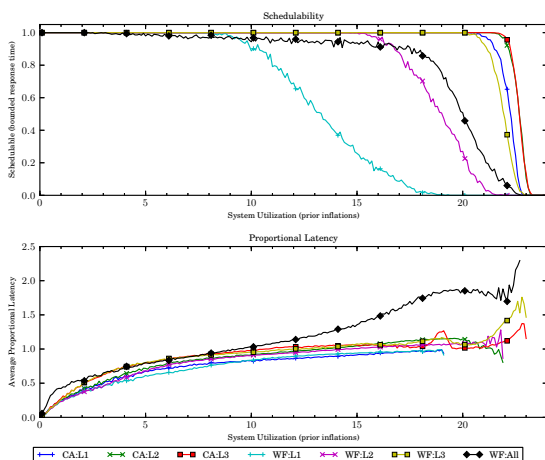


(a) Without polluter overheads.

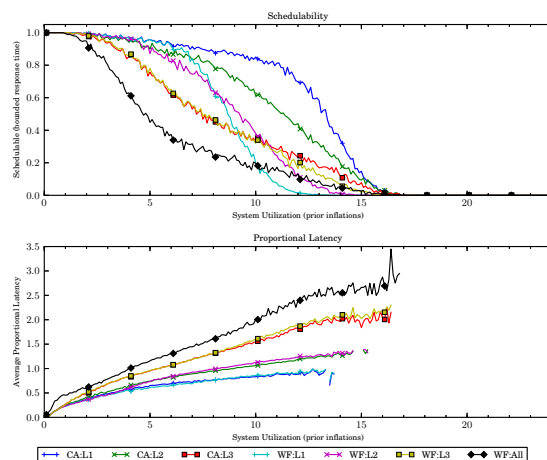


(b) With polluter overheads.

Figure 199: Results for *bimo-light* per-task utilization, *uni-long* period, *heavy-weight* EWSS, and *uni-tall* height factor.

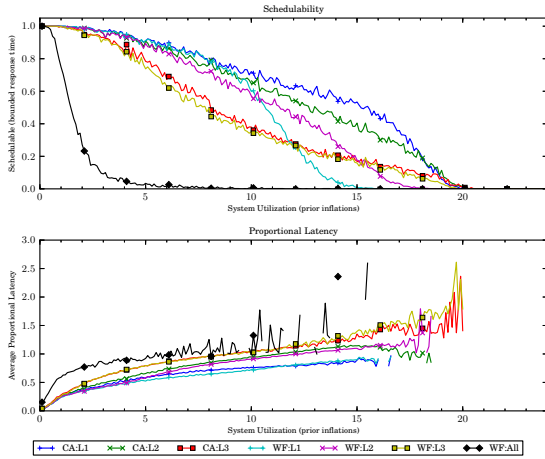


(a) Without polluter overheads.

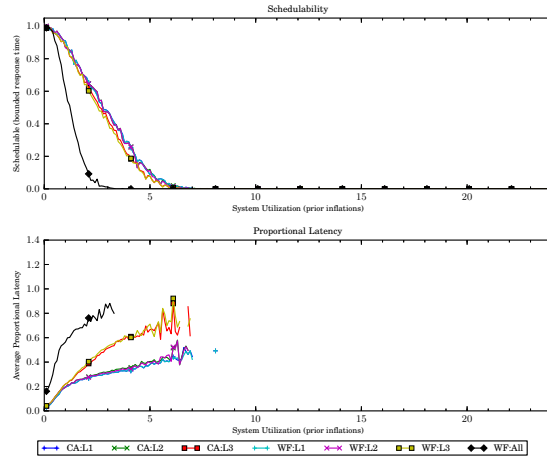


(b) With polluter overheads.

Figure 200: Results for *bimo-light* per-task utilization, *uni-long* period, *heavy-weight* EWSS, and *pipeline* height factor.

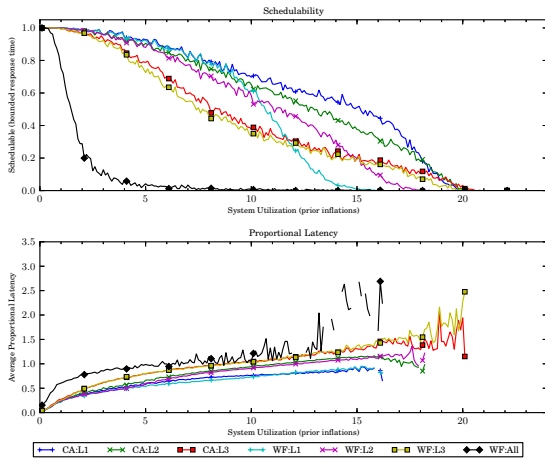


(a) Without polluter overheads.

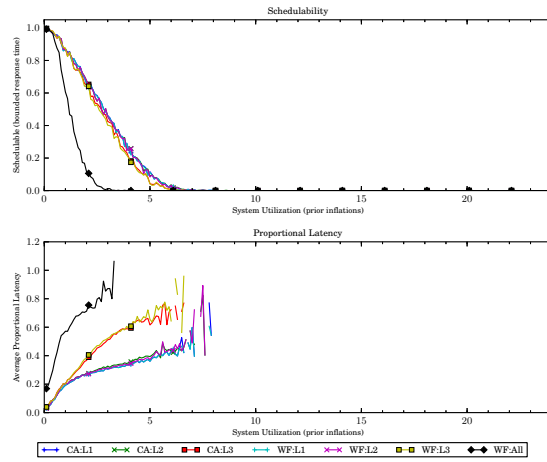


(b) With polluter overheads.

Figure 201: Results for *bimo-medium* per-task utilization, *uni-short* period, *heavy-weight* EWSS, and *uni-short* height factor.

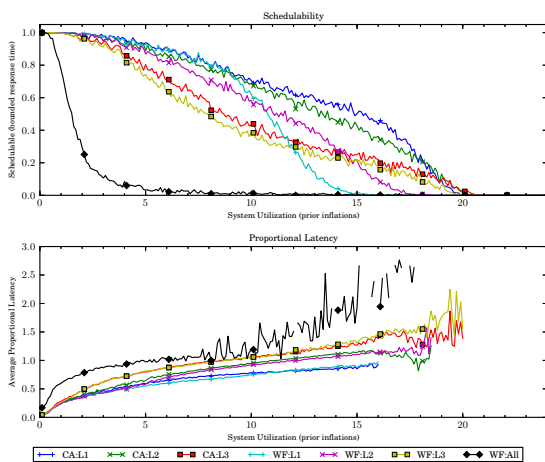


(a) Without polluter overheads.

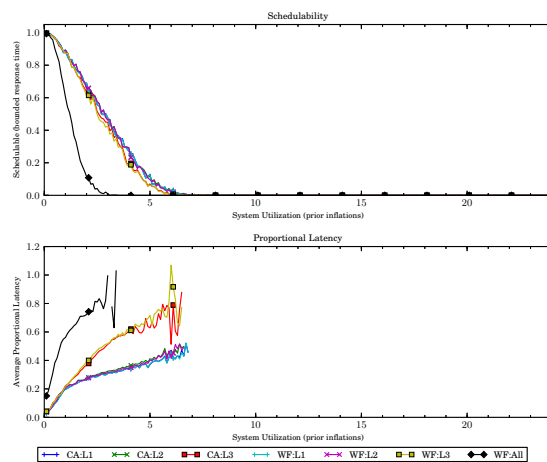


(b) With polluter overheads.

Figure 202: Results for *bimo-medium* per-task utilization, *uni-short* period, *heavy-weight* EWSS, and *uni-medium* height factor.

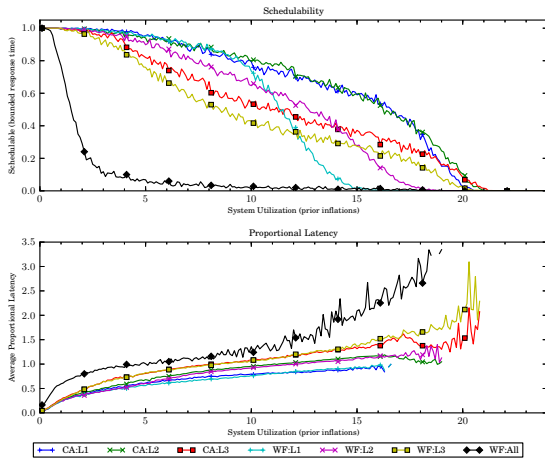


(a) Without polluter overheads.

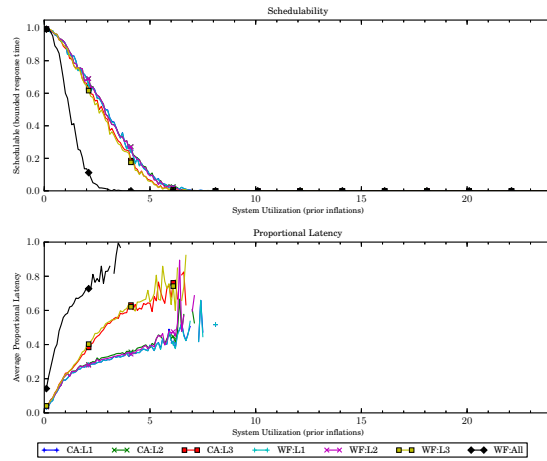


(b) With polluter overheads.

Figure 203: Results for *bimo-medium* per-task utilization, *uni-short* period, *heavy-weight* EWSS, and *uni-tall* height factor.

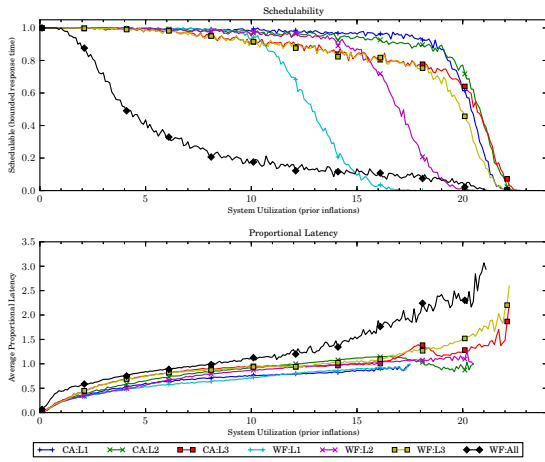


(a) Without polluter overheads.

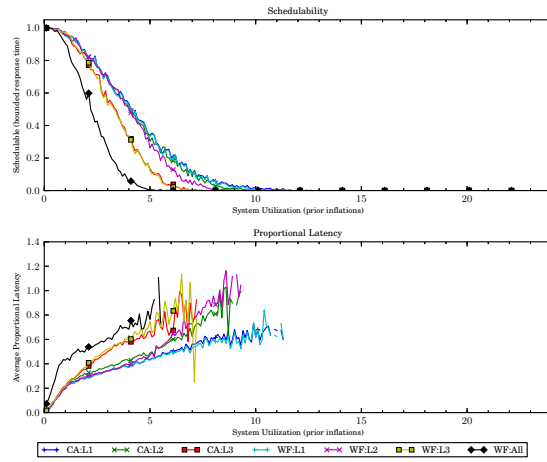


(b) With polluter overheads.

Figure 204: Results for *bimo-medium* per-task utilization, *uni-short* period, *heavy-weight* EWSS, and *pipeline* height factor.

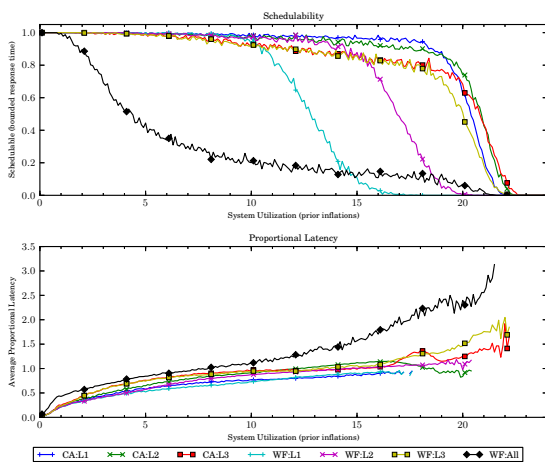


(a) Without polluter overheads.

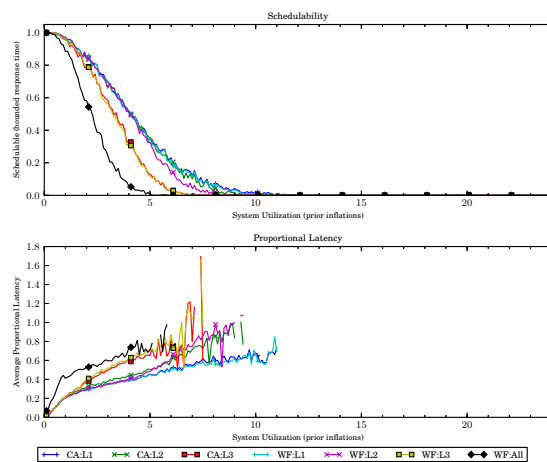


(b) With polluter overheads.

Figure 205: Results for *bimo-medium* per-task utilization, *uni-moderate* period, *heavy-weight* EWSS, and *uni-short* height factor.

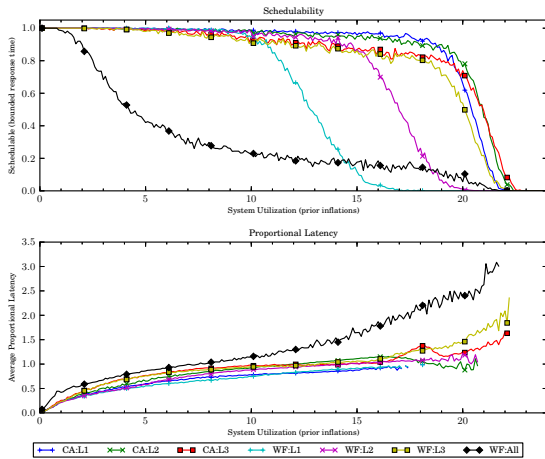


(a) Without polluter overheads.

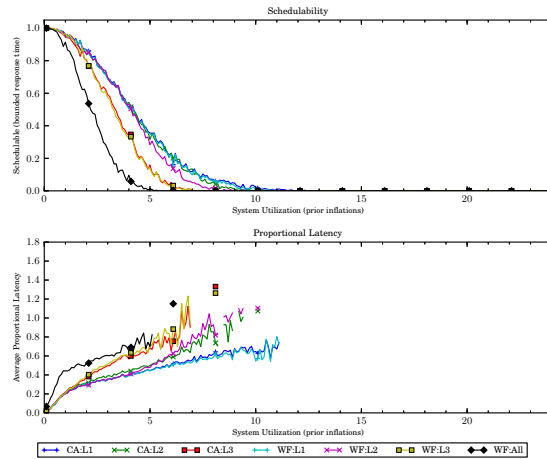


(b) With polluter overheads.

Figure 206: Results for *bimo-medium* per-task utilization, *uni-moderate* period, *heavy-weight* EWSS, and *uni-medium* height factor.

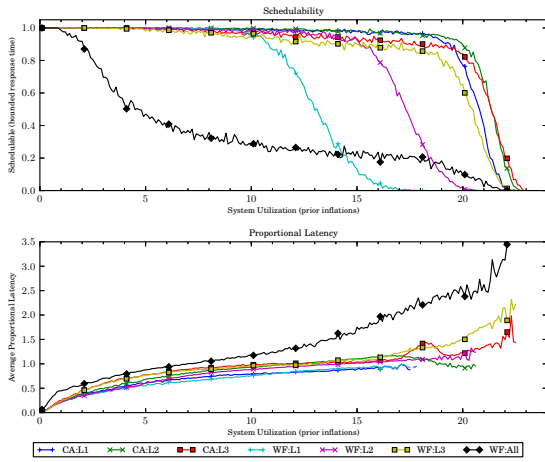


(a) Without polluter overheads.

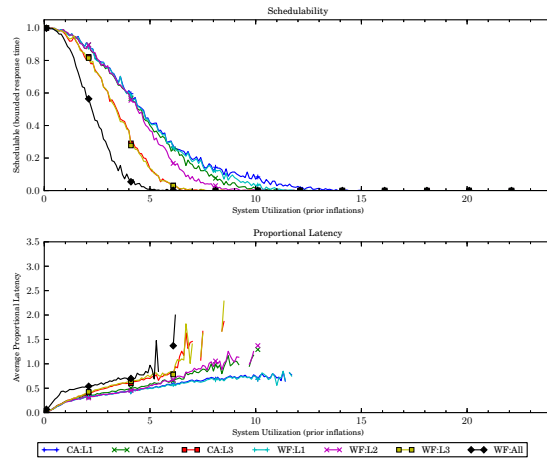


(b) With polluter overheads.

Figure 207: Results for *bimo-medium* per-task utilization, *uni-moderate* period, *heavy-weight* EWSS, and *uni-tall* height factor.

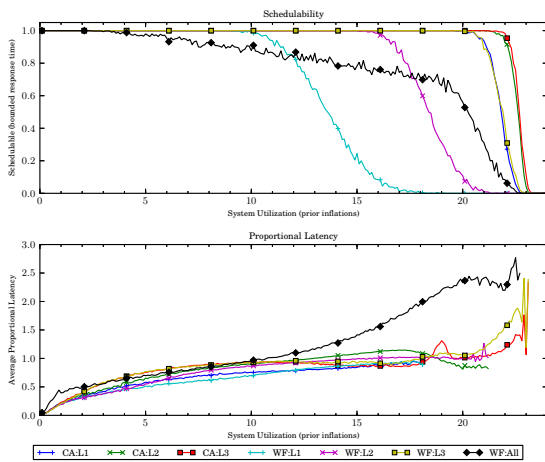


(a) Without polluter overheads.

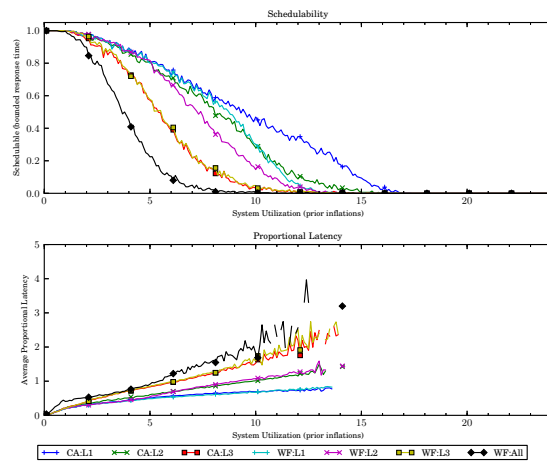


(b) With polluter overheads.

Figure 208: Results for *bimo-medium* per-task utilization, *uni-moderate* period, *heavy-weight* EWSS, and *pipeline* height factor.

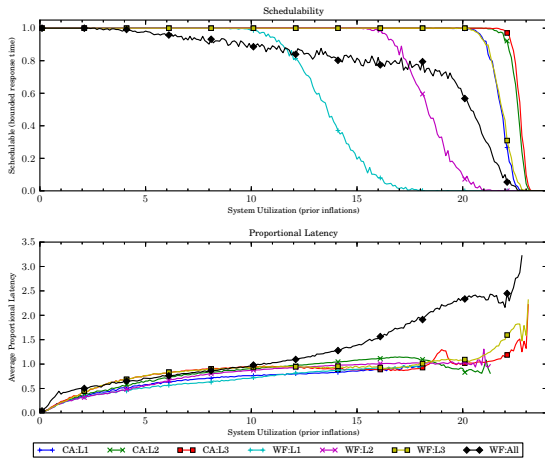


(a) Without polluter overheads.

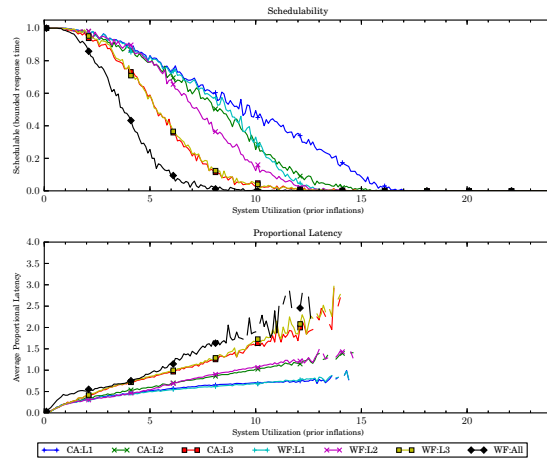


(b) With polluter overheads.

Figure 209: Results for *bimo-medium* per-task utilization, *uni-long* period, *heavy-weight* EWSS, and *uni-short* height factor.

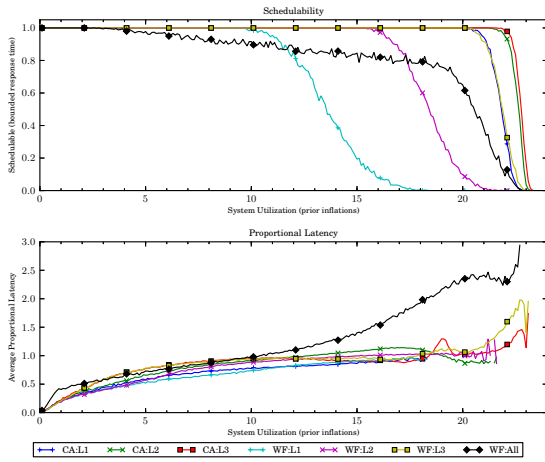


(a) Without polluter overheads.

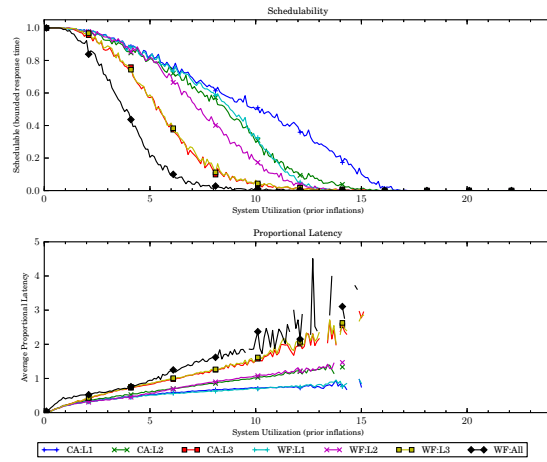


(b) With polluter overheads.

Figure 210: Results for *bimo-medium* per-task utilization, *uni-long* period, *heavy-weight* EWSS, and *uni-medium* height factor.

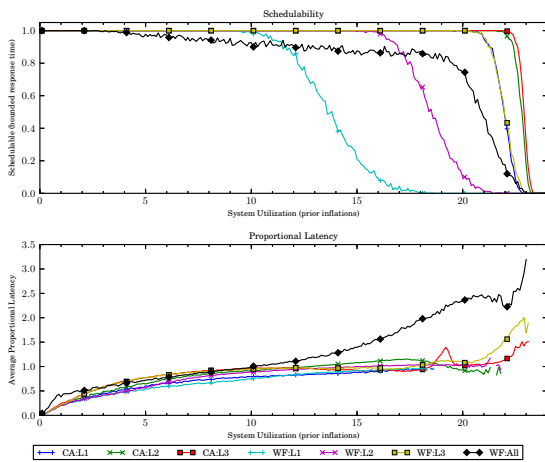


(a) Without polluter overheads.

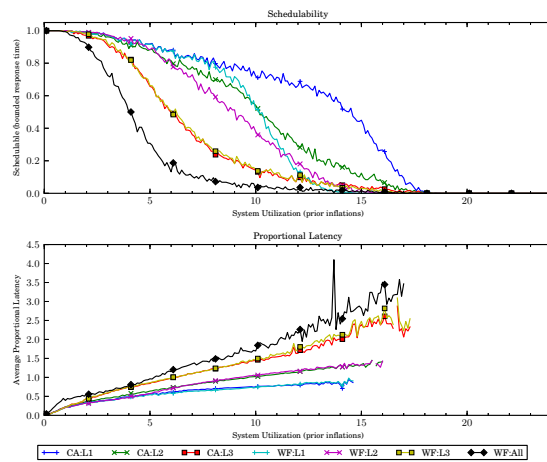


(b) With polluter overheads.

Figure 211: Results for *bimo-medium* per-task utilization, *uni-long* period, *heavy-weight* EWSS, and *uni-tall* height factor.

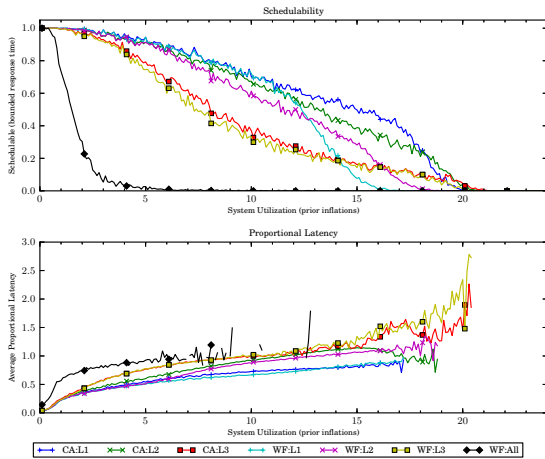


(a) Without polluter overheads.

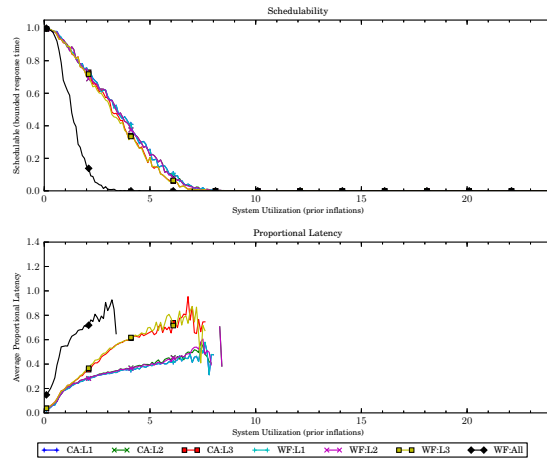


(b) With polluter overheads.

Figure 212: Results for *bimo-medium* per-task utilization, *uni-long* period, *heavy-weight* EWSS, and *pipeline* height factor.

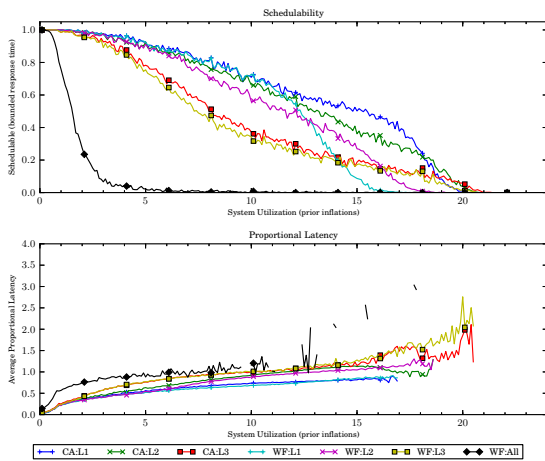


(a) Without polluter overheads.

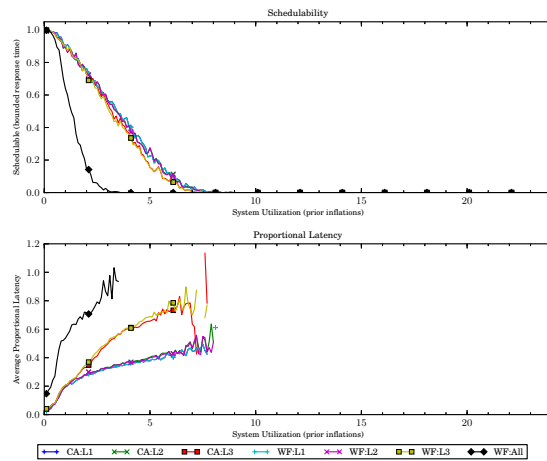


(b) With polluter overheads.

Figure 213: Results for *bimo-heavy* per-task utilization, *uni-short* period, *heavy-weight* EWSS, and *uni-short* height factor.

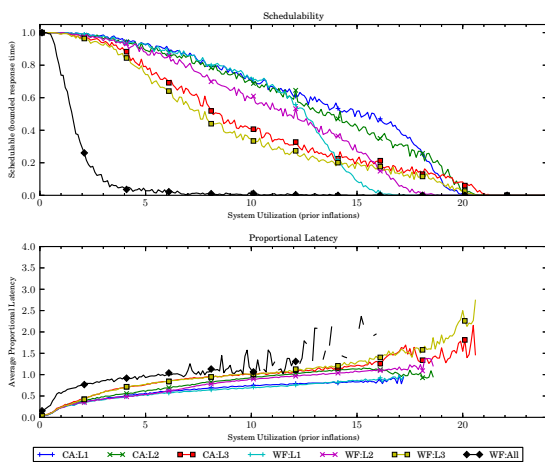


(a) Without polluter overheads.

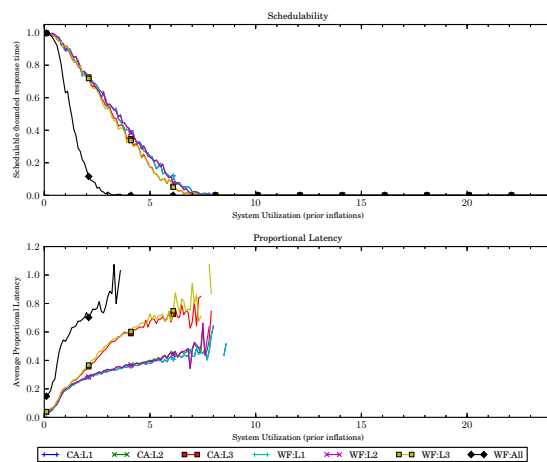


(b) With polluter overheads.

Figure 214: Results for *bimo-heavy* per-task utilization, *uni-short* period, *heavy-weight* EWSS, and *uni-medium* height factor.

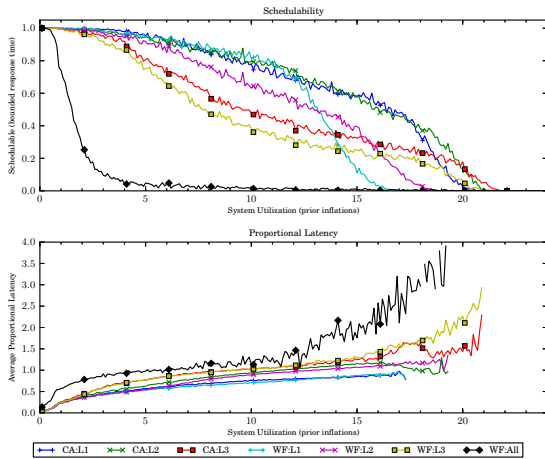


(a) Without polluter overheads.

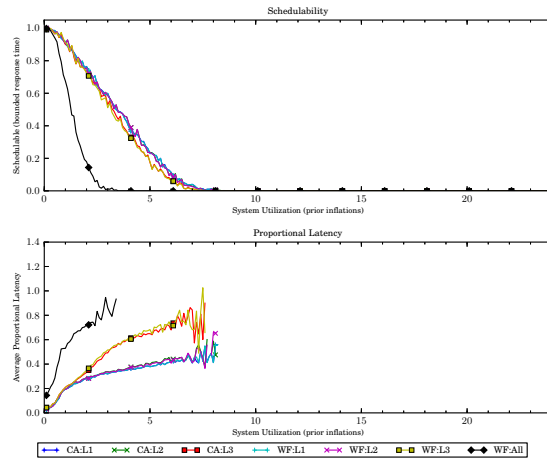


(b) With polluter overheads.

Figure 215: Results for *bimo-heavy* per-task utilization, *uni-short* period, *heavy-weight* EWSS, and *uni-tall* height factor.

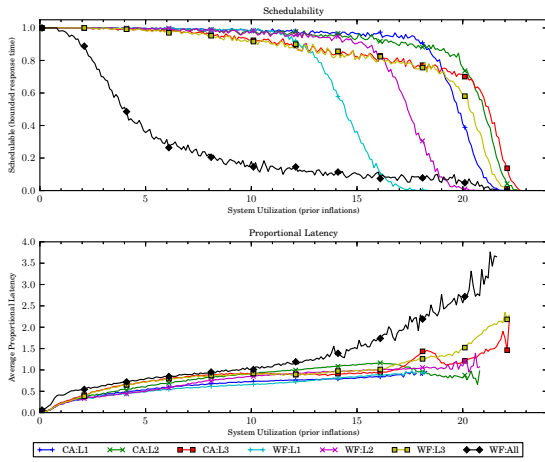


(a) Without polluter overheads.

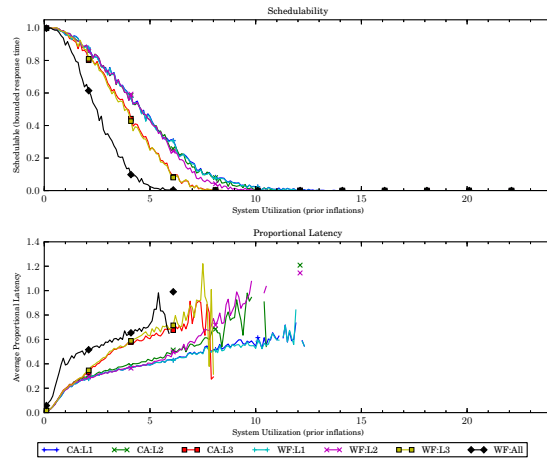


(b) With polluter overheads.

Figure 216: Results for *bimo-heavy* per-task utilization, *uni-short* period, *heavy-weight* EWSS, and *pipeline* height factor.

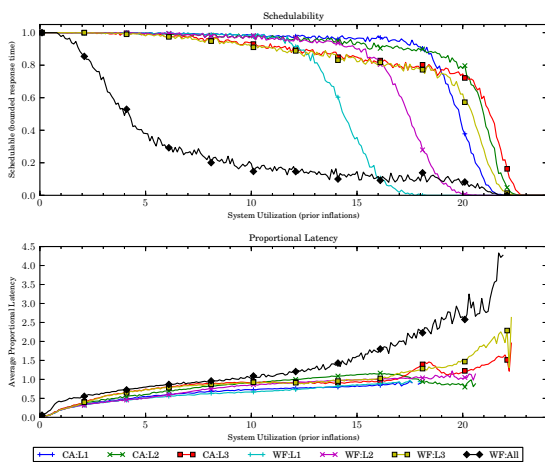


(a) Without polluter overheads.

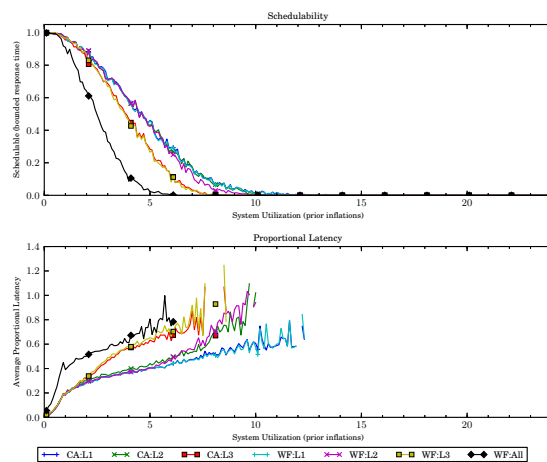


(b) With polluter overheads.

Figure 217: Results for *bimo-heavy* per-task utilization, *uni-moderate* period, *heavy-weight* EWSS, and *uni-short* height factor.

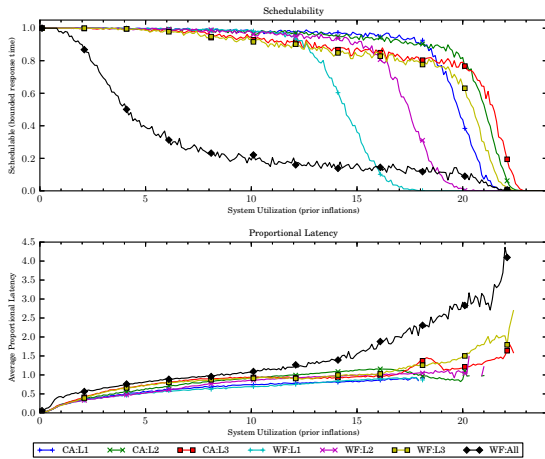


(a) Without polluter overheads.

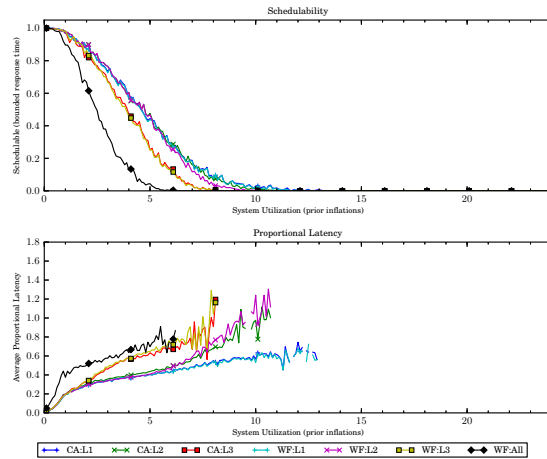


(b) With polluter overheads.

Figure 218: Results for *bimo-heavy* per-task utilization, *uni-moderate* period, *heavy-weight* EWSS, and *uni-medium* height factor.

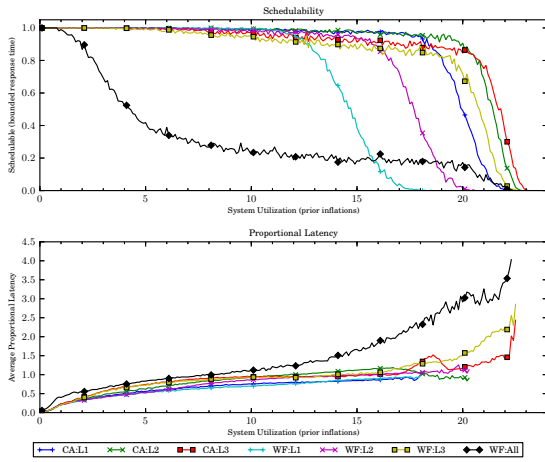


(a) Without polluter overheads.

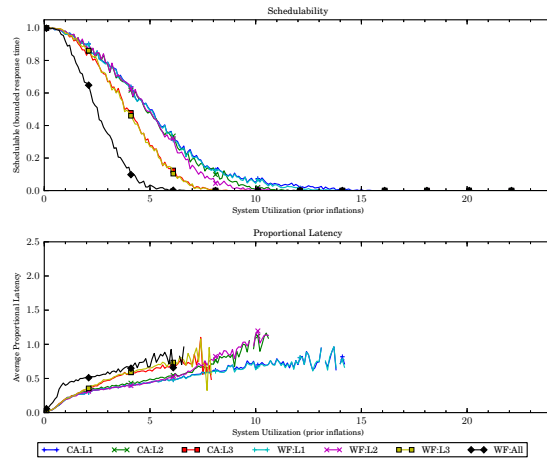


(b) With polluter overheads.

Figure 219: Results for *bimo-heavy* per-task utilization, *uni-moderate* period, *heavy-weight* EWSS, and *uni-tall* height factor.

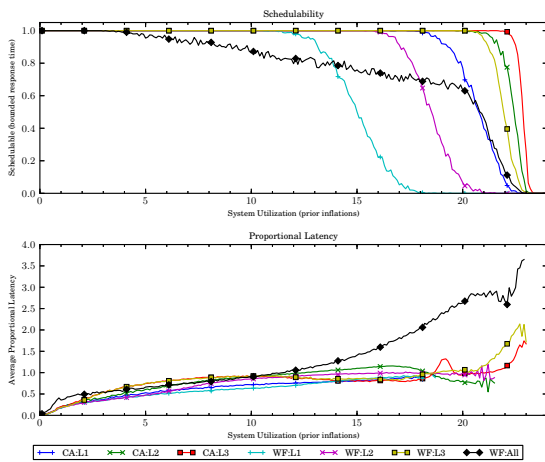


(a) Without polluter overheads.

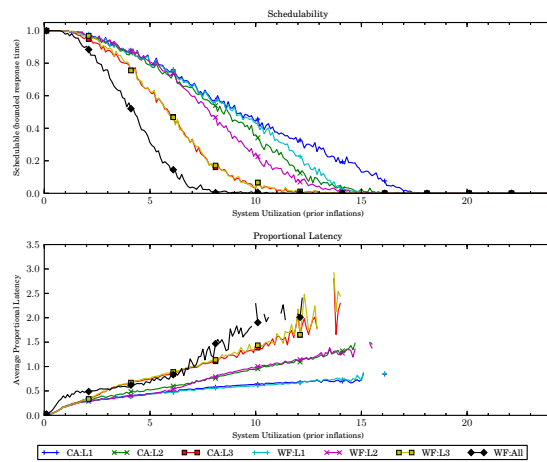


(b) With polluter overheads.

Figure 220: Results for *bimo-heavy* per-task utilization, *uni-moderate* period, *heavy-weight* EWSS, and *pipeline* height factor.

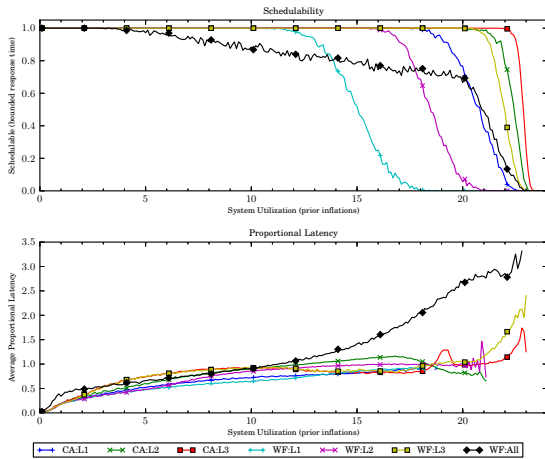


(a) Without polluter overheads.

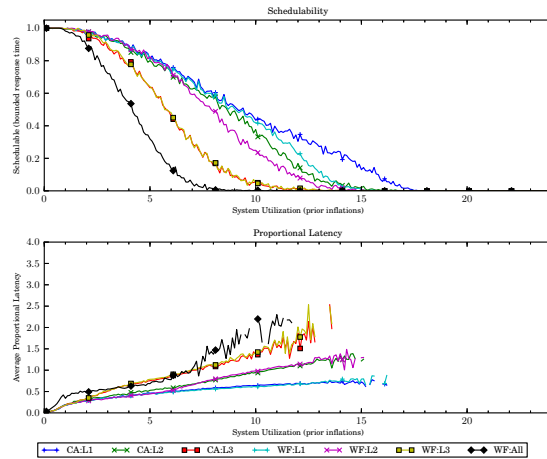


(b) With polluter overheads.

Figure 221: Results for *bimo-heavy* per-task utilization, *uni-long* period, *heavy-weight* EWSS, and *uni-short* height factor.

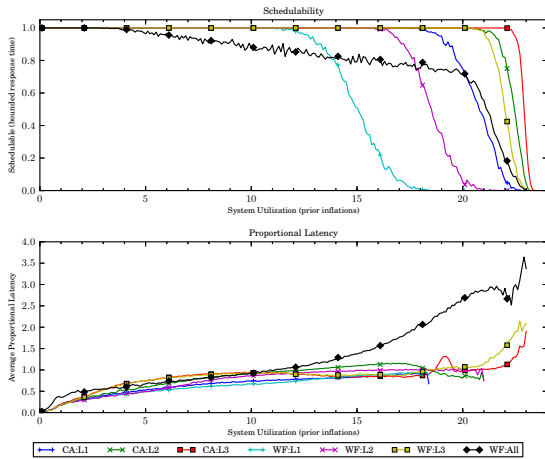


(a) Without polluter overheads.

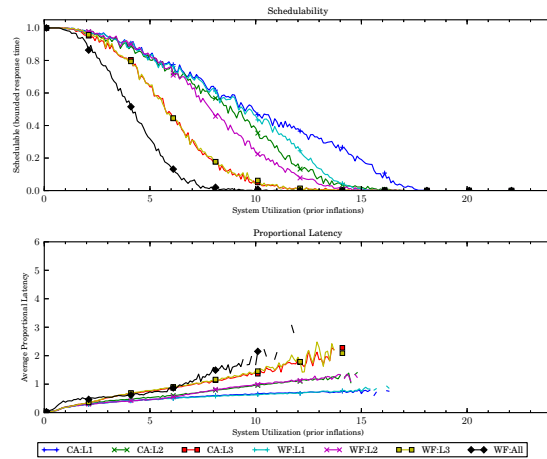


(b) With polluter overheads.

Figure 222: Results for *bimo-heavy* per-task utilization, *uni-long* period, *heavy-weight* EWSS, and *uni-medium* height factor.

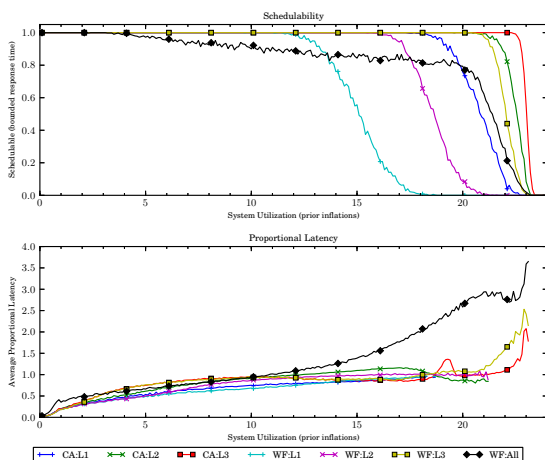


(a) Without polluter overheads.

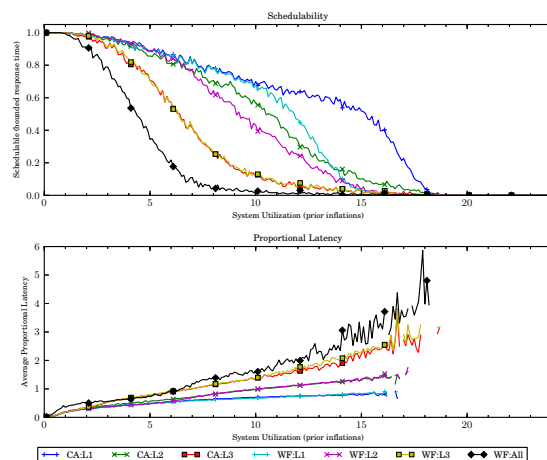


(b) With polluter overheads.

Figure 223: Results for *bimo-heavy* per-task utilization, *uni-long* period, *heavy-weight* EWSS, and *uni-tall* height factor.

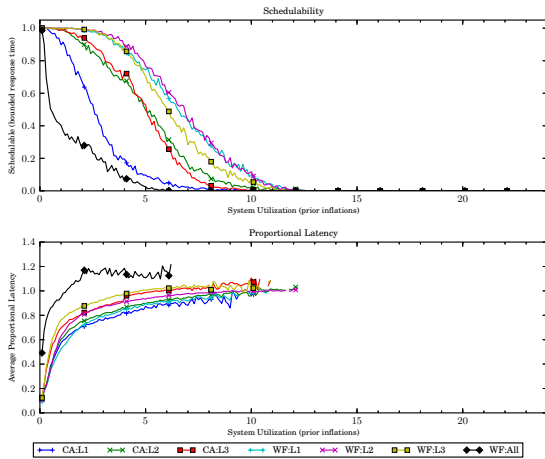


(a) Without polluter overheads.

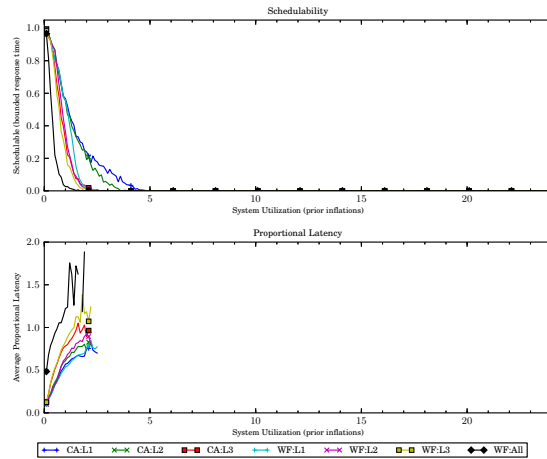


(b) With polluter overheads.

Figure 224: Results for *bimo-heavy* per-task utilization, *uni-long* period, *heavy-weight* EWSS, and *pipeline* height factor.

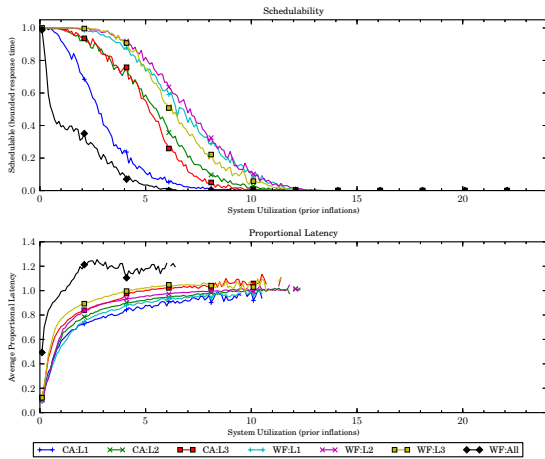


(a) Without polluter overheads.

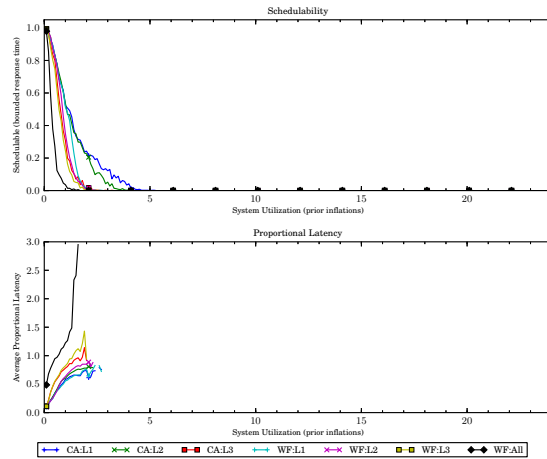


(b) With polluter overheads.

Figure 225: Results for *uni-light* per-task utilization, *uni-short* period, *bimo-light-weight* EWSS, and *uni-short* height factor.

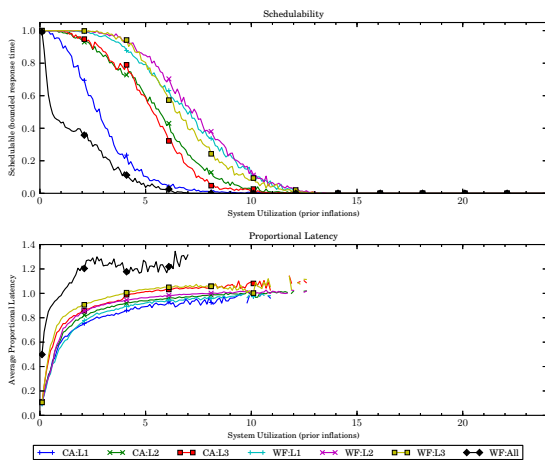


(a) Without polluter overheads.

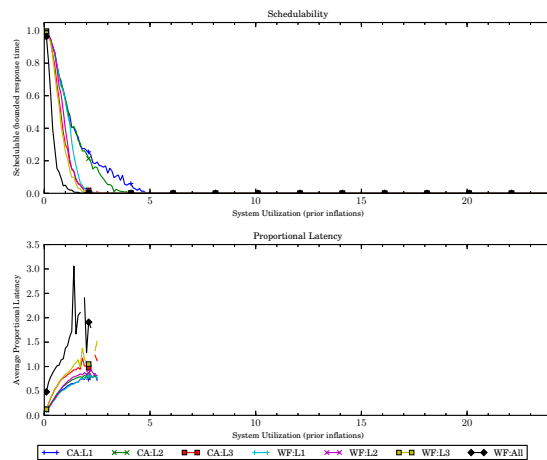


(b) With polluter overheads.

Figure 226: Results for *uni-light* per-task utilization, *uni-short* period, *bimo-light-weight* EWSS, and *uni-medium* height factor.

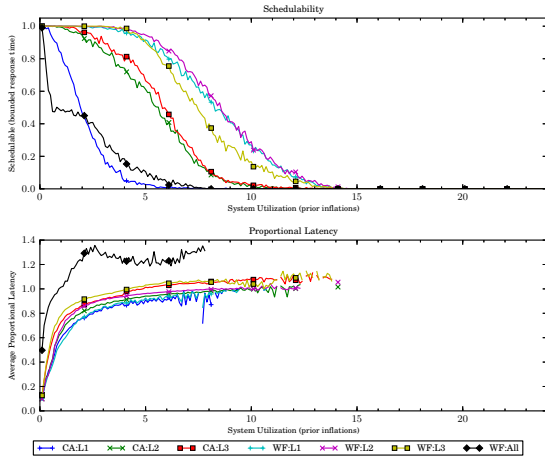


(a) Without polluter overheads.

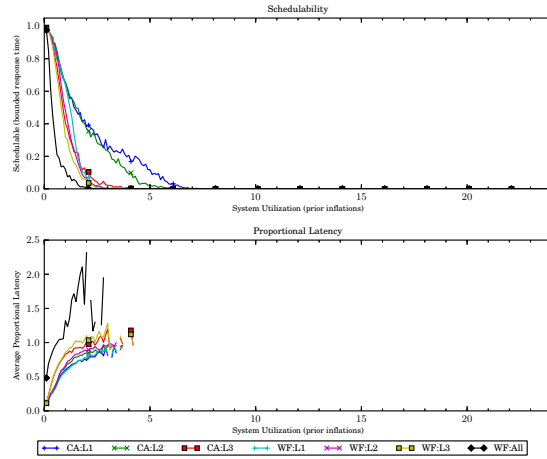


(b) With polluter overheads.

Figure 227: Results for *uni-light* per-task utilization, *uni-short* period, *bimo-light-weight* EWSS, and *uni-tall* height factor.

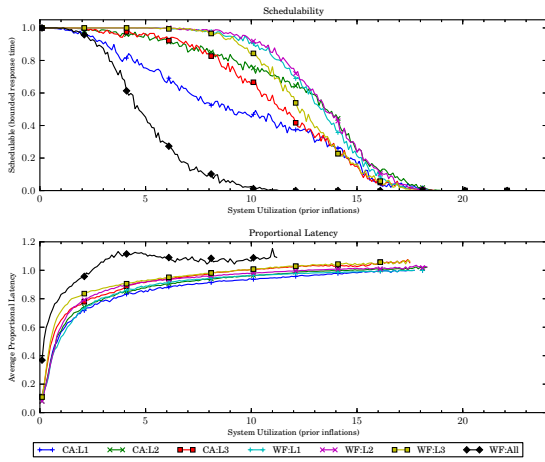


(a) Without polluter overheads.

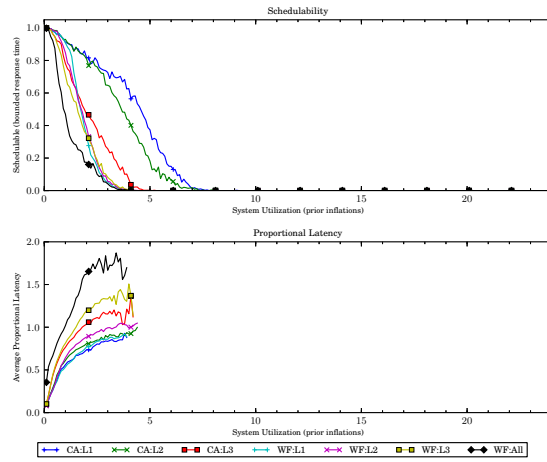


(b) With polluter overheads.

Figure 228: Results for *uni-light* per-task utilization, *uni-short* period, *bimo-light-weight* EWSS, and *pipeline* height factor.

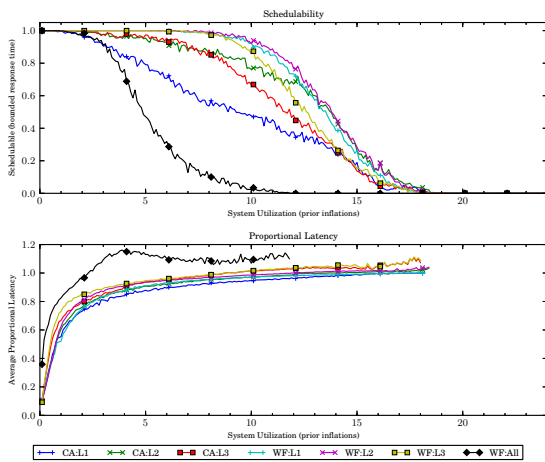


(a) Without polluter overheads.

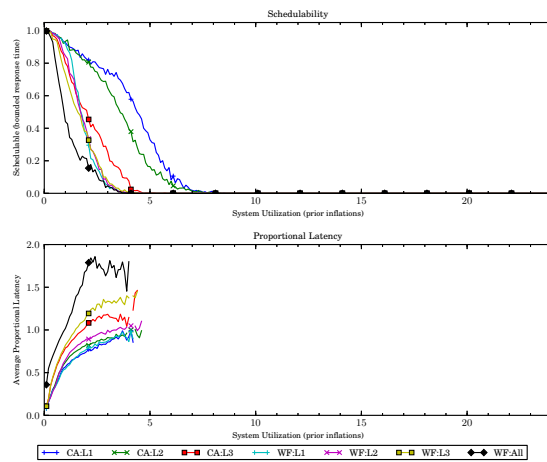


(b) With polluter overheads.

Figure 229: Results for *uni-light* per-task utilization, *uni-moderate* period, *bimo-light-weight* EWSS, and *uni-short* height factor.

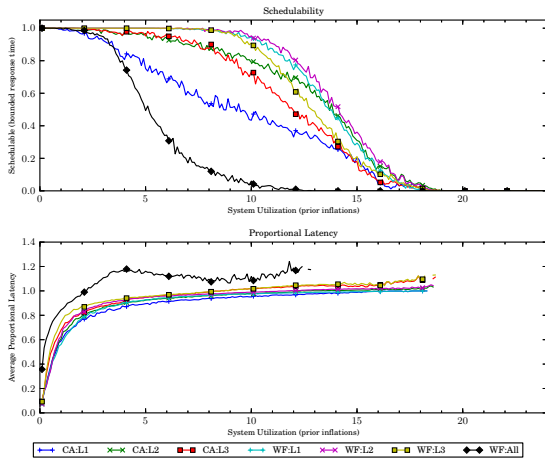


(a) Without polluter overheads.

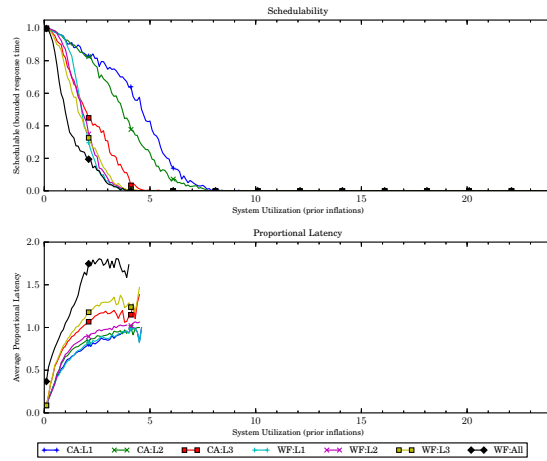


(b) With polluter overheads.

Figure 230: Results for *uni-light* per-task utilization, *uni-moderate* period, *bimo-light-weight* EWSS, and *uni-medium* height factor.

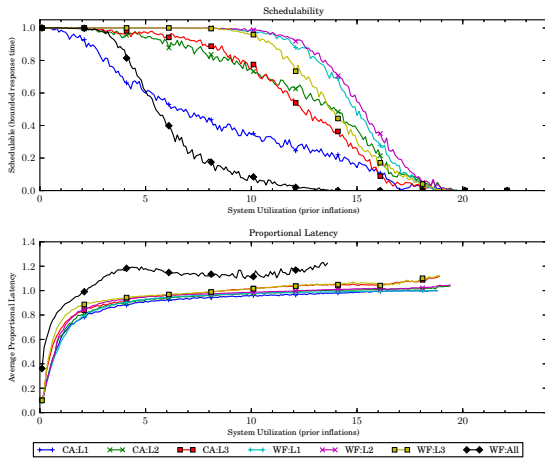


(a) Without polluter overheads.

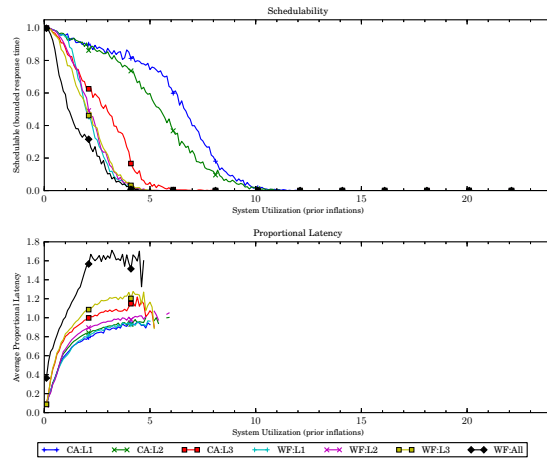


(b) With polluter overheads.

Figure 231: Results for *uni-light* per-task utilization, *uni-moderate* period, *bimo-light-weight* EWSS, and *uni-tall* height factor.

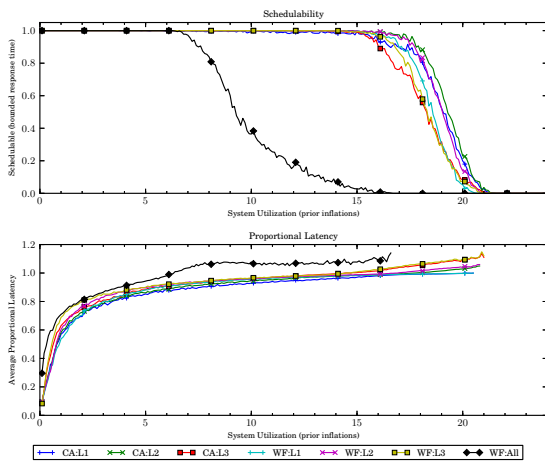


(a) Without polluter overheads.

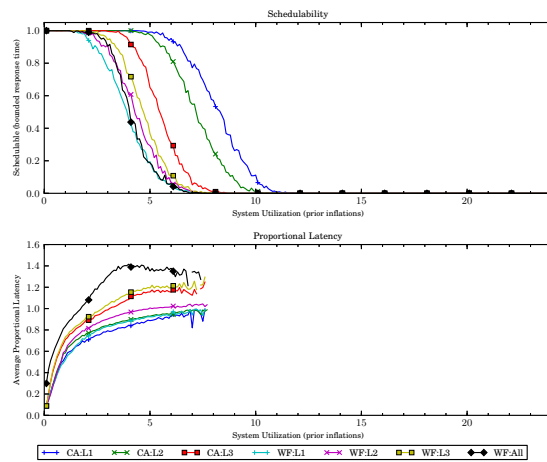


(b) With polluter overheads.

Figure 232: Results for *uni-light* per-task utilization, *uni-moderate* period, *bimo-light-weight* EWSS, and *pipeline* height factor.

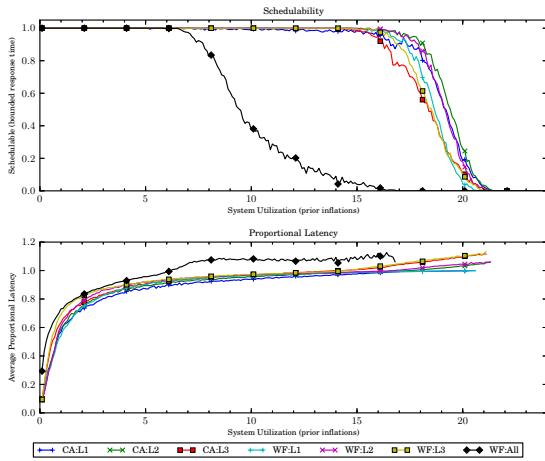


(a) Without polluter overheads.

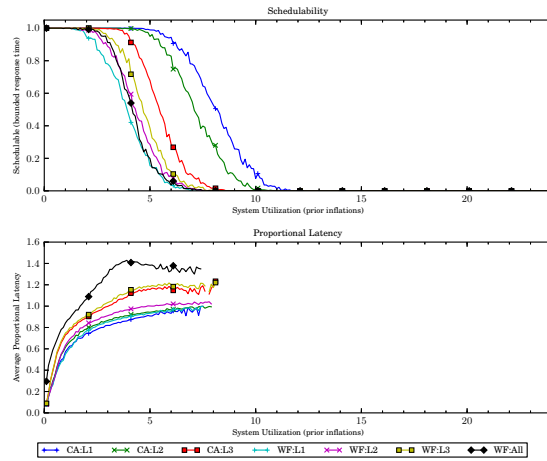


(b) With polluter overheads.

Figure 233: Results for *uni-light* per-task utilization, *uni-long* period, *bimo-light-weight* EWSS, and *uni-short* height factor.

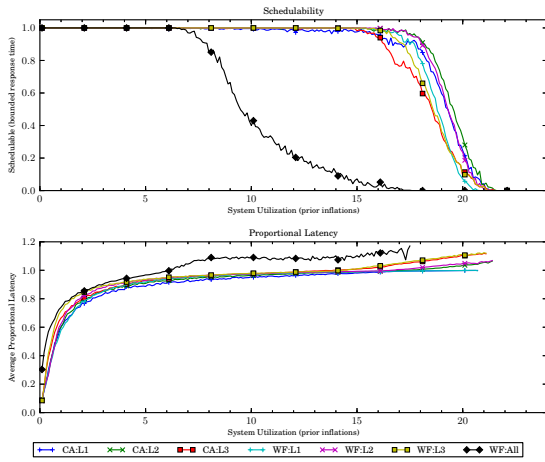


(a) Without polluter overheads.

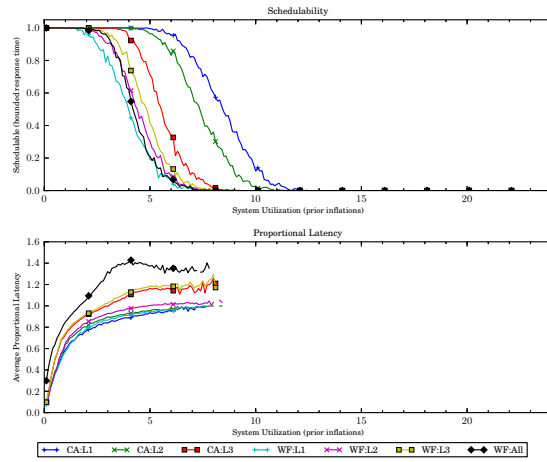


(b) With polluter overheads.

Figure 234: Results for *uni-light* per-task utilization, *uni-long* period, *bimo-light-weight* EWSS, and *uni-medium* height factor.

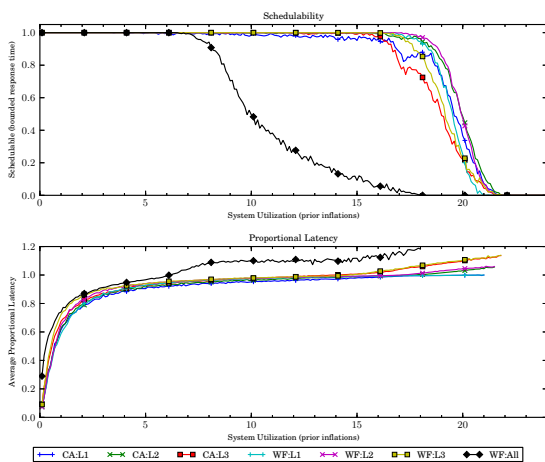


(a) Without polluter overheads.

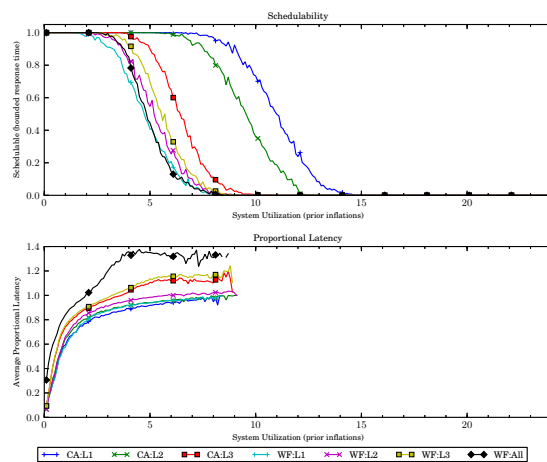


(b) With polluter overheads.

Figure 235: Results for *uni-light* per-task utilization, *uni-long* period, *bimo-light-weight* EWSS, and *uni-tall* height factor.

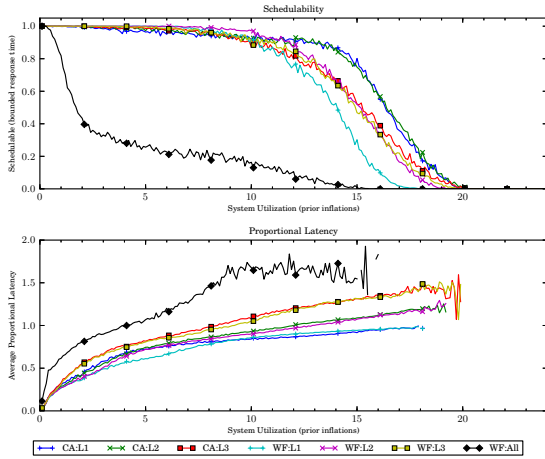


(a) Without polluter overheads.

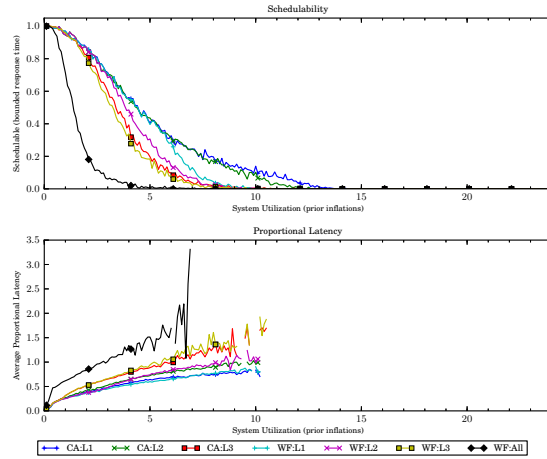


(b) With polluter overheads.

Figure 236: Results for *uni-light* per-task utilization, *uni-long* period, *bimo-light-weight* EWSS, and *pipeline* height factor.

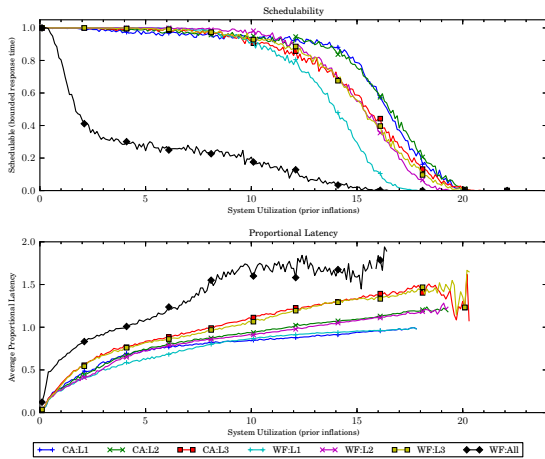


(a) Without polluter overheads.

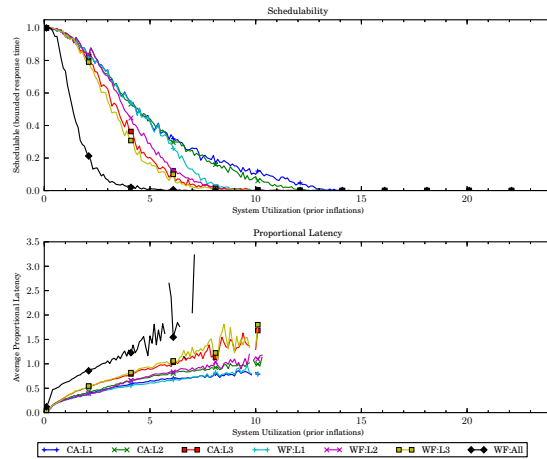


(b) With polluter overheads.

Figure 237: Results for *uni-medium* per-task utilization, *uni-short* period, *bimo-light-weight* EWSS, and *uni-short* height factor.

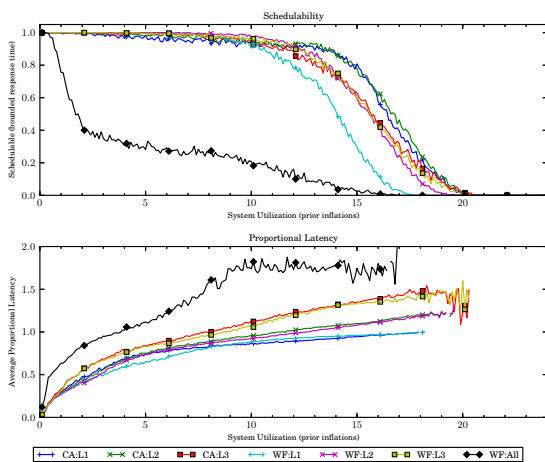


(a) Without polluter overheads.

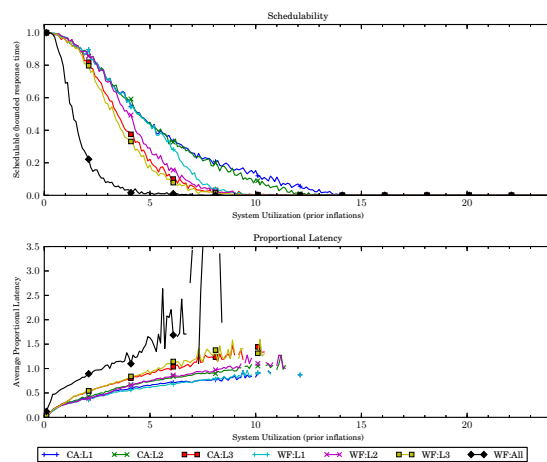


(b) With polluter overheads.

Figure 238: Results for *uni-medium* per-task utilization, *uni-short* period, *bimo-light-weight* EWSS, and *uni-medium* height factor.

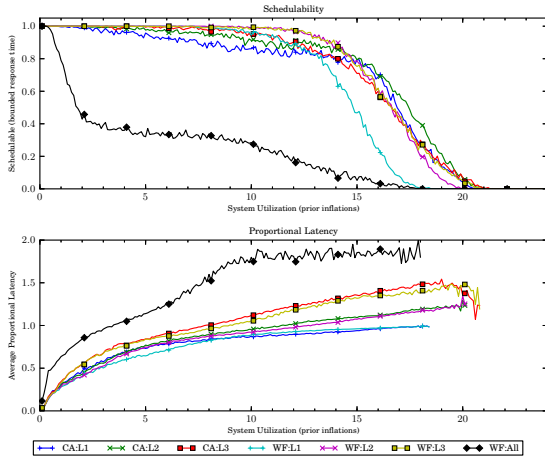


(a) Without polluter overheads.

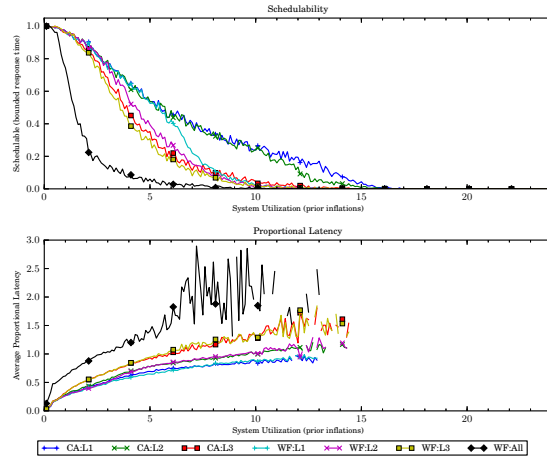


(b) With polluter overheads.

Figure 239: Results for *uni-medium* per-task utilization, *uni-short* period, *bimo-light-weight* EWSS, and *uni-tall* height factor.

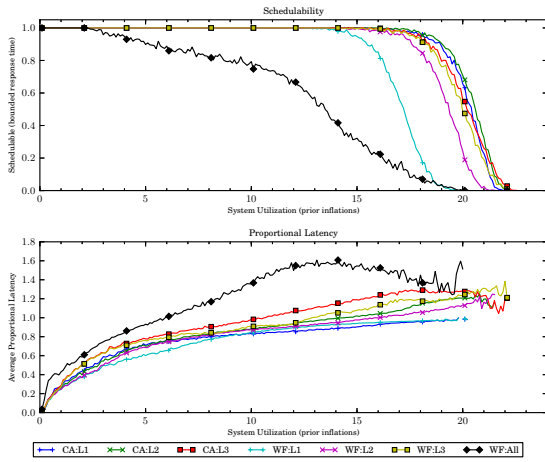


(a) Without polluter overheads.

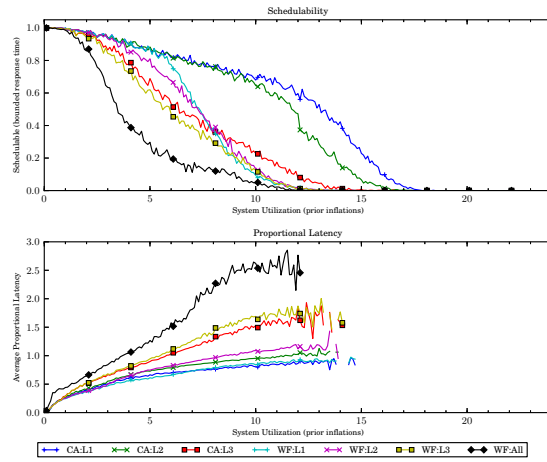


(b) With polluter overheads.

Figure 240: Results for *uni-medium* per-task utilization, *uni-short* period, *bimo-light-weight* EWSS, and *pipeline* height factor.

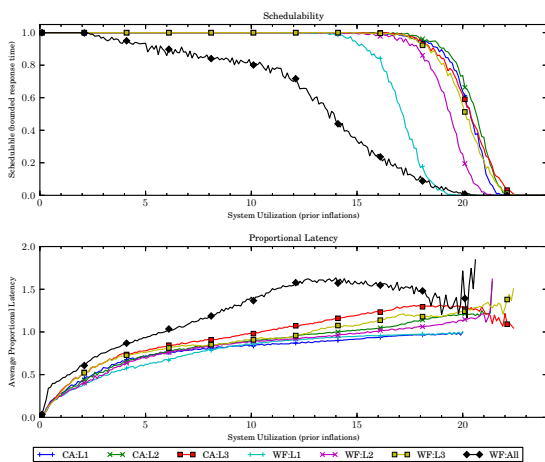


(a) Without polluter overheads.

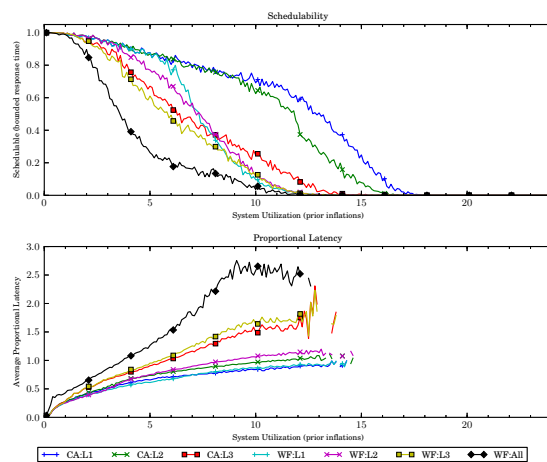


(b) With polluter overheads.

Figure 241: Results for *uni-medium* per-task utilization, *uni-moderate* period, *bimo-light-weight* EWSS, and *uni-short* height factor.

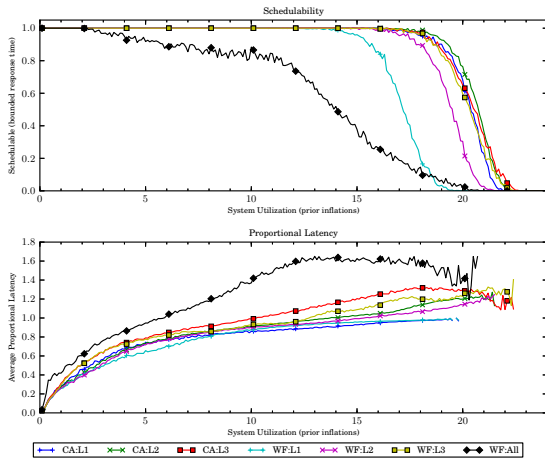


(a) Without polluter overheads.

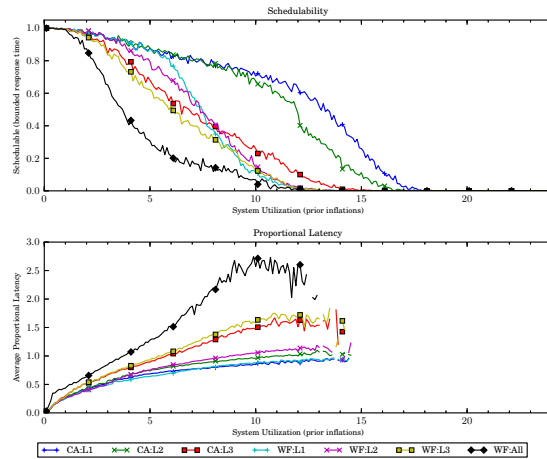


(b) With polluter overheads.

Figure 242: Results for *uni-medium* per-task utilization, *uni-moderate* period, *bimo-light-weight* EWSS, and *uni-medium* height factor.

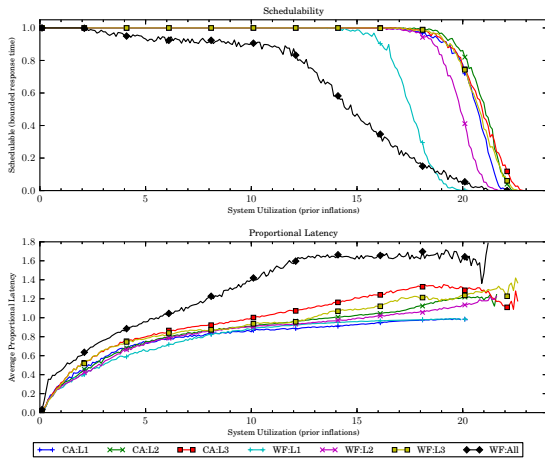


(a) Without polluter overheads.

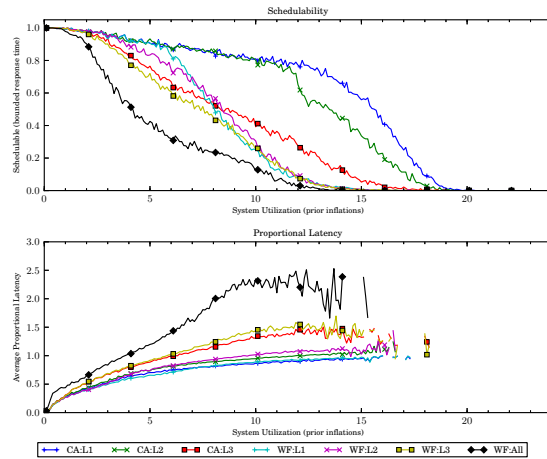


(b) With polluter overheads.

Figure 243: Results for *uni-medium* per-task utilization, *uni-moderate* period, *bimo-light-weight* EWSS, and *uni-tall* height factor.

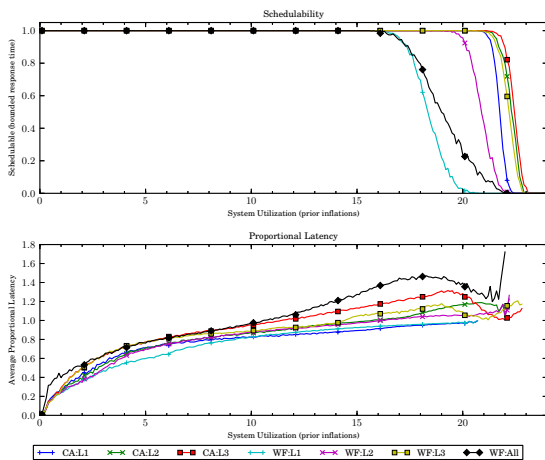


(a) Without polluter overheads.

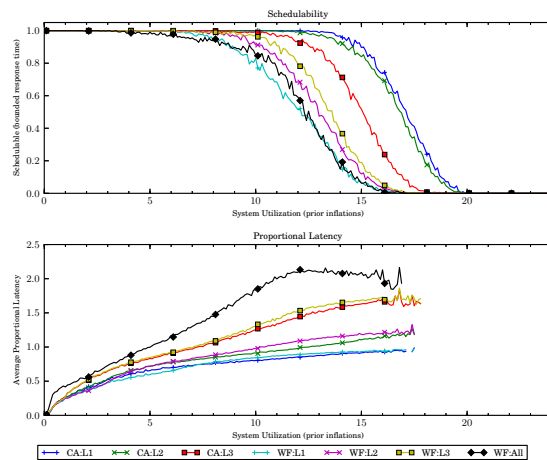


(b) With polluter overheads.

Figure 244: Results for *uni-medium* per-task utilization, *uni-moderate* period, *bimo-light-weight* EWSS, and *pipeline* height factor.

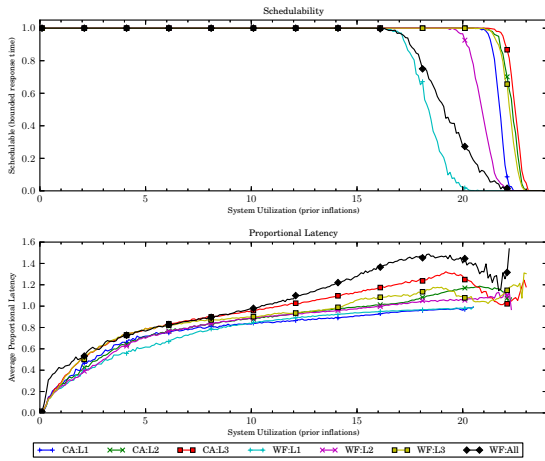


(a) Without polluter overheads.

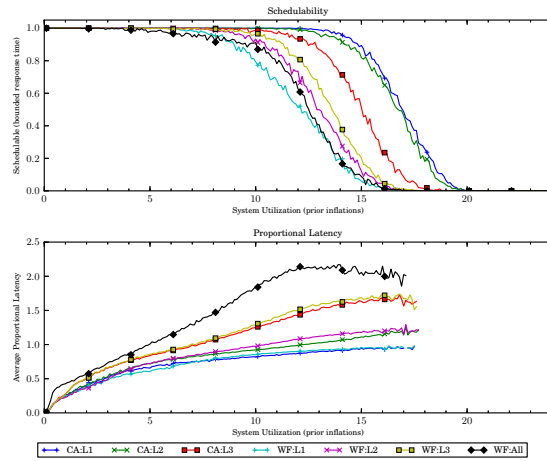


(b) With polluter overheads.

Figure 245: Results for *uni-medium* per-task utilization, *uni-long* period, *bimo-light-weight* EWSS, and *uni-short* height factor.

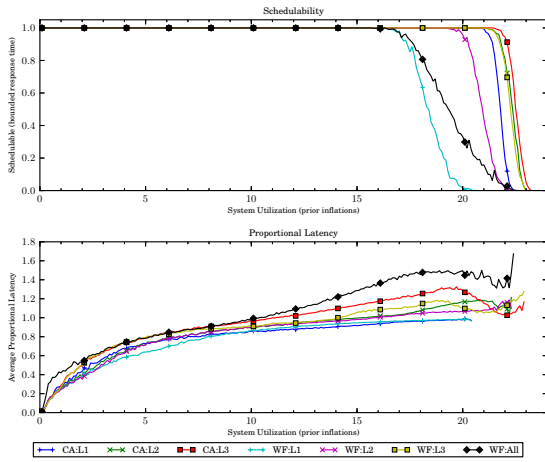


(a) Without polluter overheads.

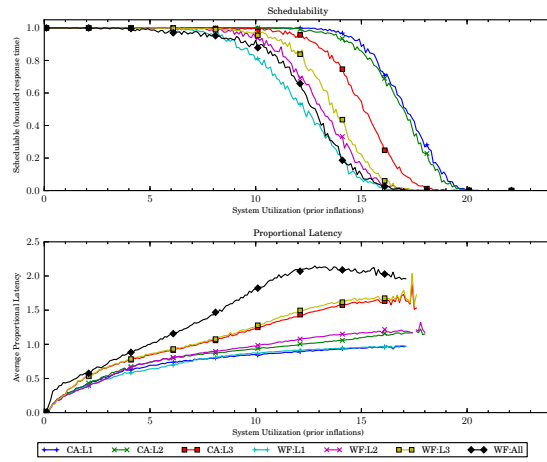


(b) With polluter overheads.

Figure 246: Results for *uni-medium* per-task utilization, *uni-long* period, *bimo-light-weight* EWSS, and *uni-medium* height factor.

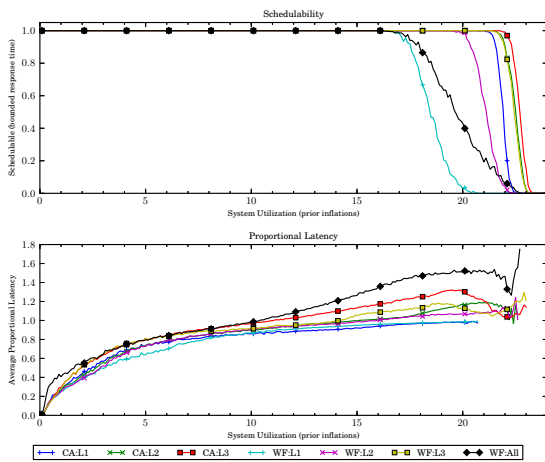


(a) Without polluter overheads.

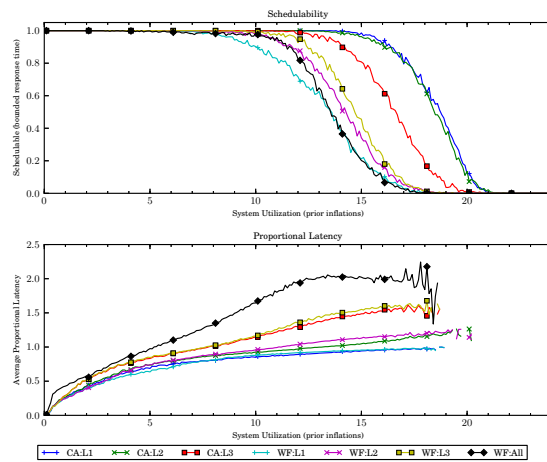


(b) With polluter overheads.

Figure 247: Results for *uni-medium* per-task utilization, *uni-long* period, *bimo-light-weight* EWSS, and *uni-tall* height factor.

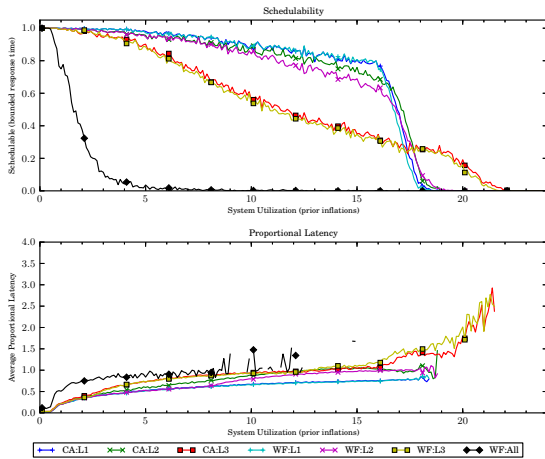


(a) Without polluter overheads.

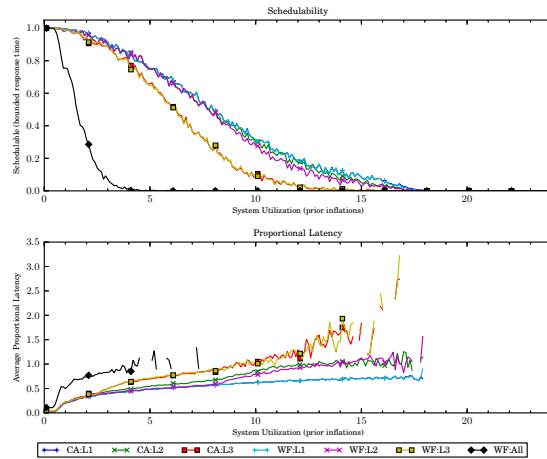


(b) With polluter overheads.

Figure 248: Results for *uni-medium* per-task utilization, *uni-long* period, *bimo-light-weight* EWSS, and *pipeline* height factor.

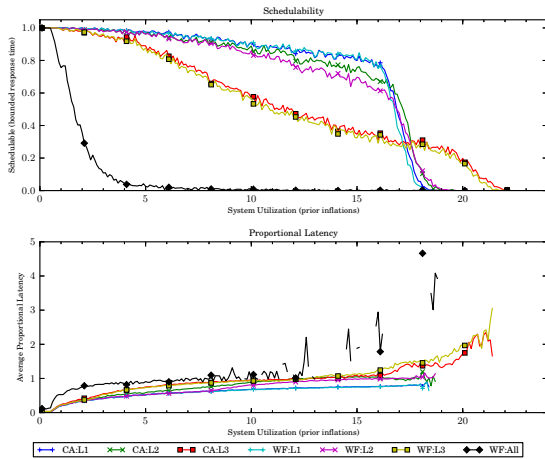


(a) Without polluter overheads.

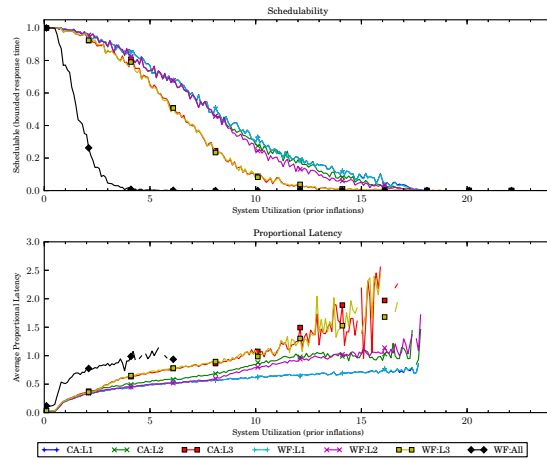


(b) With polluter overheads.

Figure 249: Results for *uni-heavy* per-task utilization, *uni-short* period, *bimo-light-weight* EWSS, and *uni-short* height factor.

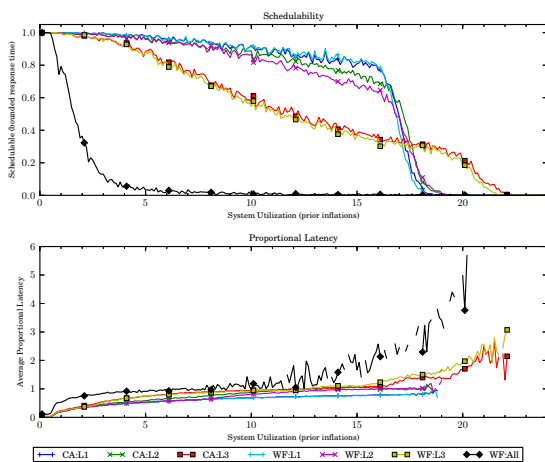


(a) Without polluter overheads.

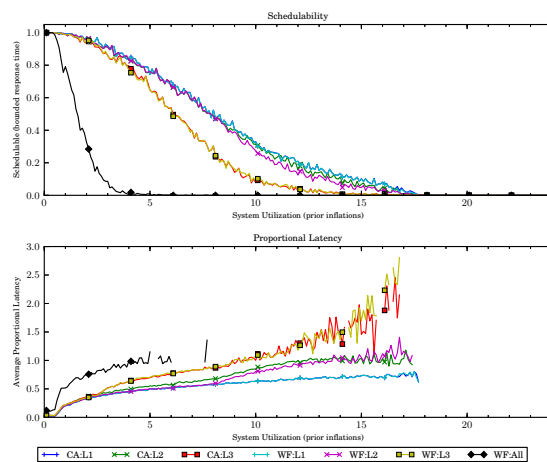


(b) With polluter overheads.

Figure 250: Results for *uni-heavy* per-task utilization, *uni-short* period, *bimo-light-weight* EWSS, and *uni-medium* height factor.

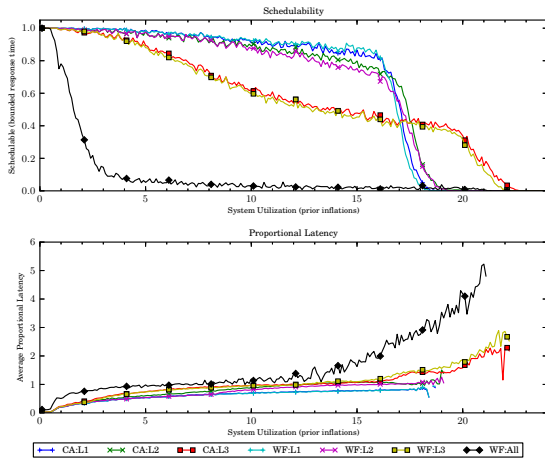


(a) Without polluter overheads.

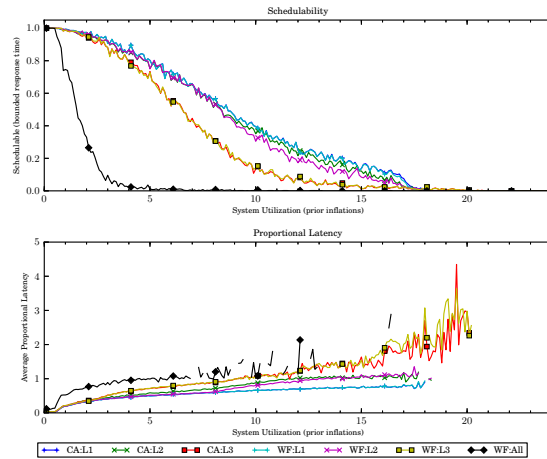


(b) With polluter overheads.

Figure 251: Results for *uni-heavy* per-task utilization, *uni-short* period, *bimo-light-weight* EWSS, and *uni-tall* height factor.

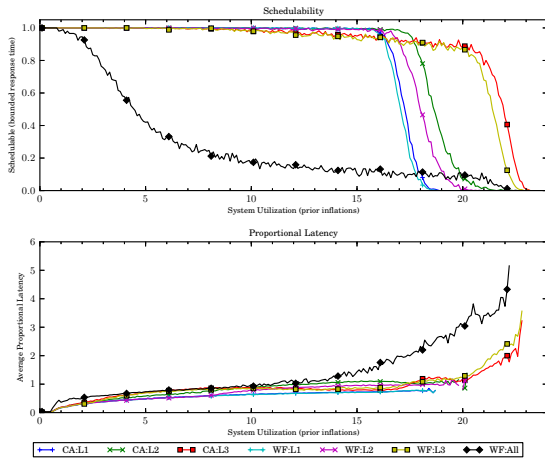


(a) Without polluter overheads.

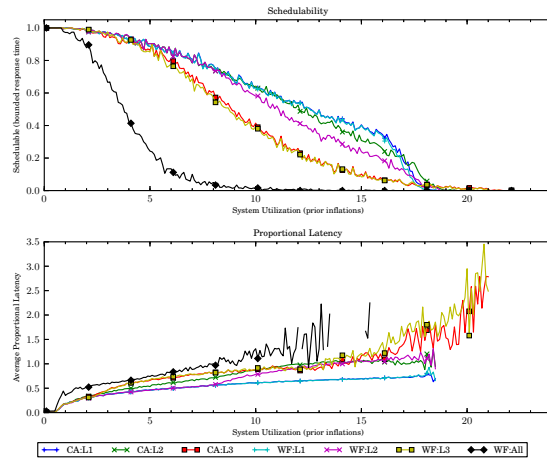


(b) With polluter overheads.

Figure 252: Results for *uni-heavy* per-task utilization, *uni-short* period, *bimo-light-weight* EWSS, and *pipeline* height factor.

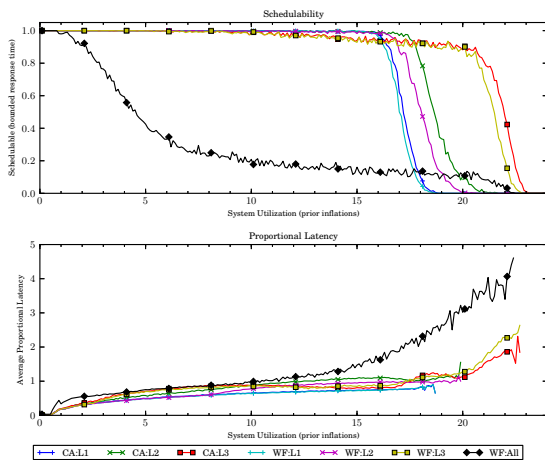


(a) Without polluter overheads.

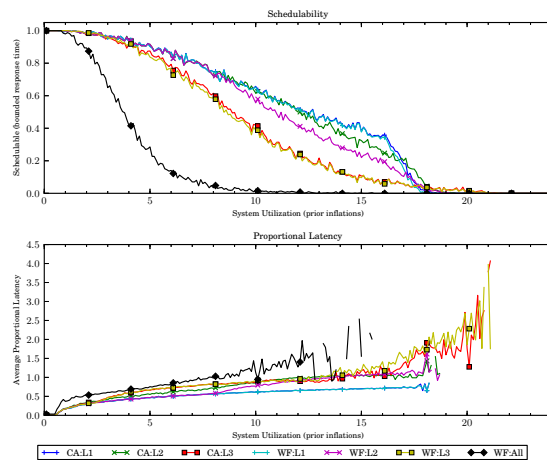


(b) With polluter overheads.

Figure 253: Results for *uni-heavy* per-task utilization, *uni-moderate* period, *bimo-light-weight* EWSS, and *uni-short* height factor.

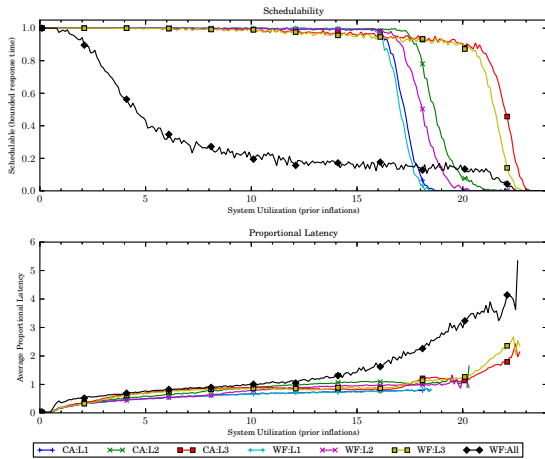


(a) Without polluter overheads.

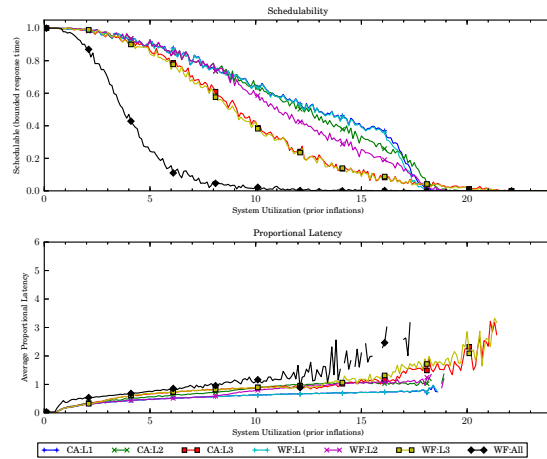


(b) With polluter overheads.

Figure 254: Results for *uni-heavy* per-task utilization, *uni-moderate* period, *bimo-light-weight* EWSS, and *uni-medium* height factor.

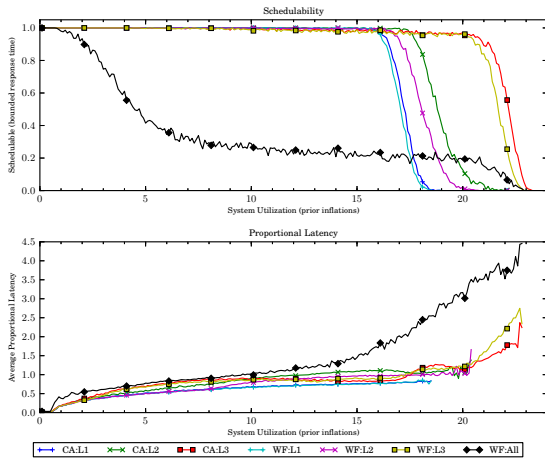


(a) Without polluter overheads.

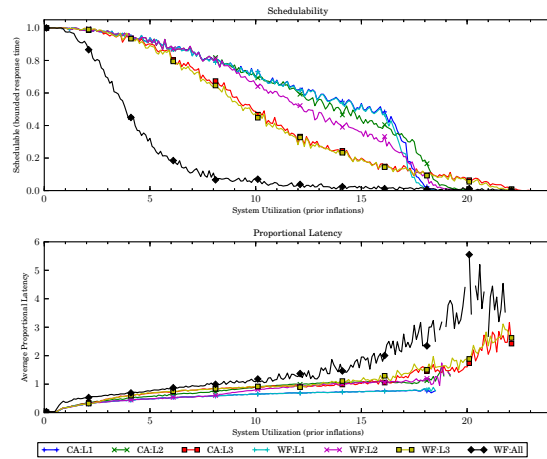


(b) With polluter overheads.

Figure 255: Results for *uni-heavy* per-task utilization, *uni-moderate* period, *bimo-light-weight* EWSS, and *uni-tall* height factor.

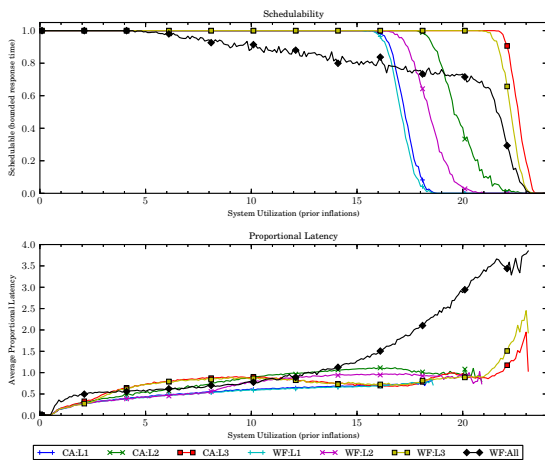


(a) Without polluter overheads.

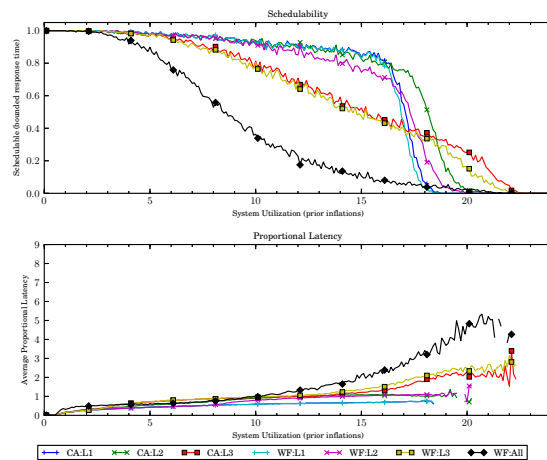


(b) With polluter overheads.

Figure 256: Results for *uni-heavy* per-task utilization, *uni-moderate* period, *bimo-light-weight* EWSS, and *pipeline* height factor.

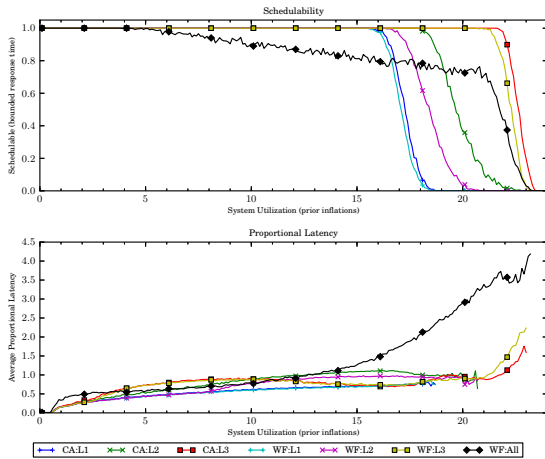


(a) Without polluter overheads.

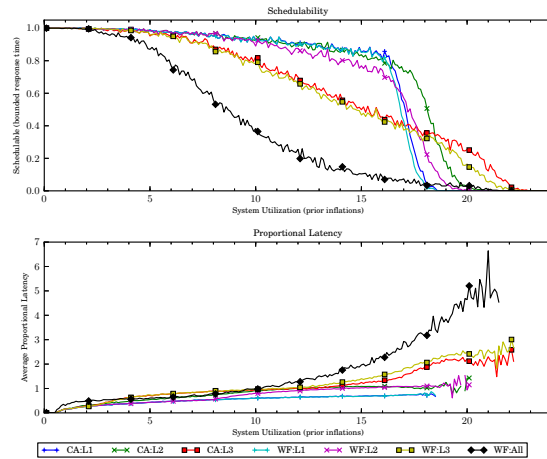


(b) With polluter overheads.

Figure 257: Results for *uni-heavy* per-task utilization, *uni-long* period, *bimo-light-weight* EWSS, and *uni-short* height factor.

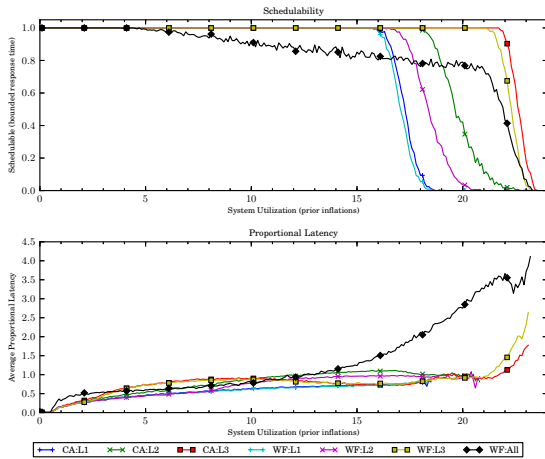


(a) Without polluter overheads.

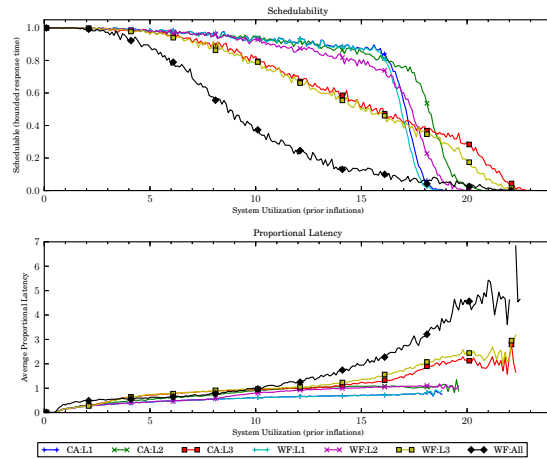


(b) With polluter overheads.

Figure 258: Results for *uni-heavy* per-task utilization, *uni-long* period, *bimo-light-weight* EWSS, and *uni-medium* height factor.

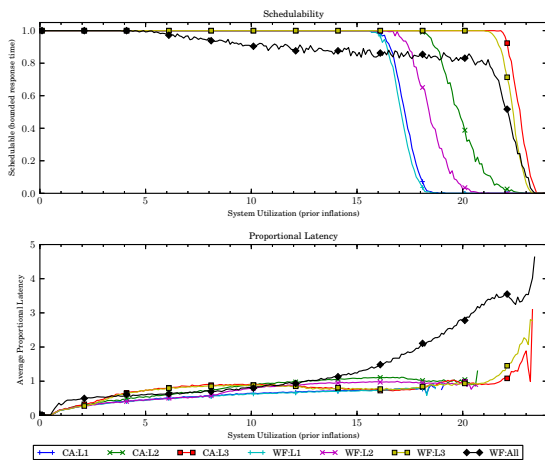


(a) Without polluter overheads.

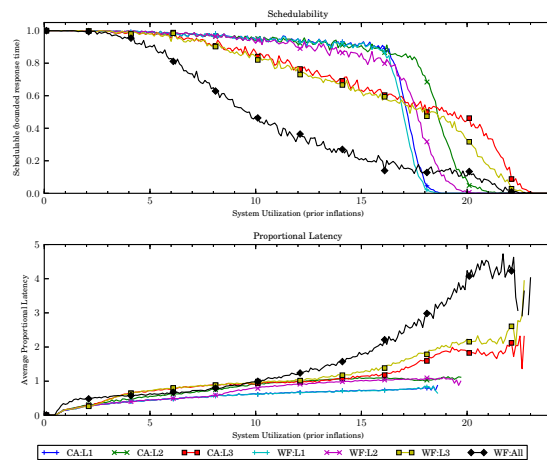


(b) With polluter overheads.

Figure 259: Results for *uni-heavy* per-task utilization, *uni-long* period, *bimo-light-weight* EWSS, and *uni-tall* height factor.

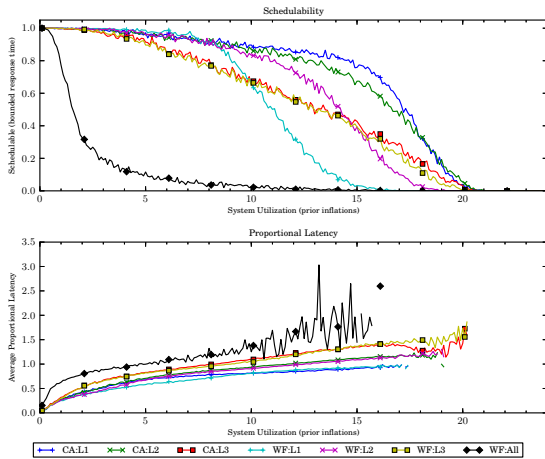


(a) Without polluter overheads.

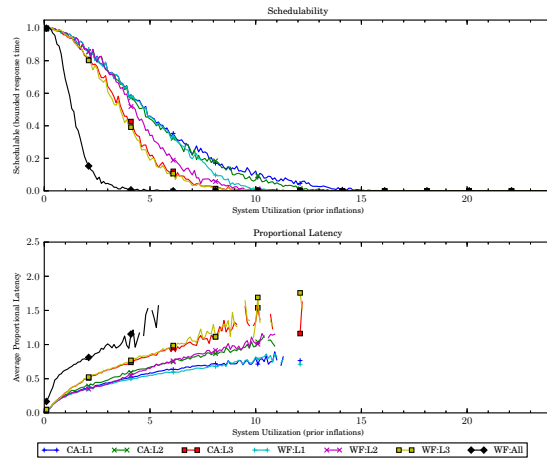


(b) With polluter overheads.

Figure 260: Results for *uni-heavy* per-task utilization, *uni-long* period, *bimo-light-weight* EWSS, and *pipeline* height factor.

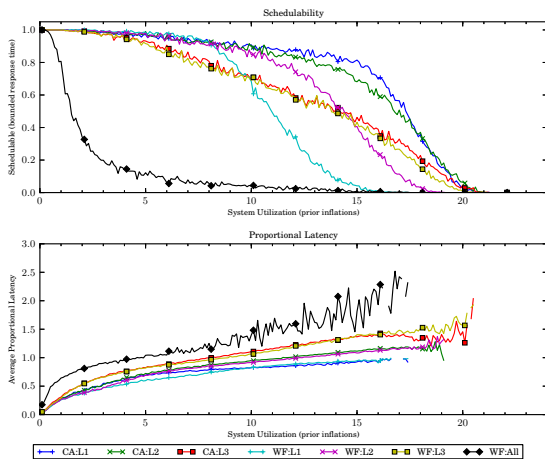


(a) Without polluter overheads.

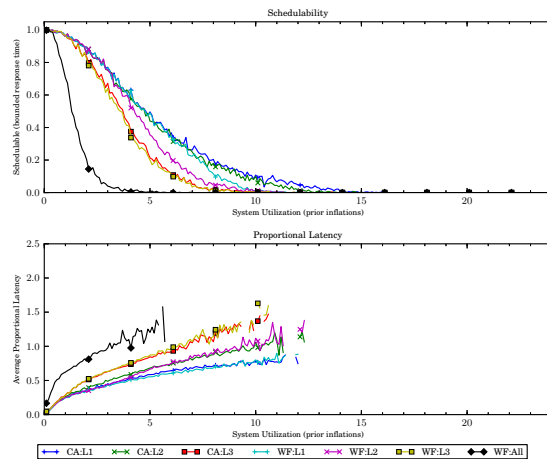


(b) With polluter overheads.

Figure 261: Results for *bimo-light* per-task utilization, *uni-short* period, *bimo-light-weight* EWSS, and *uni-short* height factor.

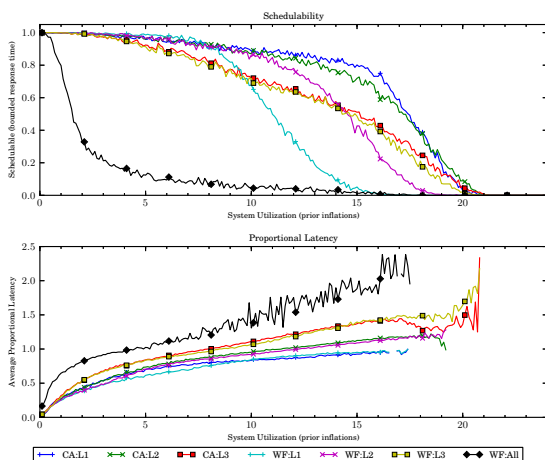


(a) Without polluter overheads.

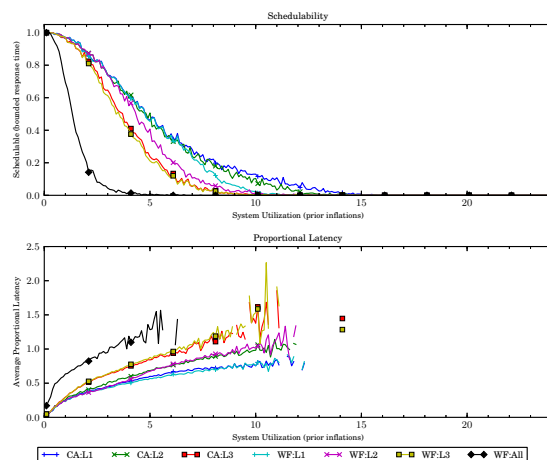


(b) With polluter overheads.

Figure 262: Results for *bimo-light* per-task utilization, *uni-short* period, *bimo-light-weight* EWSS, and *uni-medium* height factor.

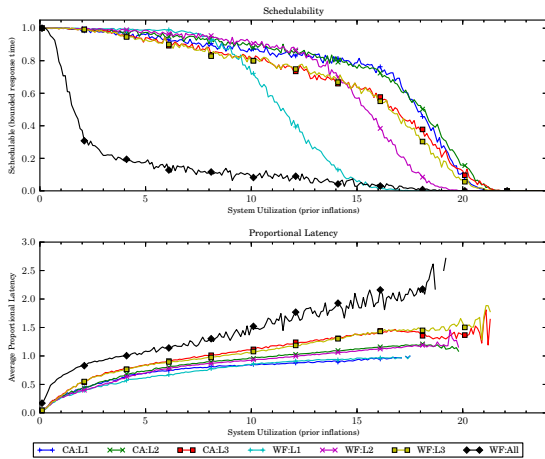


(a) Without polluter overheads.

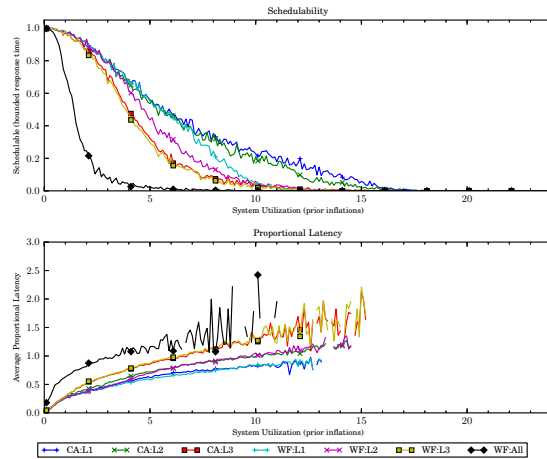


(b) With polluter overheads.

Figure 263: Results for *bimo-light* per-task utilization, *uni-short* period, *bimo-light-weight* EWSS, and *uni-tall* height factor.

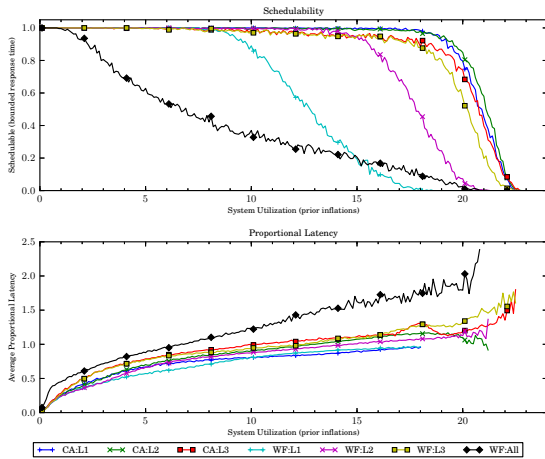


(a) Without polluter overheads.

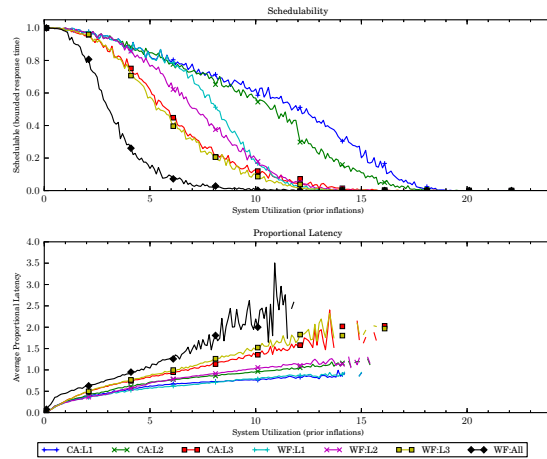


(b) With polluter overheads.

Figure 264: Results for *bimo-light* per-task utilization, *uni-short* period, *bimo-light-weight* EWSS, and *pipeline* height factor.

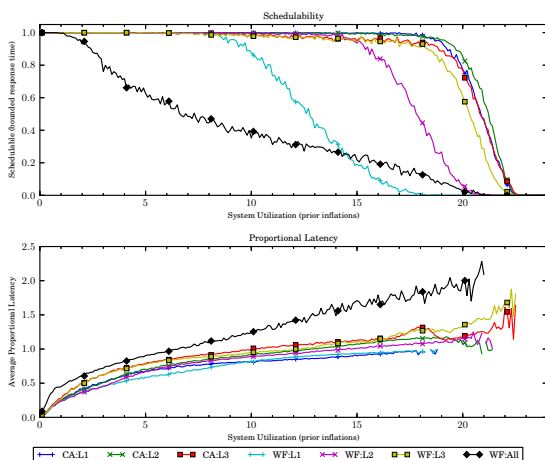


(a) Without polluter overheads.

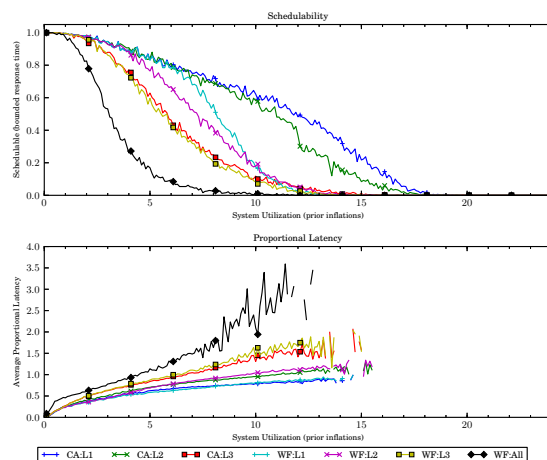


(b) With polluter overheads.

Figure 265: Results for *bimo-light* per-task utilization, *uni-moderate* period, *bimo-light-weight* EWSS, and *uni-short* height factor.

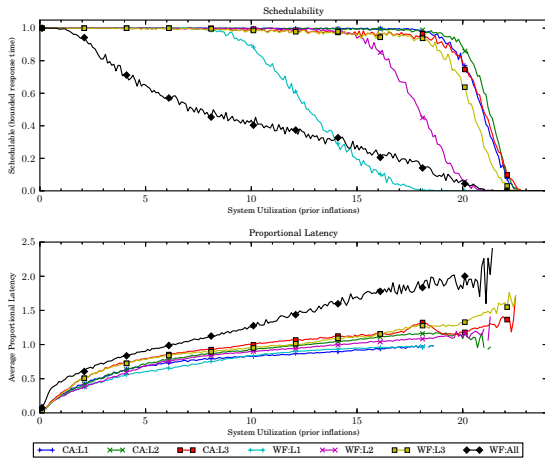


(a) Without polluter overheads.

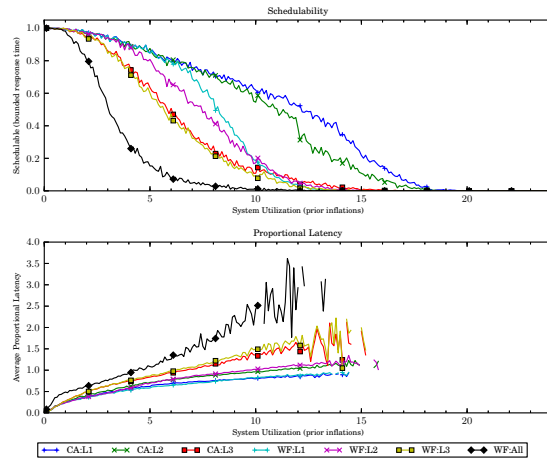


(b) With polluter overheads.

Figure 266: Results for *bimo-light* per-task utilization, *uni-moderate* period, *bimo-light-weight* EWSS, and *uni-medium* height factor.

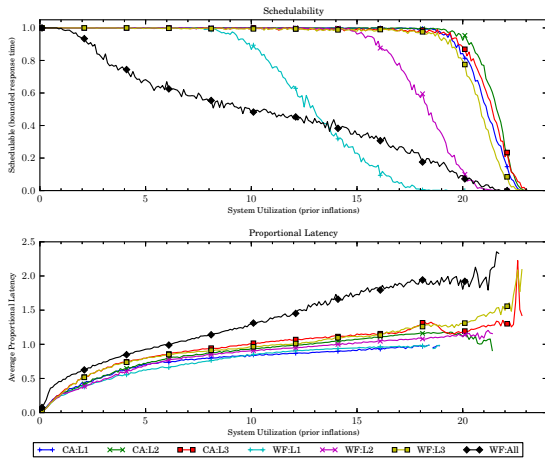


(a) Without polluter overheads.

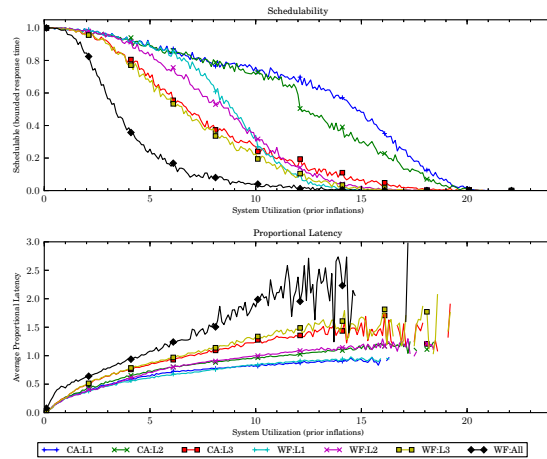


(b) With polluter overheads.

Figure 267: Results for *bimo-light* per-task utilization, *uni-moderate* period, *bimo-light-weight* EWSS, and *uni-tall* height factor.

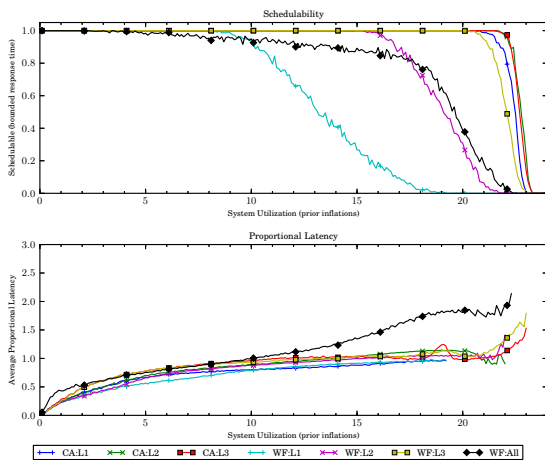


(a) Without polluter overheads.

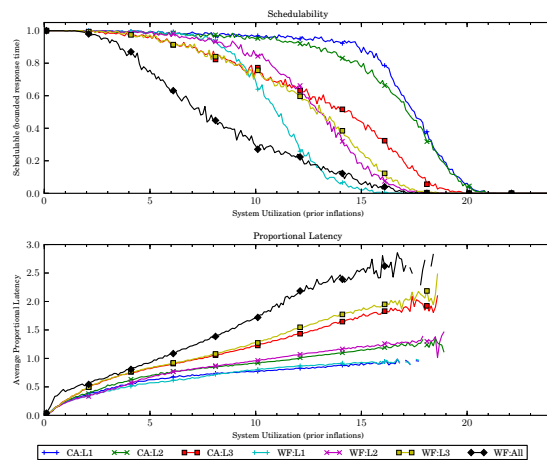


(b) With polluter overheads.

Figure 268: Results for *bimo-light* per-task utilization, *uni-moderate* period, *bimo-light-weight* EWSS, and *pipeline* height factor.

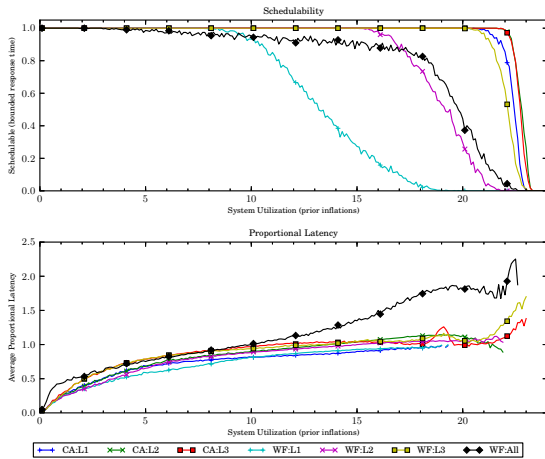


(a) Without polluter overheads.

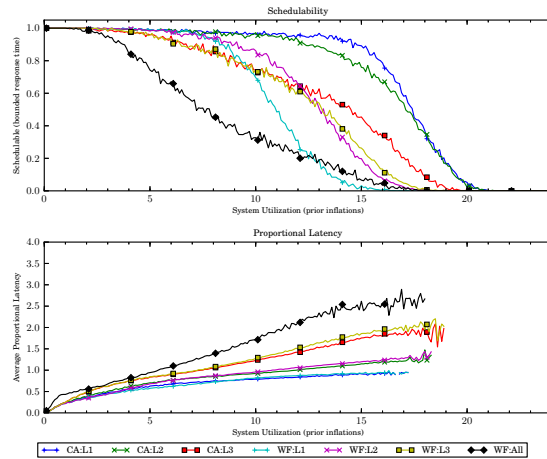


(b) With polluter overheads.

Figure 269: Results for *bimo-light* per-task utilization, *uni-long* period, *bimo-light-weight* EWSS, and *uni-short* height factor.

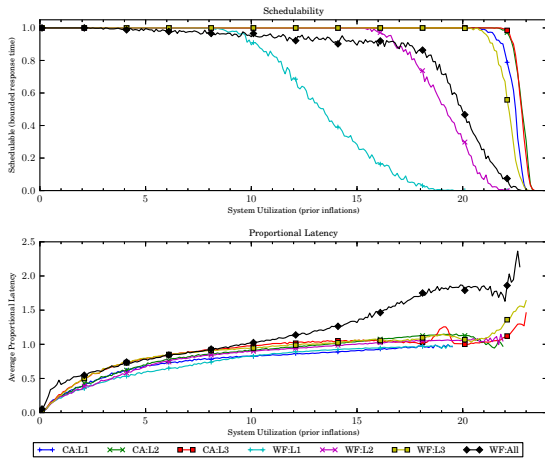


(a) Without polluter overheads.

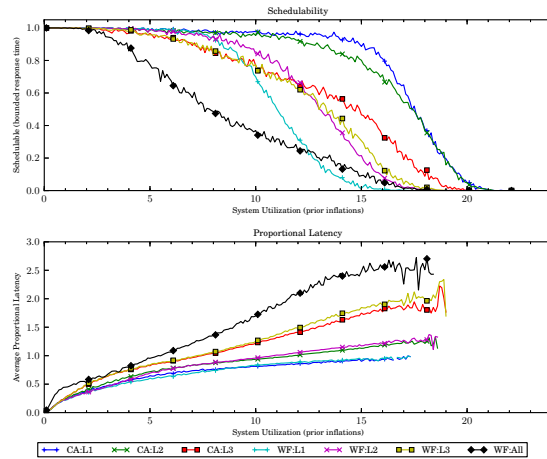


(b) With polluter overheads.

Figure 270: Results for *bimo-light* per-task utilization, *uni-long* period, *bimo-light-weight* EWSS, and *uni-medium* height factor.

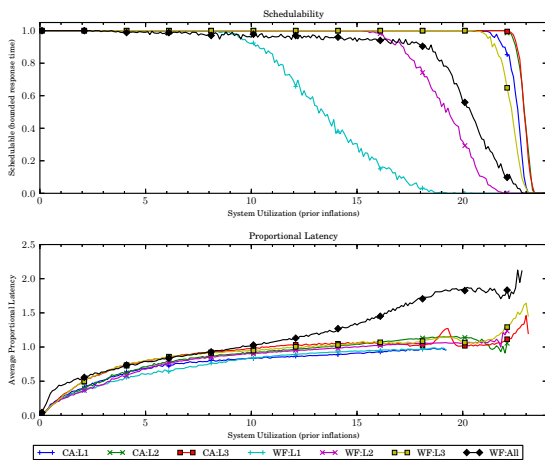


(a) Without polluter overheads.

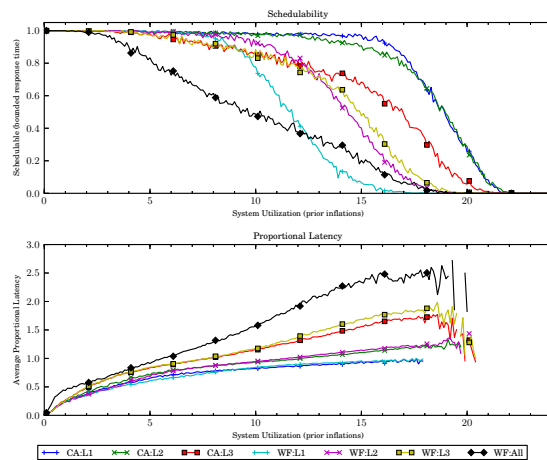


(b) With polluter overheads.

Figure 271: Results for *bimo-light* per-task utilization, *uni-long* period, *bimo-light-weight* EWSS, and *uni-tall* height factor.

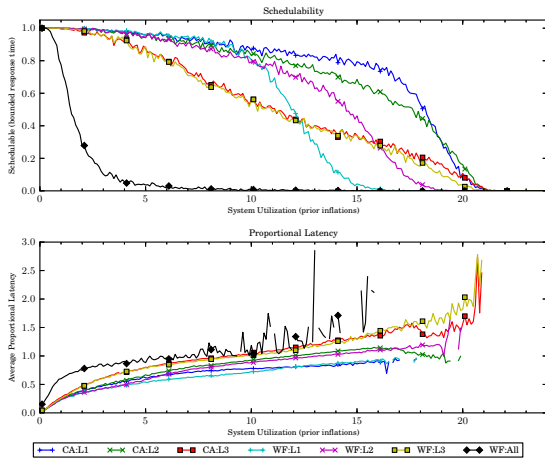


(a) Without polluter overheads.

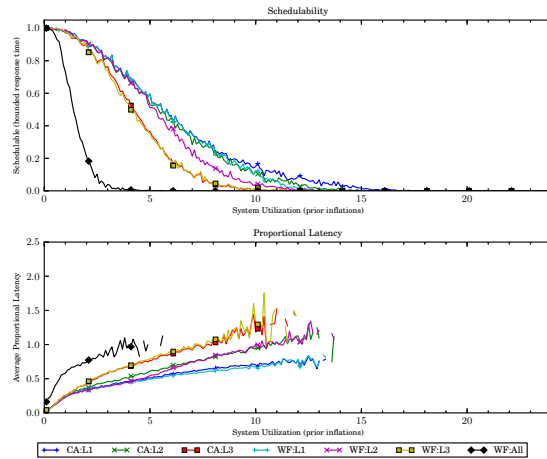


(b) With polluter overheads.

Figure 272: Results for *bimo-light* per-task utilization, *uni-long* period, *bimo-light-weight* EWSS, and *pipeline* height factor.

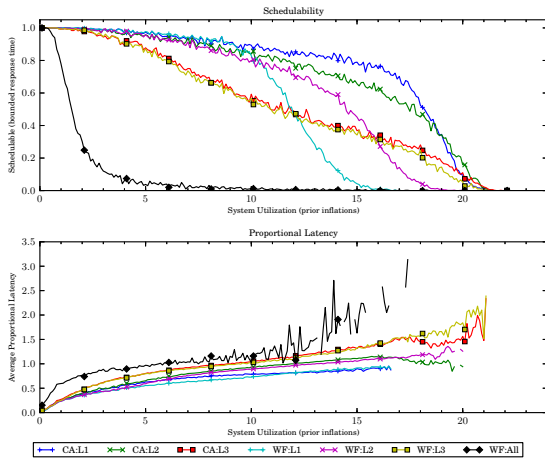


(a) Without polluter overheads.

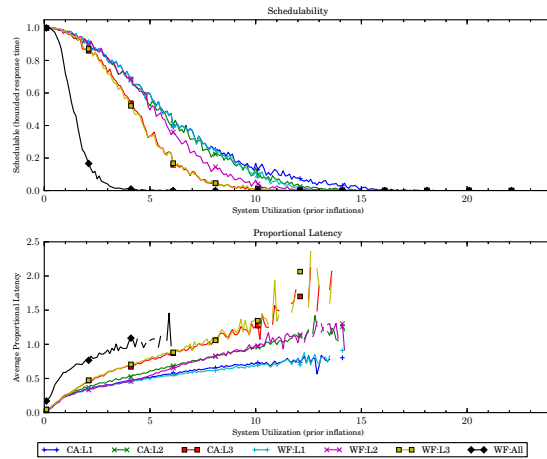


(b) With polluter overheads.

Figure 273: Results for *bimo-medium* per-task utilization, *uni-short* period, *bimo-light-weight* EWSS, and *uni-short* height factor.

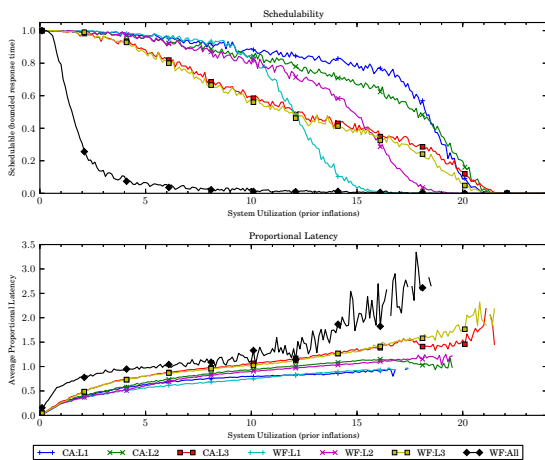


(a) Without polluter overheads.

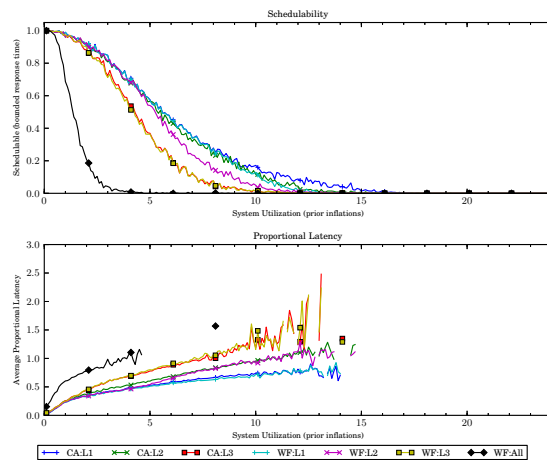


(b) With polluter overheads.

Figure 274: Results for *bimo-medium* per-task utilization, *uni-short* period, *bimo-light-weight* EWSS, and *uni-medium* height factor.

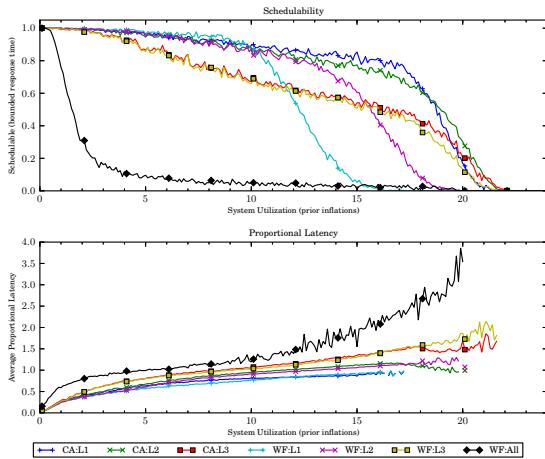


(a) Without polluter overheads.

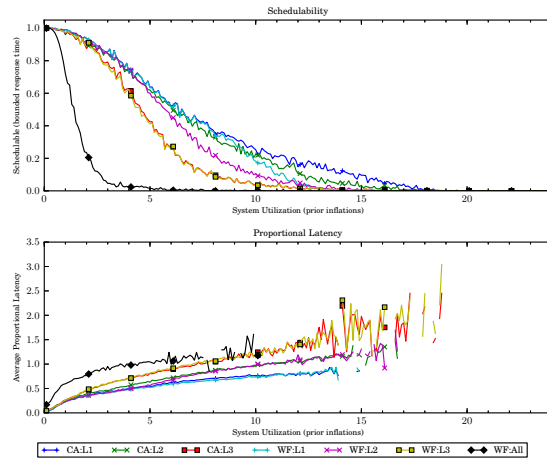


(b) With polluter overheads.

Figure 275: Results for *bimo-medium* per-task utilization, *uni-short* period, *bimo-light-weight* EWSS, and *uni-tall* height factor.

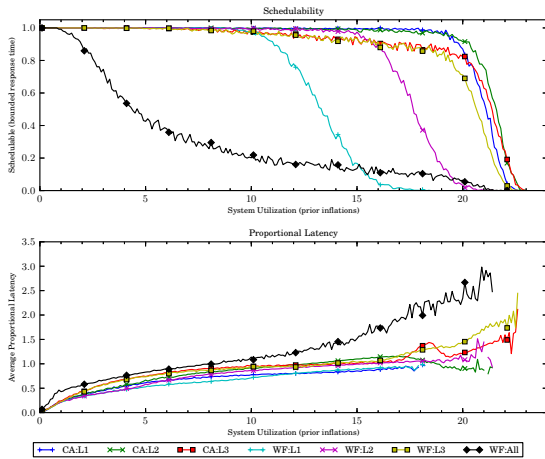


(a) Without polluter overheads.

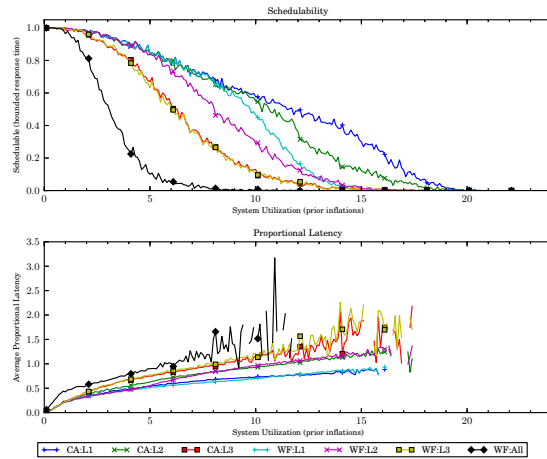


(b) With polluter overheads.

Figure 276: Results for *bimo-medium* per-task utilization, *uni-short* period, *bimo-light-weight* EWSS, and *pipeline* height factor.

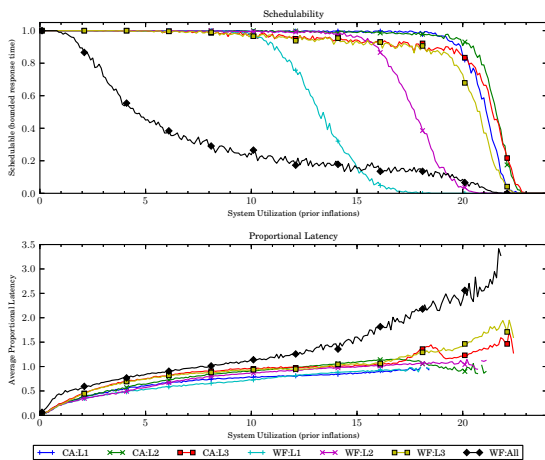


(a) Without polluter overheads.

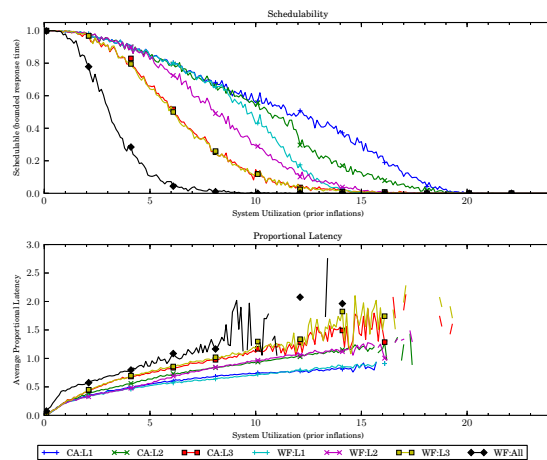


(b) With polluter overheads.

Figure 277: Results for *bimo-medium* per-task utilization, *uni-moderate* period, *bimo-light-weight* EWSS, and *uni-short* height factor.

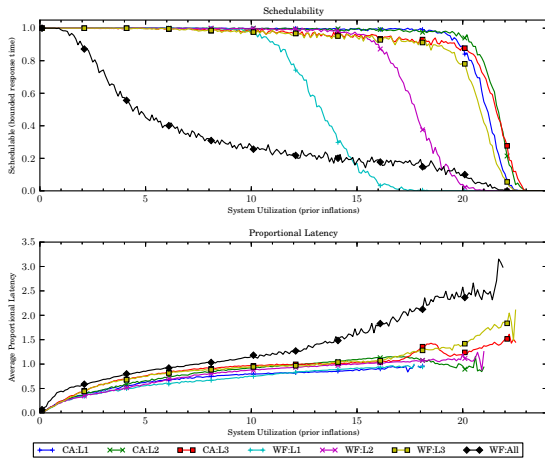


(a) Without polluter overheads.

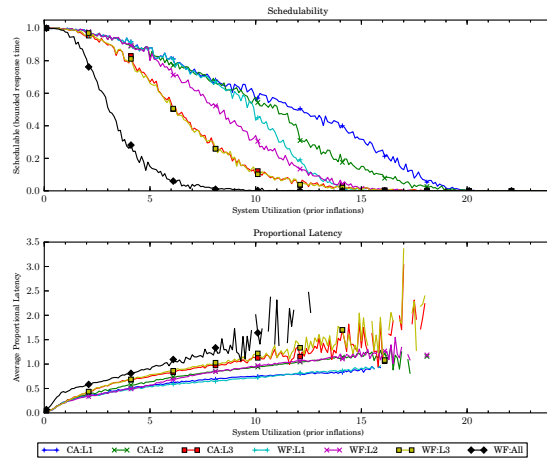


(b) With polluter overheads.

Figure 278: Results for *bimo-medium* per-task utilization, *uni-moderate* period, *bimo-light-weight* EWSS, and *uni-medium* height factor.

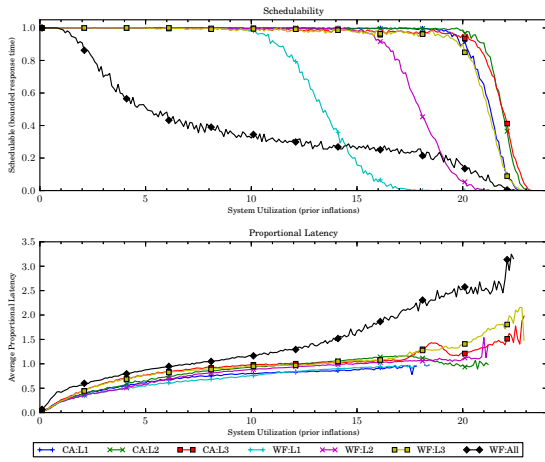


(a) Without polluter overheads.

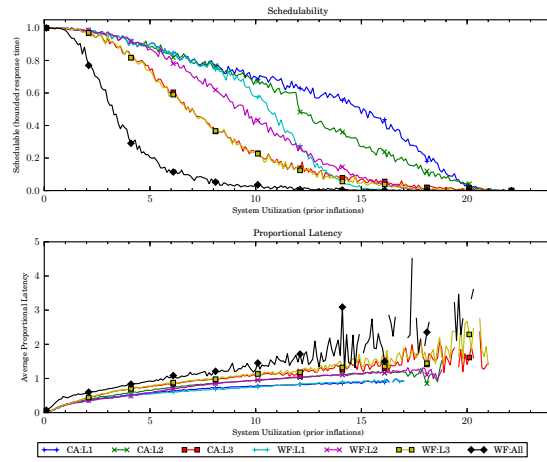


(b) With polluter overheads.

Figure 279: Results for *bimo-medium* per-task utilization, *uni-moderate* period, *bimo-light-weight* EWSS, and *uni-tall* height factor.

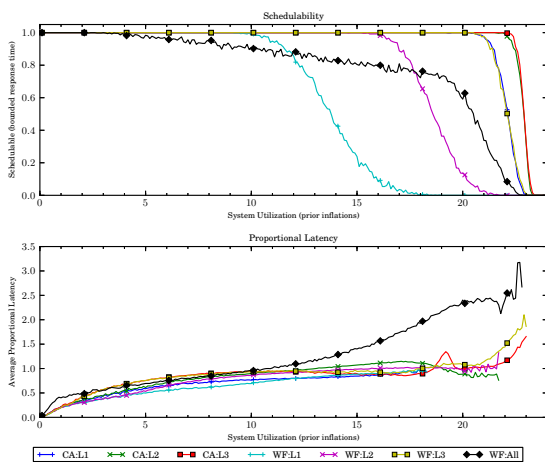


(a) Without polluter overheads.

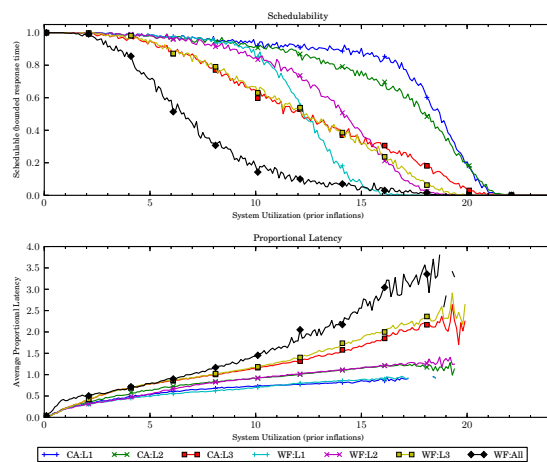


(b) With polluter overheads.

Figure 280: Results for *bimo-medium* per-task utilization, *uni-moderate* period, *bimo-light-weight* EWSS, and *pipeline* height factor.

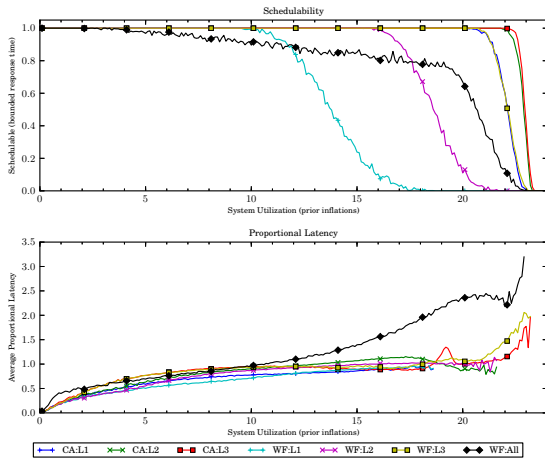


(a) Without polluter overheads.

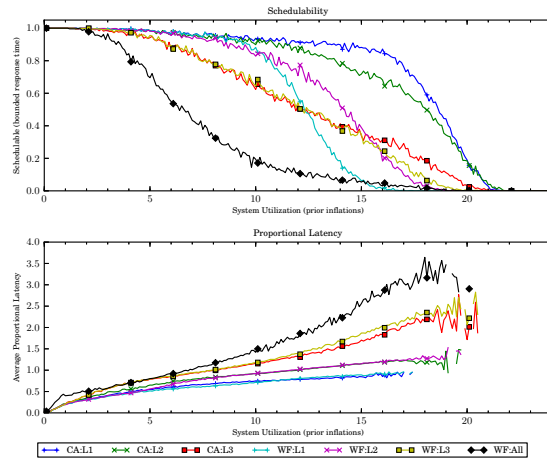


(b) With polluter overheads.

Figure 281: Results for *bimo-medium* per-task utilization, *uni-long* period, *bimo-light-weight* EWSS, and *uni-short* height factor.

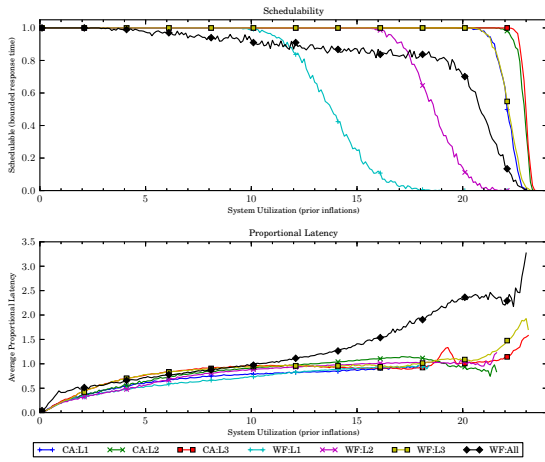


(a) Without polluter overheads.

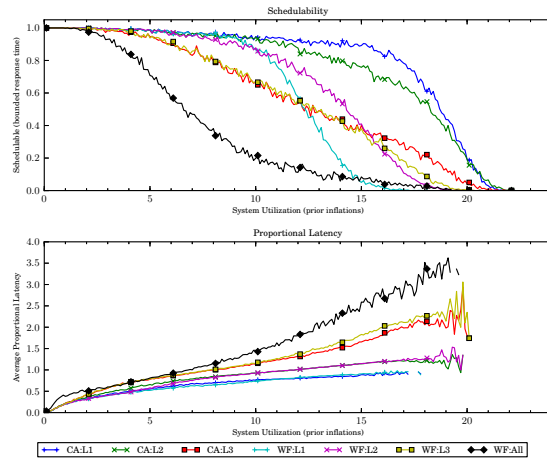


(b) With polluter overheads.

Figure 282: Results for *bimo-medium* per-task utilization, *uni-long* period, *bimo-light-weight* EWSS, and *uni-medium* height factor.

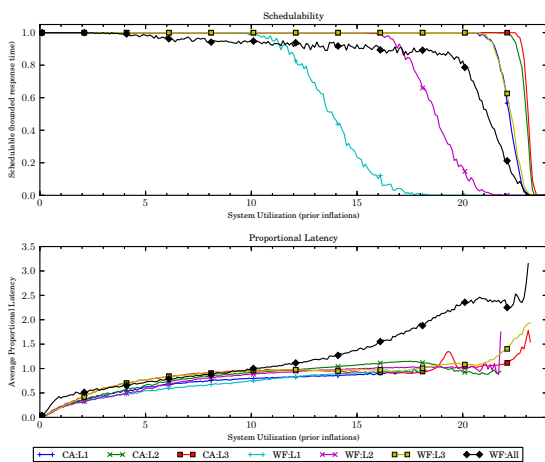


(a) Without polluter overheads.

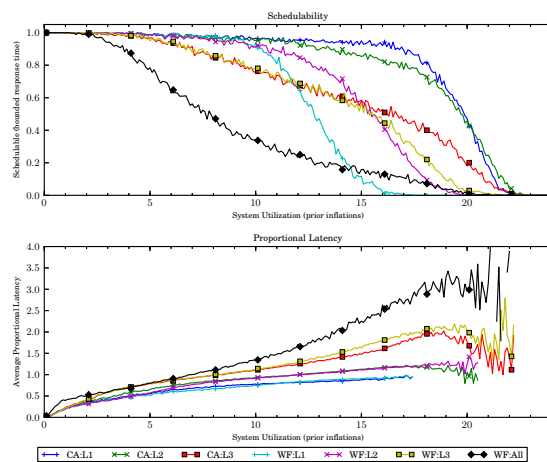


(b) With polluter overheads.

Figure 283: Results for *bimo-medium* per-task utilization, *uni-long* period, *bimo-light-weight* EWSS, and *uni-tall* height factor.

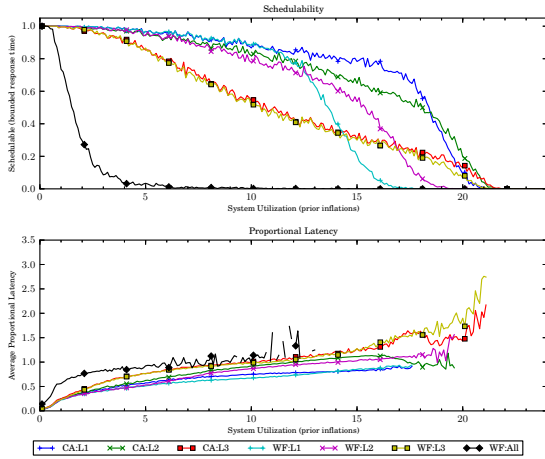


(a) Without polluter overheads.

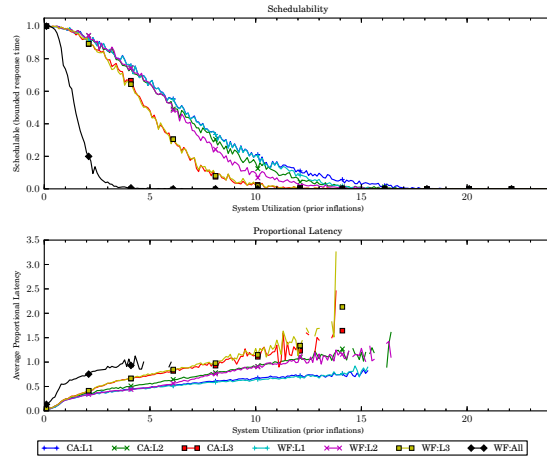


(b) With polluter overheads.

Figure 284: Results for *bimo-medium* per-task utilization, *uni-long* period, *bimo-light-weight* EWSS, and *pipeline* height factor.

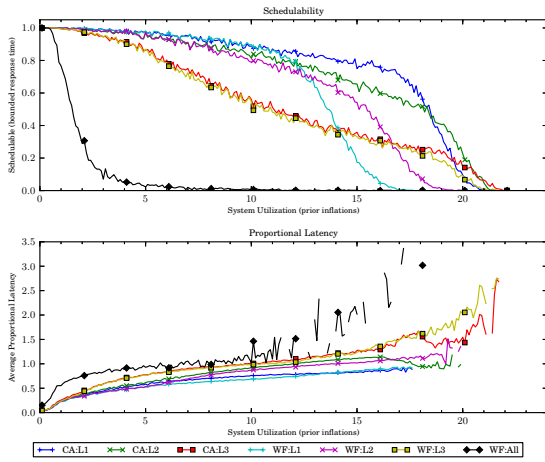


(a) Without polluter overheads.

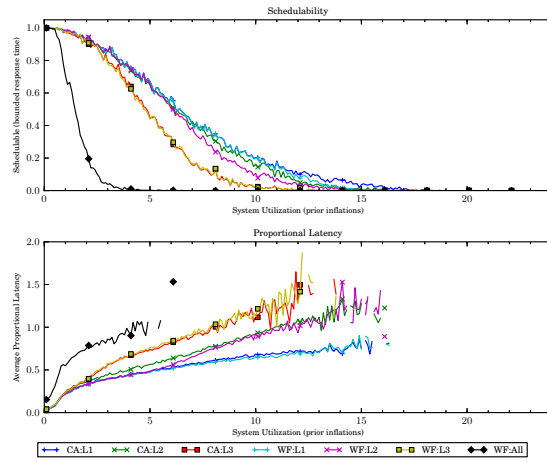


(b) With polluter overheads.

Figure 285: Results for *bimo-heavy* per-task utilization, *uni-short* period, *bimo-light-weight* EWSS, and *uni-short* height factor.

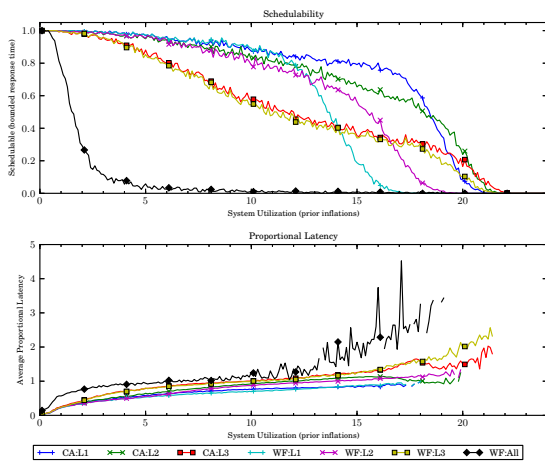


(a) Without polluter overheads.

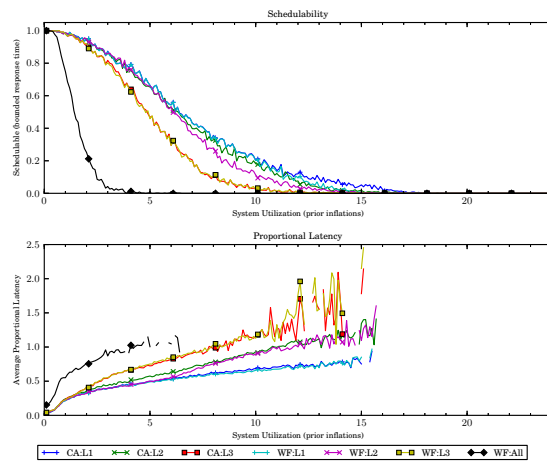


(b) With polluter overheads.

Figure 286: Results for *bimo-heavy* per-task utilization, *uni-short* period, *bimo-light-weight* EWSS, and *uni-medium* height factor.

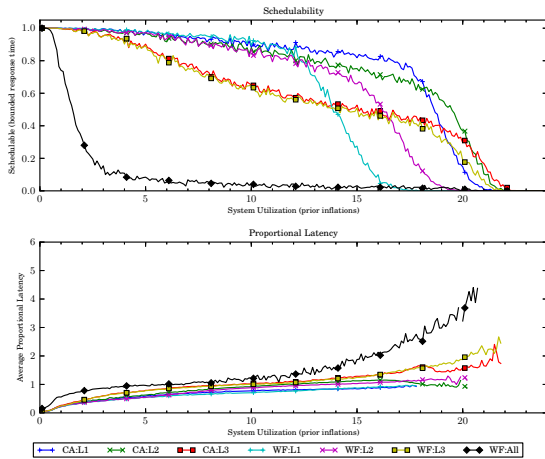


(a) Without polluter overheads.

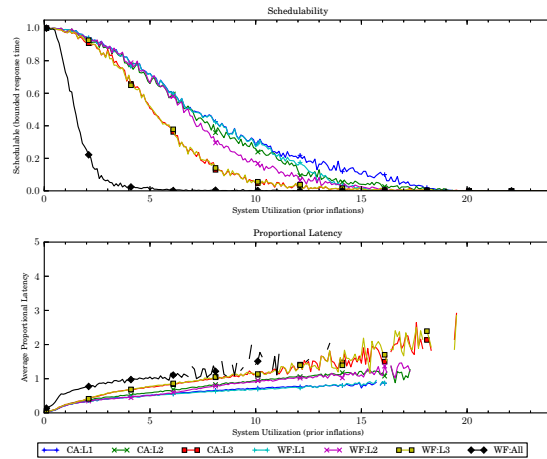


(b) With polluter overheads.

Figure 287: Results for *bimo-heavy* per-task utilization, *uni-short* period, *bimo-light-weight* EWSS, and *uni-tall* height factor.

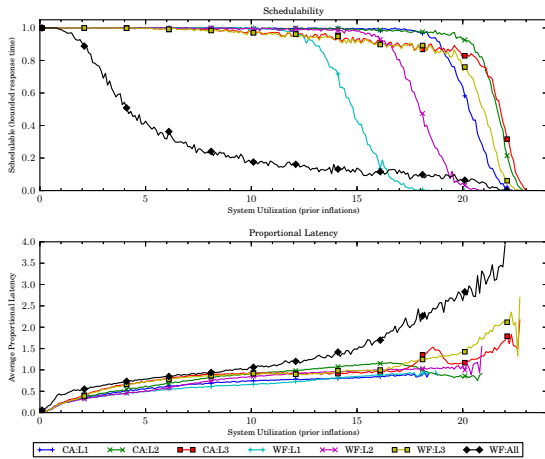


(a) Without polluter overheads.

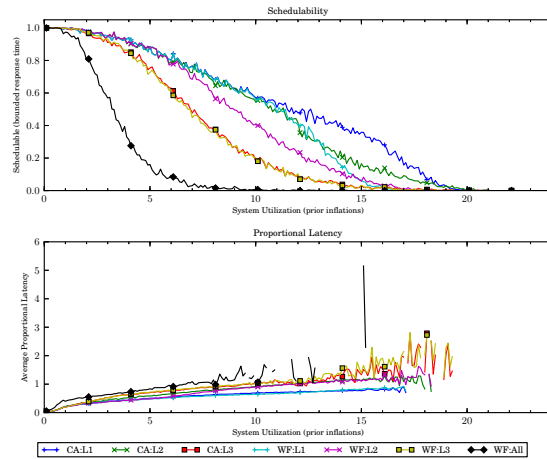


(b) With polluter overheads.

Figure 288: Results for *bimo-heavy* per-task utilization, *uni-short* period, *bimo-light-weight* EWSS, and *pipeline* height factor.

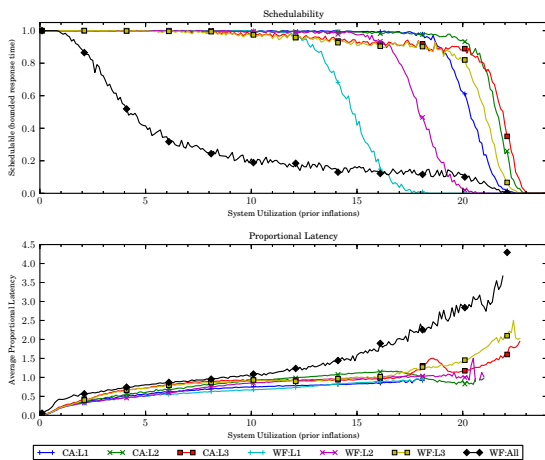


(a) Without polluter overheads.

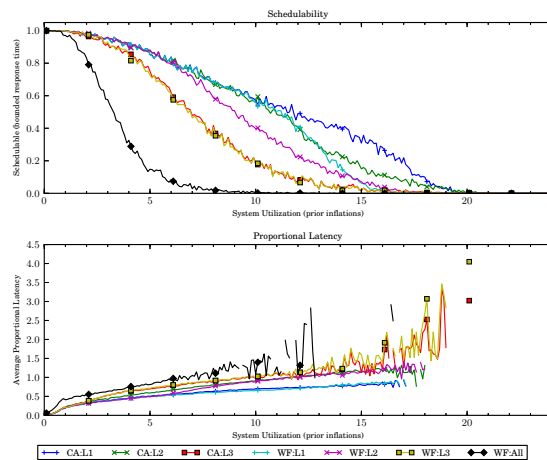


(b) With polluter overheads.

Figure 289: Results for *bimo-heavy* per-task utilization, *uni-moderate* period, *bimo-light-weight* EWSS, and *uni-short* height factor.

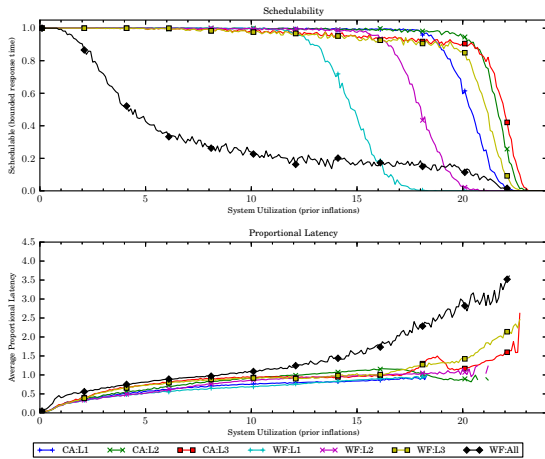


(a) Without polluter overheads.

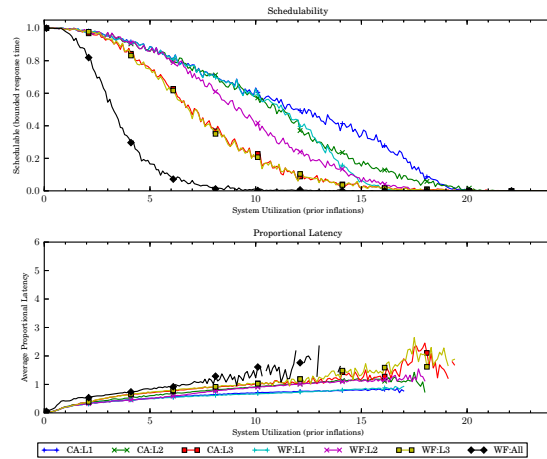


(b) With polluter overheads.

Figure 290: Results for *bimo-heavy* per-task utilization, *uni-moderate* period, *bimo-light-weight* EWSS, and *uni-medium* height factor.

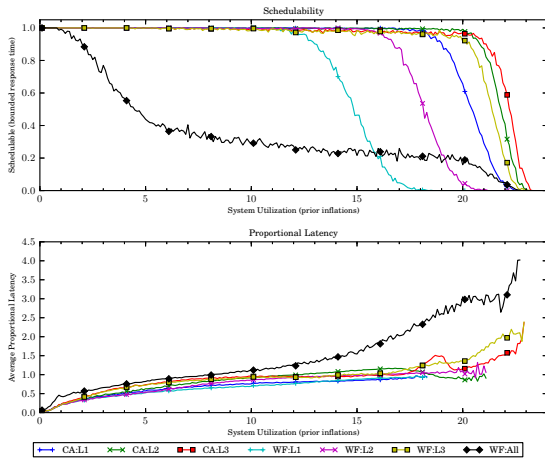


(a) Without polluter overheads.

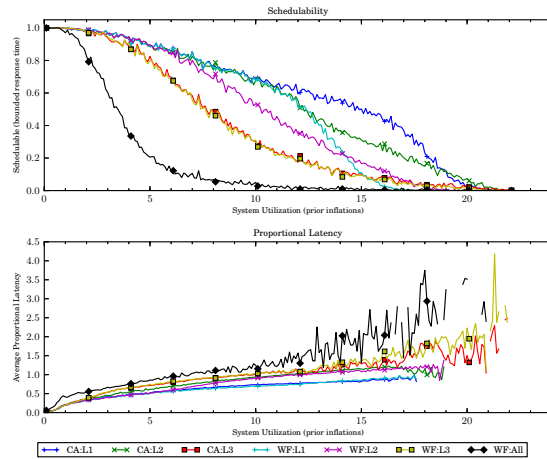


(b) With polluter overheads.

Figure 291: Results for *bimo-heavy* per-task utilization, *uni-moderate* period, *bimo-light-weight* EWSS, and *uni-tall* height factor.

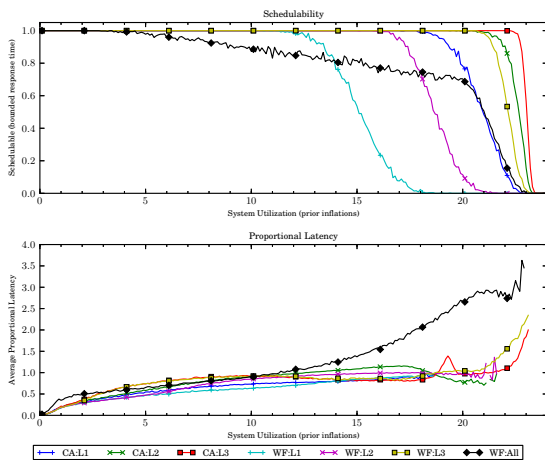


(a) Without polluter overheads.

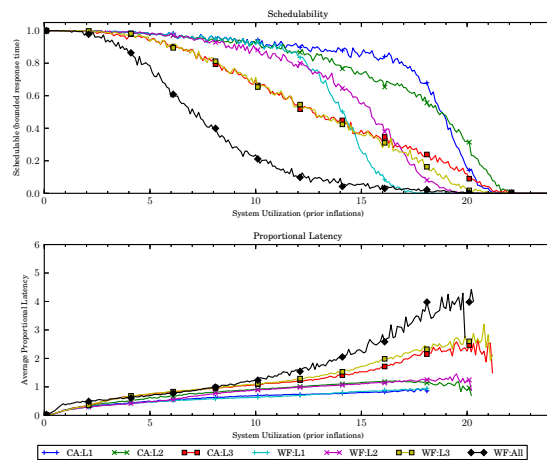


(b) With polluter overheads.

Figure 292: Results for *bimo-heavy* per-task utilization, *uni-moderate* period, *bimo-light-weight* EWSS, and *pipeline* height factor.

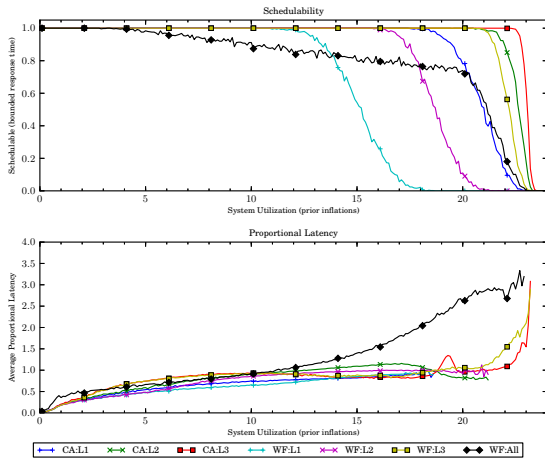


(a) Without polluter overheads.

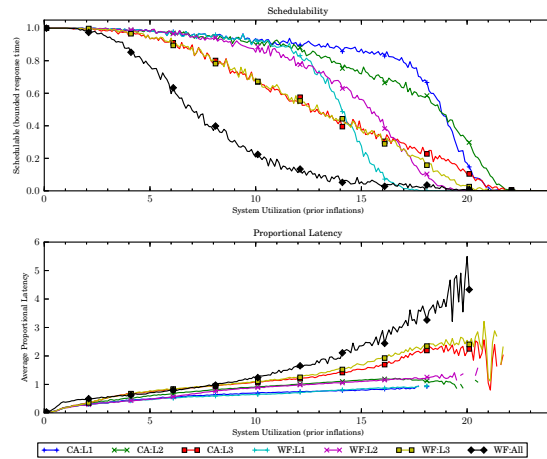


(b) With polluter overheads.

Figure 293: Results for *bimo-heavy* per-task utilization, *uni-long* period, *bimo-light-weight* EWSS, and *uni-short* height factor.

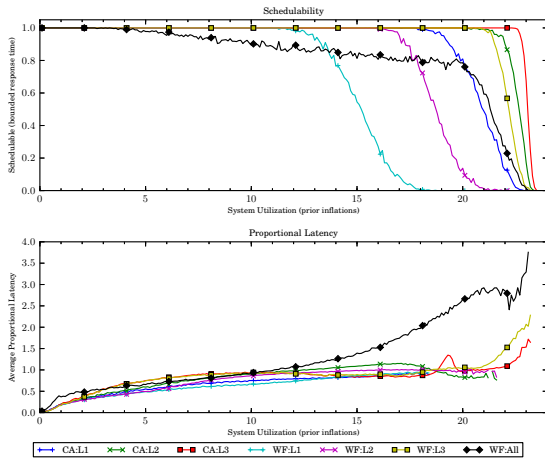


(a) Without polluter overheads.

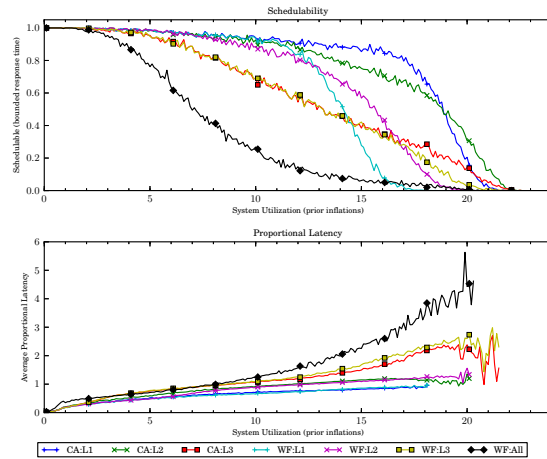


(b) With polluter overheads.

Figure 294: Results for *bimo-heavy* per-task utilization, *uni-long* period, *bimo-light-weight* EWSS, and *uni-medium* height factor.

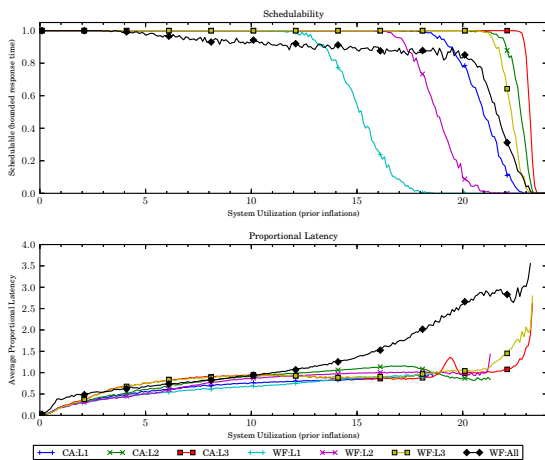


(a) Without polluter overheads.

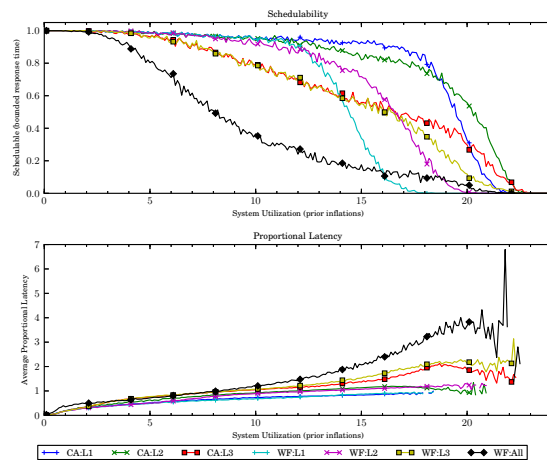


(b) With polluter overheads.

Figure 295: Results for *bimo-heavy* per-task utilization, *uni-long* period, *bimo-light-weight* EWSS, and *uni-tall* height factor.

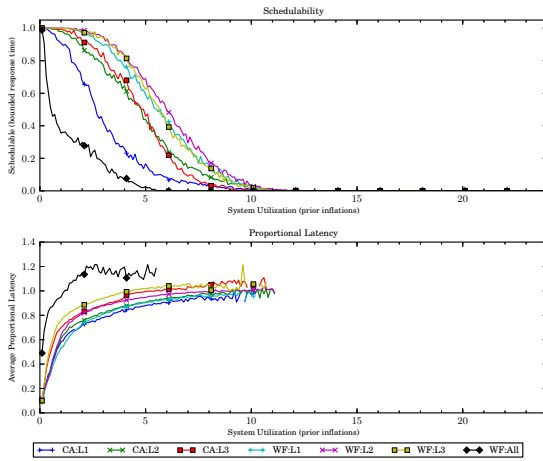


(a) Without polluter overheads.

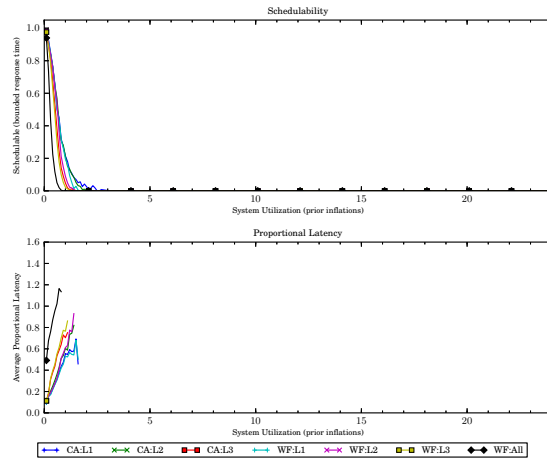


(b) With polluter overheads.

Figure 296: Results for *bimo-heavy* per-task utilization, *uni-long* period, *bimo-light-weight* EWSS, and *pipeline* height factor.

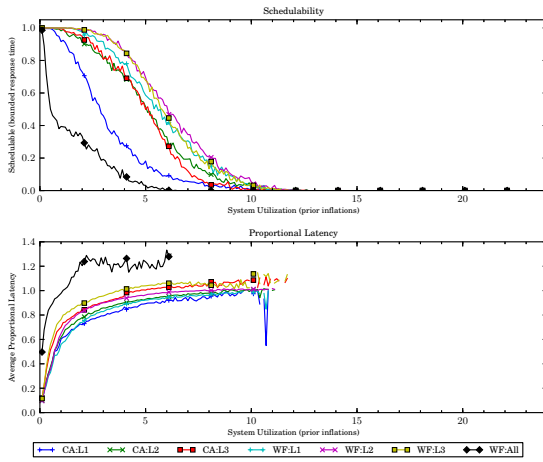


(a) Without polluter overheads.

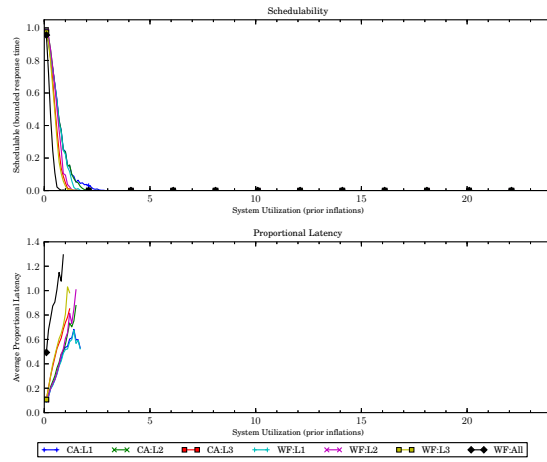


(b) With polluter overheads.

Figure 297: Results for *uni-light* per-task utilization, *uni-short* period, *bimo-medium-weight* EWSS, and *uni-short* height factor.

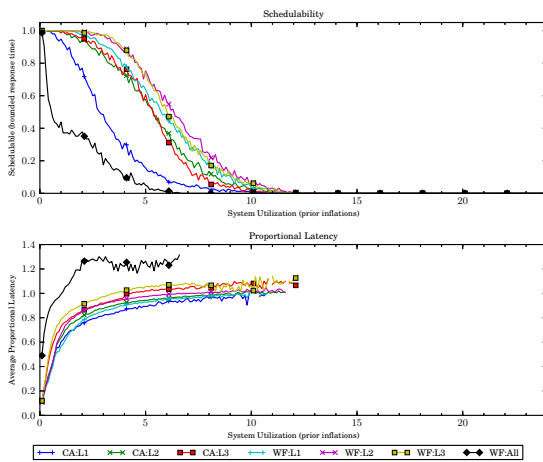


(a) Without polluter overheads.

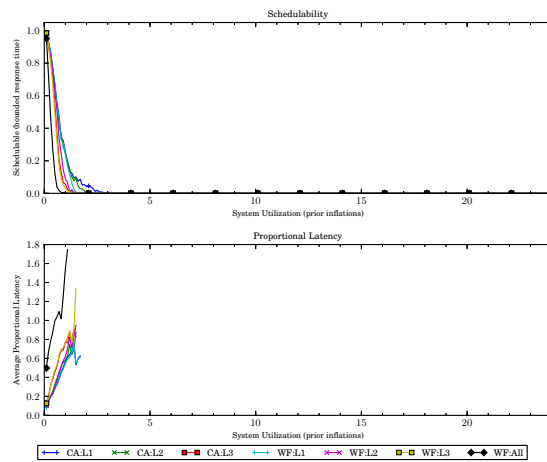


(b) With polluter overheads.

Figure 298: Results for *uni-light* per-task utilization, *uni-short* period, *bimo-medium-weight* EWSS, and *uni-medium* height factor.

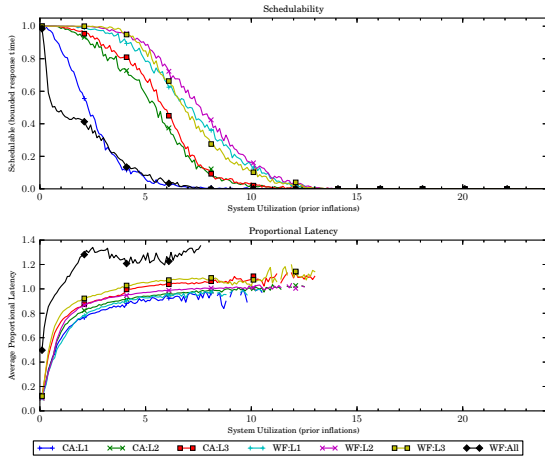


(a) Without polluter overheads.

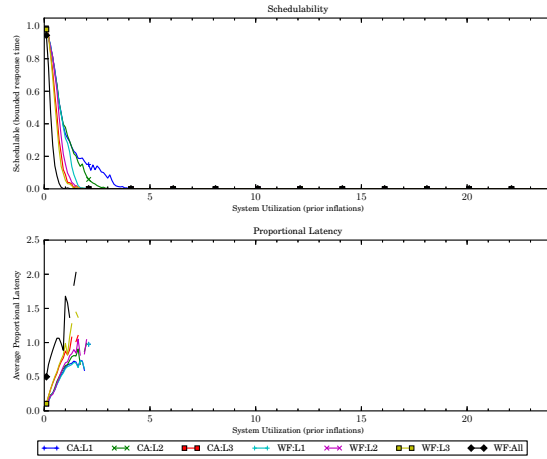


(b) With polluter overheads.

Figure 299: Results for *uni-light* per-task utilization, *uni-short* period, *bimo-medium-weight* EWSS, and *uni-tall* height factor.

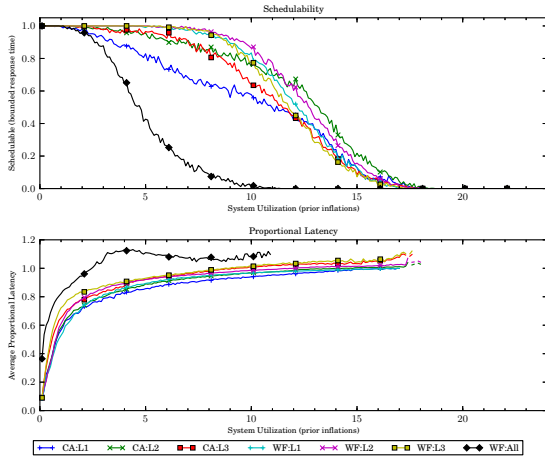


(a) Without polluter overheads.

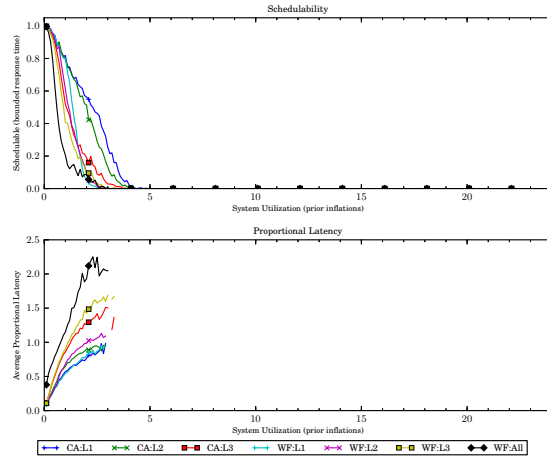


(b) With polluter overheads.

Figure 300: Results for *uni-light* per-task utilization, *uni-short* period, *bimo-medium-weight* EWSS, and *pipeline* height factor.

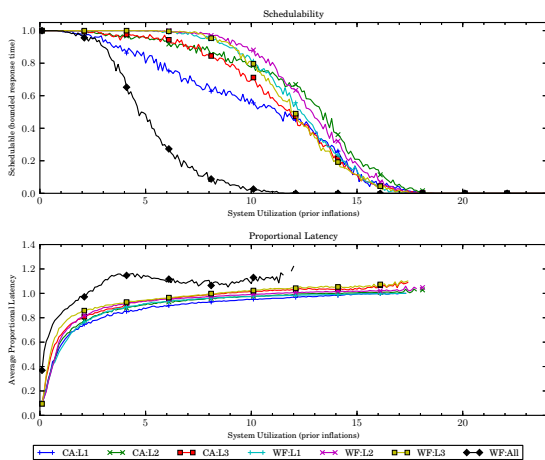


(a) Without polluter overheads.

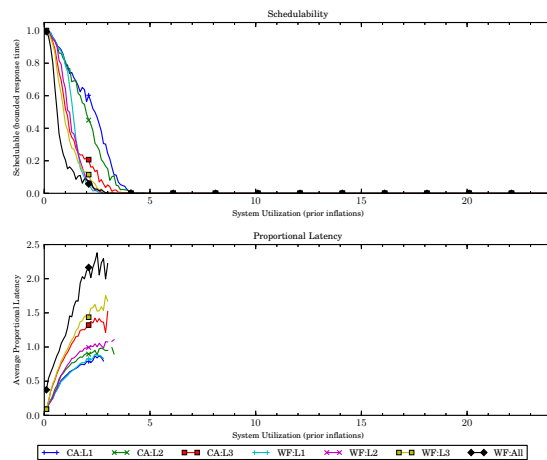


(b) With polluter overheads.

Figure 301: Results for *uni-light* per-task utilization, *uni-moderate* period, *bimo-medium-weight* EWSS, and *uni-short* height factor.

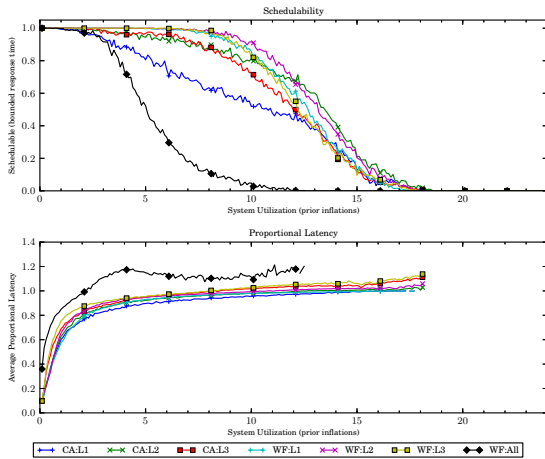


(a) Without polluter overheads.

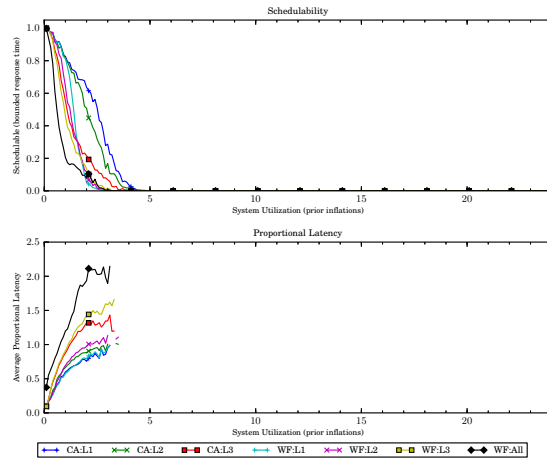


(b) With polluter overheads.

Figure 302: Results for *uni-light* per-task utilization, *uni-moderate* period, *bimo-medium-weight* EWSS, and *uni-medium* height factor.

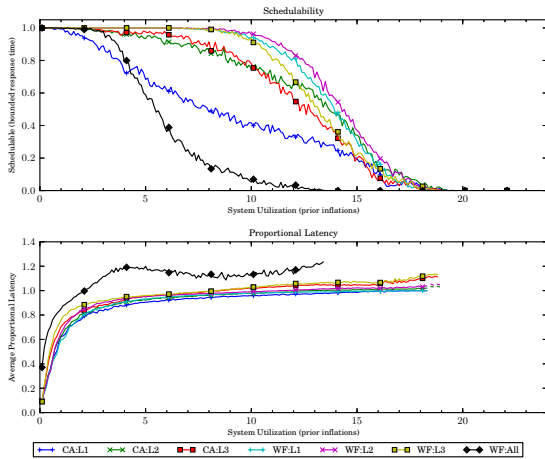


(a) Without polluter overheads.

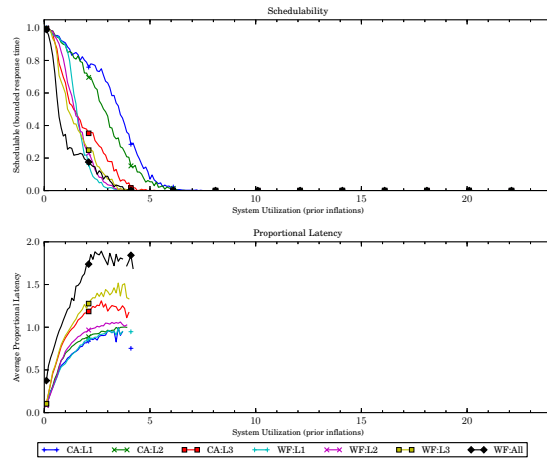


(b) With polluter overheads.

Figure 303: Results for *uni-light* per-task utilization, *uni-moderate* period, *bimo-medium-weight* EWSS, and *uni-tall* height factor.

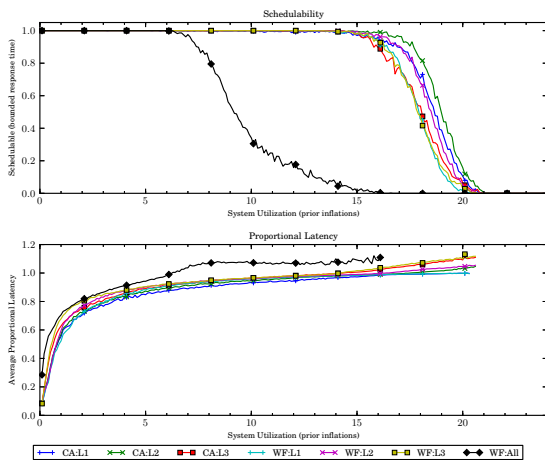


(a) Without polluter overheads.

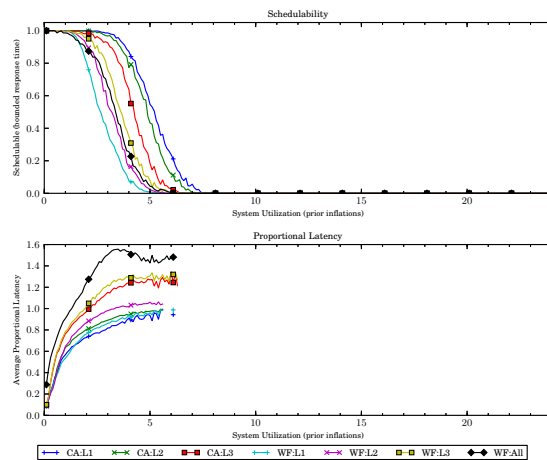


(b) With polluter overheads.

Figure 304: Results for *uni-light* per-task utilization, *uni-moderate* period, *bimo-medium-weight* EWSS, and *pipeline* height factor.

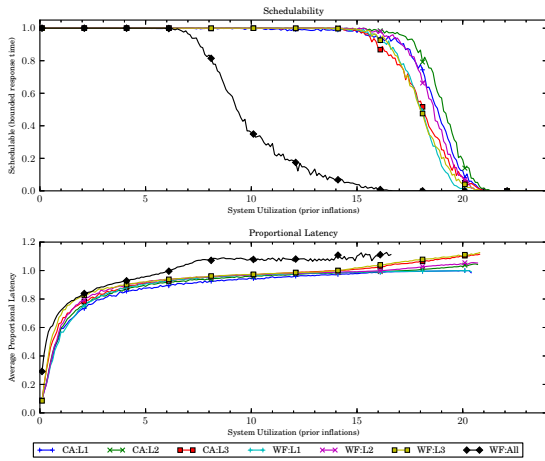


(a) Without polluter overheads.

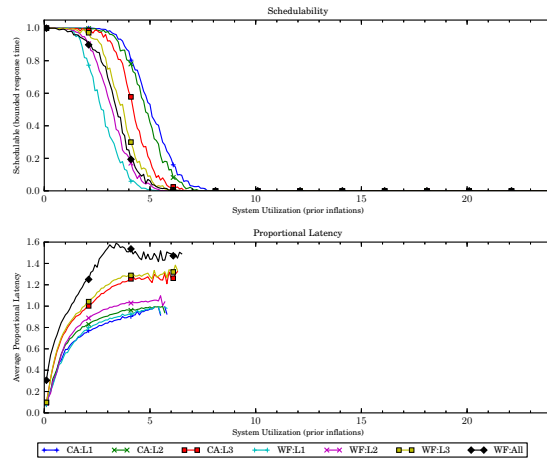


(b) With polluter overheads.

Figure 305: Results for *uni-light* per-task utilization, *uni-long* period, *bimo-medium-weight* EWSS, and *uni-short* height factor.

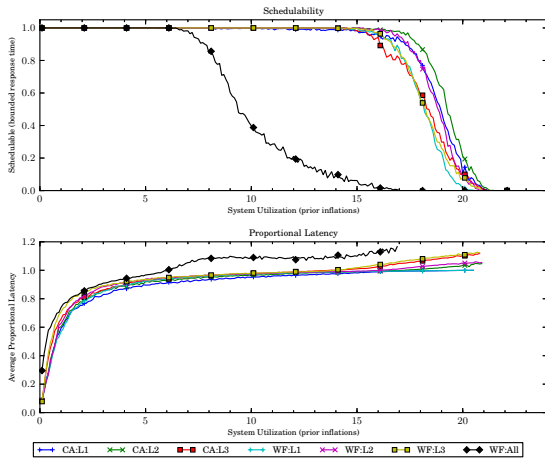


(a) Without polluter overheads.

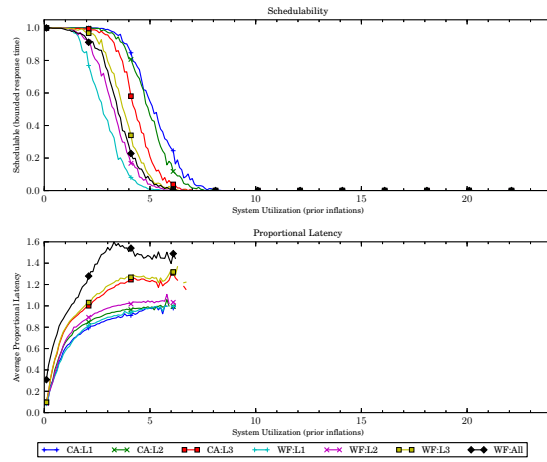


(b) With polluter overheads.

Figure 306: Results for *uni-light* per-task utilization, *uni-long* period, *bimo-medium-weight* EWSS, and *uni-medium* height factor.

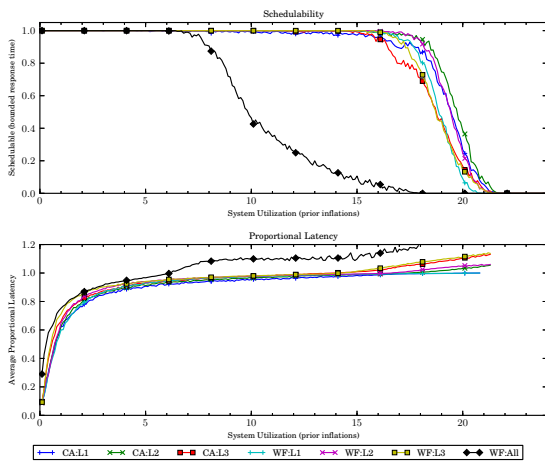


(a) Without polluter overheads.

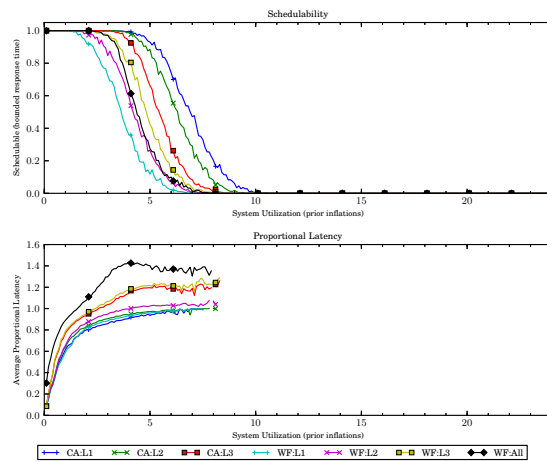


(b) With polluter overheads.

Figure 307: Results for *uni-light* per-task utilization, *uni-long* period, *bimo-medium-weight* EWSS, and *uni-tall* height factor.

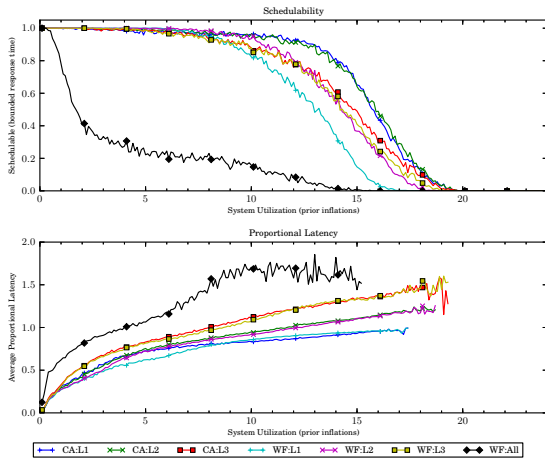


(a) Without polluter overheads.

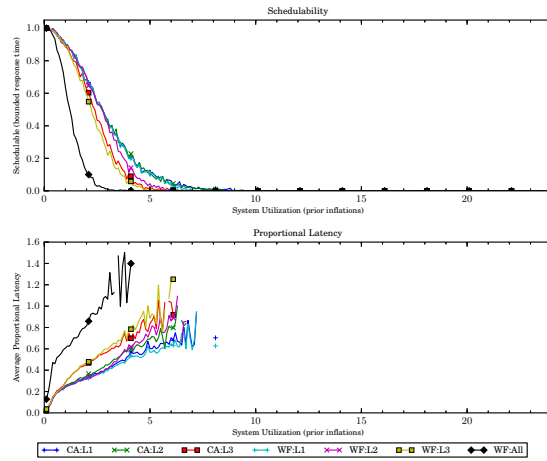


(b) With polluter overheads.

Figure 308: Results for *uni-light* per-task utilization, *uni-long* period, *bimo-medium-weight* EWSS, and *pipeline* height factor.

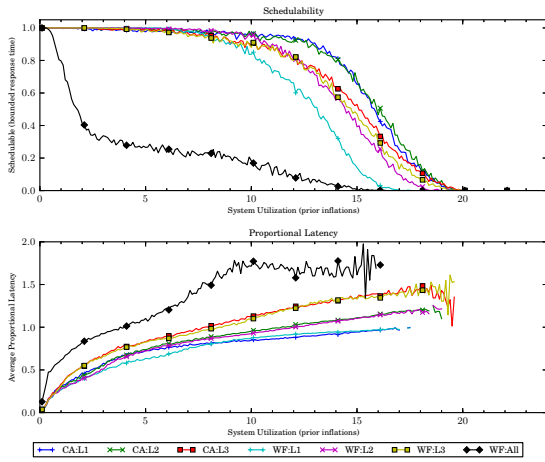


(a) Without polluter overheads.

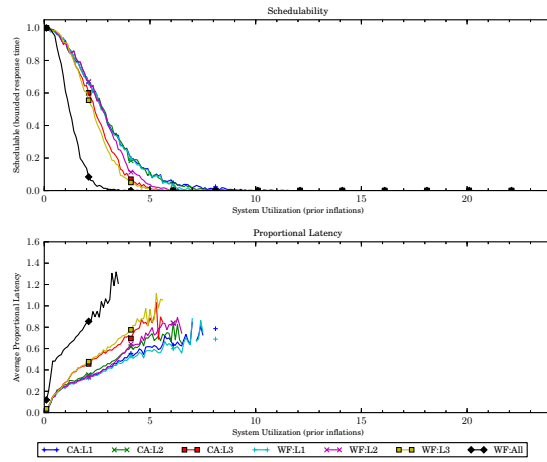


(b) With polluter overheads.

Figure 309: Results for *uni-medium* per-task utilization, *uni-short* period, *bimo-medium-weight* EWSS, and *uni-short* height factor.

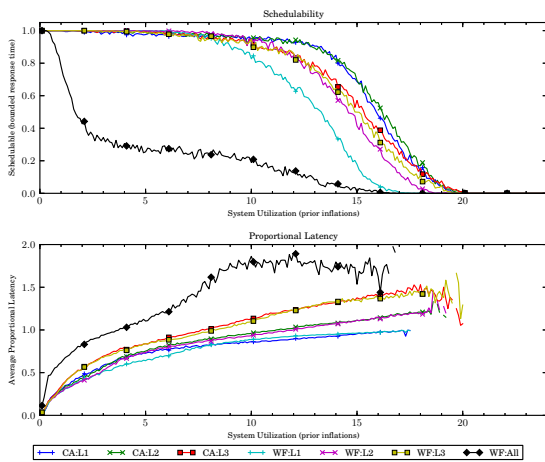


(a) Without polluter overheads.

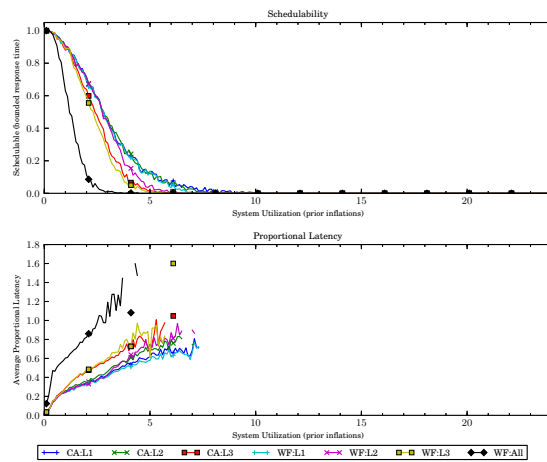


(b) With polluter overheads.

Figure 310: Results for *uni-medium* per-task utilization, *uni-short* period, *bimo-medium-weight* EWSS, and *uni-medium* height factor.

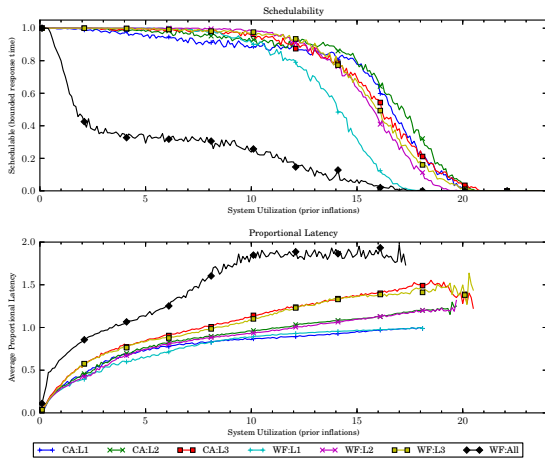


(a) Without polluter overheads.

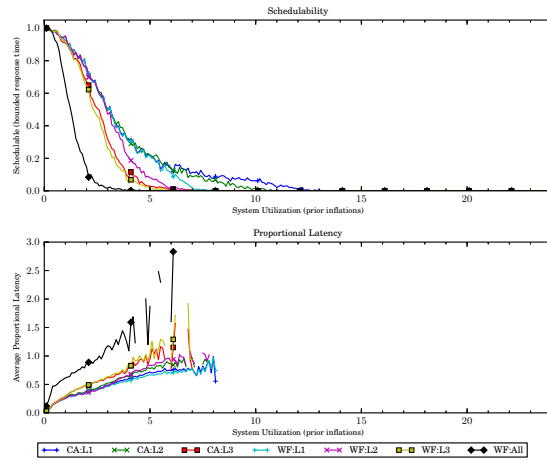


(b) With polluter overheads.

Figure 311: Results for *uni-medium* per-task utilization, *uni-short* period, *bimo-medium-weight* EWSS, and *uni-tall* height factor.

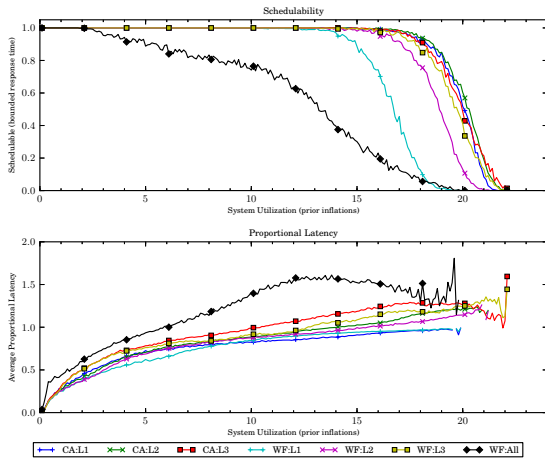


(a) Without polluter overheads.

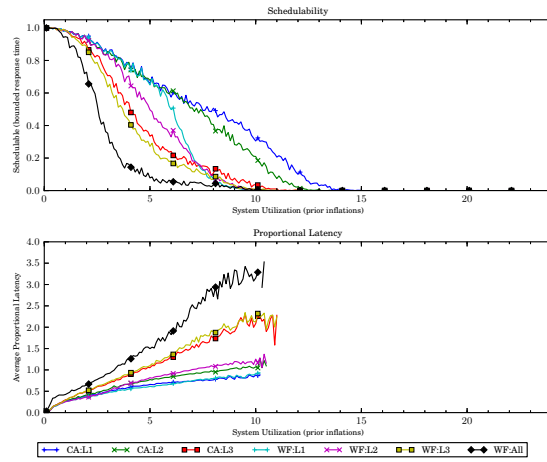


(b) With polluter overheads.

Figure 312: Results for *uni-medium* per-task utilization, *uni-short* period, *bimo-medium-weight* EWSS, and *pipeline* height factor.

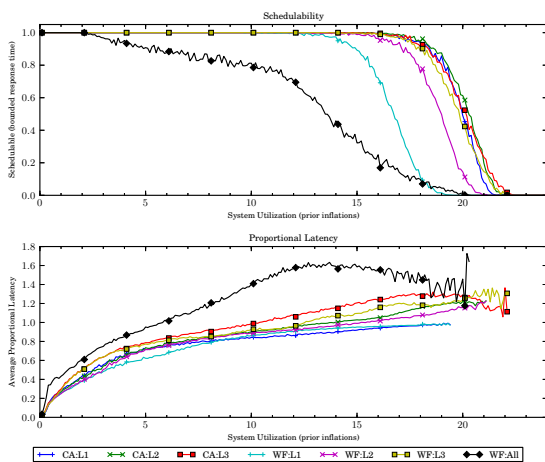


(a) Without polluter overheads.

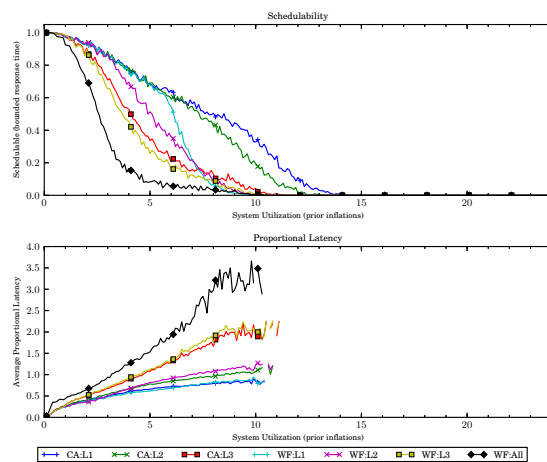


(b) With polluter overheads.

Figure 313: Results for *uni-medium* per-task utilization, *uni-moderate* period, *bimo-medium-weight* EWSS, and *uni-short* height factor.

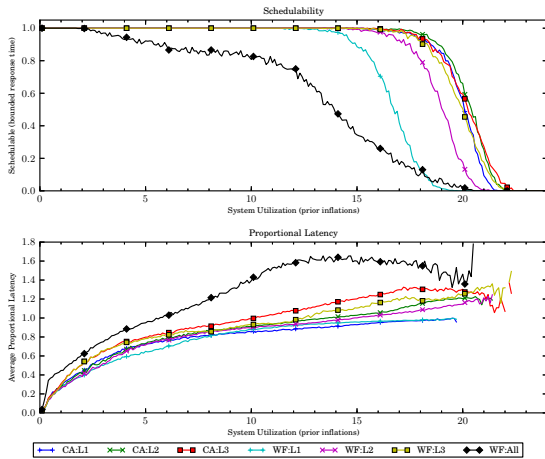


(a) Without polluter overheads.

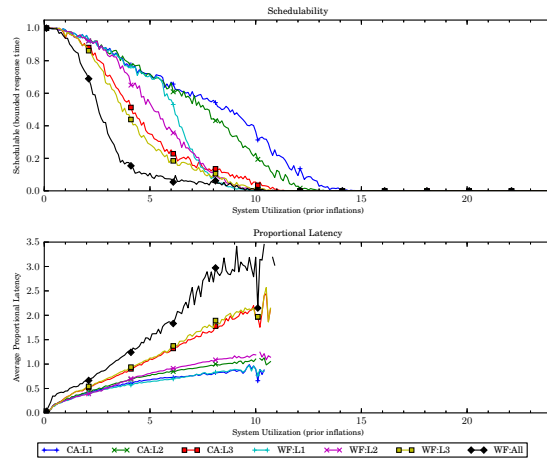


(b) With polluter overheads.

Figure 314: Results for *uni-medium* per-task utilization, *uni-moderate* period, *bimo-medium-weight* EWSS, and *uni-medium* height factor.

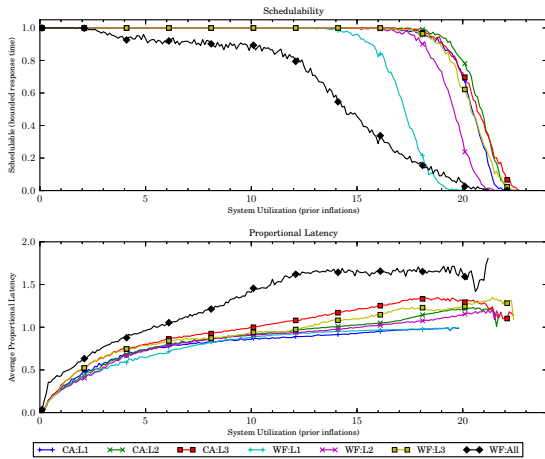


(a) Without polluter overheads.

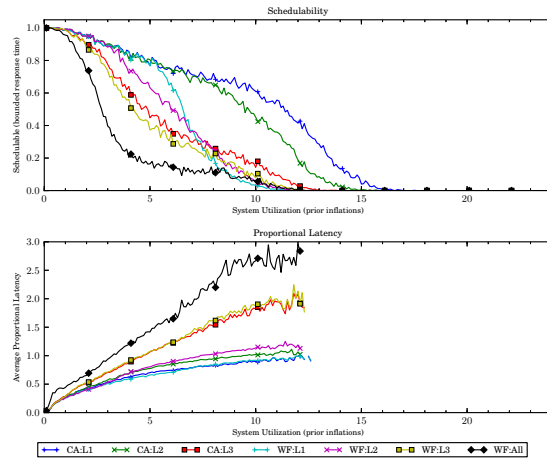


(b) With polluter overheads.

Figure 315: Results for *uni-medium* per-task utilization, *uni-moderate* period, *bimo-medium-weight* EWSS, and *uni-tall* height factor.

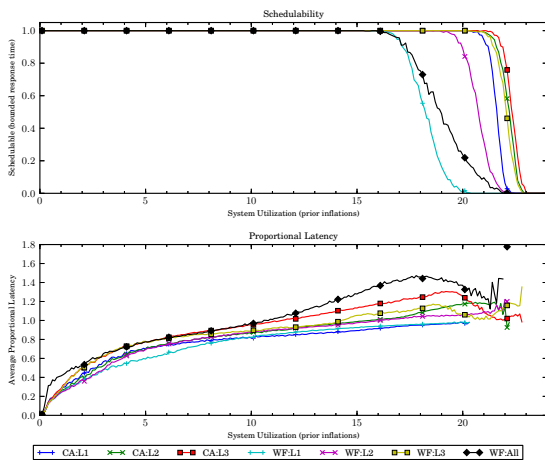


(a) Without polluter overheads.

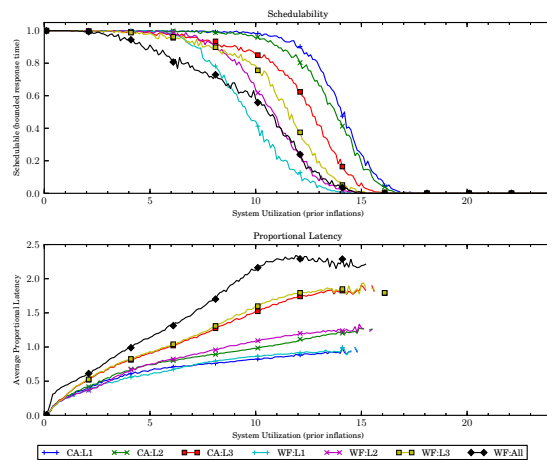


(b) With polluter overheads.

Figure 316: Results for *uni-medium* per-task utilization, *uni-moderate* period, *bimo-medium-weight* EWSS, and *pipeline* height factor.

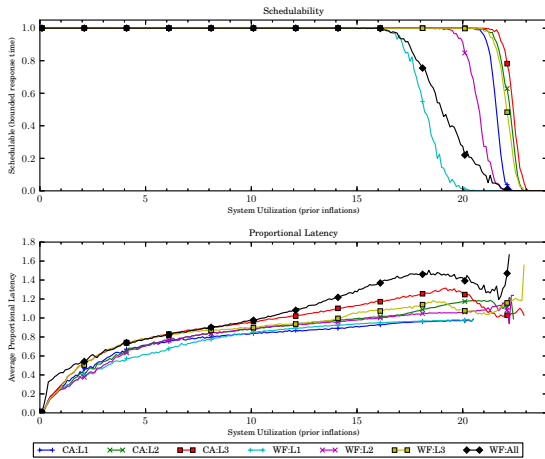


(a) Without polluter overheads.

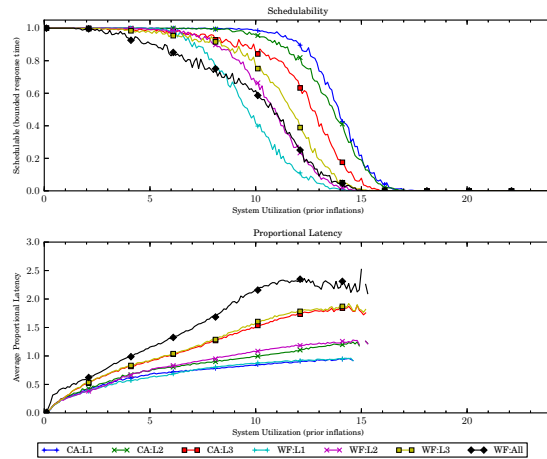


(b) With polluter overheads.

Figure 317: Results for *uni-medium* per-task utilization, *uni-long* period, *bimo-medium-weight* EWSS, and *uni-short* height factor.

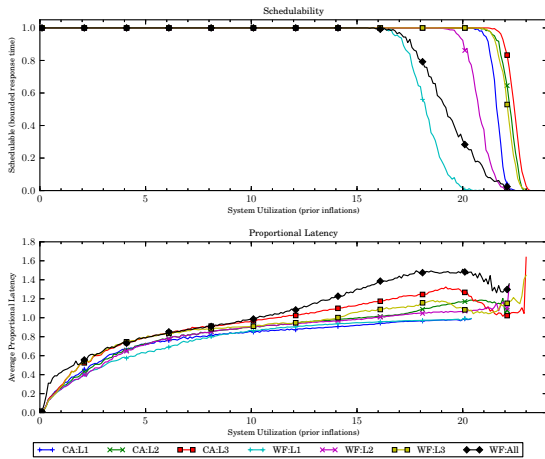


(a) Without polluter overheads.

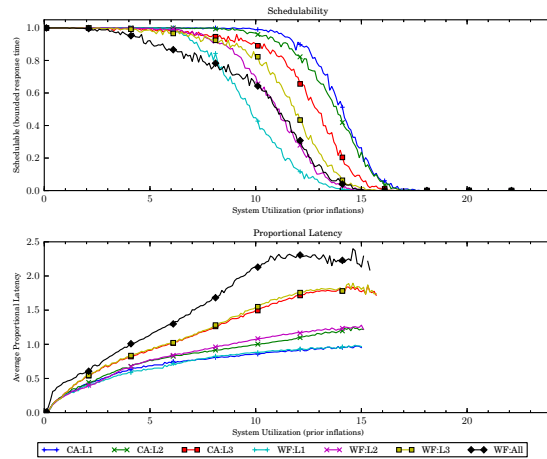


(b) With polluter overheads.

Figure 318: Results for *uni-medium* per-task utilization, *uni-long* period, *bimo-medium-weight* EWSS, and *uni-medium* height factor.

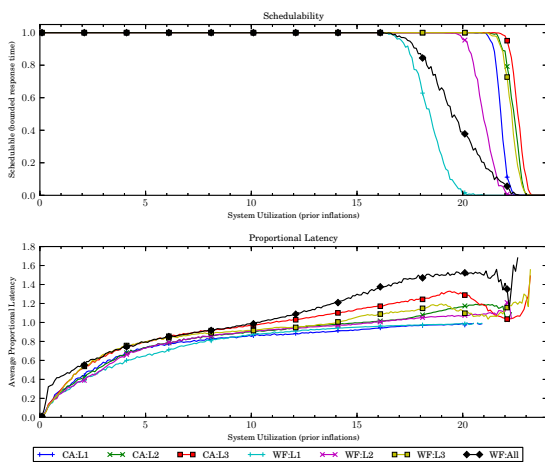


(a) Without polluter overheads.

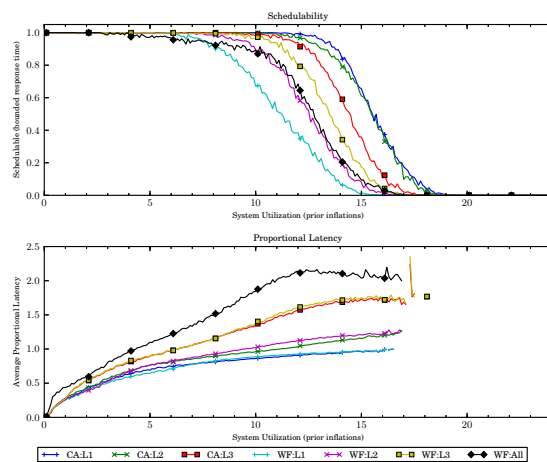


(b) With polluter overheads.

Figure 319: Results for *uni-medium* per-task utilization, *uni-long* period, *bimo-medium-weight* EWSS, and *uni-tall* height factor.

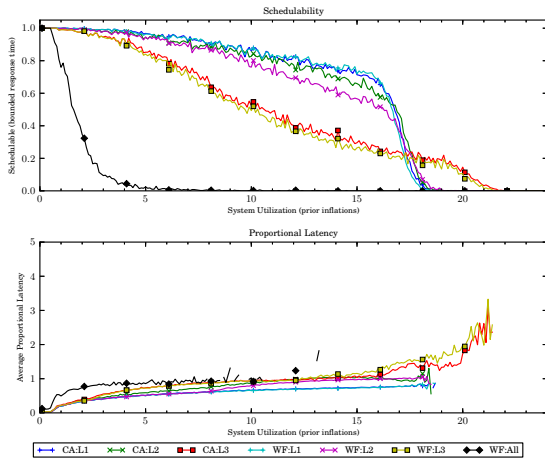


(a) Without polluter overheads.

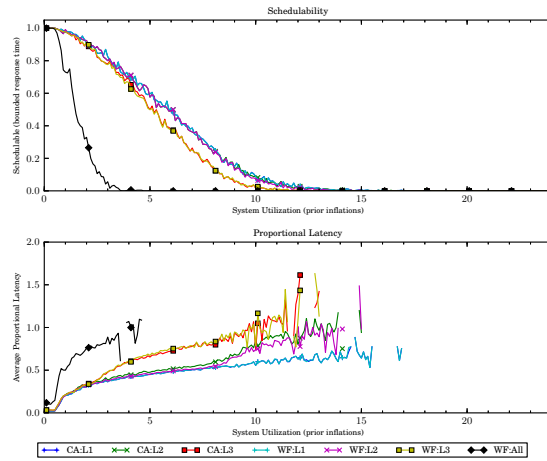


(b) With polluter overheads.

Figure 320: Results for *uni-medium* per-task utilization, *uni-long* period, *bimo-medium-weight* EWSS, and *pipeline* height factor.

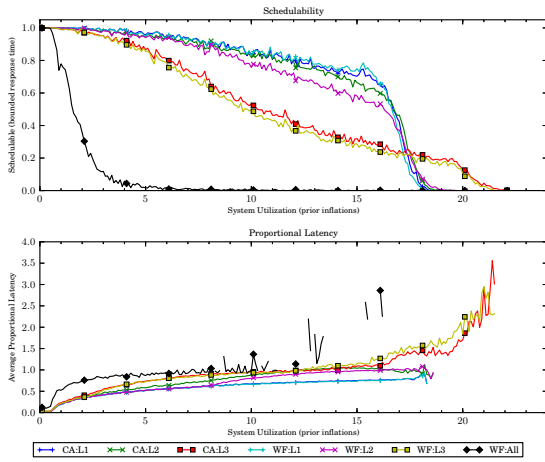


(a) Without polluter overheads.

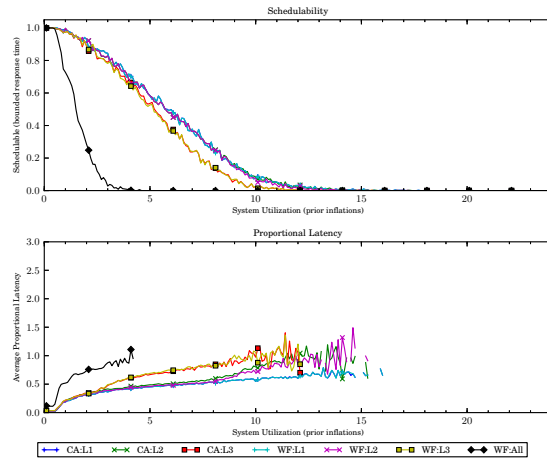


(b) With polluter overheads.

Figure 321: Results for *uni-heavy* per-task utilization, *uni-short* period, *bimo-medium-weight* EWSS, and *uni-short* height factor.

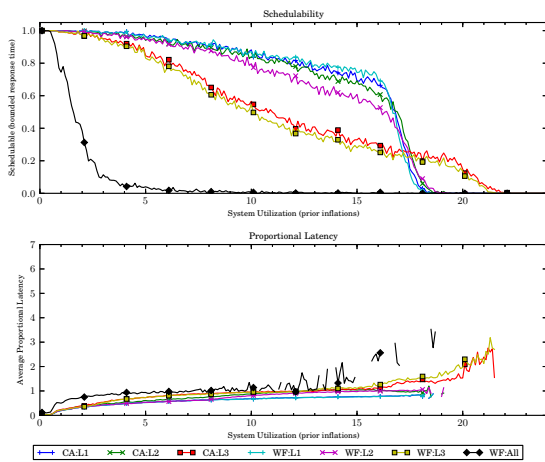


(a) Without polluter overheads.

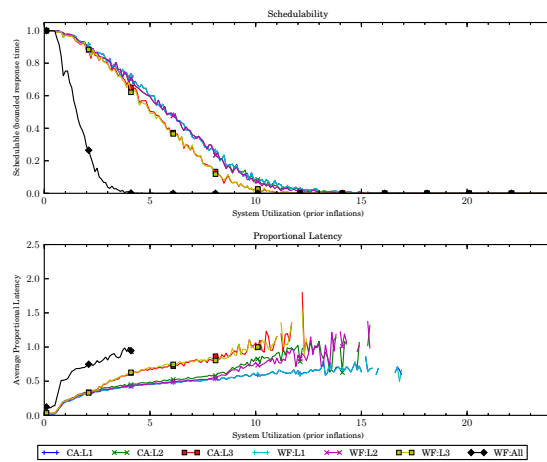


(b) With polluter overheads.

Figure 322: Results for *uni-heavy* per-task utilization, *uni-short* period, *bimo-medium-weight* EWSS, and *uni-medium* height factor.

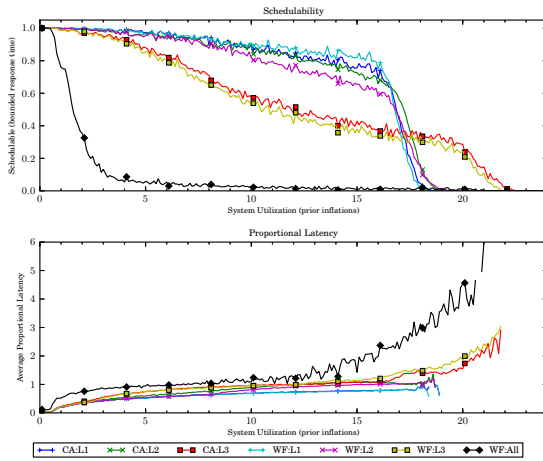


(a) Without polluter overheads.

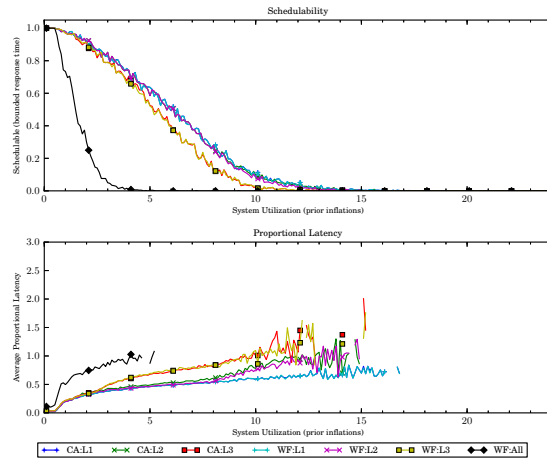


(b) With polluter overheads.

Figure 323: Results for *uni-heavy* per-task utilization, *uni-short* period, *bimo-medium-weight* EWSS, and *uni-tall* height factor.

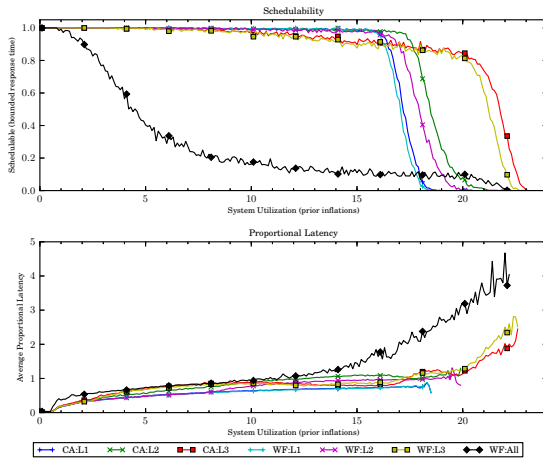


(a) Without polluter overheads.

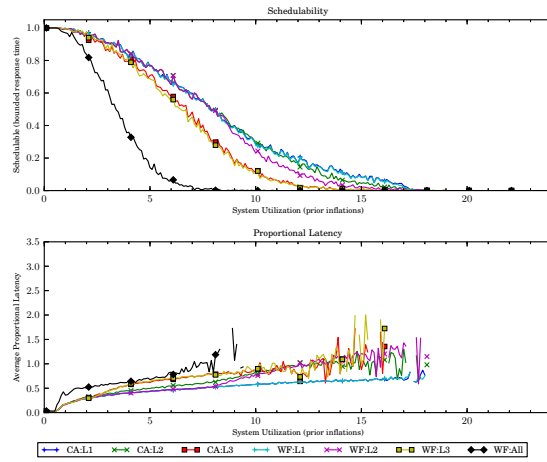


(b) With polluter overheads.

Figure 324: Results for *uni-heavy* per-task utilization, *uni-short* period, *bimo-medium-weight* EWSS, and *pipeline* height factor.

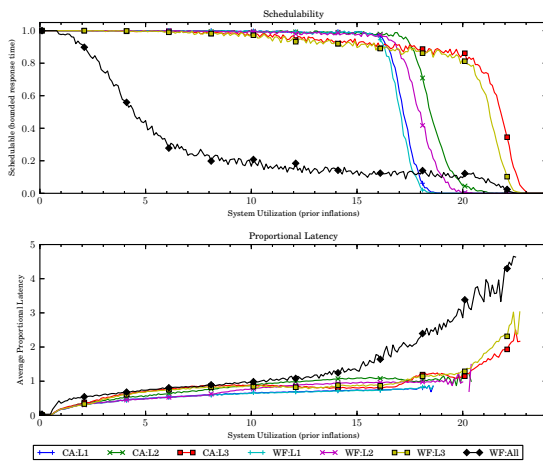


(a) Without polluter overheads.

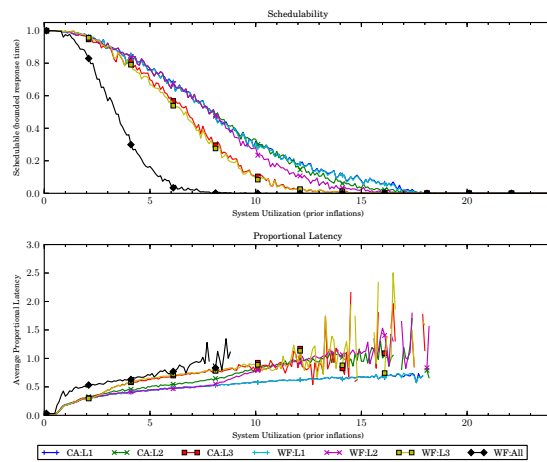


(b) With polluter overheads.

Figure 325: Results for *uni-heavy* per-task utilization, *uni-moderate* period, *bimo-medium-weight* EWSS, and *uni-short* height factor.

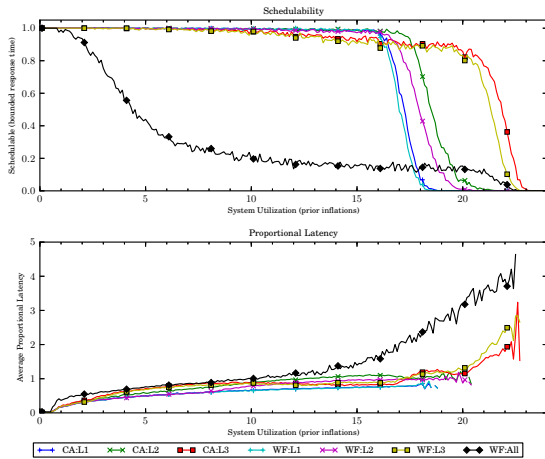


(a) Without polluter overheads.

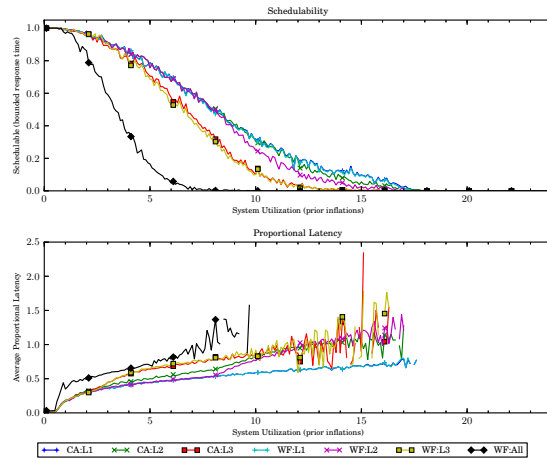


(b) With polluter overheads.

Figure 326: Results for *uni-heavy* per-task utilization, *uni-moderate* period, *bimo-medium-weight* EWSS, and *uni-medium* height factor.

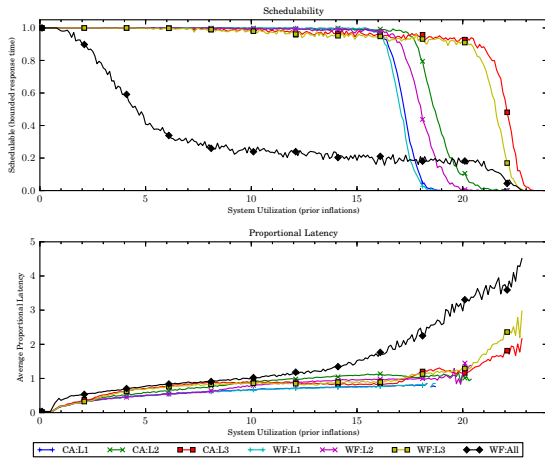


(a) Without polluter overheads.

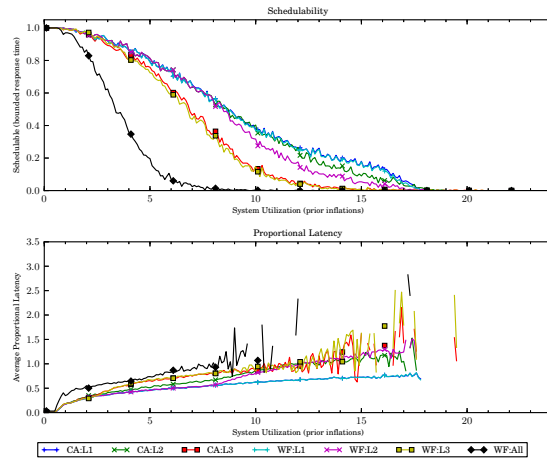


(b) With polluter overheads.

Figure 327: Results for *uni-heavy* per-task utilization, *uni-moderate* period, *bimo-medium-weight* EWSS, and *uni-tall* height factor.

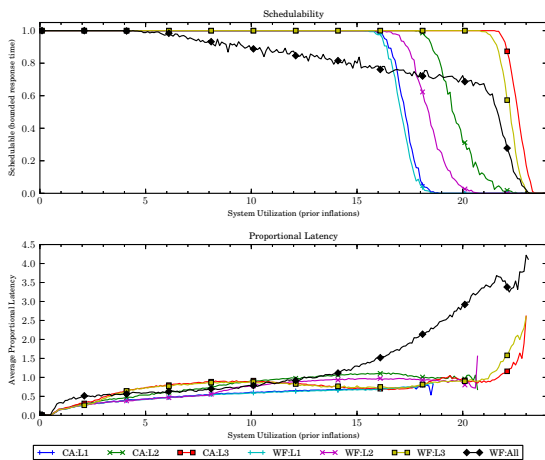


(a) Without polluter overheads.

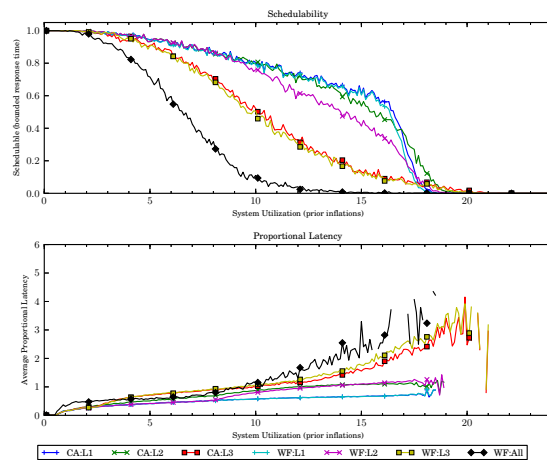


(b) With polluter overheads.

Figure 328: Results for *uni-heavy* per-task utilization, *uni-moderate* period, *bimo-medium-weight* EWSS, and *pipeline* height factor.

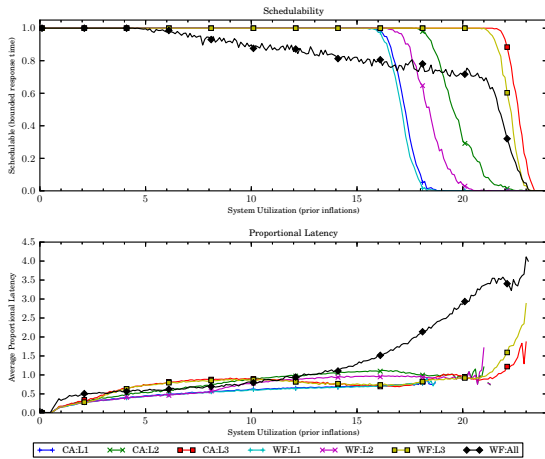


(a) Without polluter overheads.

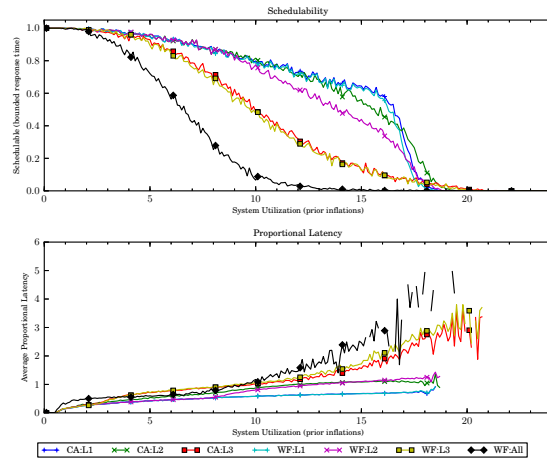


(b) With polluter overheads.

Figure 329: Results for *uni-heavy* per-task utilization, *uni-long* period, *bimo-medium-weight* EWSS, and *uni-short* height factor.

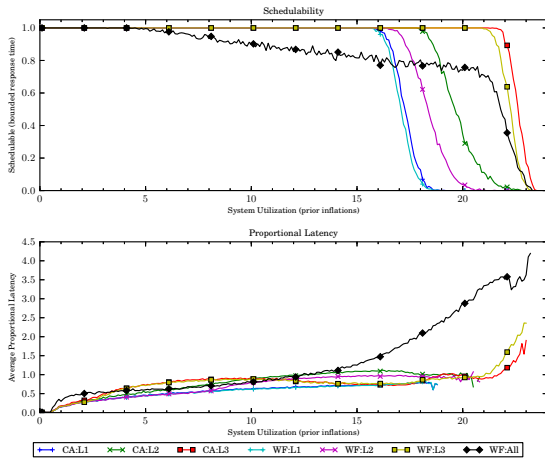


(a) Without polluter overheads.

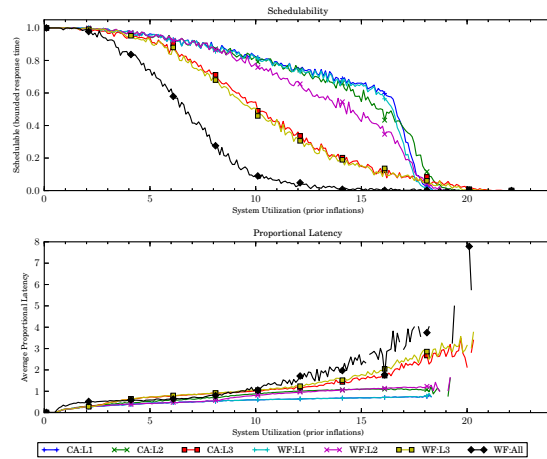


(b) With polluter overheads.

Figure 330: Results for *uni-heavy* per-task utilization, *uni-long* period, *bimo-medium-weight* EWSS, and *uni-medium* height factor.

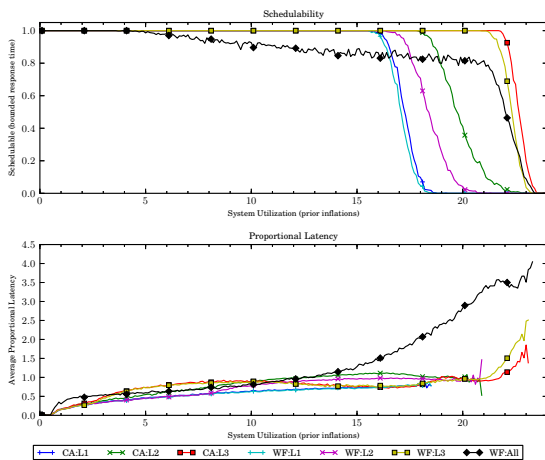


(a) Without polluter overheads.

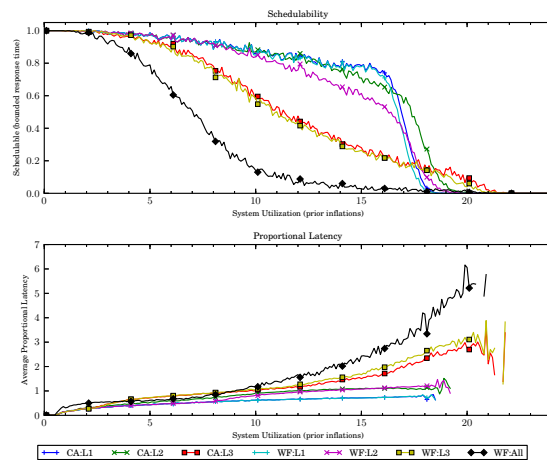


(b) With polluter overheads.

Figure 331: Results for *uni-heavy* per-task utilization, *uni-long* period, *bimo-medium-weight* EWSS, and *uni-tall* height factor.

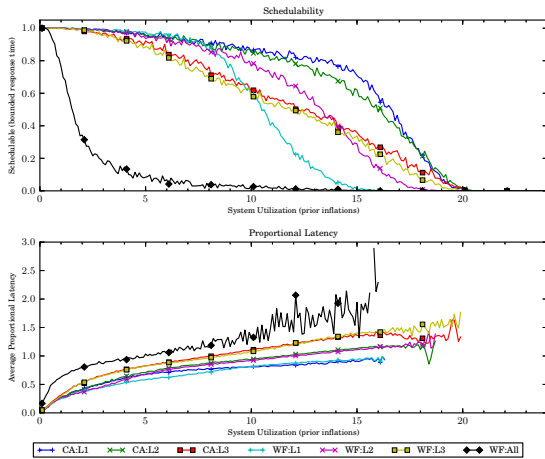


(a) Without polluter overheads.

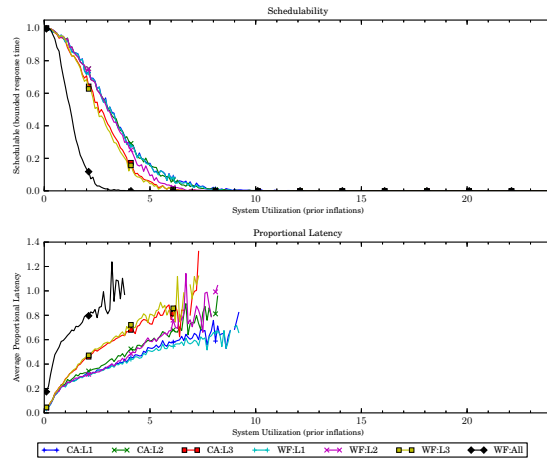


(b) With polluter overheads.

Figure 332: Results for *uni-heavy* per-task utilization, *uni-long* period, *bimo-medium-weight* EWSS, and *pipeline* height factor.

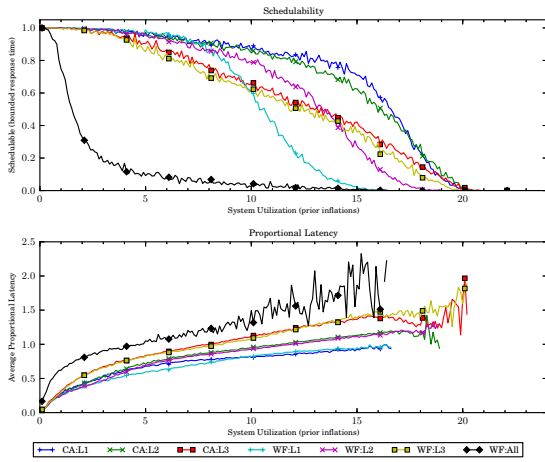


(a) Without polluter overheads.

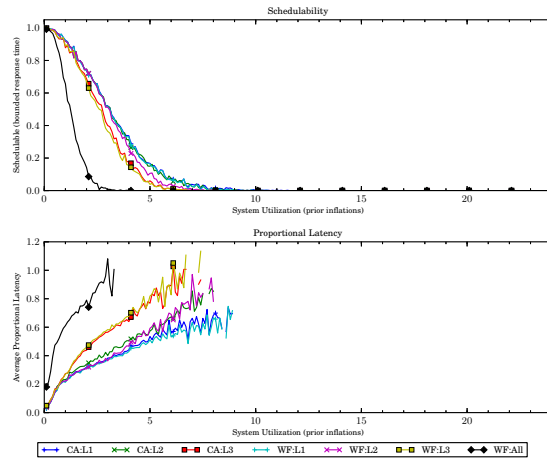


(b) With polluter overheads.

Figure 333: Results for *bimo-light* per-task utilization, *uni-short* period, *bimo-medium-weight* EWSS, and *uni-short* height factor.

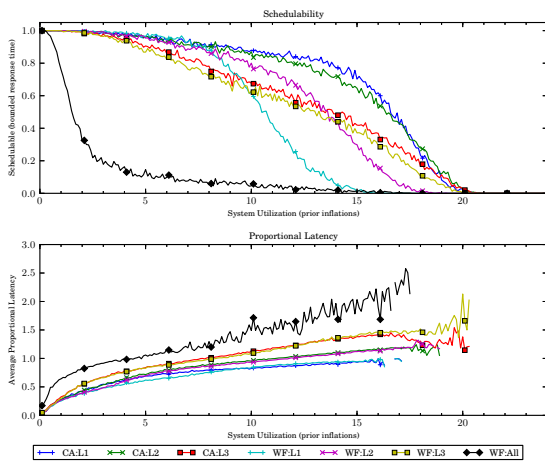


(a) Without polluter overheads.

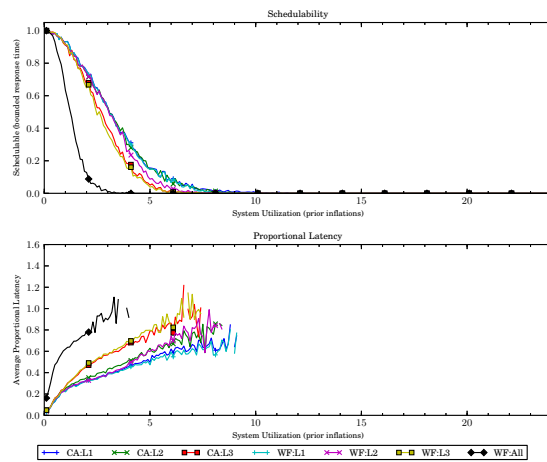


(b) With polluter overheads.

Figure 334: Results for *bimo-light* per-task utilization, *uni-short* period, *bimo-medium-weight* EWSS, and *uni-medium* height factor.

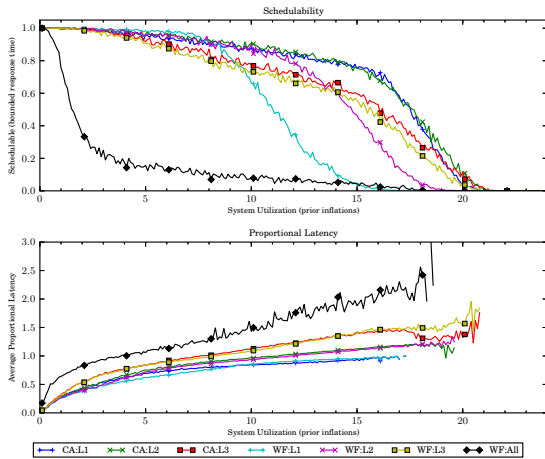


(a) Without polluter overheads.

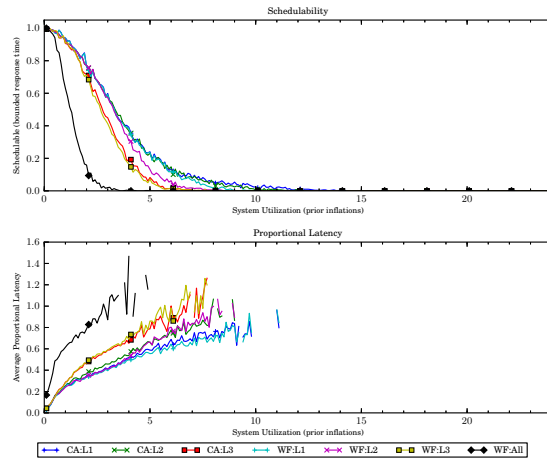


(b) With polluter overheads.

Figure 335: Results for *bimo-light* per-task utilization, *uni-short* period, *bimo-medium-weight* EWSS, and *uni-tall* height factor.

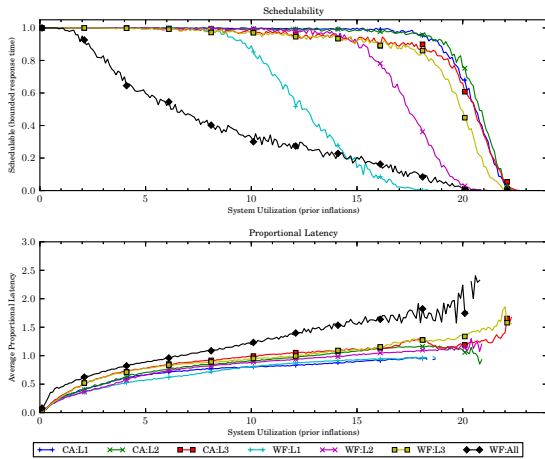


(a) Without polluter overheads.

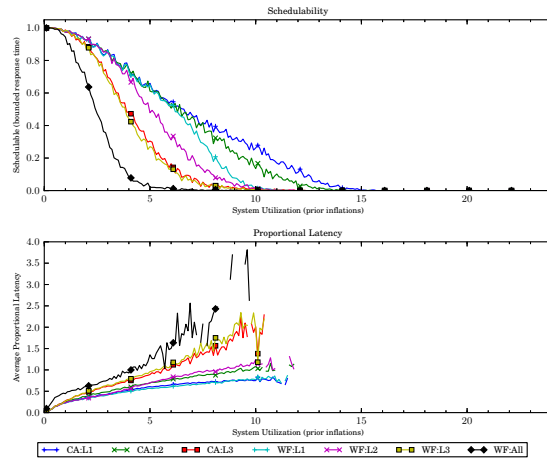


(b) With polluter overheads.

Figure 336: Results for *bimo-light* per-task utilization, *uni-short* period, *bimo-medium-weight* EWSS, and *pipeline* height factor.

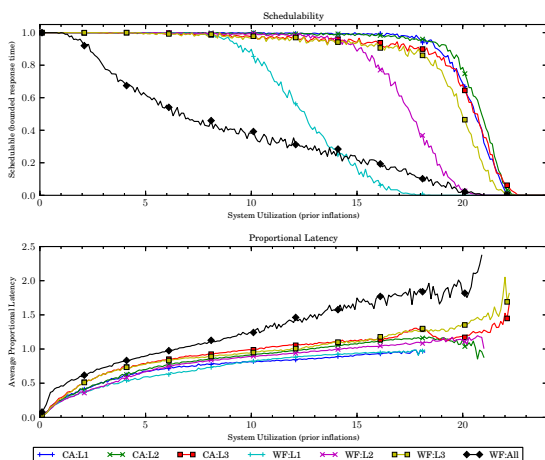


(a) Without polluter overheads.

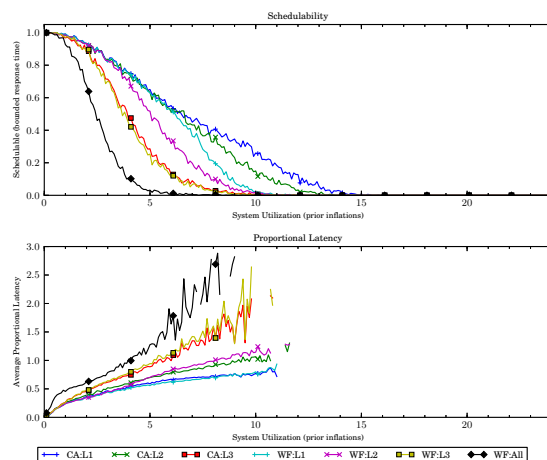


(b) With polluter overheads.

Figure 337: Results for *bimo-light* per-task utilization, *uni-moderate* period, *bimo-medium-weight* EWSS, and *uni-short* height factor.

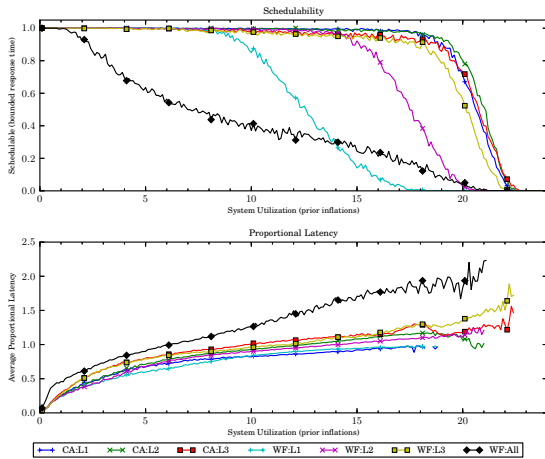


(a) Without polluter overheads.

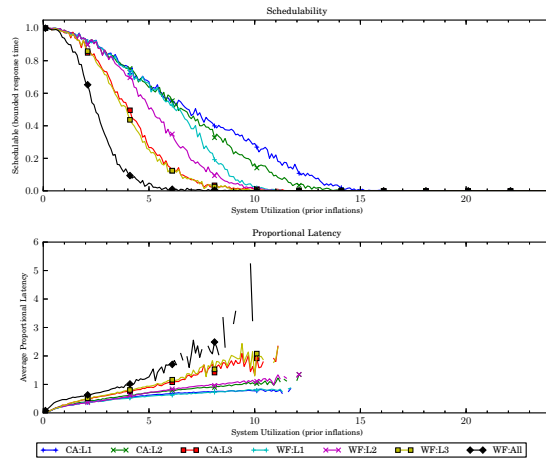


(b) With polluter overheads.

Figure 338: Results for *bimo-light* per-task utilization, *uni-moderate* period, *bimo-medium-weight* EWSS, and *uni-medium* height factor.

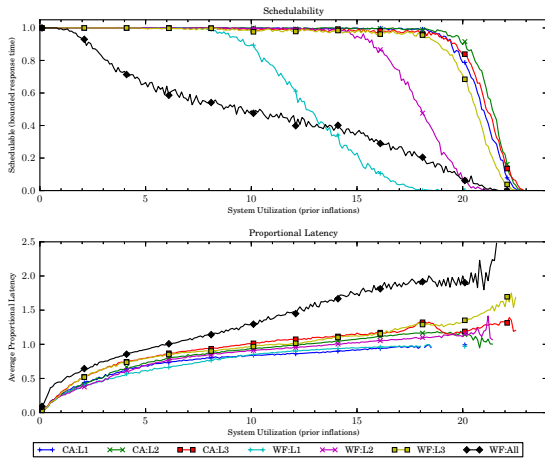


(a) Without polluter overheads.

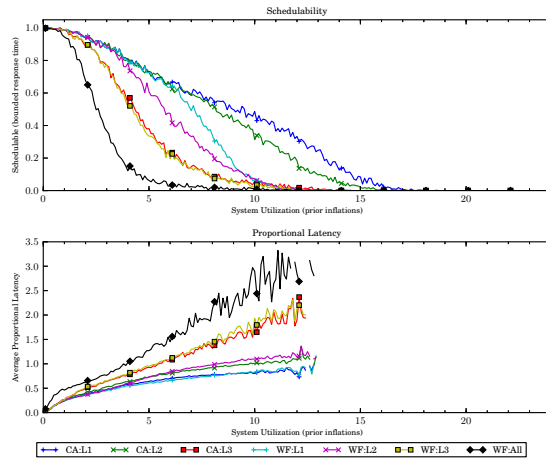


(b) With polluter overheads.

Figure 339: Results for *bimo-light* per-task utilization, *uni-moderate* period, *bimo-medium-weight* EWSS, and *uni-tall* height factor.

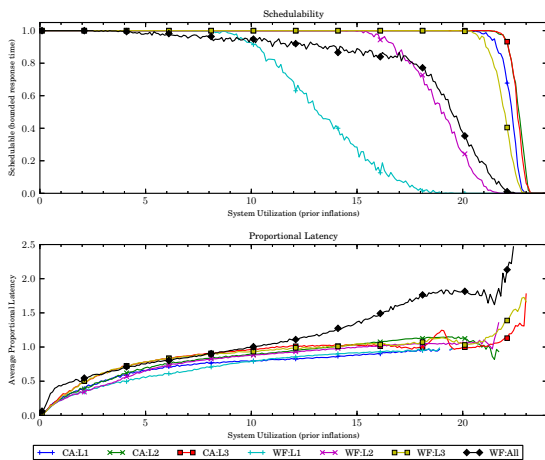


(a) Without polluter overheads.

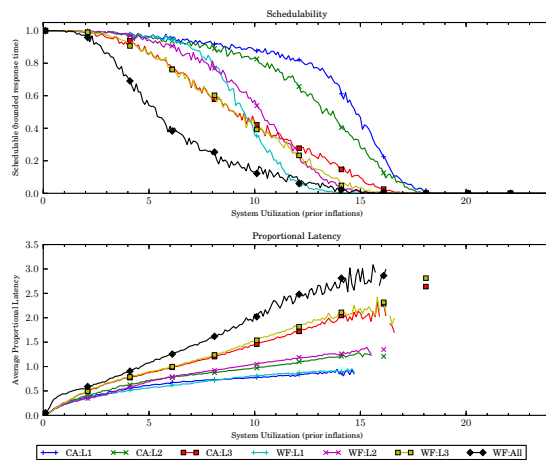


(b) With polluter overheads.

Figure 340: Results for *bimo-light* per-task utilization, *uni-moderate* period, *bimo-medium-weight* EWSS, and *pipeline* height factor.

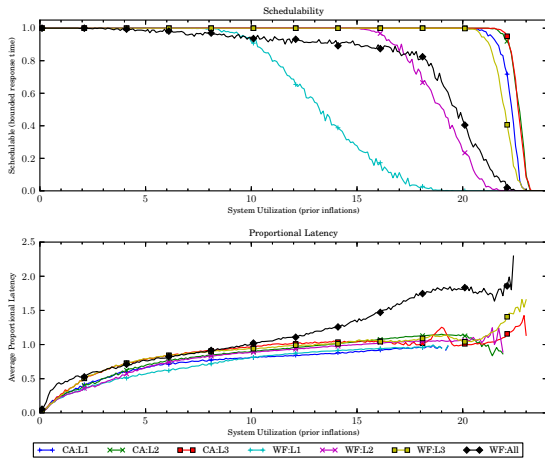


(a) Without polluter overheads.

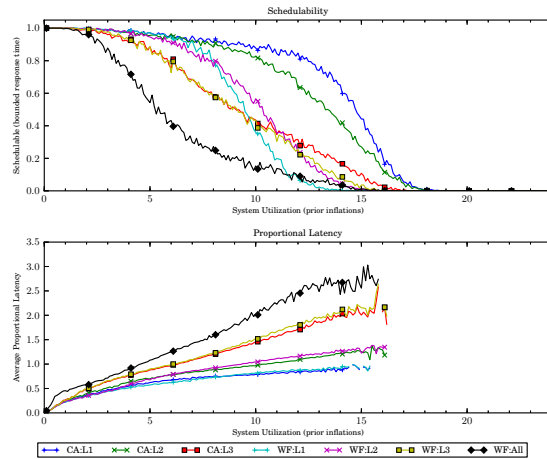


(b) With polluter overheads.

Figure 341: Results for *bimo-light* per-task utilization, *uni-long* period, *bimo-medium-weight* EWSS, and *uni-short* height factor.

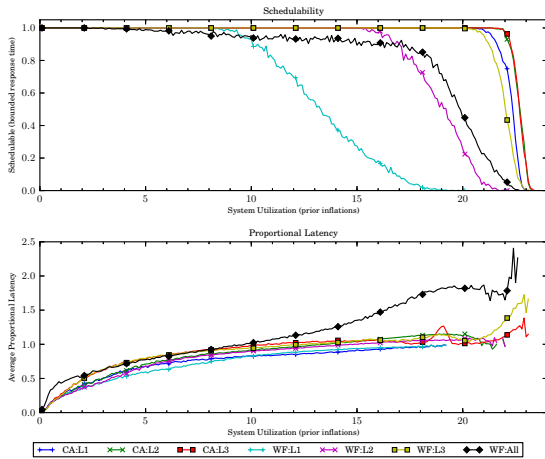


(a) Without polluter overheads.

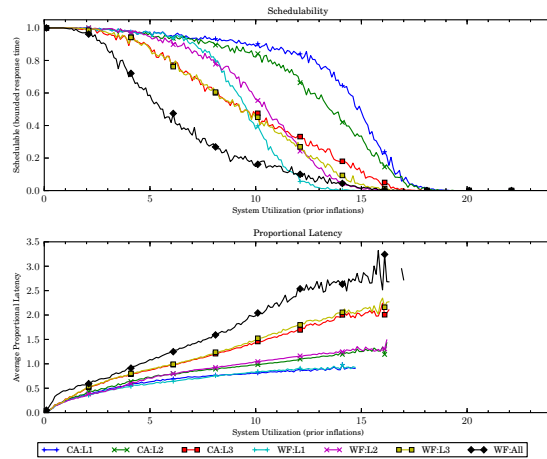


(b) With polluter overheads.

Figure 342: Results for *bimo-light* per-task utilization, *uni-long* period, *bimo-medium-weight* EWSS, and *uni-medium* height factor.

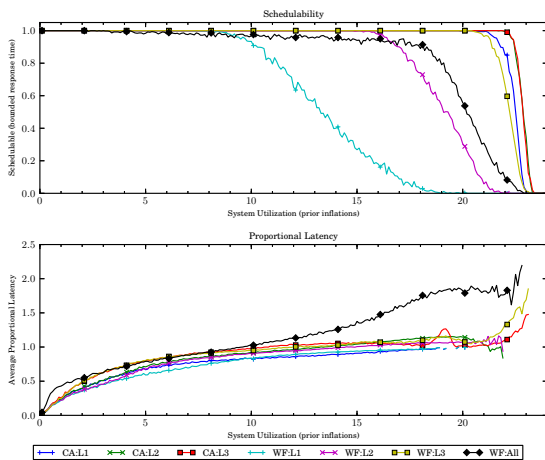


(a) Without polluter overheads.

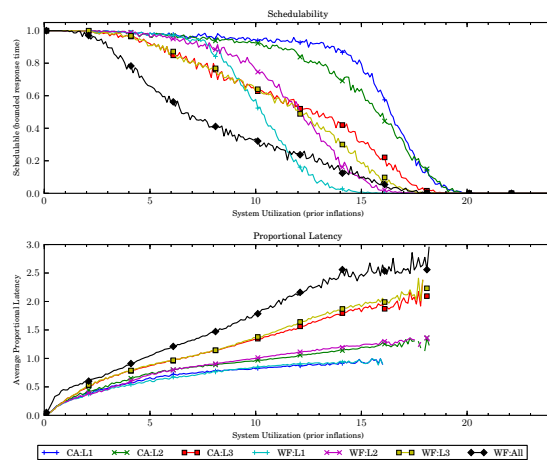


(b) With polluter overheads.

Figure 343: Results for *bimo-light* per-task utilization, *uni-long* period, *bimo-medium-weight* EWSS, and *uni-tall* height factor.

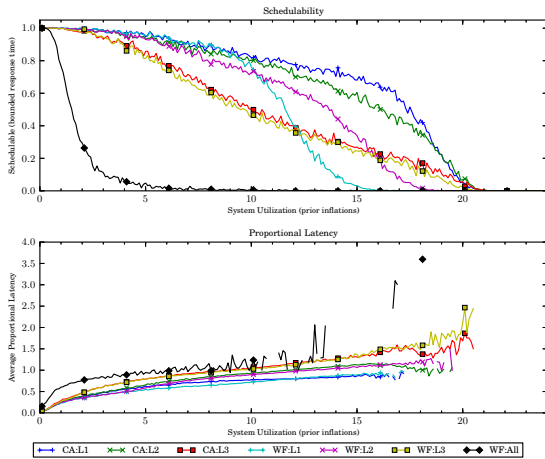


(a) Without polluter overheads.

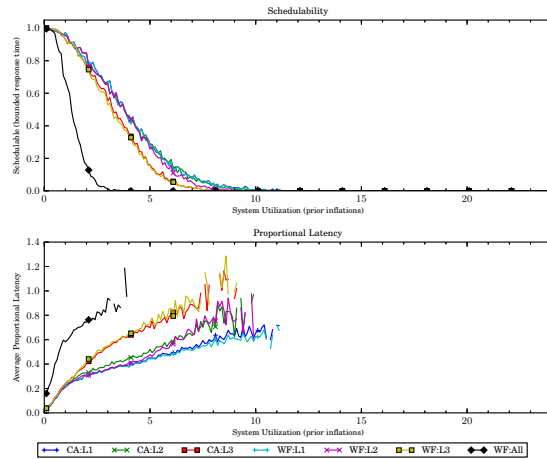


(b) With polluter overheads.

Figure 344: Results for *bimo-light* per-task utilization, *uni-long* period, *bimo-medium-weight* EWSS, and *pipeline* height factor.

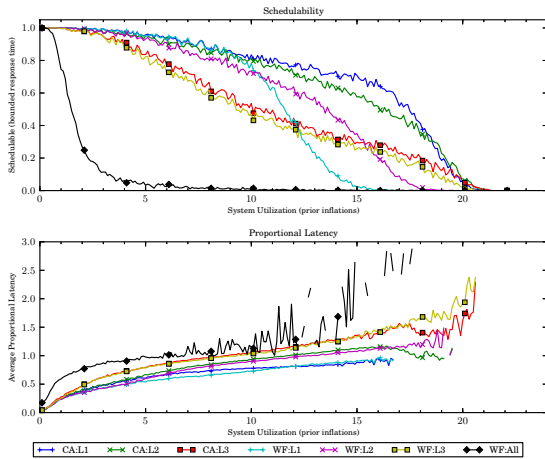


(a) Without polluter overheads.

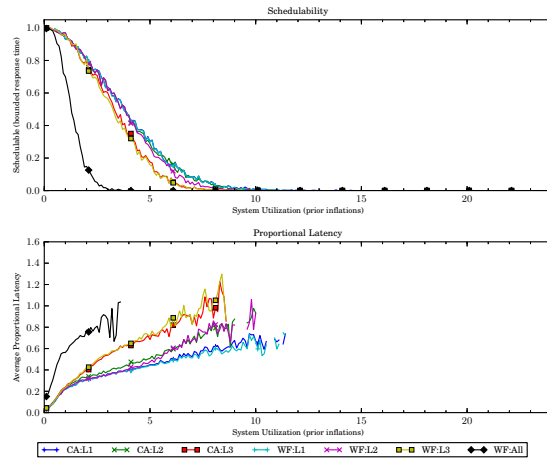


(b) With polluter overheads.

Figure 345: Results for *bimo-medium* per-task utilization, *uni-short* period, *bimo-medium-weight* EWSS, and *uni-short* height factor.

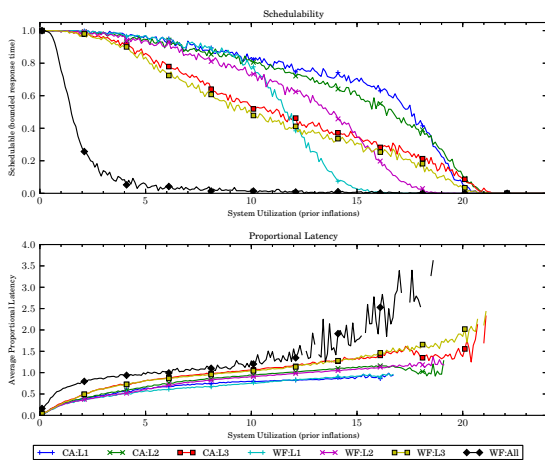


(a) Without polluter overheads.

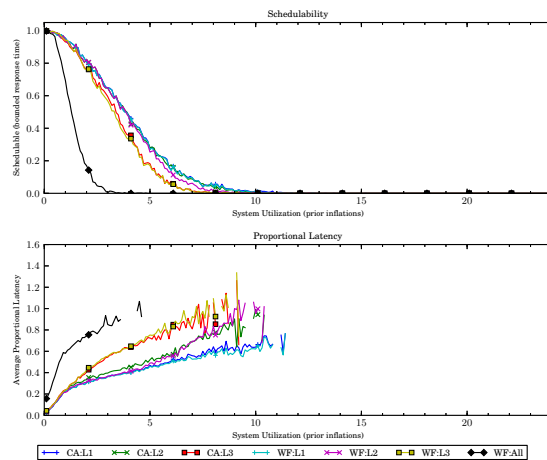


(b) With polluter overheads.

Figure 346: Results for *bimo-medium* per-task utilization, *uni-short* period, *bimo-medium-weight* EWSS, and *uni-medium* height factor.

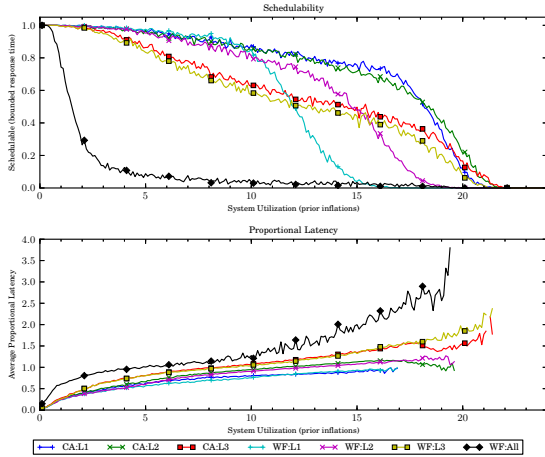


(a) Without polluter overheads.

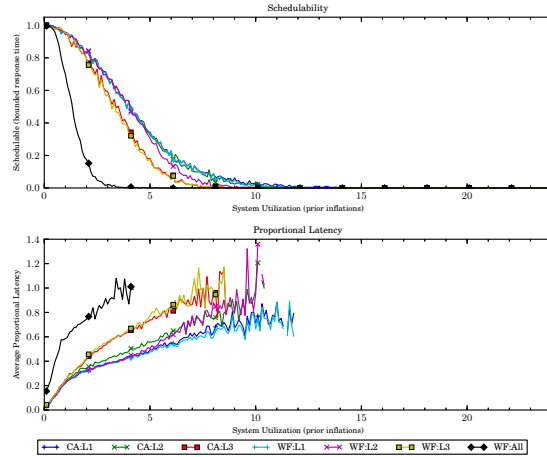


(b) With polluter overheads.

Figure 347: Results for *bimo-medium* per-task utilization, *uni-short* period, *bimo-medium-weight* EWSS, and *uni-tall* height factor.

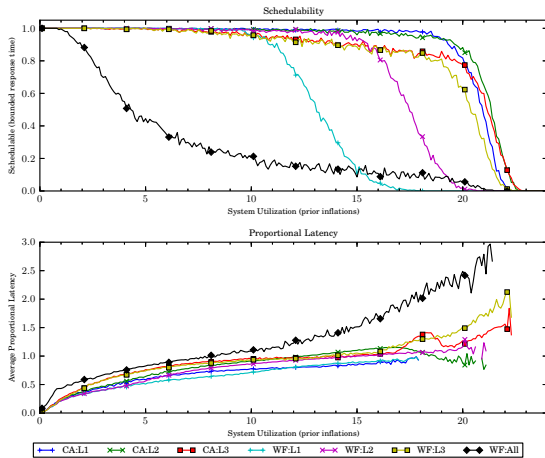


(a) Without polluter overheads.

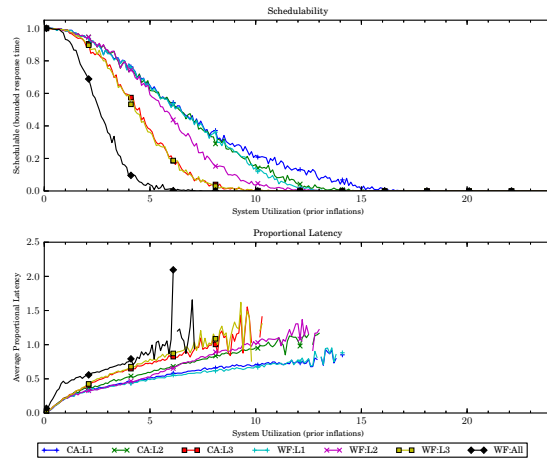


(b) With polluter overheads.

Figure 348: Results for *bimo-medium* per-task utilization, *uni-short* period, *bimo-medium-weight* EWSS, and *pipeline* height factor.

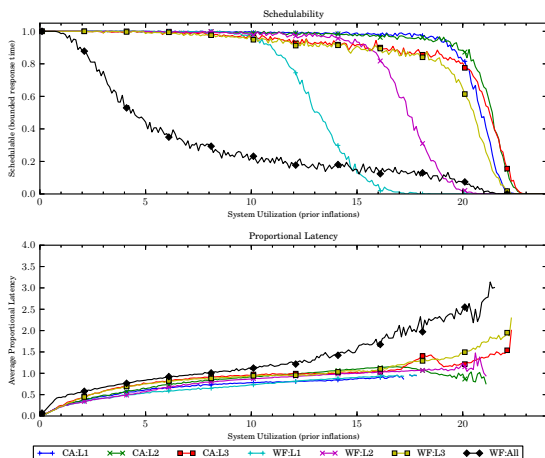


(a) Without polluter overheads.

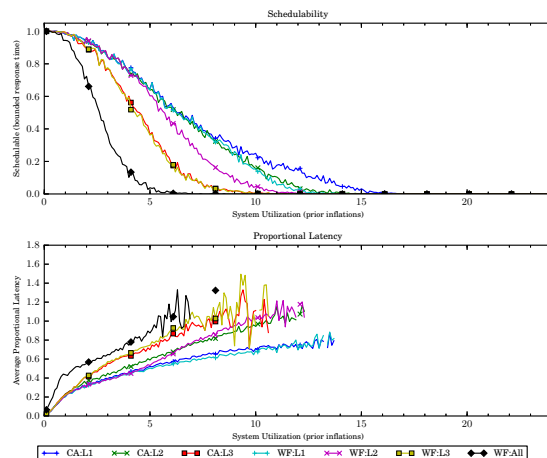


(b) With polluter overheads.

Figure 349: Results for *bimo-medium* per-task utilization, *uni-moderate* period, *bimo-medium-weight* EWSS, and *uni-short* height factor.

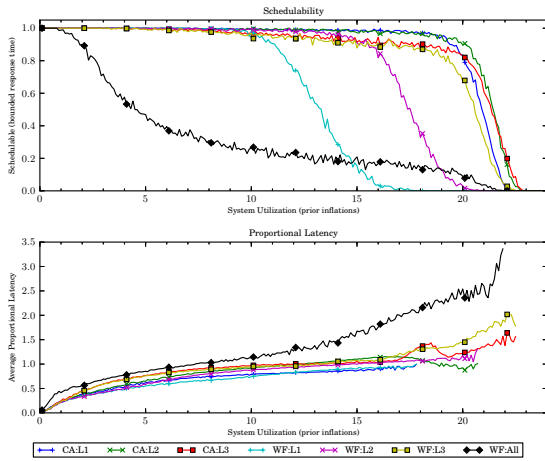


(a) Without polluter overheads.

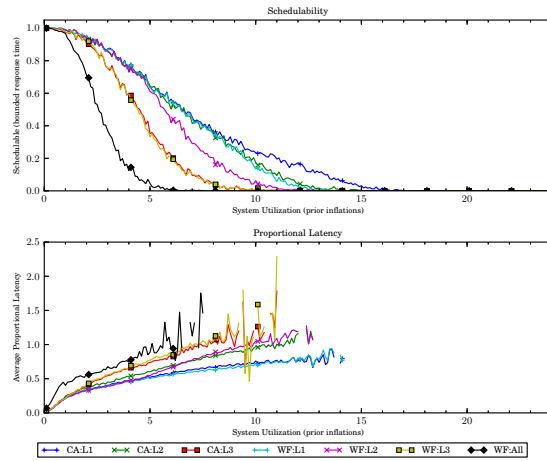


(b) With polluter overheads.

Figure 350: Results for *bimo-medium* per-task utilization, *uni-moderate* period, *bimo-medium-weight* EWSS, and *uni-medium* height factor.

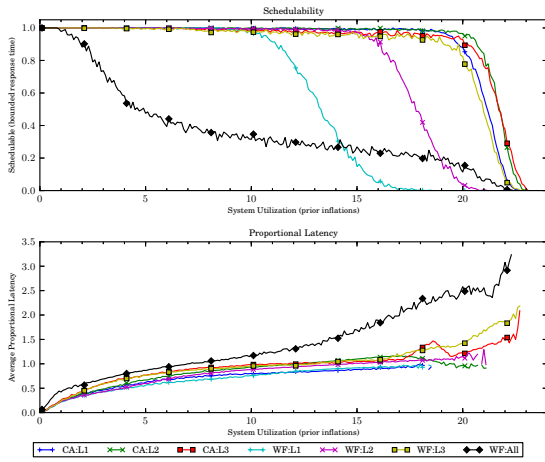


(a) Without polluter overheads.

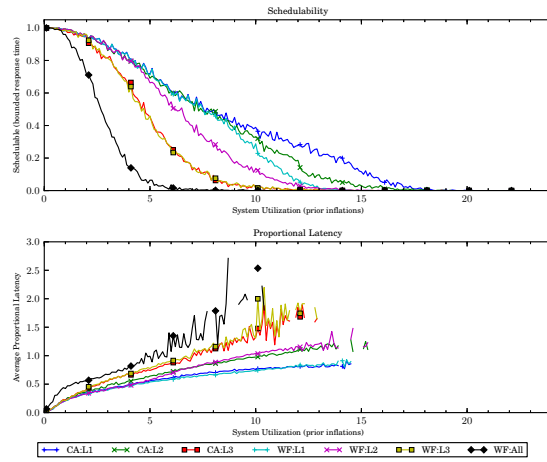


(b) With polluter overheads.

Figure 351: Results for *bimo-medium* per-task utilization, *uni-moderate* period, *bimo-medium-weight* EWSS, and *uni-tall* height factor.

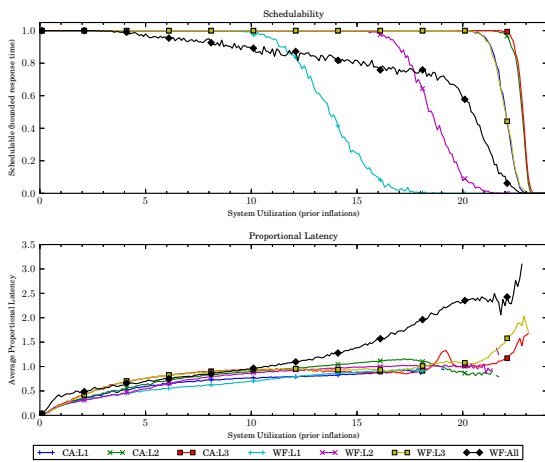


(a) Without polluter overheads.

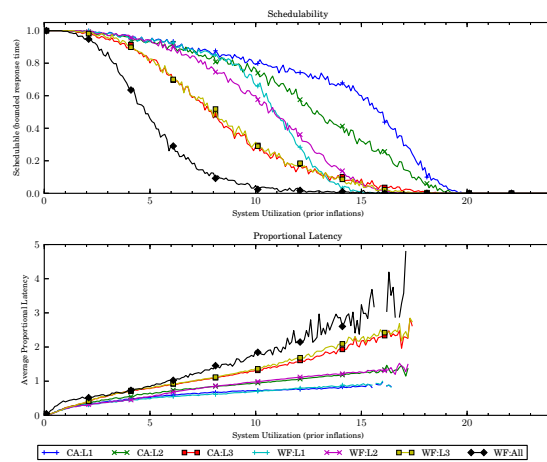


(b) With polluter overheads.

Figure 352: Results for *bimo-medium* per-task utilization, *uni-moderate* period, *bimo-medium-weight* EWSS, and *pipeline* height factor.

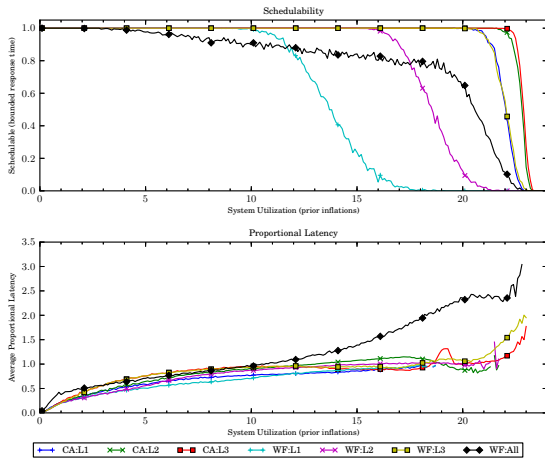


(a) Without polluter overheads.

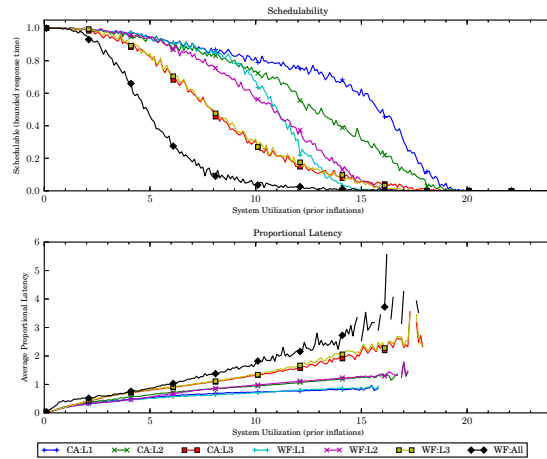


(b) With polluter overheads.

Figure 353: Results for *bimo-medium* per-task utilization, *uni-long* period, *bimo-medium-weight* EWSS, and *uni-short* height factor.

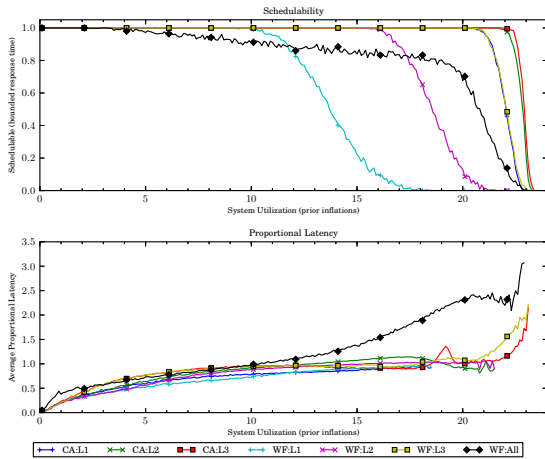


(a) Without polluter overheads.

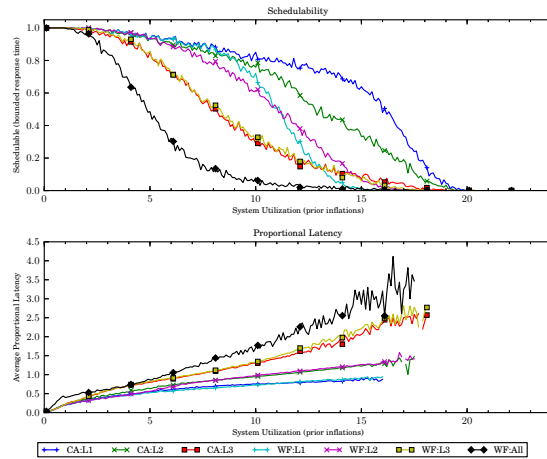


(b) With polluter overheads.

Figure 354: Results for *bimo-medium* per-task utilization, *uni-long* period, *bimo-medium-weight* EWSS, and *uni-medium* height factor.

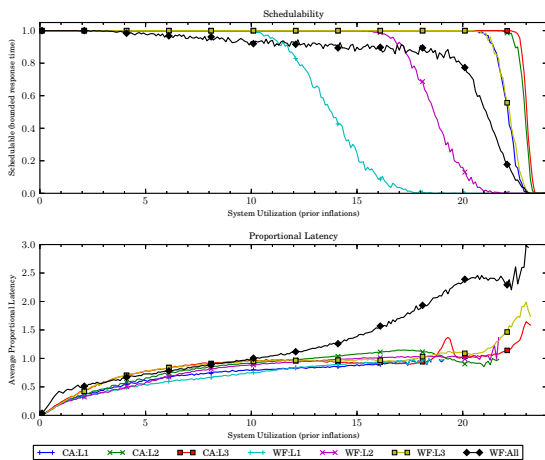


(a) Without polluter overheads.

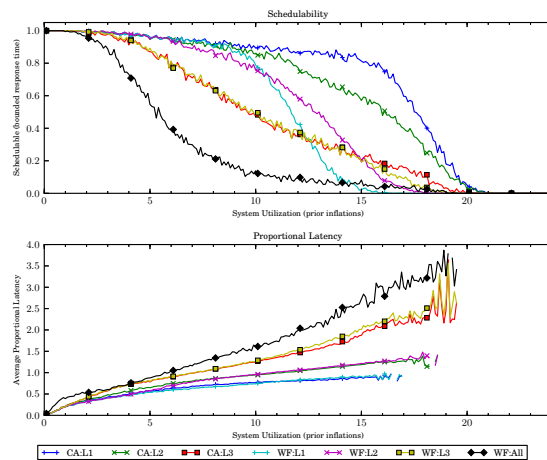


(b) With polluter overheads.

Figure 355: Results for *bimo-medium* per-task utilization, *uni-long* period, *bimo-medium-weight* EWSS, and *uni-tall* height factor.

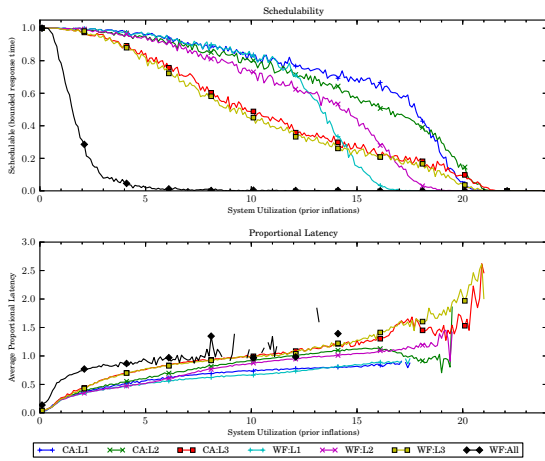


(a) Without polluter overheads.

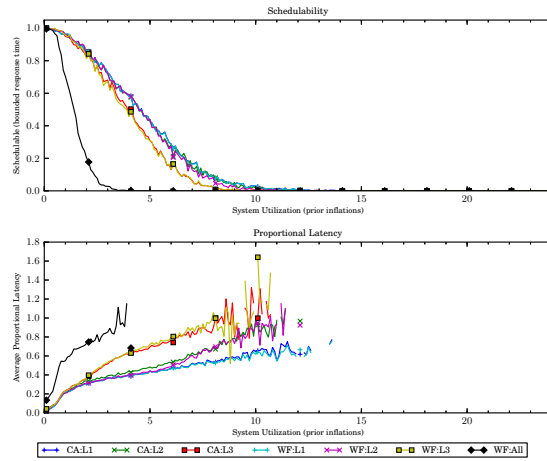


(b) With polluter overheads.

Figure 356: Results for *bimo-medium* per-task utilization, *uni-long* period, *bimo-medium-weight* EWSS, and *pipeline* height factor.

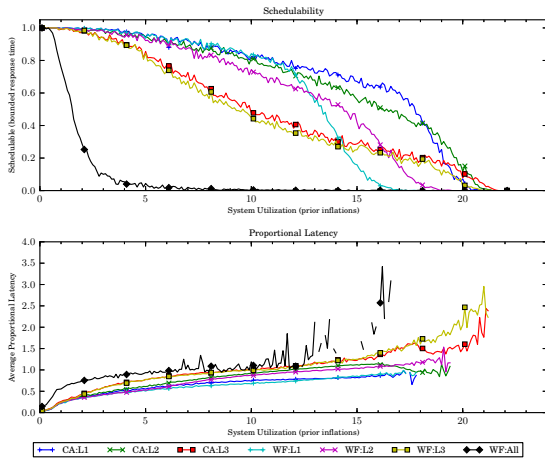


(a) Without polluter overheads.

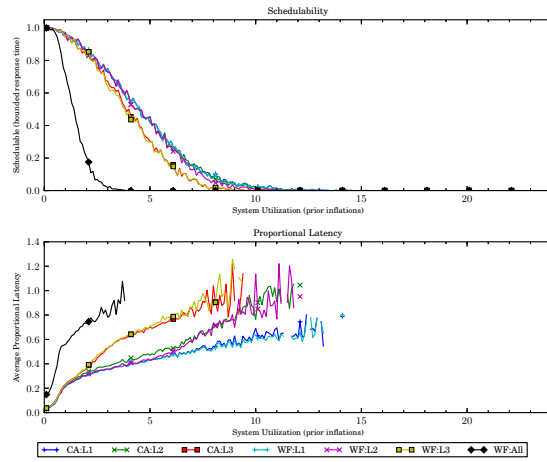


(b) With polluter overheads.

Figure 357: Results for *bimo-heavy* per-task utilization, *uni-short* period, *bimo-medium-weight* EWSS, and *uni-short* height factor.

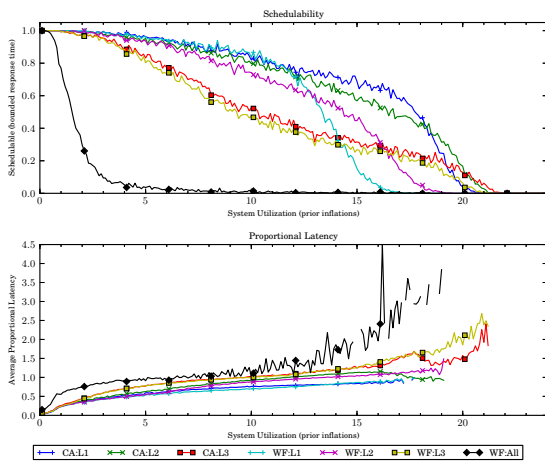


(a) Without polluter overheads.

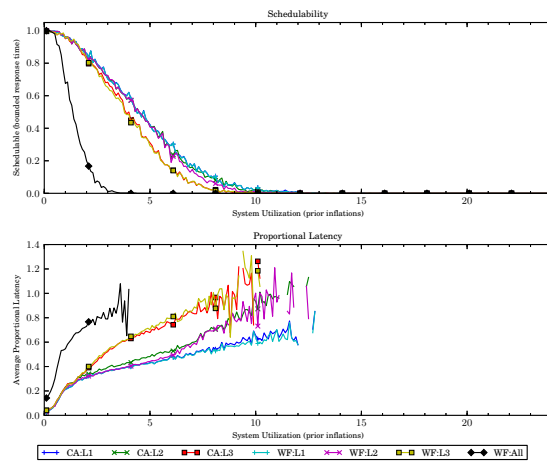


(b) With polluter overheads.

Figure 358: Results for *bimo-heavy* per-task utilization, *uni-short* period, *bimo-medium-weight* EWSS, and *uni-medium* height factor.

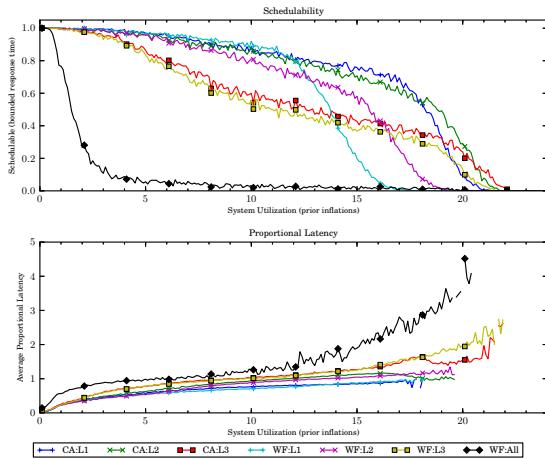


(a) Without polluter overheads.

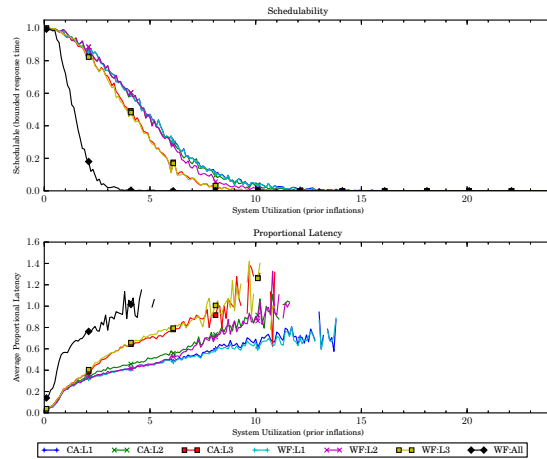


(b) With polluter overheads.

Figure 359: Results for *bimo-heavy* per-task utilization, *uni-short* period, *bimo-medium-weight* EWSS, and *uni-tall* height factor.

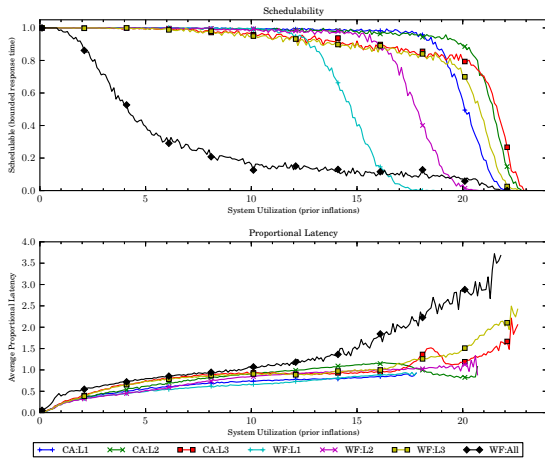


(a) Without polluter overheads.

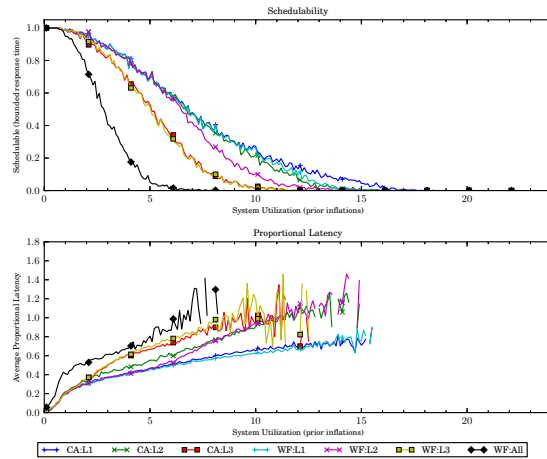


(b) With polluter overheads.

Figure 360: Results for *bimo-heavy* per-task utilization, *uni-short* period, *bimo-medium-weight* EWSS, and *pipeline* height factor.

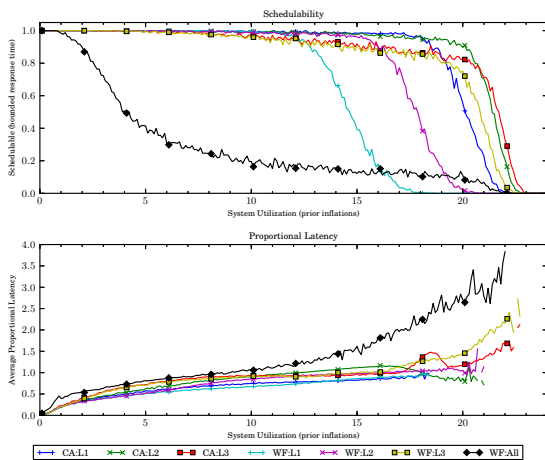


(a) Without polluter overheads.

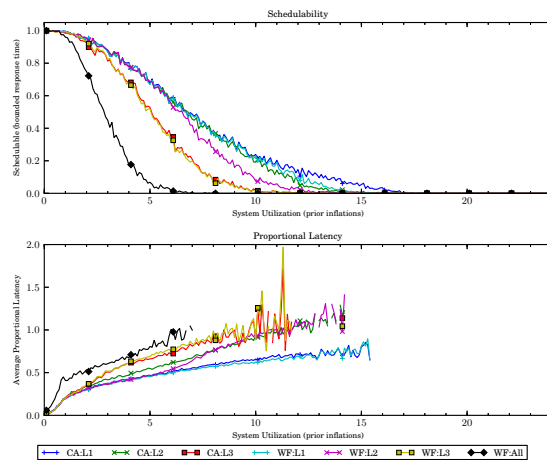


(b) With polluter overheads.

Figure 361: Results for *bimo-heavy* per-task utilization, *uni-moderate* period, *bimo-medium-weight* EWSS, and *uni-short* height factor.

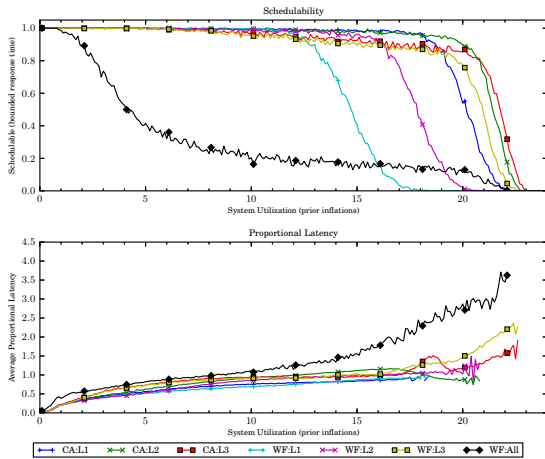


(a) Without polluter overheads.

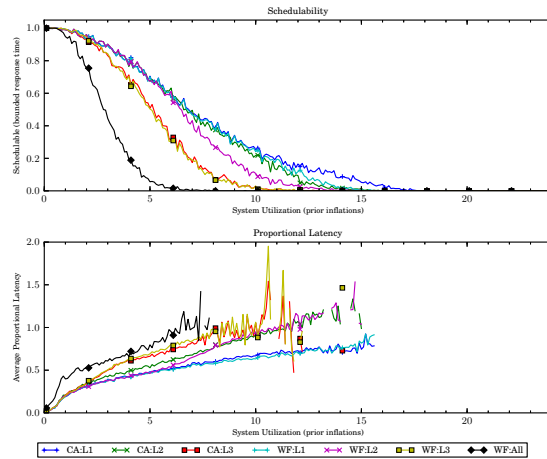


(b) With polluter overheads.

Figure 362: Results for *bimo-heavy* per-task utilization, *uni-moderate* period, *bimo-medium-weight* EWSS, and *uni-medium* height factor.

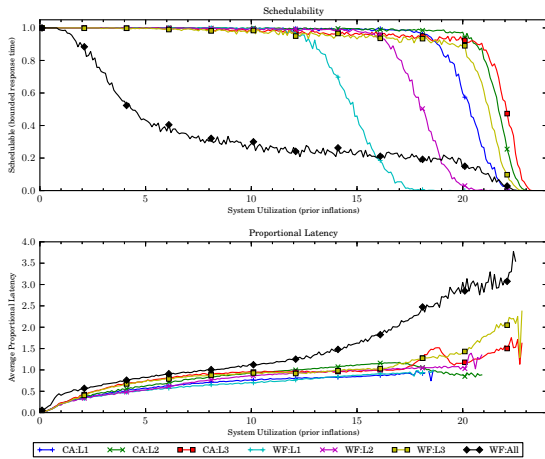


(a) Without polluter overheads.

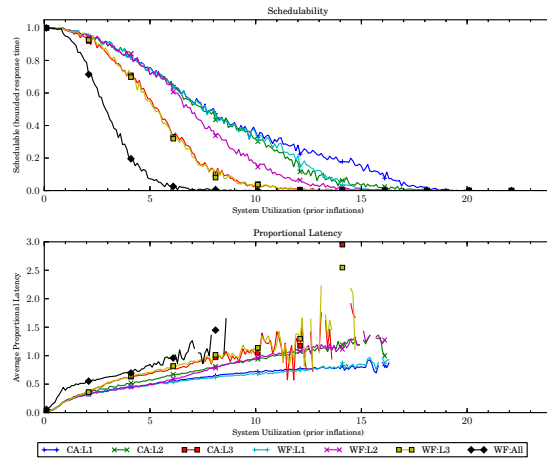


(b) With polluter overheads.

Figure 363: Results for *bimo-heavy* per-task utilization, *uni-moderate* period, *bimo-medium-weight* EWSS, and *uni-tall* height factor.

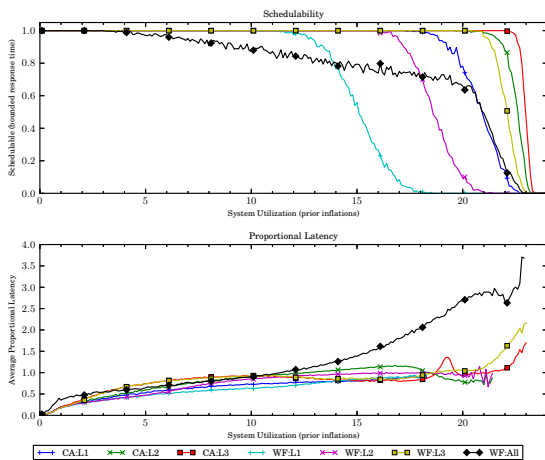


(a) Without polluter overheads.

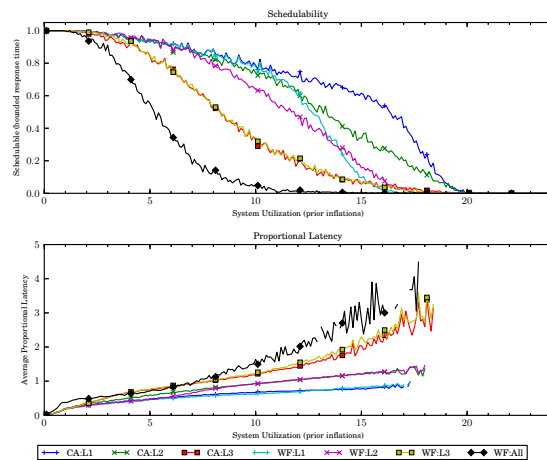


(b) With polluter overheads.

Figure 364: Results for *bimo-heavy* per-task utilization, *uni-moderate* period, *bimo-medium-weight* EWSS, and *pipeline* height factor.

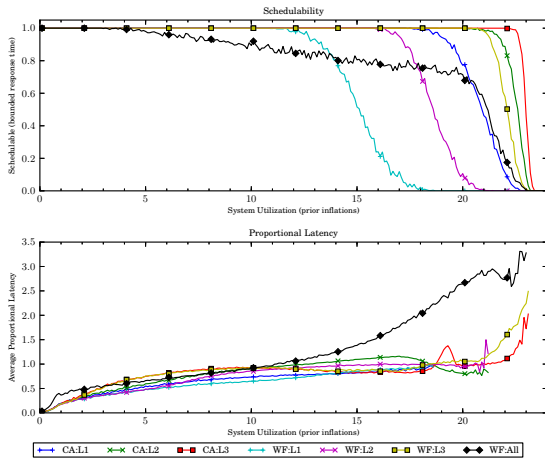


(a) Without polluter overheads.

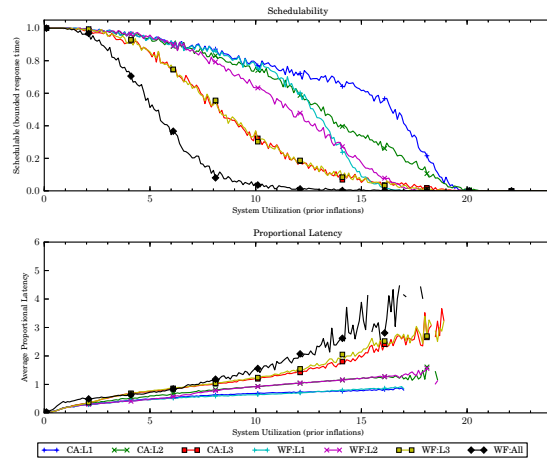


(b) With polluter overheads.

Figure 365: Results for *bimo-heavy* per-task utilization, *uni-long* period, *bimo-medium-weight* EWSS, and *uni-short* height factor.

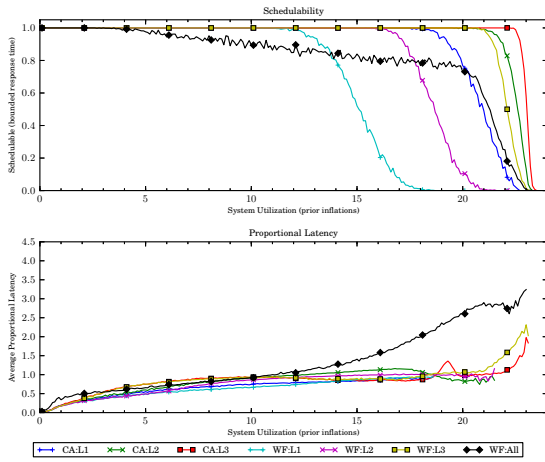


(a) Without polluter overheads.

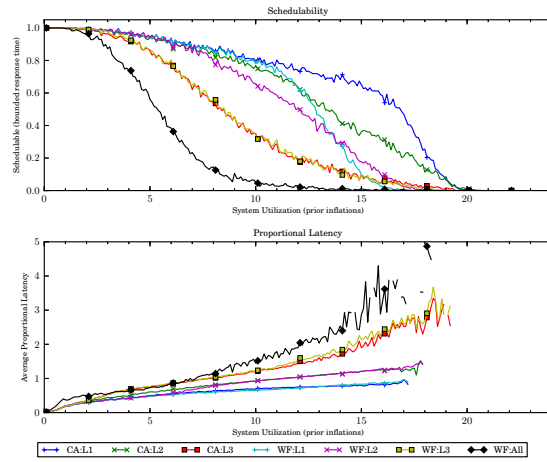


(b) With polluter overheads.

Figure 366: Results for *bimo-heavy* per-task utilization, *uni-long* period, *bimo-medium-weight* EWSS, and *uni-medium* height factor.

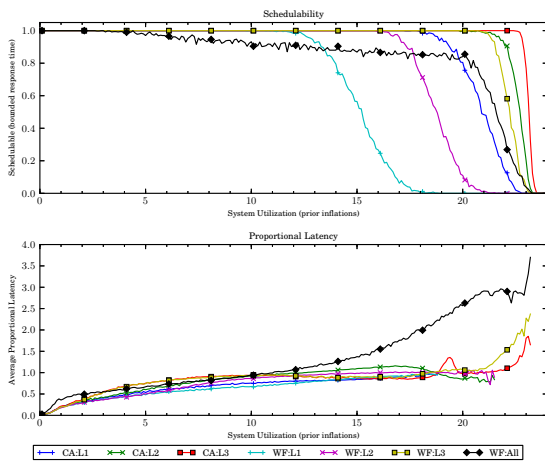


(a) Without polluter overheads.

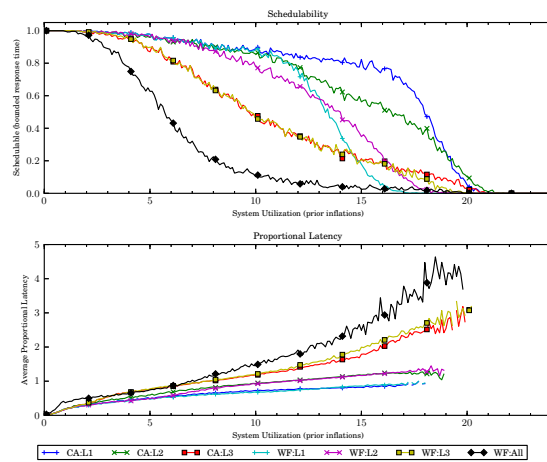


(b) With polluter overheads.

Figure 367: Results for *bimo-heavy* per-task utilization, *uni-long* period, *bimo-medium-weight* EWSS, and *uni-tall* height factor.

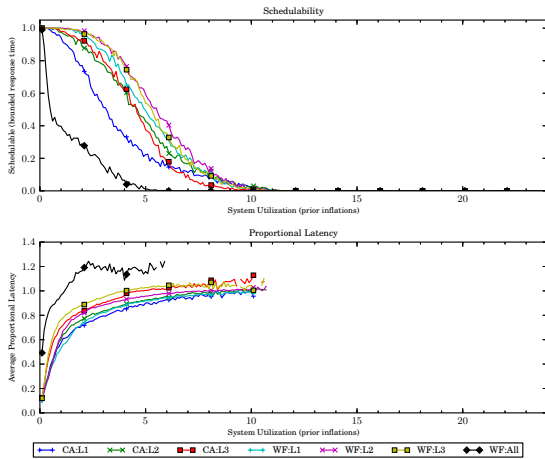


(a) Without polluter overheads.

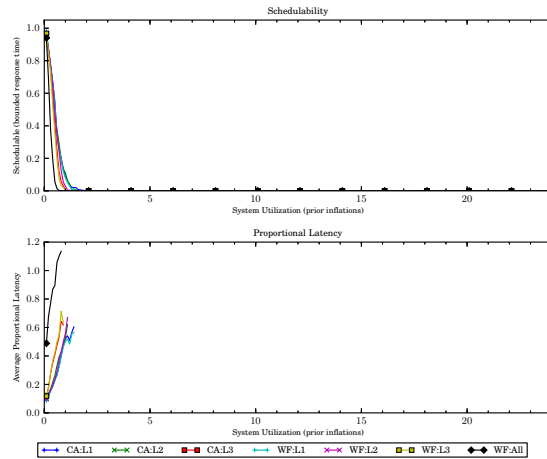


(b) With polluter overheads.

Figure 368: Results for *bimo-heavy* per-task utilization, *uni-long* period, *bimo-medium-weight* EWSS, and *pipeline* height factor.

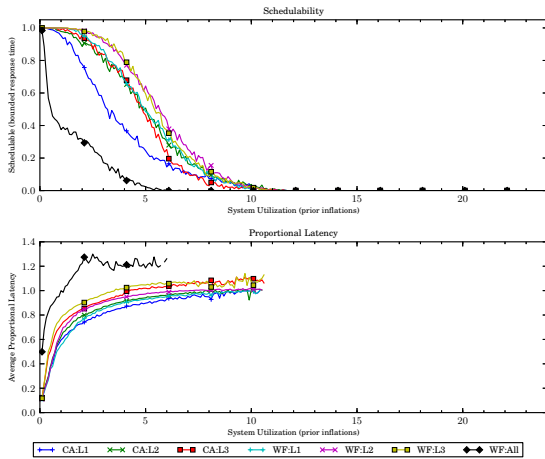


(a) Without polluter overheads.

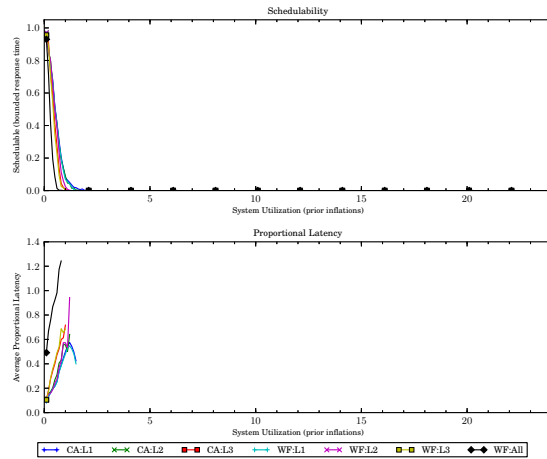


(b) With polluter overheads.

Figure 369: Results for *uni-light* per-task utilization, *uni-short* period, *bimo-heavy-weight* EWSS, and *uni-short* height factor.

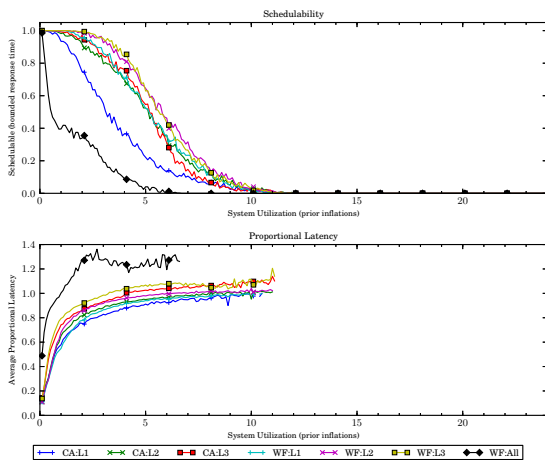


(a) Without polluter overheads.

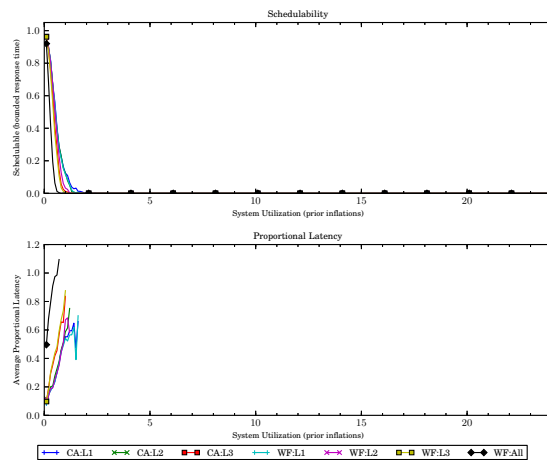


(b) With polluter overheads.

Figure 370: Results for *uni-light* per-task utilization, *uni-short* period, *bimo-heavy-weight* EWSS, and *uni-medium* height factor.

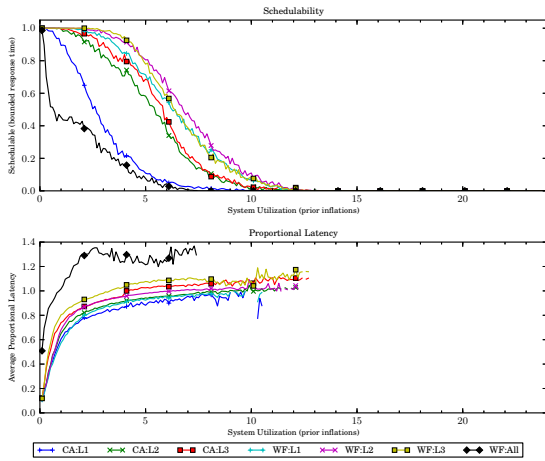


(a) Without polluter overheads.

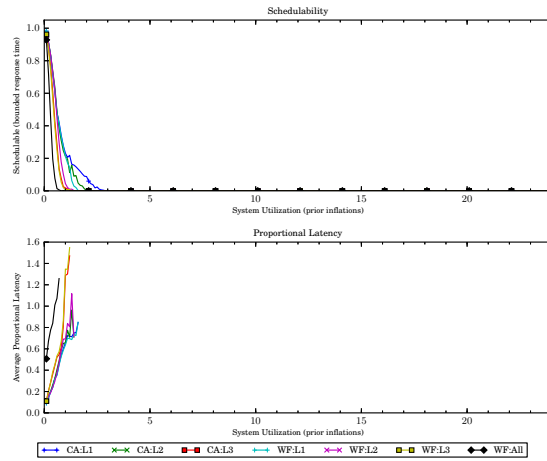


(b) With polluter overheads.

Figure 371: Results for *uni-light* per-task utilization, *uni-short* period, *bimo-heavy-weight* EWSS, and *uni-tall* height factor.

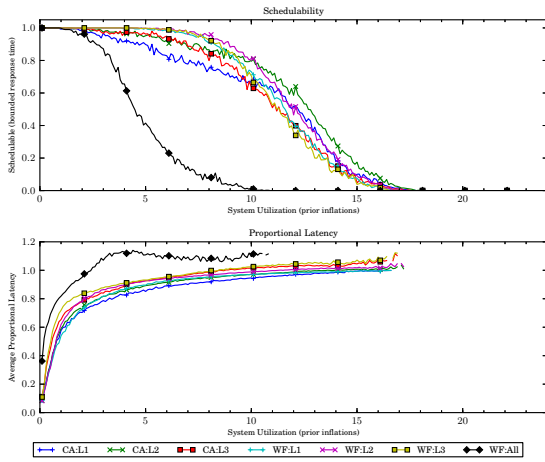


(a) Without polluter overheads.

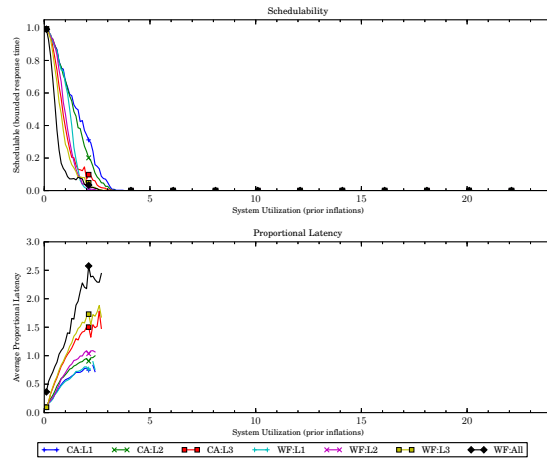


(b) With polluter overheads.

Figure 372: Results for *uni-light* per-task utilization, *uni-short* period, *bimo-heavy-weight* EWSS, and *pipeline* height factor.

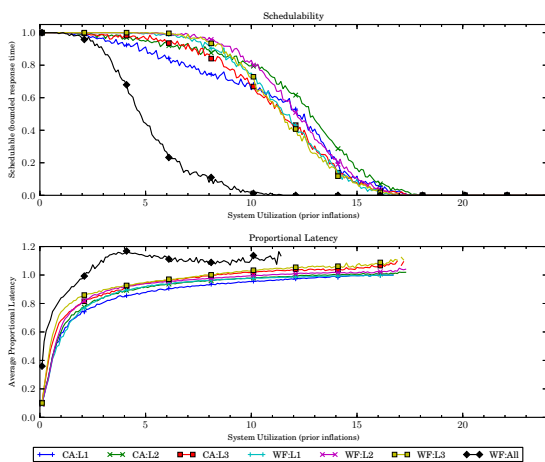


(a) Without polluter overheads.

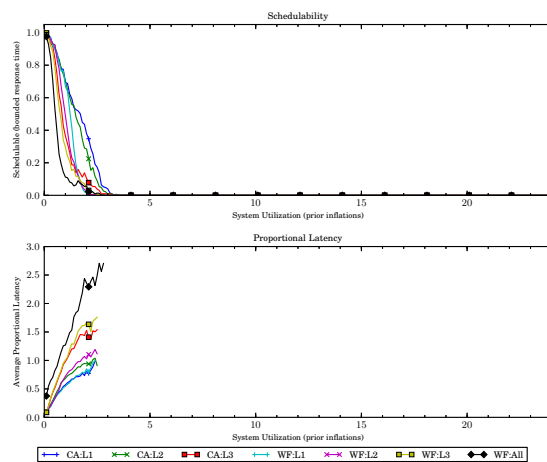


(b) With polluter overheads.

Figure 373: Results for *uni-light* per-task utilization, *uni-moderate* period, *bimo-heavy-weight* EWSS, and *uni-short* height factor.

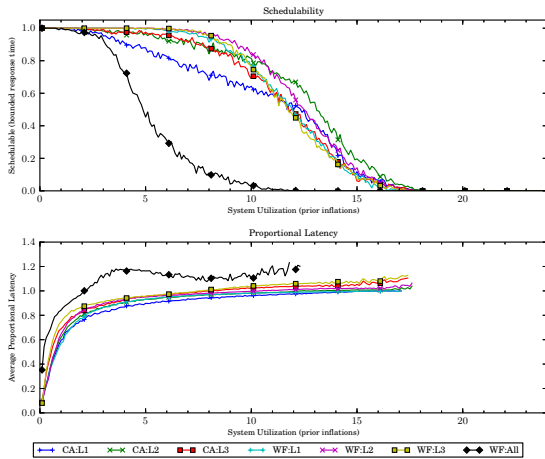


(a) Without polluter overheads.

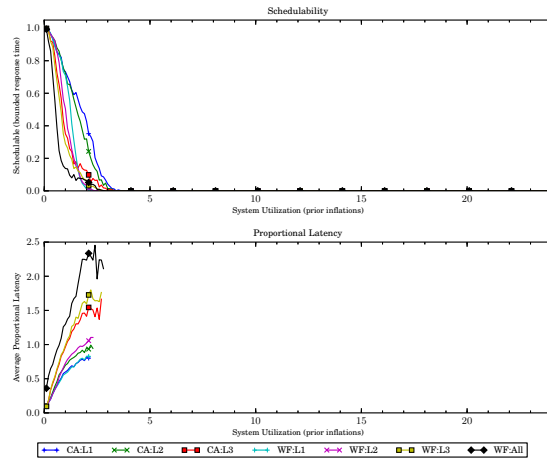


(b) With polluter overheads.

Figure 374: Results for *uni-light* per-task utilization, *uni-moderate* period, *bimo-heavy-weight* EWSS, and *uni-medium* height factor.

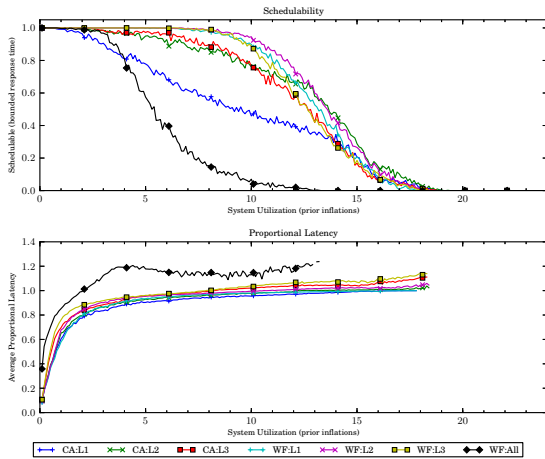


(a) Without polluter overheads.

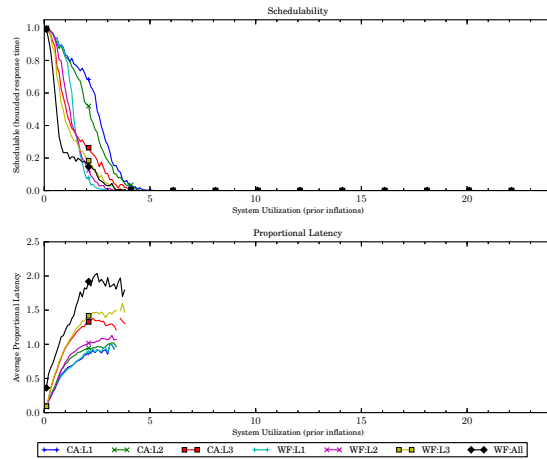


(b) With polluter overheads.

Figure 375: Results for *uni-light* per-task utilization, *uni-moderate* period, *bimo-heavy-weight* EWSS, and *uni-tall* height factor.

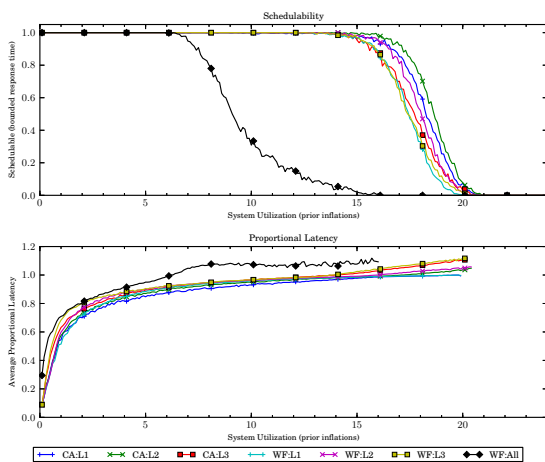


(a) Without polluter overheads.

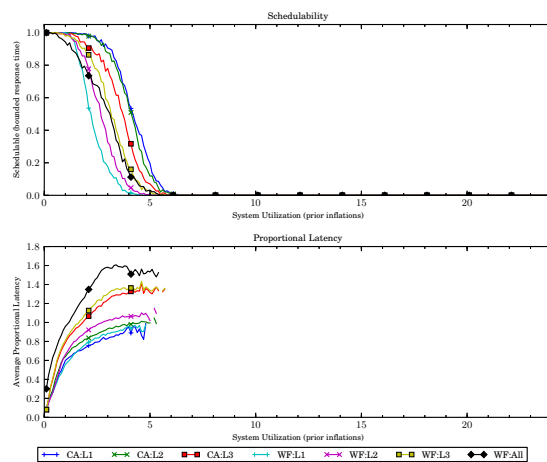


(b) With polluter overheads.

Figure 376: Results for *uni-light* per-task utilization, *uni-moderate* period, *bimo-heavy-weight* EWSS, and *pipeline* height factor.

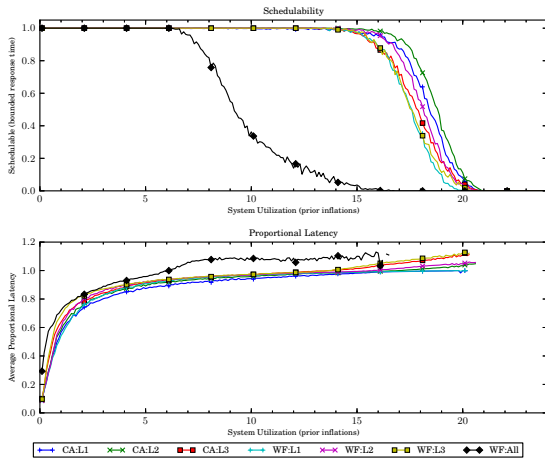


(a) Without polluter overheads.

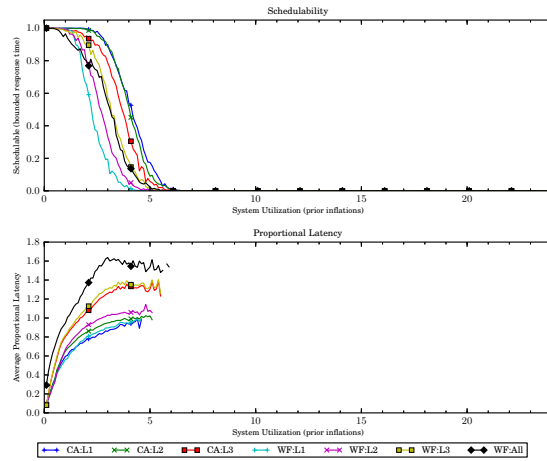


(b) With polluter overheads.

Figure 377: Results for *uni-light* per-task utilization, *uni-long* period, *bimo-heavy-weight* EWSS, and *uni-short* height factor.

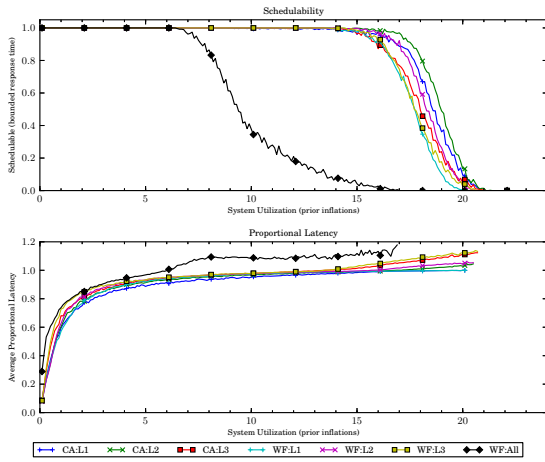


(a) Without polluter overheads.

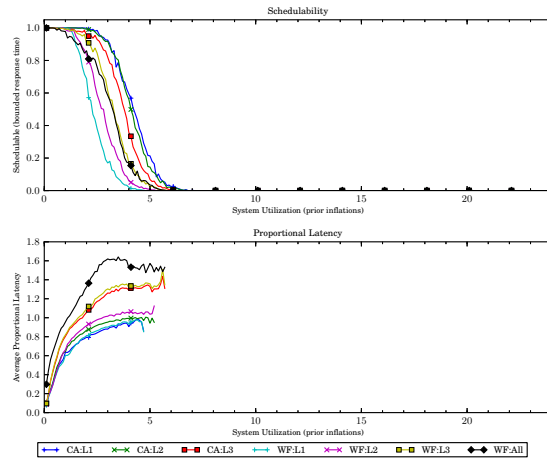


(b) With polluter overheads.

Figure 378: Results for *uni-light* per-task utilization, *uni-long* period, *bimo-heavy-weight* EWSS, and *uni-medium* height factor.

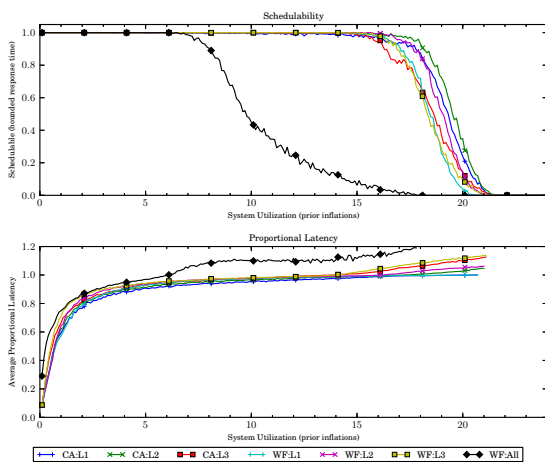


(a) Without polluter overheads.

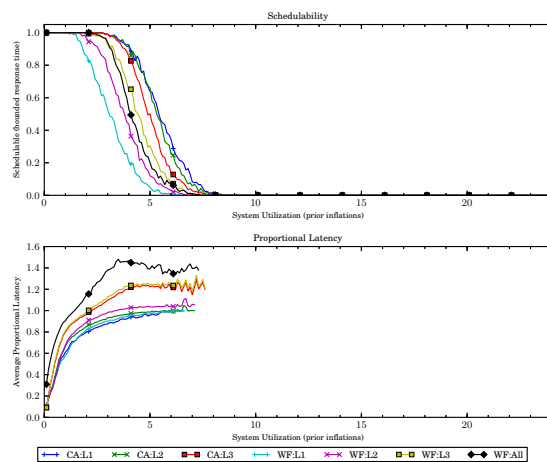


(b) With polluter overheads.

Figure 379: Results for *uni-light* per-task utilization, *uni-long* period, *bimo-heavy-weight* EWSS, and *uni-tall* height factor.

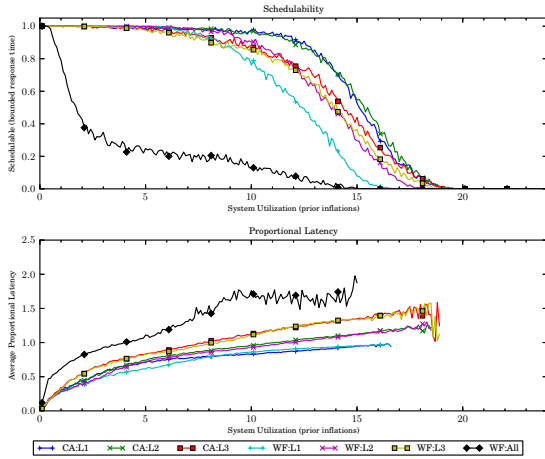


(a) Without polluter overheads.

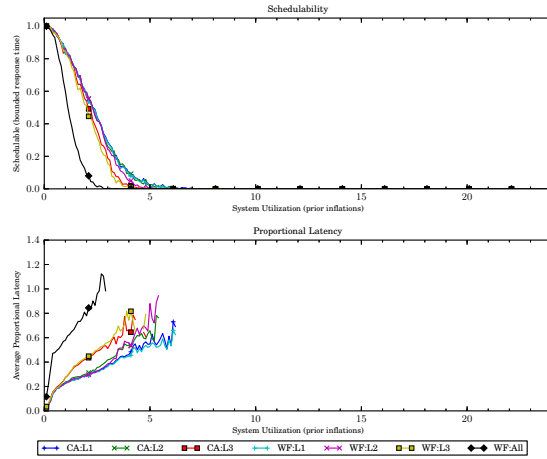


(b) With polluter overheads.

Figure 380: Results for *uni-light* per-task utilization, *uni-long* period, *bimo-heavy-weight* EWSS, and *pipeline* height factor.

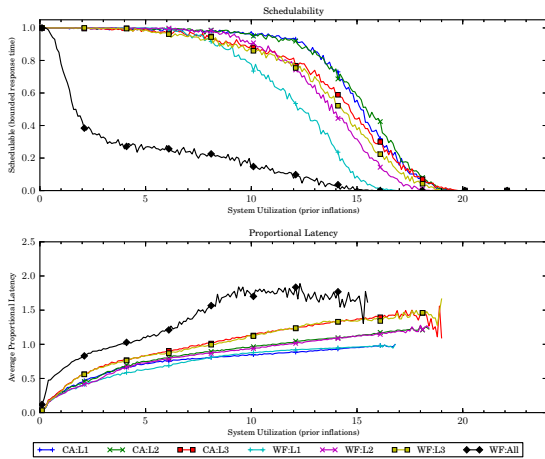


(a) Without polluter overheads.

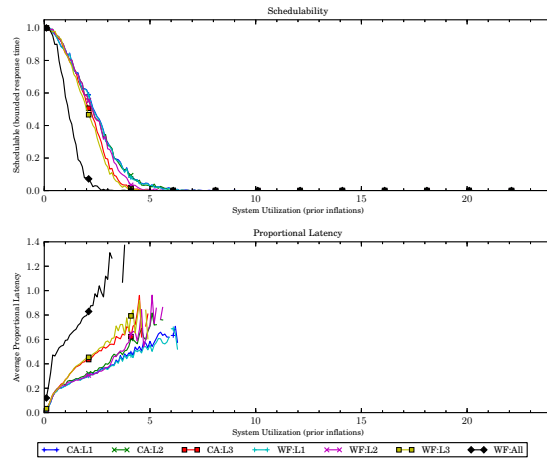


(b) With polluter overheads.

Figure 381: Results for *uni-medium* per-task utilization, *uni-short* period, *bimo-heavy-weight* EWSS, and *uni-short* height factor.

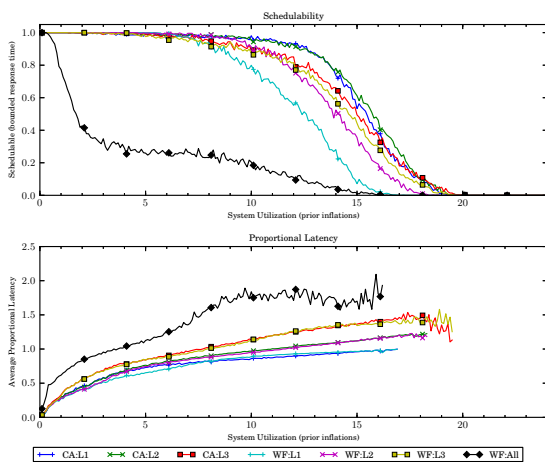


(a) Without polluter overheads.

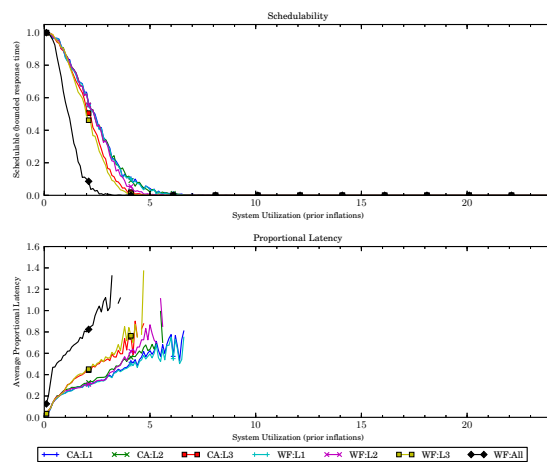


(b) With polluter overheads.

Figure 382: Results for *uni-medium* per-task utilization, *uni-short* period, *bimo-heavy-weight* EWSS, and *uni-medium* height factor.

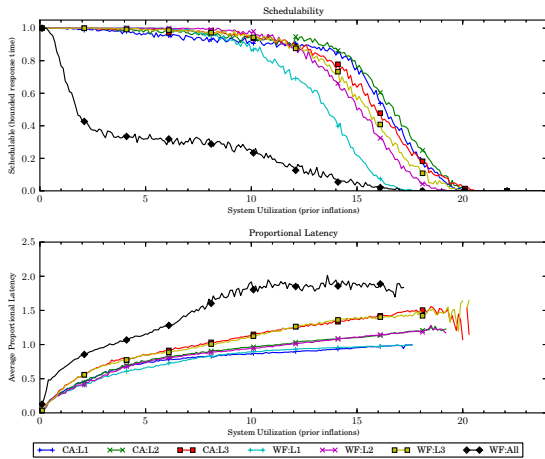


(a) Without polluter overheads.

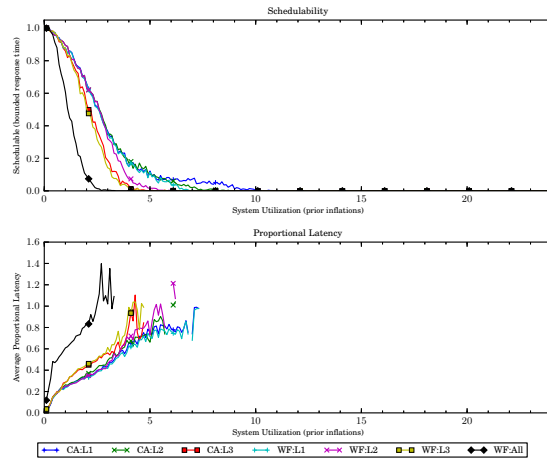


(b) With polluter overheads.

Figure 383: Results for *uni-medium* per-task utilization, *uni-short* period, *bimo-heavy-weight* EWSS, and *uni-tall* height factor.

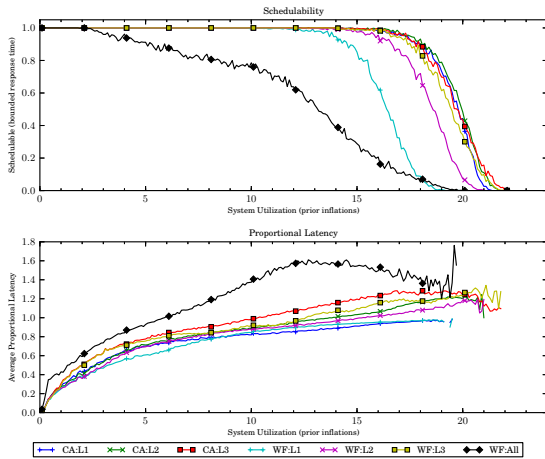


(a) Without polluter overheads.

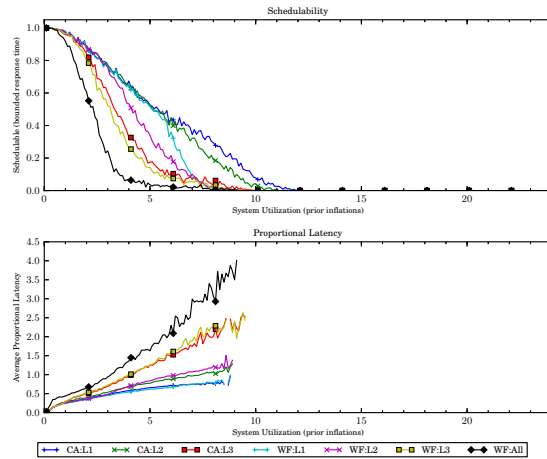


(b) With polluter overheads.

Figure 384: Results for *uni-medium* per-task utilization, *uni-short* period, *bimo-heavy-weight* EWSS, and *pipeline* height factor.

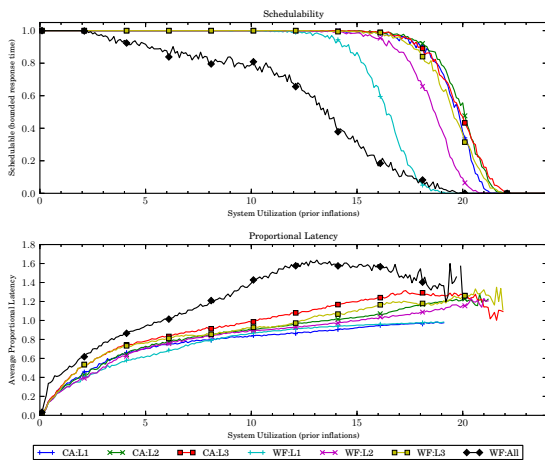


(a) Without polluter overheads.

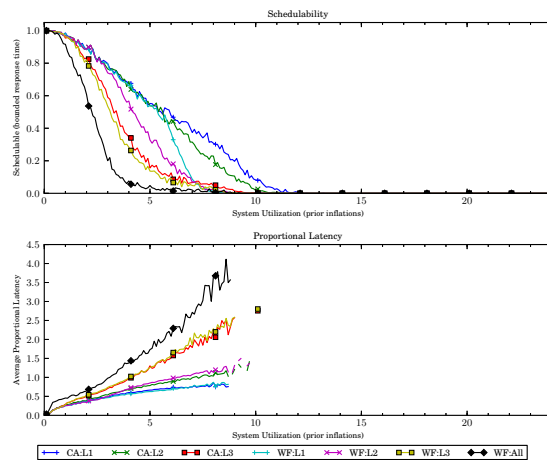


(b) With polluter overheads.

Figure 385: Results for *uni-medium* per-task utilization, *uni-moderate* period, *bimo-heavy-weight* EWSS, and *uni-short* height factor.

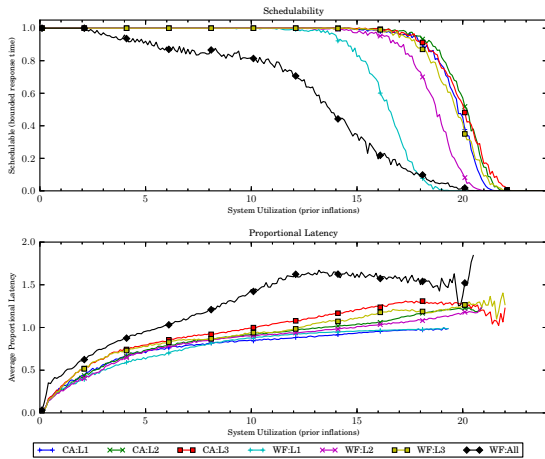


(a) Without polluter overheads.

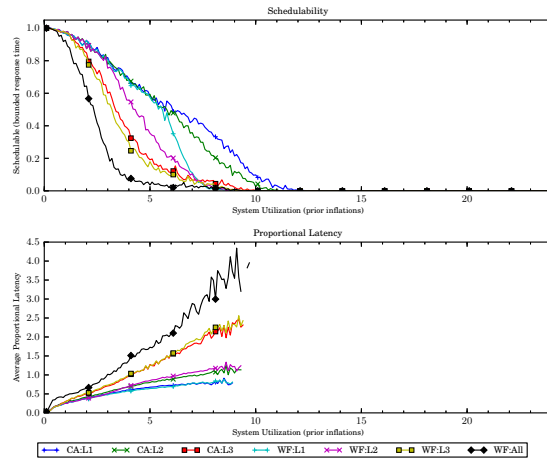


(b) With polluter overheads.

Figure 386: Results for *uni-medium* per-task utilization, *uni-moderate* period, *bimo-heavy-weight* EWSS, and *uni-medium* height factor.

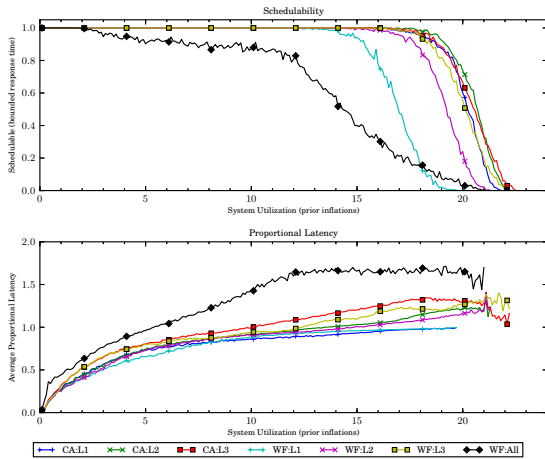


(a) Without polluter overheads.

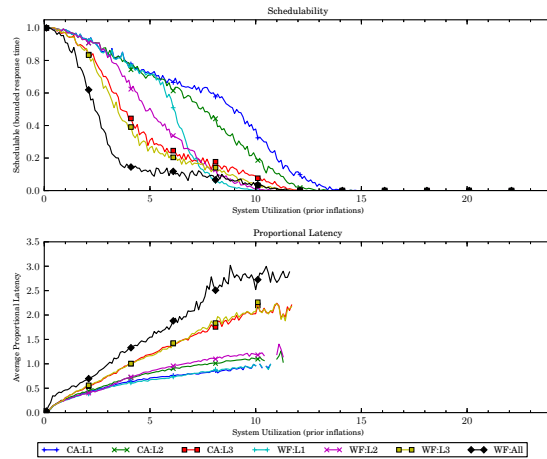


(b) With polluter overheads.

Figure 387: Results for *uni-medium* per-task utilization, *uni-moderate* period, *bimo-heavy-weight* EWSS, and *uni-tall* height factor.

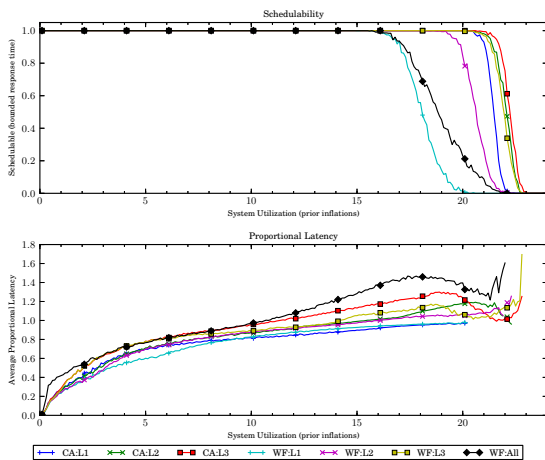


(a) Without polluter overheads.

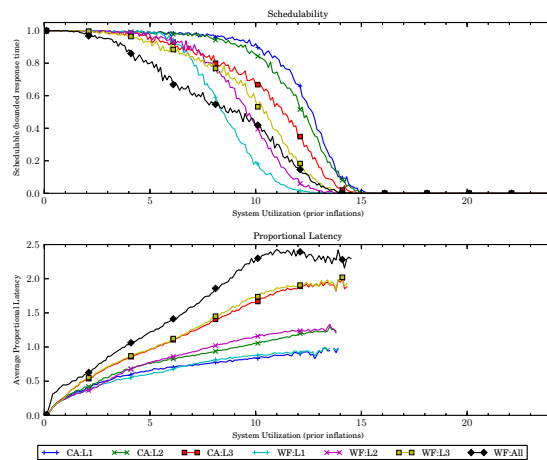


(b) With polluter overheads.

Figure 388: Results for *uni-medium* per-task utilization, *uni-moderate* period, *bimo-heavy-weight* EWSS, and *pipeline* height factor.

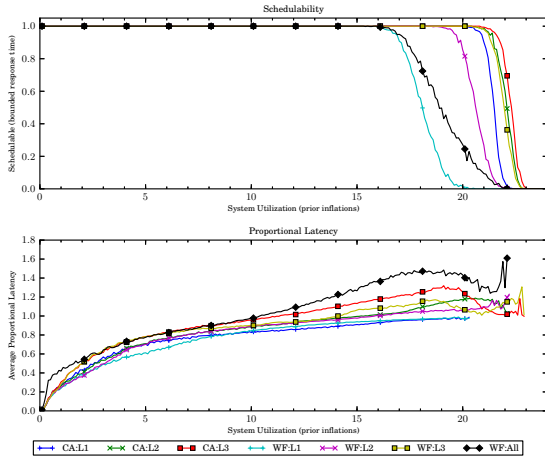


(a) Without polluter overheads.

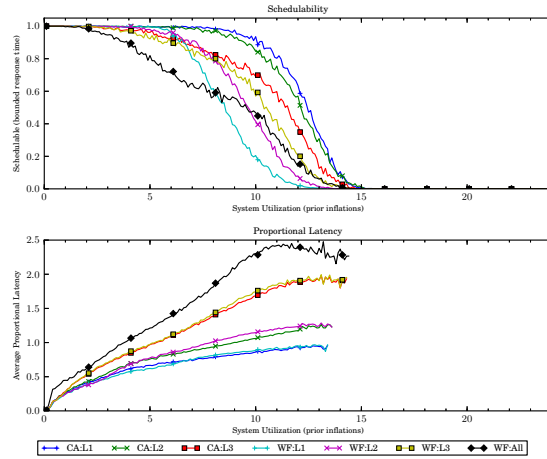


(b) With polluter overheads.

Figure 389: Results for *uni-medium* per-task utilization, *uni-long* period, *bimo-heavy-weight* EWSS, and *uni-short* height factor.

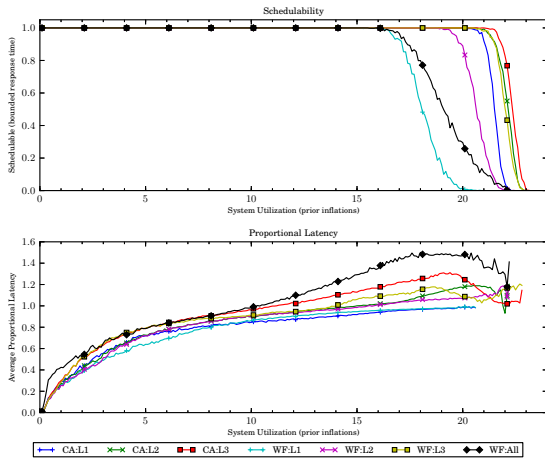


(a) Without polluter overheads.

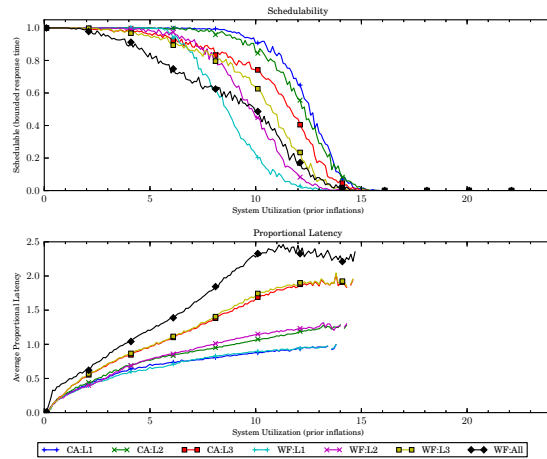


(b) With polluter overheads.

Figure 390: Results for *uni-medium* per-task utilization, *uni-long* period, *bimo-heavy-weight* EWSS, and *uni-medium* height factor.

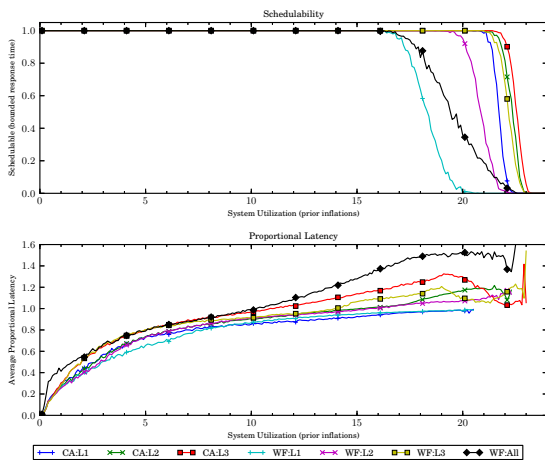


(a) Without polluter overheads.

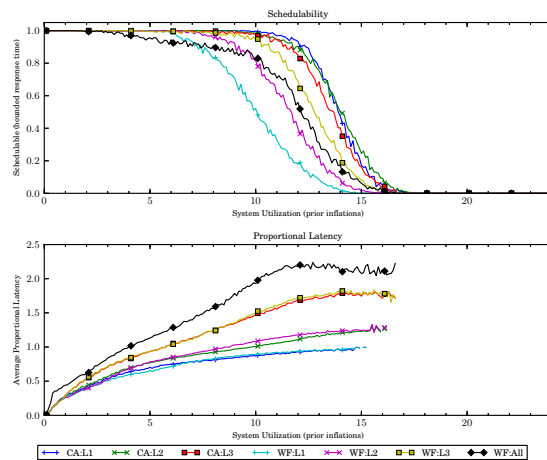


(b) With polluter overheads.

Figure 391: Results for *uni-medium* per-task utilization, *uni-long* period, *bimo-heavy-weight* EWSS, and *uni-tall* height factor.

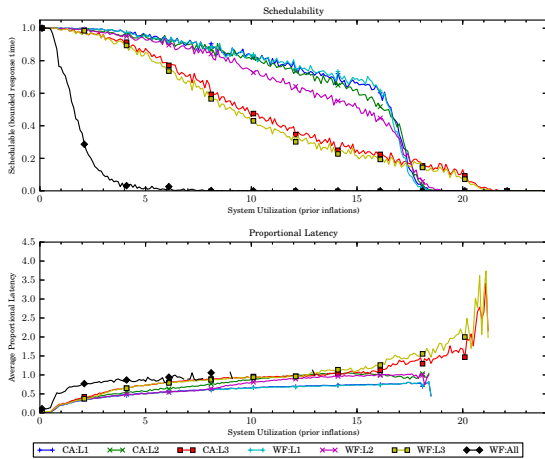


(a) Without polluter overheads.

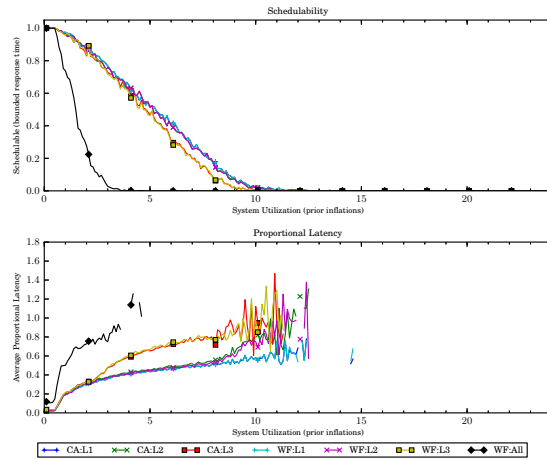


(b) With polluter overheads.

Figure 392: Results for *uni-medium* per-task utilization, *uni-long* period, *bimo-heavy-weight* EWSS, and *pipeline* height factor.

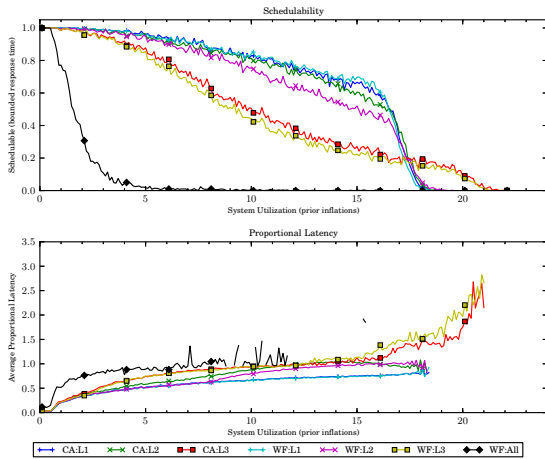


(a) Without polluter overheads.

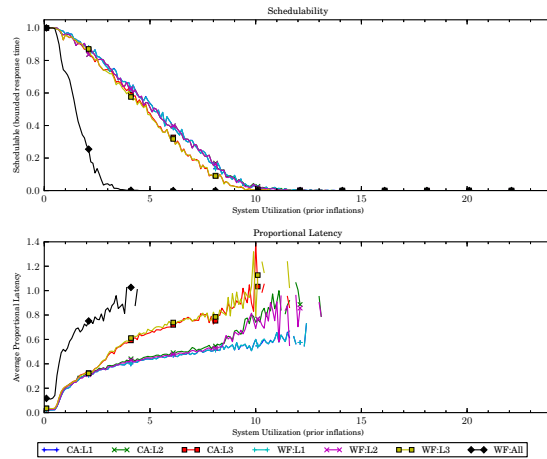


(b) With polluter overheads.

Figure 393: Results for *uni-heavy* per-task utilization, *uni-short* period, *bimo-heavy-weight* EWSS, and *uni-short* height factor.

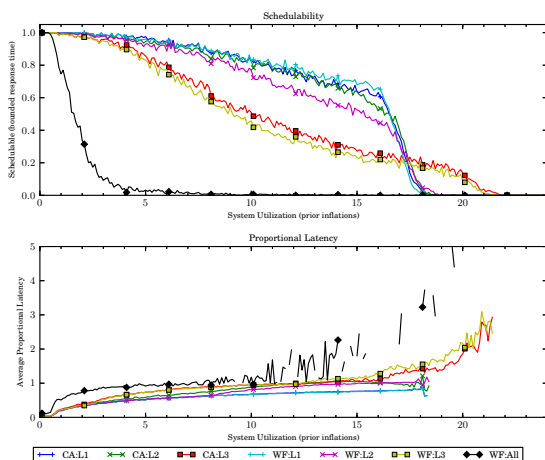


(a) Without polluter overheads.

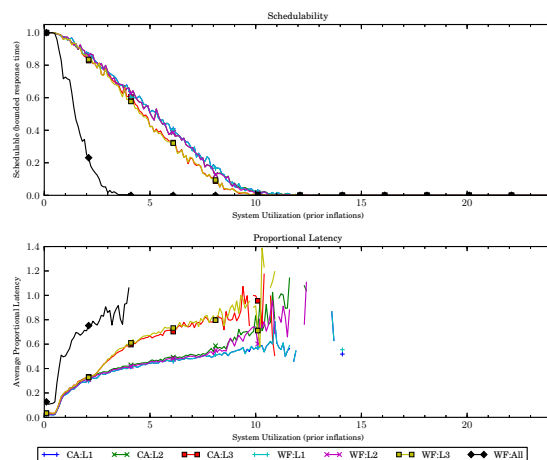


(b) With polluter overheads.

Figure 394: Results for *uni-heavy* per-task utilization, *uni-short* period, *bimo-heavy-weight* EWSS, and *uni-medium* height factor.

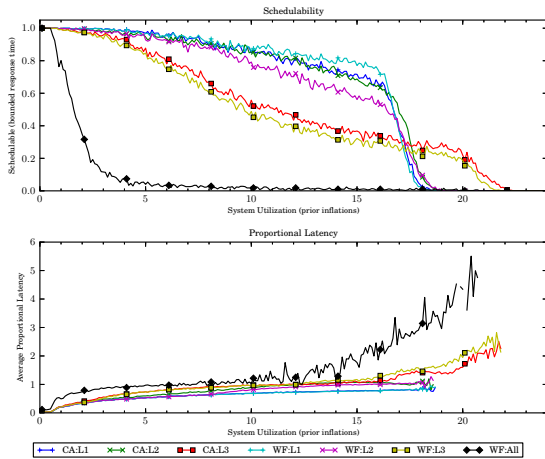


(a) Without polluter overheads.

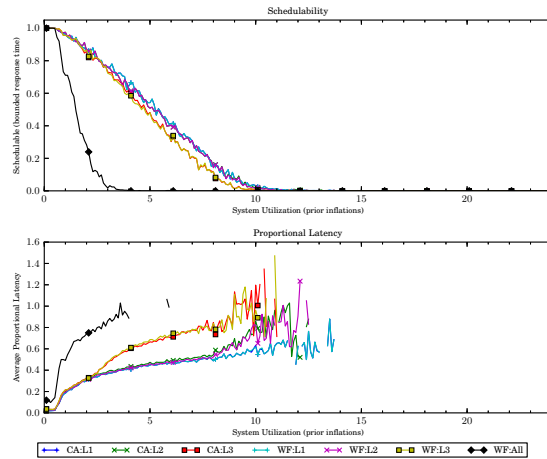


(b) With polluter overheads.

Figure 395: Results for *uni-heavy* per-task utilization, *uni-short* period, *bimo-heavy-weight* EWSS, and *uni-tall* height factor.

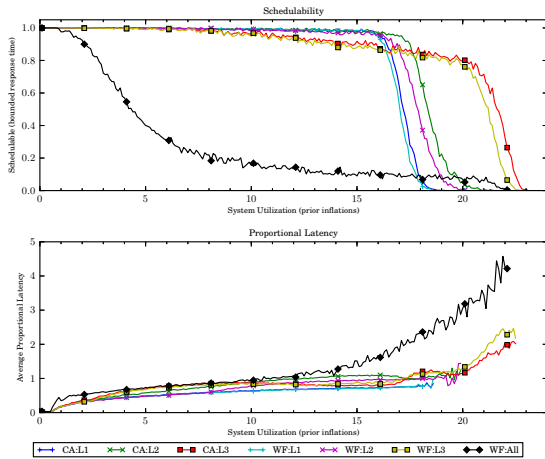


(a) Without polluter overheads.

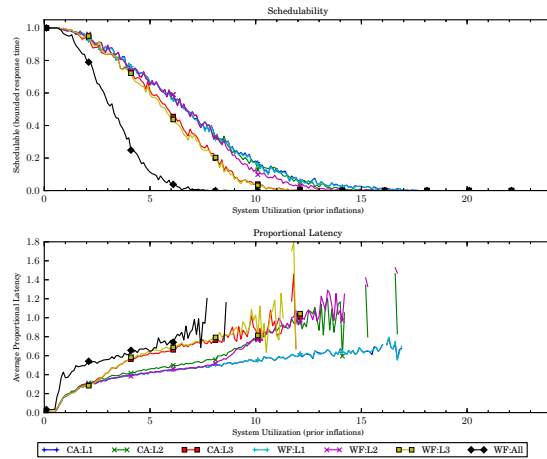


(b) With polluter overheads.

Figure 396: Results for *uni-heavy* per-task utilization, *uni-short* period, *bimo-heavy-weight* EWSS, and *pipeline* height factor.

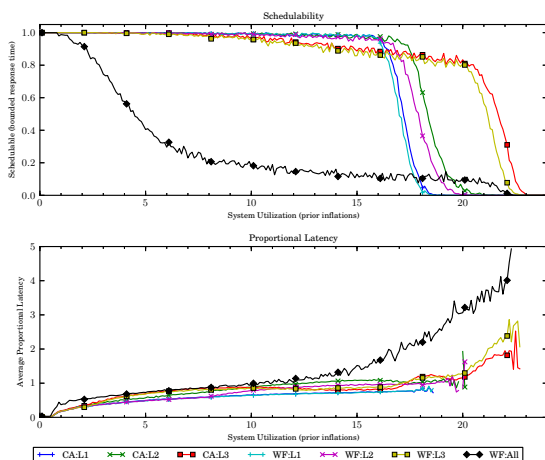


(a) Without polluter overheads.

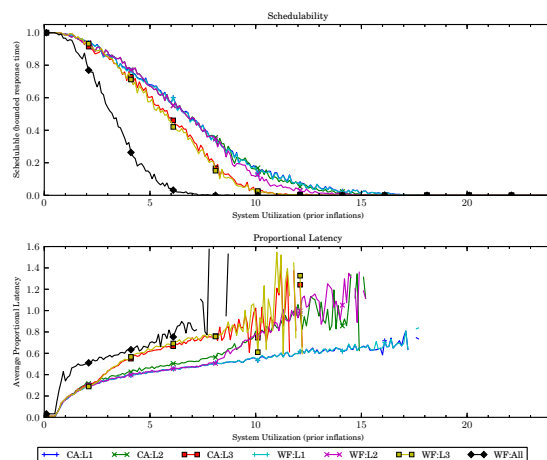


(b) With polluter overheads.

Figure 397: Results for *uni-heavy* per-task utilization, *uni-moderate* period, *bimo-heavy-weight* EWSS, and *uni-short* height factor.

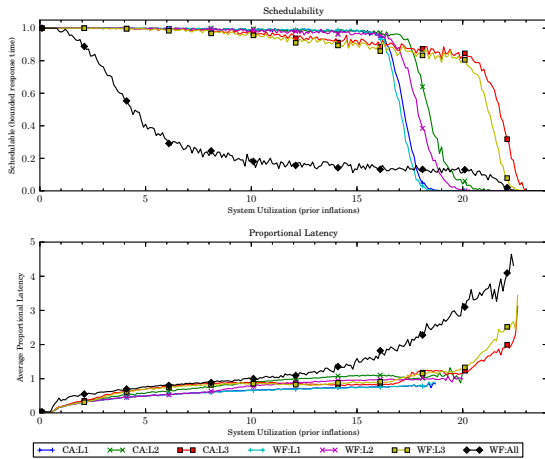


(a) Without polluter overheads.

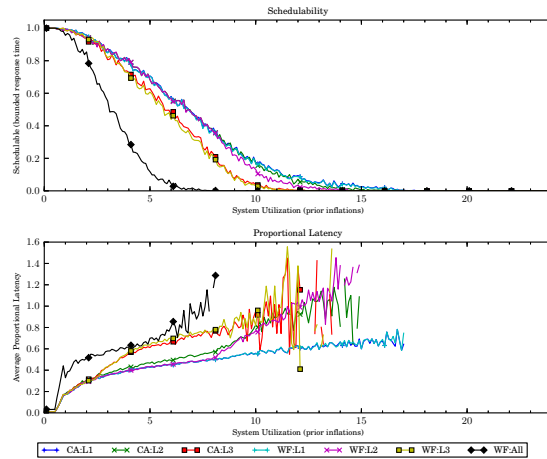


(b) With polluter overheads.

Figure 398: Results for *uni-heavy* per-task utilization, *uni-moderate* period, *bimo-heavy-weight* EWSS, and *uni-medium* height factor.

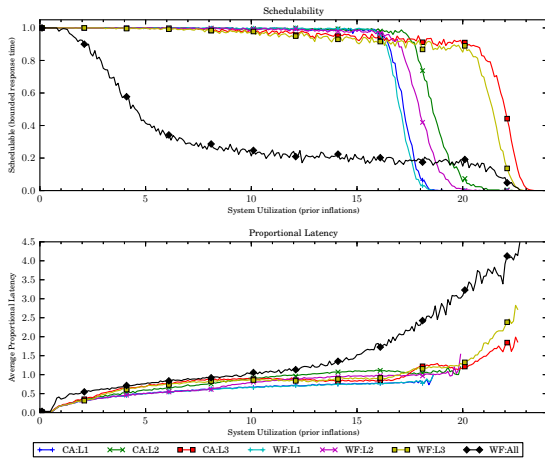


(a) Without polluter overheads.

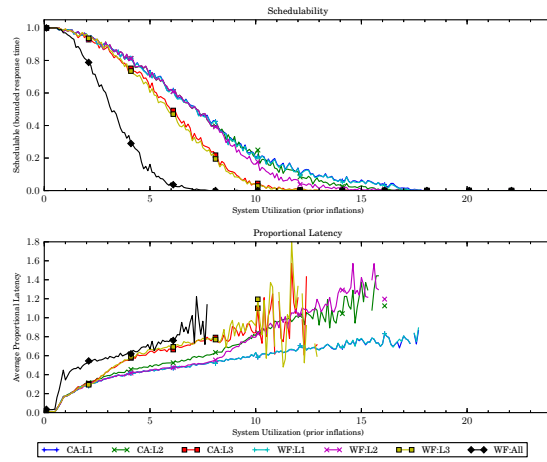


(b) With polluter overheads.

Figure 399: Results for *uni-heavy* per-task utilization, *uni-moderate* period, *bimo-heavy-weight* EWSS, and *uni-tall* height factor.

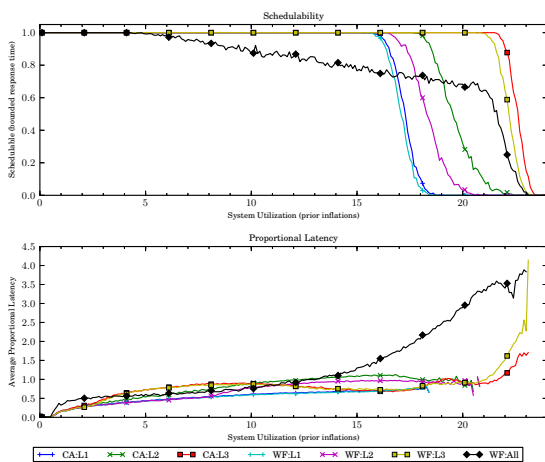


(a) Without polluter overheads.

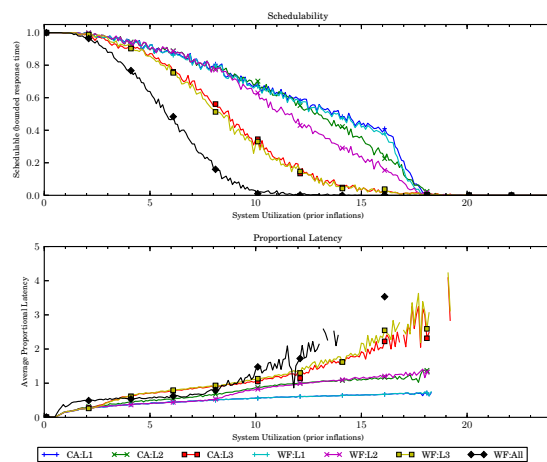


(b) With polluter overheads.

Figure 400: Results for *uni-heavy* per-task utilization, *uni-moderate* period, *bimo-heavy-weight* EWSS, and *pipeline* height factor.

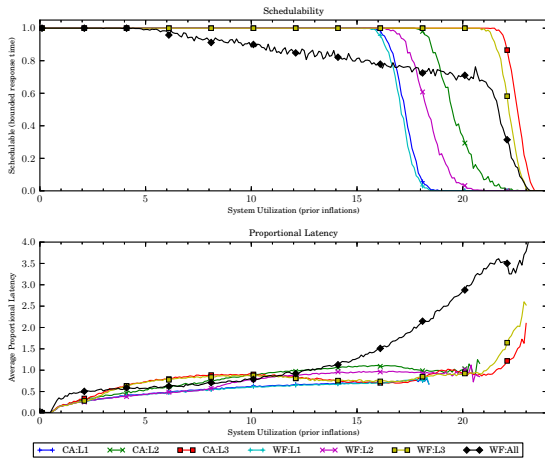


(a) Without polluter overheads.

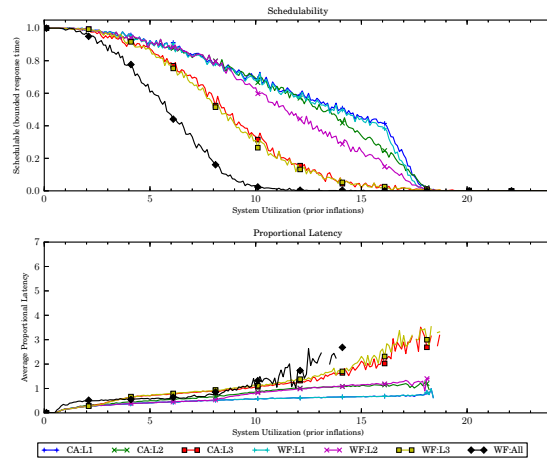


(b) With polluter overheads.

Figure 401: Results for *uni-heavy* per-task utilization, *uni-long* period, *bimo-heavy-weight* EWSS, and *uni-short* height factor.

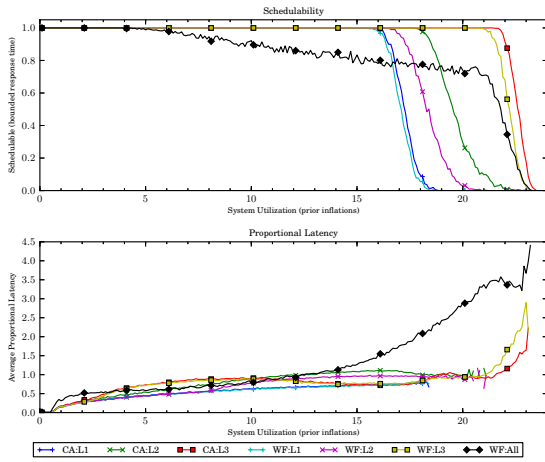


(a) Without polluter overheads.

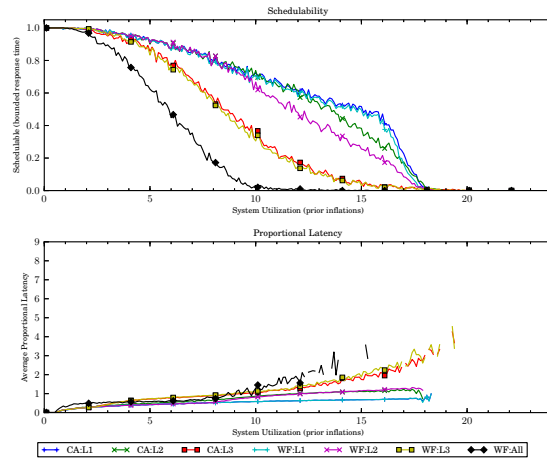


(b) With polluter overheads.

Figure 402: Results for *uni-heavy* per-task utilization, *uni-long* period, *bimo-heavy-weight* EWSS, and *uni-medium* height factor.

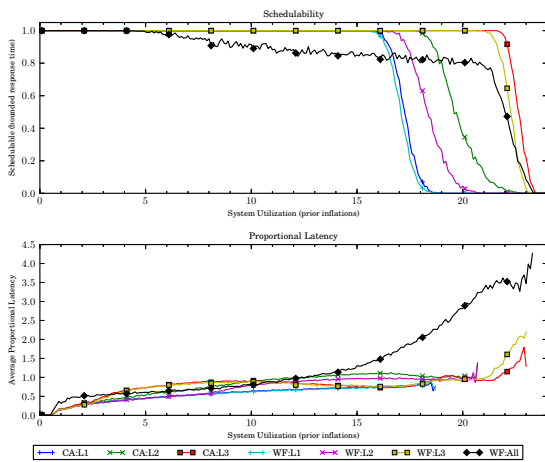


(a) Without polluter overheads.

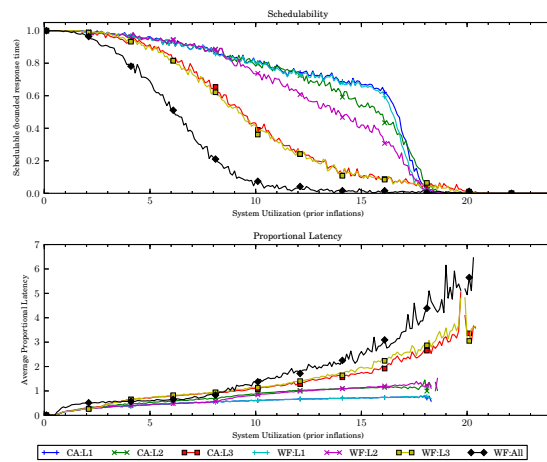


(b) With polluter overheads.

Figure 403: Results for *uni-heavy* per-task utilization, *uni-long* period, *bimo-heavy-weight* EWSS, and *uni-tall* height factor.

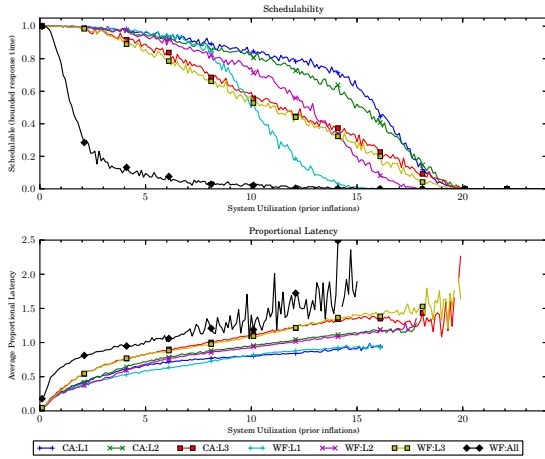


(a) Without polluter overheads.

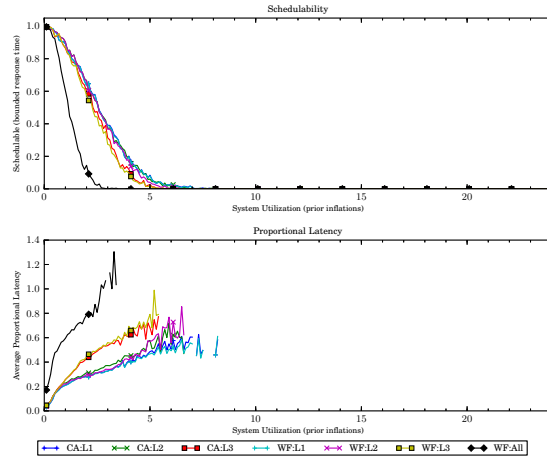


(b) With polluter overheads.

Figure 404: Results for *uni-heavy* per-task utilization, *uni-long* period, *bimo-heavy-weight* EWSS, and *pipeline* height factor.

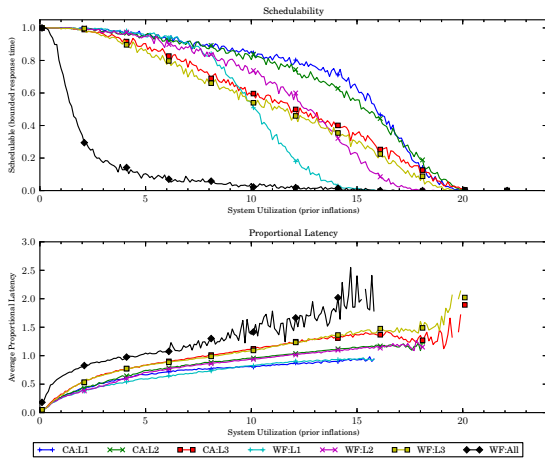


(a) Without polluter overheads.

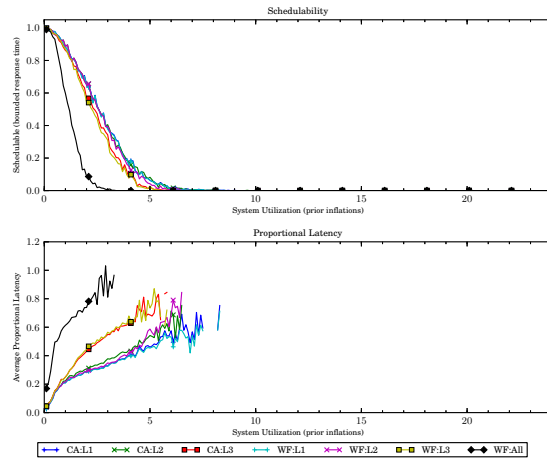


(b) With polluter overheads.

Figure 405: Results for *bimo-light* per-task utilization, *uni-short* period, *bimo-heavy-weight* EWSS, and *uni-short* height factor.

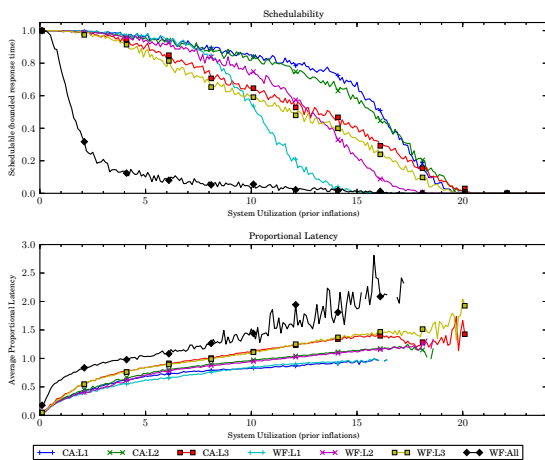


(a) Without polluter overheads.

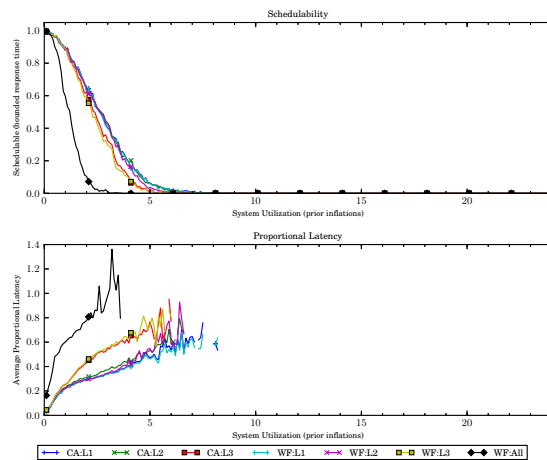


(b) With polluter overheads.

Figure 406: Results for *bimo-light* per-task utilization, *uni-short* period, *bimo-heavy-weight* EWSS, and *uni-medium* height factor.

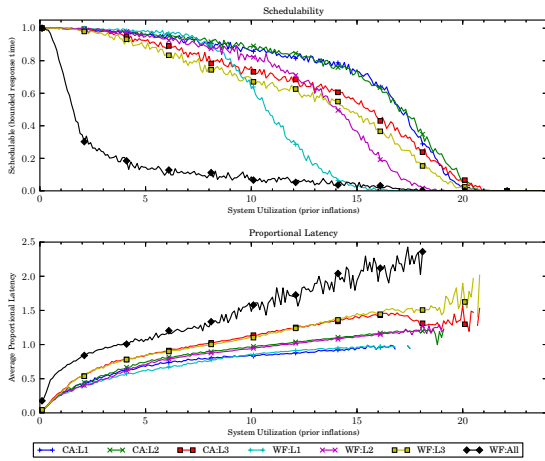


(a) Without polluter overheads.

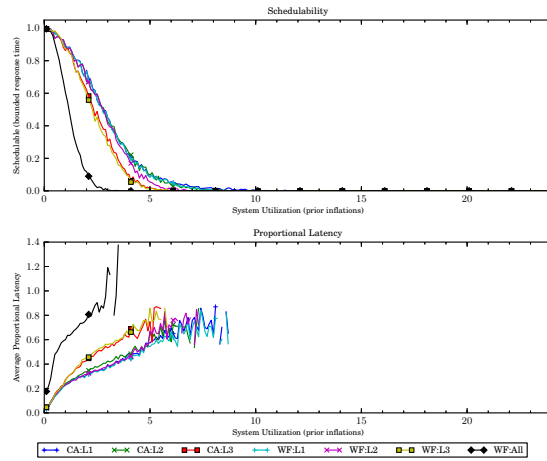


(b) With polluter overheads.

Figure 407: Results for *bimo-light* per-task utilization, *uni-short* period, *bimo-heavy-weight* EWSS, and *uni-tall* height factor.

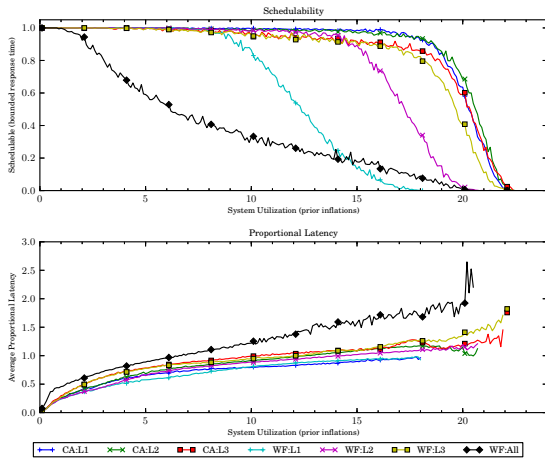


(a) Without polluter overheads.

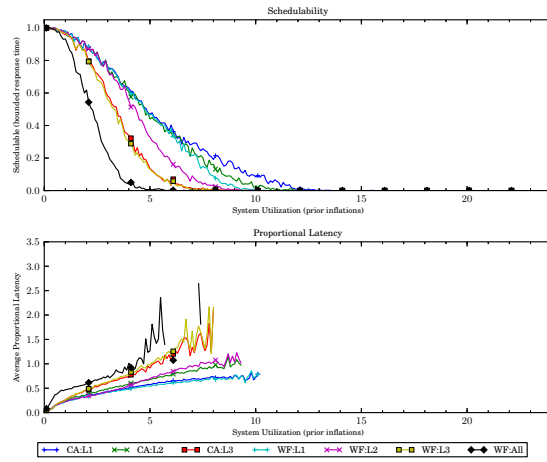


(b) With polluter overheads.

Figure 408: Results for *bimo-light* per-task utilization, *uni-short* period, *bimo-heavy-weight* EWSS, and *pipeline* height factor.

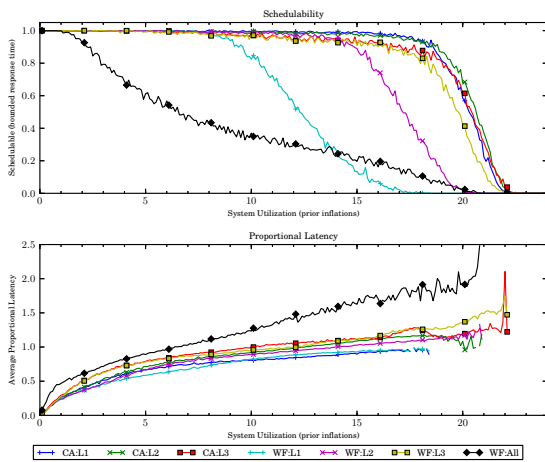


(a) Without polluter overheads.

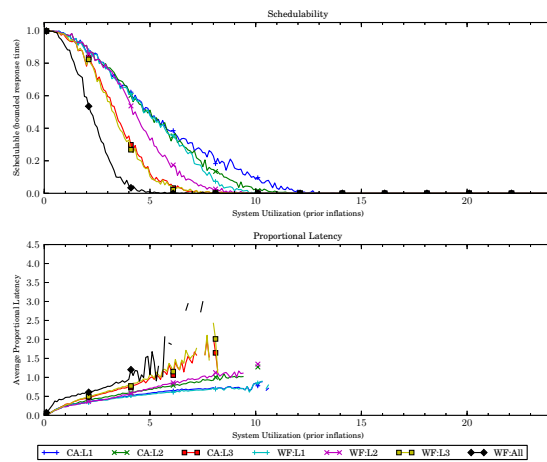


(b) With polluter overheads.

Figure 409: Results for *bimo-light* per-task utilization, *uni-moderate* period, *bimo-heavy-weight* EWSS, and *uni-short* height factor.

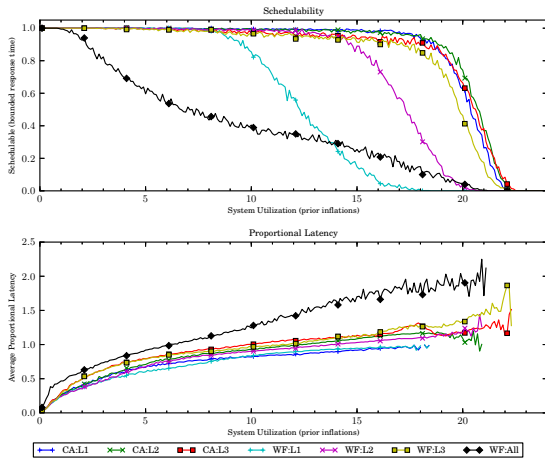


(a) Without polluter overheads.

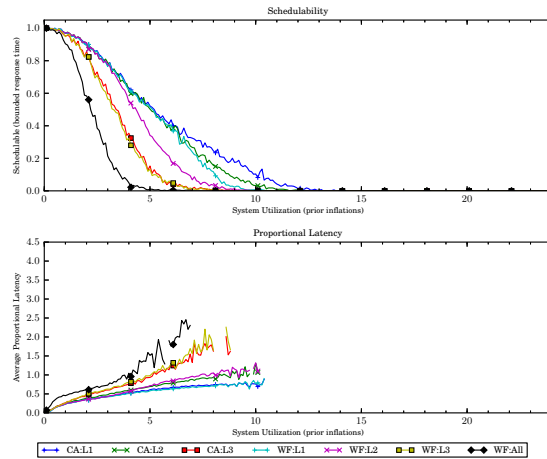


(b) With polluter overheads.

Figure 410: Results for *bimo-light* per-task utilization, *uni-moderate* period, *bimo-heavy-weight* EWSS, and *uni-medium* height factor.

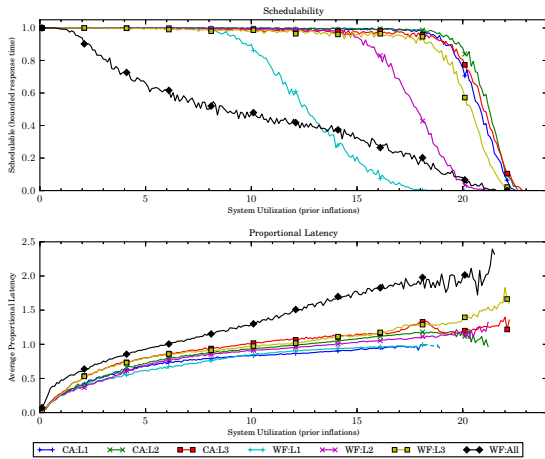


(a) Without polluter overheads.

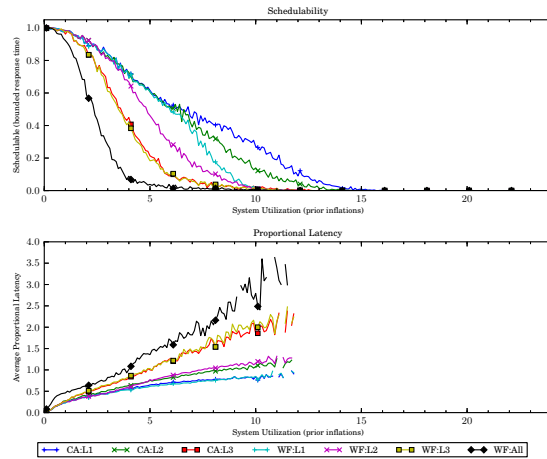


(b) With polluter overheads.

Figure 411: Results for *bimo-light* per-task utilization, *uni-moderate* period, *bimo-heavy-weight* EWSS, and *uni-tall* height factor.

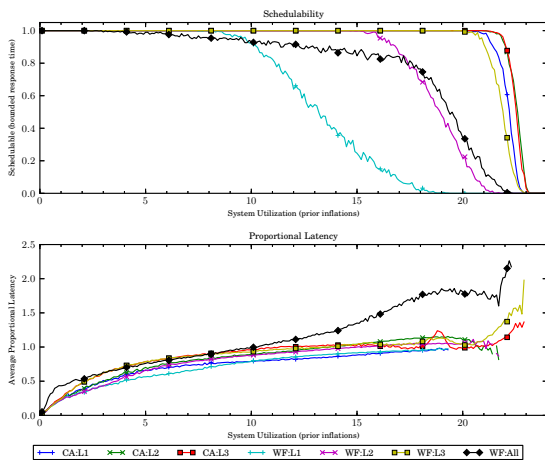


(a) Without polluter overheads.

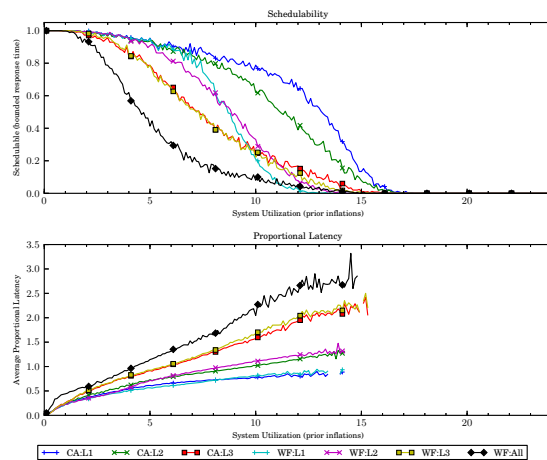


(b) With polluter overheads.

Figure 412: Results for *bimo-light* per-task utilization, *uni-moderate* period, *bimo-heavy-weight* EWSS, and *pipeline* height factor.

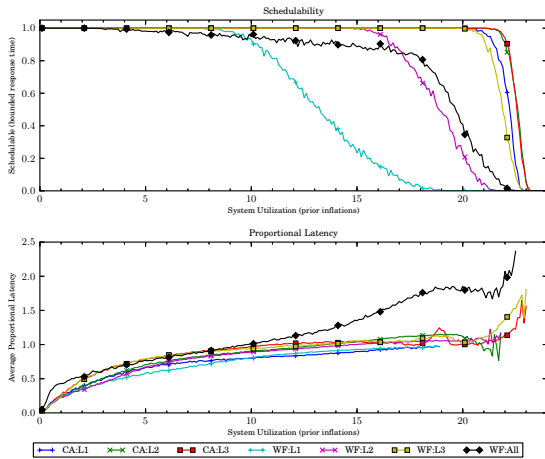


(a) Without polluter overheads.

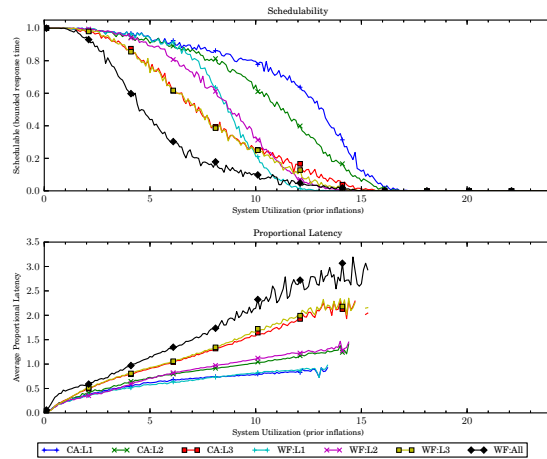


(b) With polluter overheads.

Figure 413: Results for *bimo-light* per-task utilization, *uni-long* period, *bimo-heavy-weight* EWSS, and *uni-short* height factor.

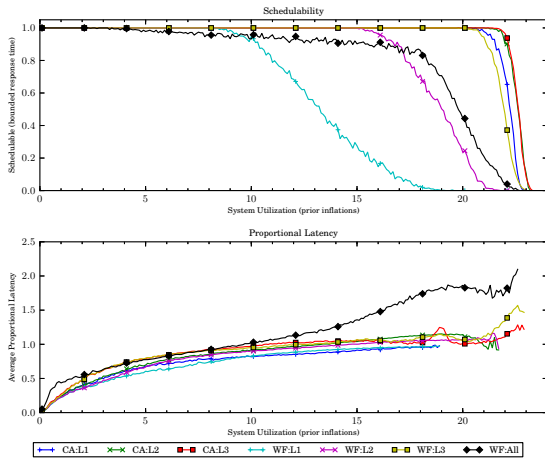


(a) Without polluter overheads.

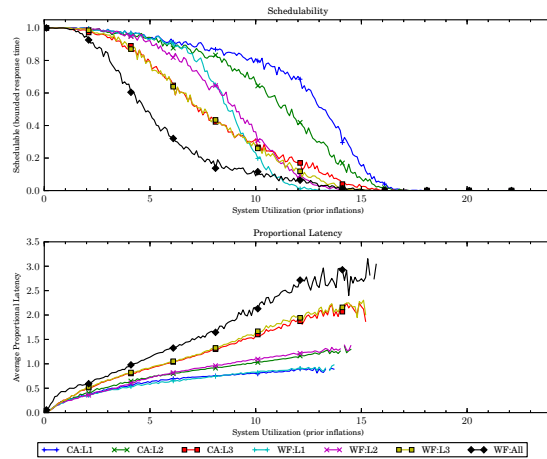


(b) With polluter overheads.

Figure 414: Results for *bimo-light* per-task utilization, *uni-long* period, *bimo-heavy-weight* EWSS, and *uni-medium* height factor.

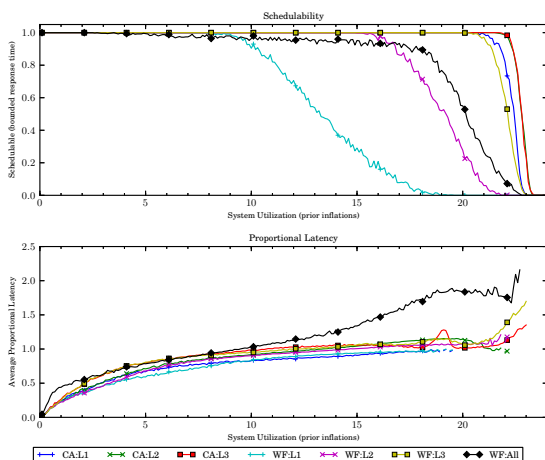


(a) Without polluter overheads.

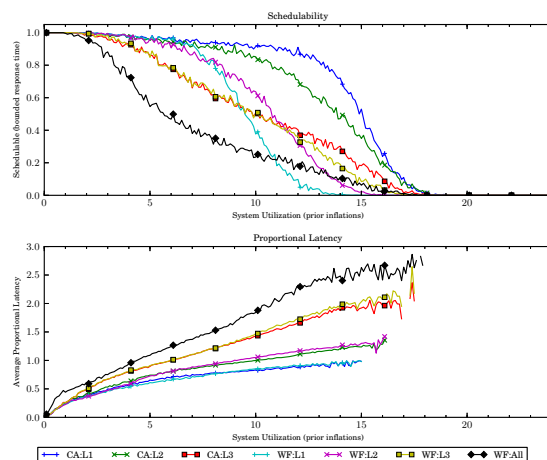


(b) With polluter overheads.

Figure 415: Results for *bimo-light* per-task utilization, *uni-long* period, *bimo-heavy-weight* EWSS, and *uni-tall* height factor.

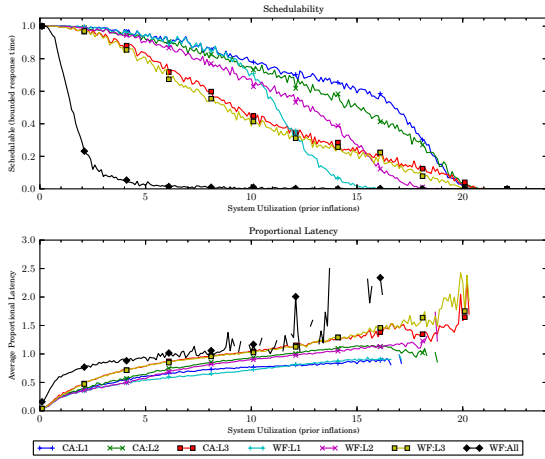


(a) Without polluter overheads.

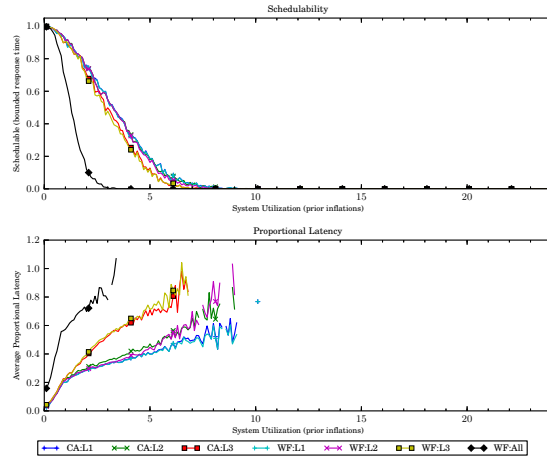


(b) With polluter overheads.

Figure 416: Results for *bimo-light* per-task utilization, *uni-long* period, *bimo-heavy-weight* EWSS, and *pipeline* height factor.

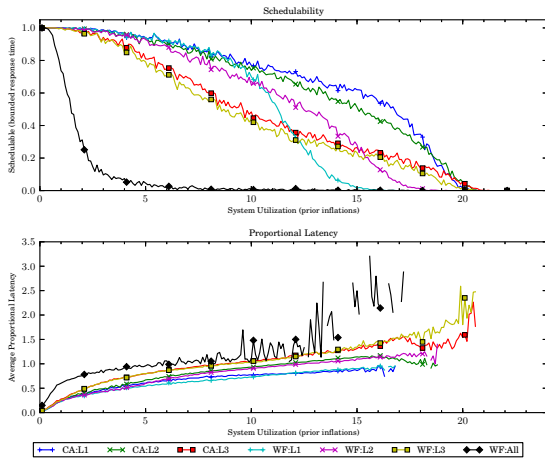


(a) Without polluter overheads.

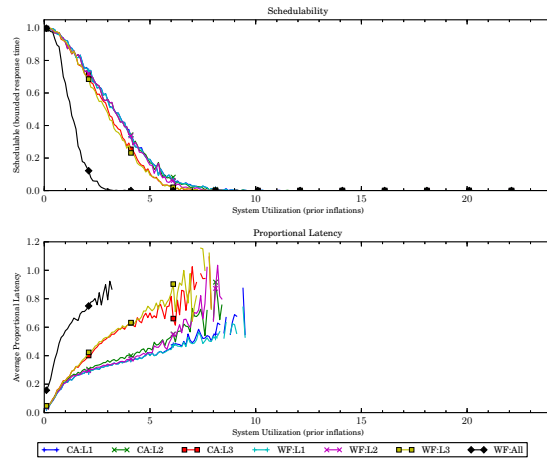


(b) With polluter overheads.

Figure 417: Results for *bimo-medium* per-task utilization, *uni-short* period, *bimo-heavy-weight* EWSS, and *uni-short* height factor.

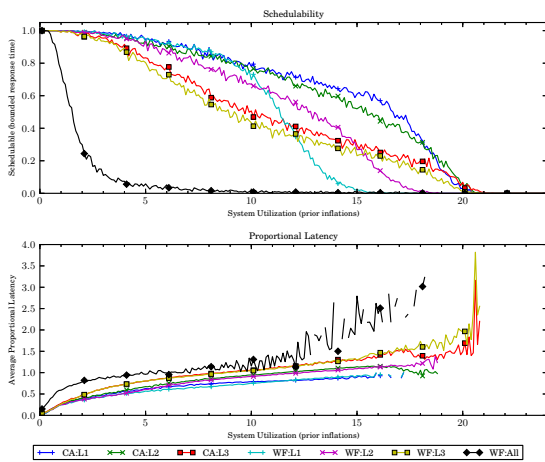


(a) Without polluter overheads.

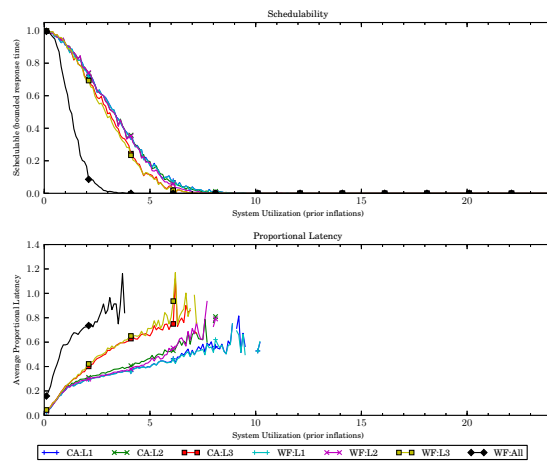


(b) With polluter overheads.

Figure 418: Results for *bimo-medium* per-task utilization, *uni-short* period, *bimo-heavy-weight* EWSS, and *uni-medium* height factor.

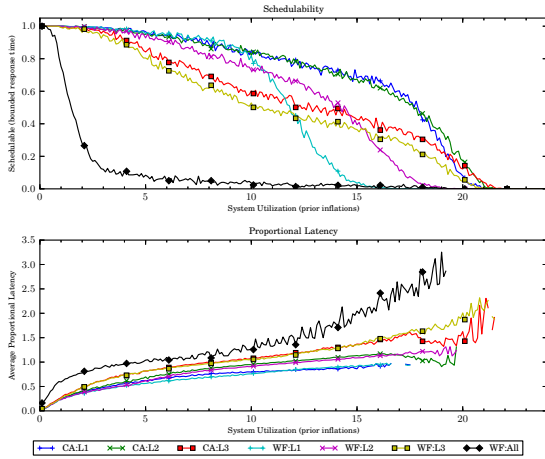


(a) Without polluter overheads.

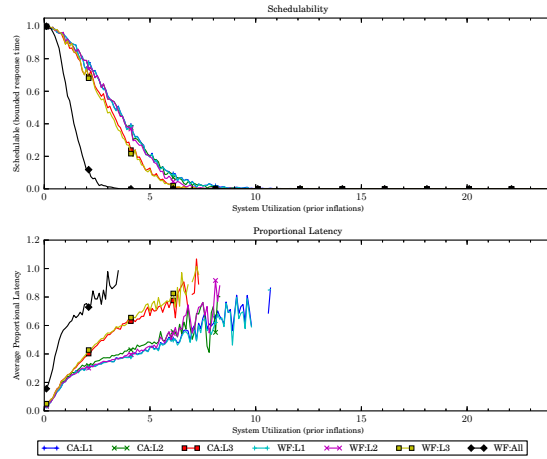


(b) With polluter overheads.

Figure 419: Results for *bimo-medium* per-task utilization, *uni-short* period, *bimo-heavy-weight* EWSS, and *uni-tall* height factor.

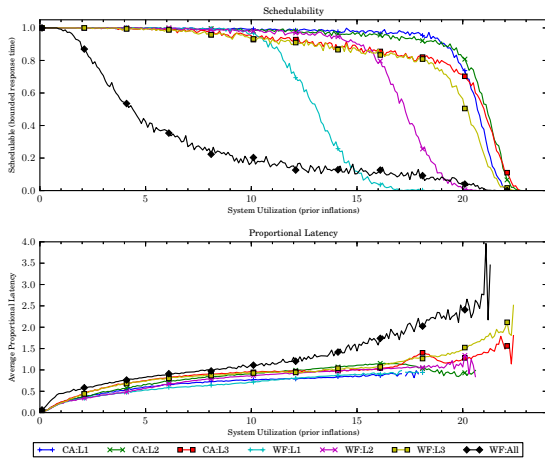


(a) Without polluter overheads.

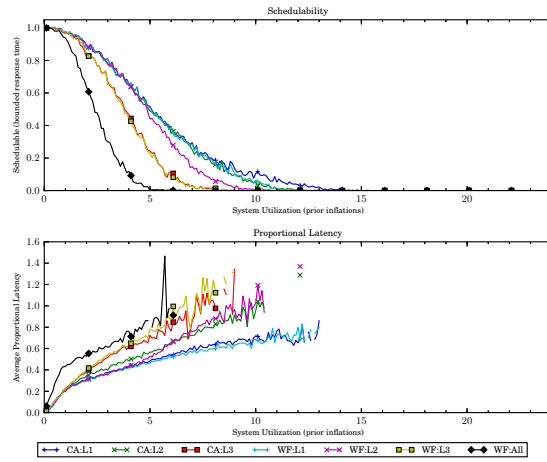


(b) With polluter overheads.

Figure 420: Results for *bimo-medium* per-task utilization, *uni-short* period, *bimo-heavy-weight* EWSS, and *pipeline* height factor.

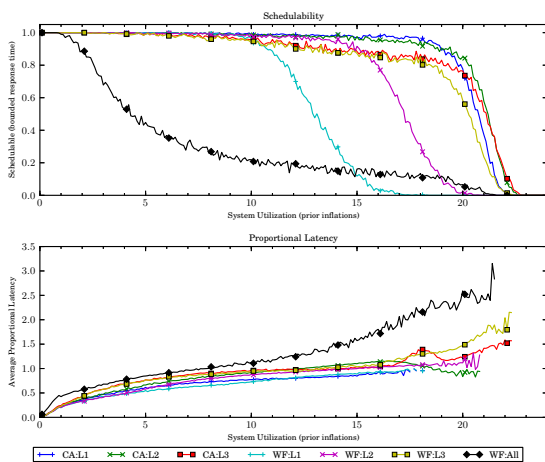


(a) Without polluter overheads.

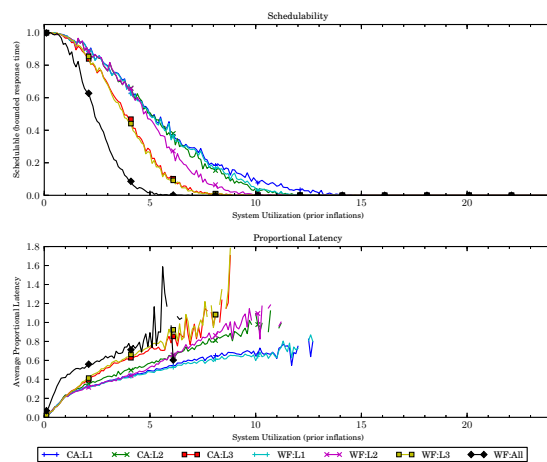


(b) With polluter overheads.

Figure 421: Results for *bimo-medium* per-task utilization, *uni-moderate* period, *bimo-heavy-weight* EWSS, and *uni-short* height factor.

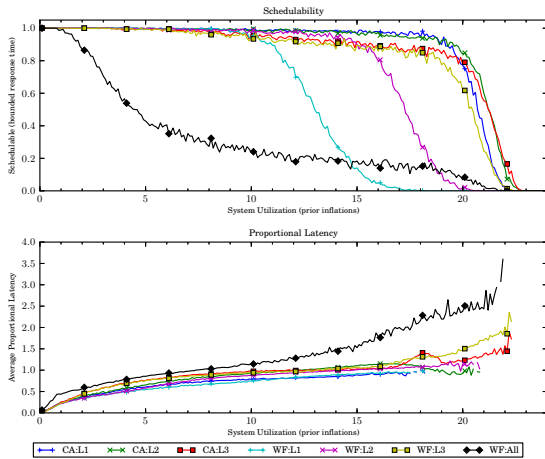


(a) Without polluter overheads.

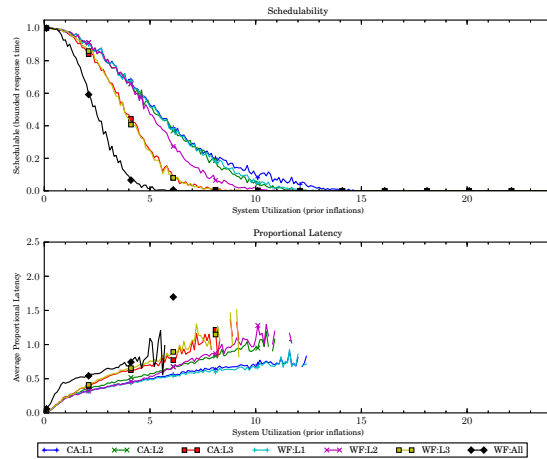


(b) With polluter overheads.

Figure 422: Results for *bimo-medium* per-task utilization, *uni-moderate* period, *bimo-heavy-weight* EWSS, and *uni-medium* height factor.

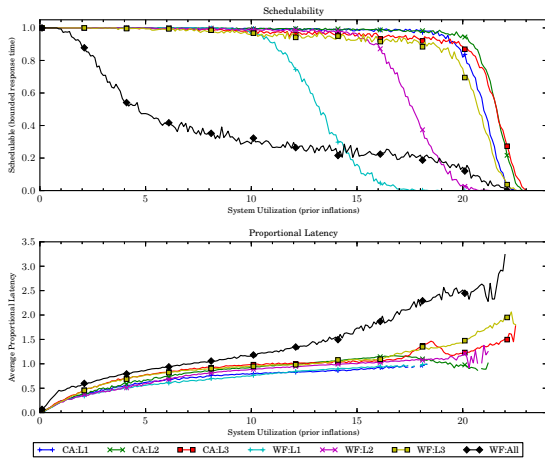


(a) Without polluter overheads.

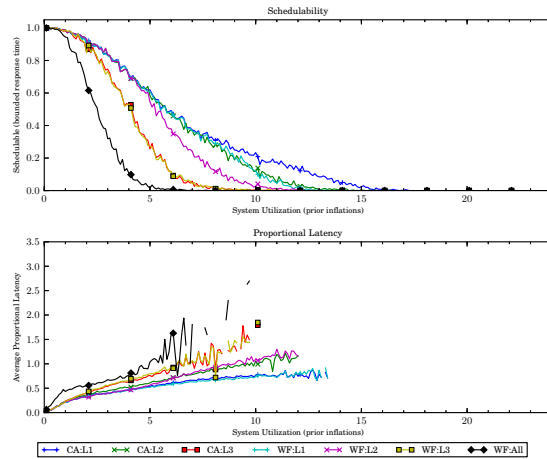


(b) With polluter overheads.

Figure 423: Results for *bimo-medium* per-task utilization, *uni-moderate* period, *bimo-heavy-weight* EWSS, and *uni-tall* height factor.

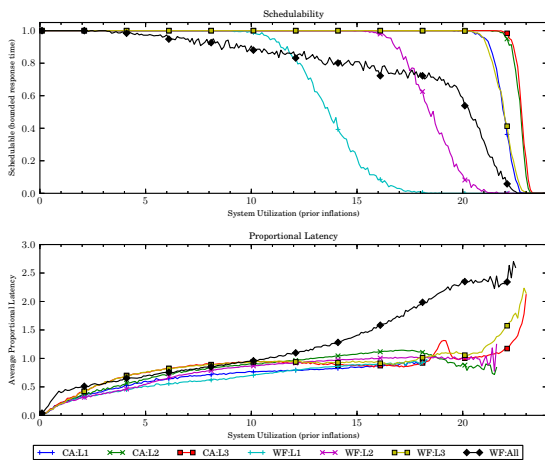


(a) Without polluter overheads.

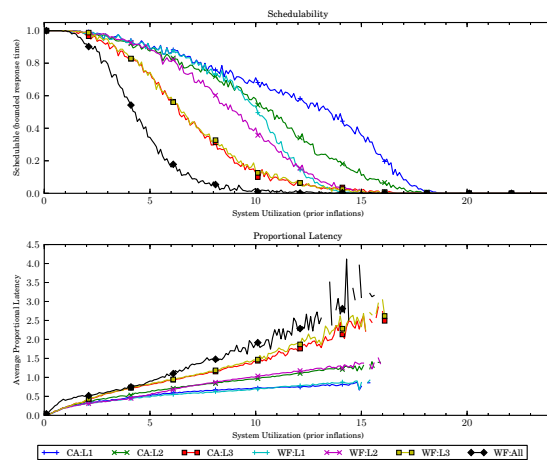


(b) With polluter overheads.

Figure 424: Results for *bimo-medium* per-task utilization, *uni-moderate* period, *bimo-heavy-weight* EWSS, and *pipeline* height factor.

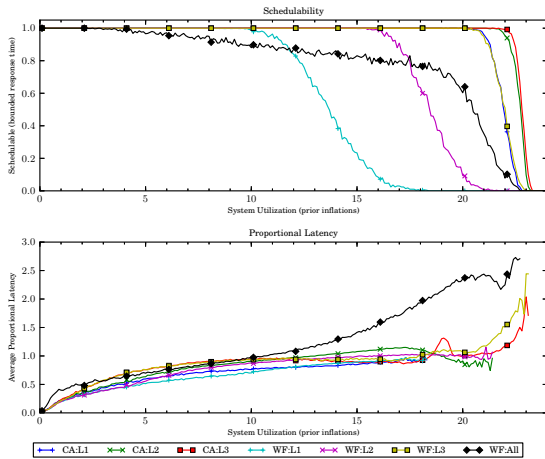


(a) Without polluter overheads.

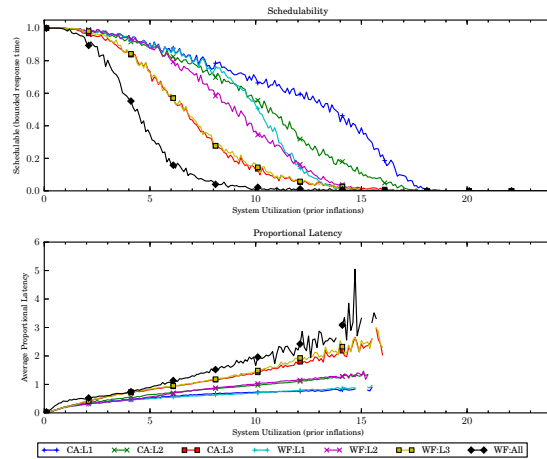


(b) With polluter overheads.

Figure 425: Results for *bimo-medium* per-task utilization, *uni-long* period, *bimo-heavy-weight* EWSS, and *uni-short* height factor.

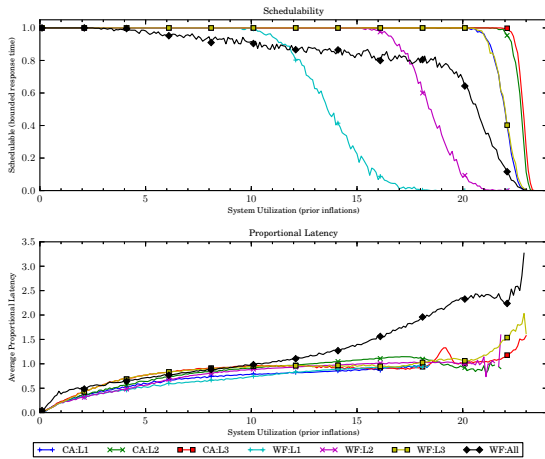


(a) Without polluter overheads.

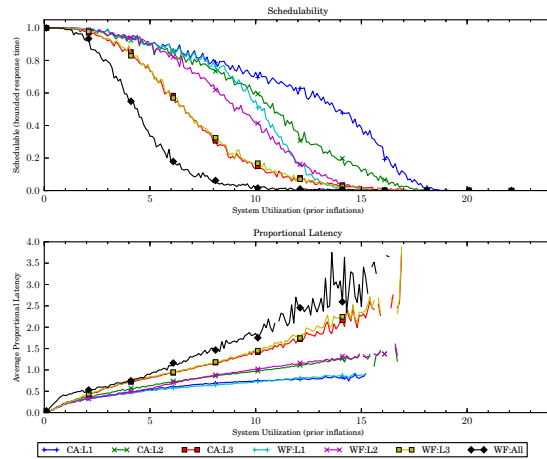


(b) With polluter overheads.

Figure 426: Results for *bimo-medium* per-task utilization, *uni-long* period, *bimo-heavy-weight* EWSS, and *uni-medium* height factor.

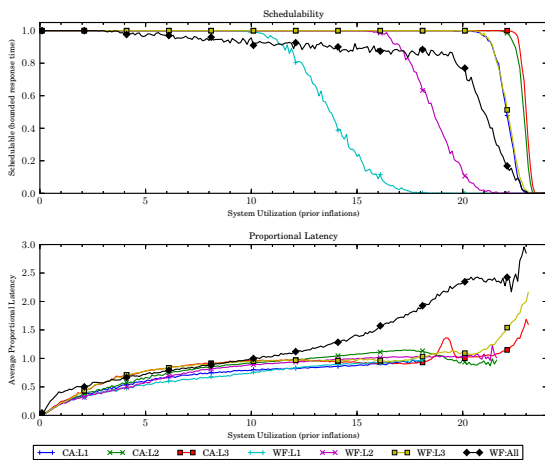


(a) Without polluter overheads.

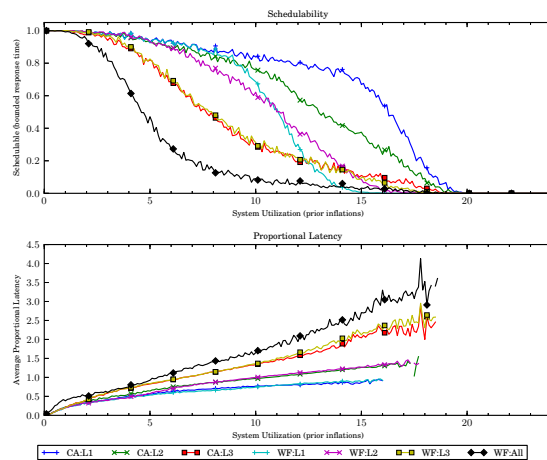


(b) With polluter overheads.

Figure 427: Results for *bimo-medium* per-task utilization, *uni-long* period, *bimo-heavy-weight* EWSS, and *uni-tall* height factor.

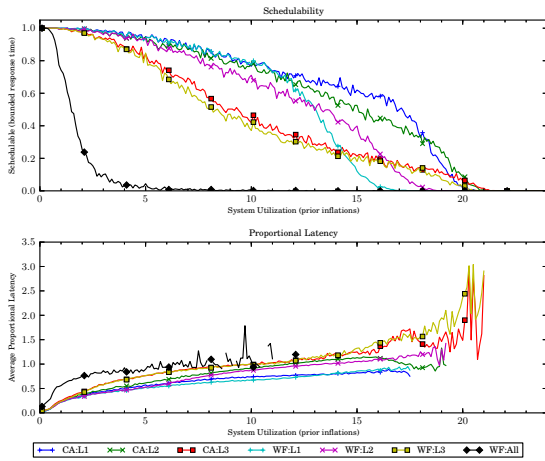


(a) Without polluter overheads.

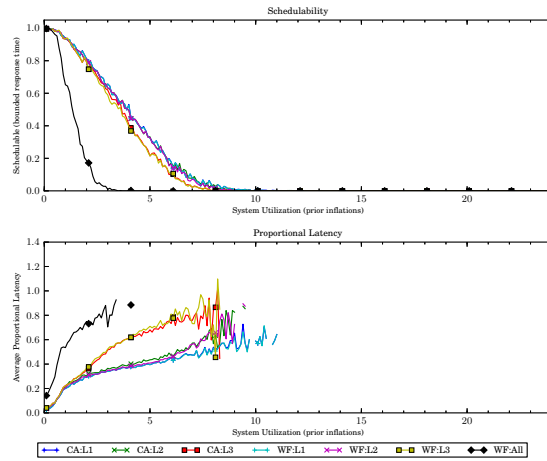


(b) With polluter overheads.

Figure 428: Results for *bimo-medium* per-task utilization, *uni-long* period, *bimo-heavy-weight* EWSS, and *pipeline* height factor.

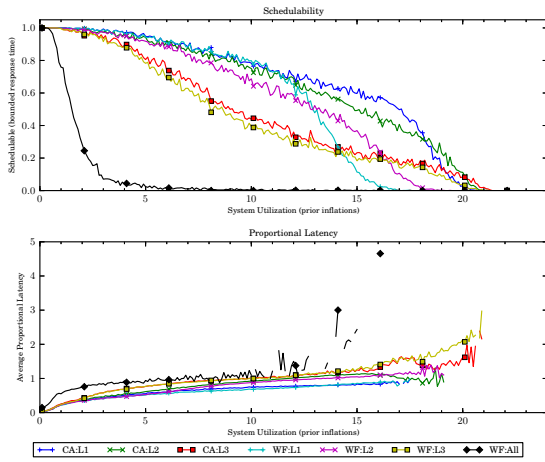


(a) Without polluter overheads.

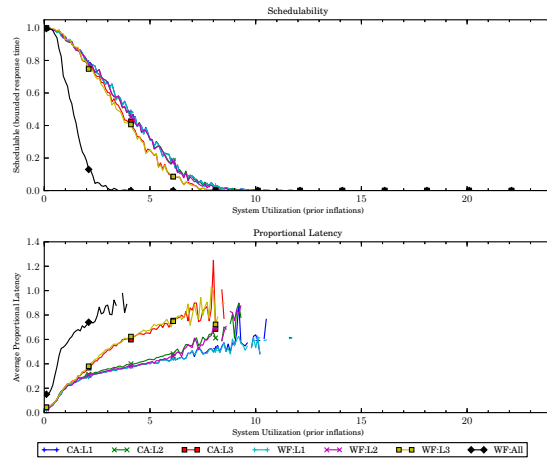


(b) With polluter overheads.

Figure 429: Results for *bimo-heavy* per-task utilization, *uni-short* period, *bimo-heavy-weight* EWSS, and *uni-short* height factor.

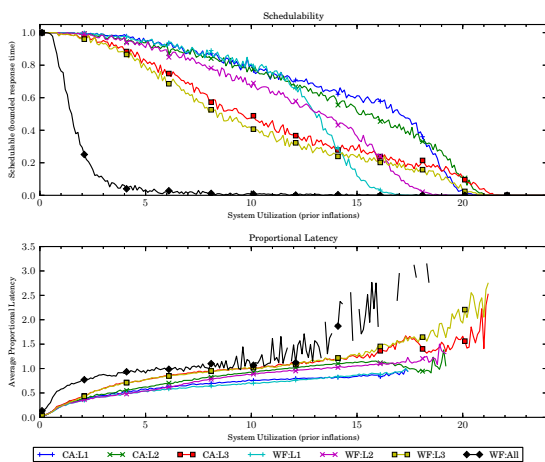


(a) Without polluter overheads.

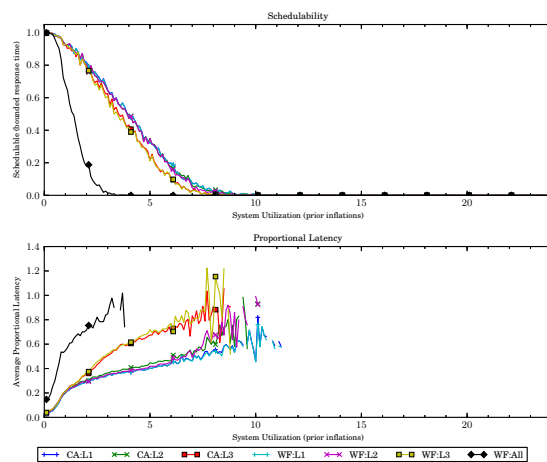


(b) With polluter overheads.

Figure 430: Results for *bimo-heavy* per-task utilization, *uni-short* period, *bimo-heavy-weight* EWSS, and *uni-medium* height factor.

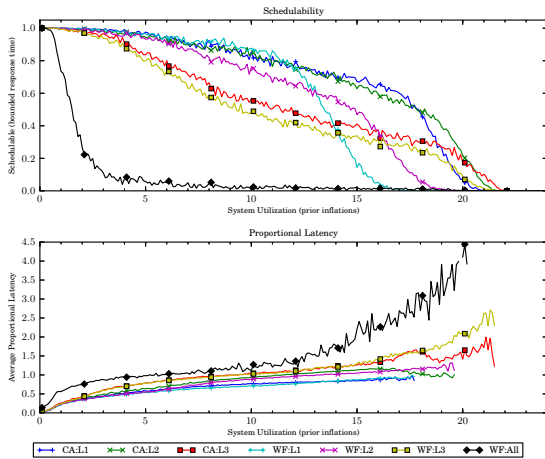


(a) Without polluter overheads.

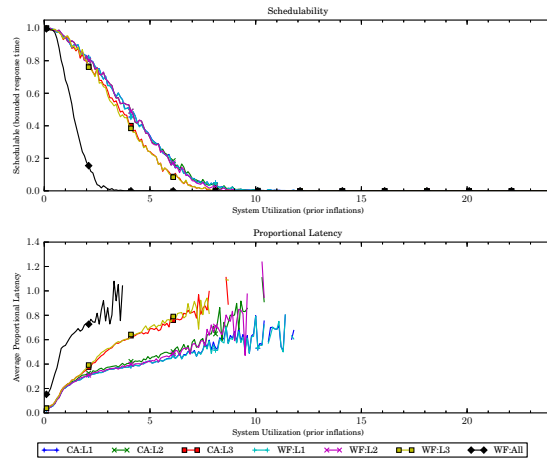


(b) With polluter overheads.

Figure 431: Results for *bimo-heavy* per-task utilization, *uni-short* period, *bimo-heavy-weight* EWSS, and *uni-tall* height factor.

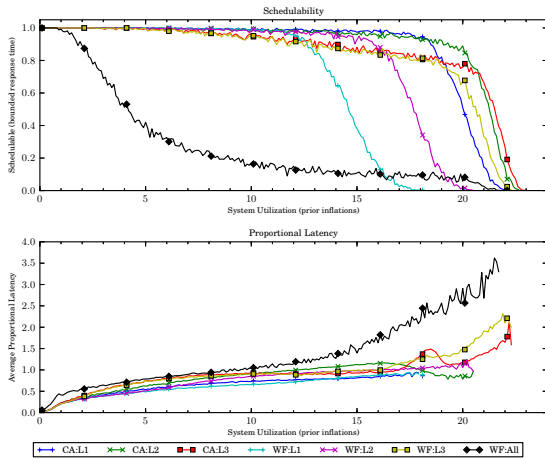


(a) Without polluter overheads.

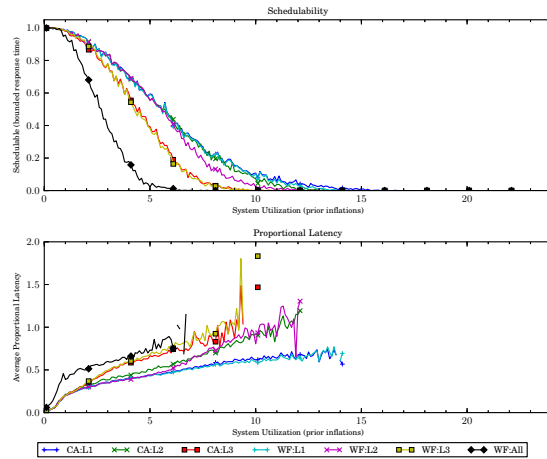


(b) With polluter overheads.

Figure 432: Results for *bimo-heavy* per-task utilization, *uni-short* period, *bimo-heavy-weight* EWSS, and *pipeline* height factor.

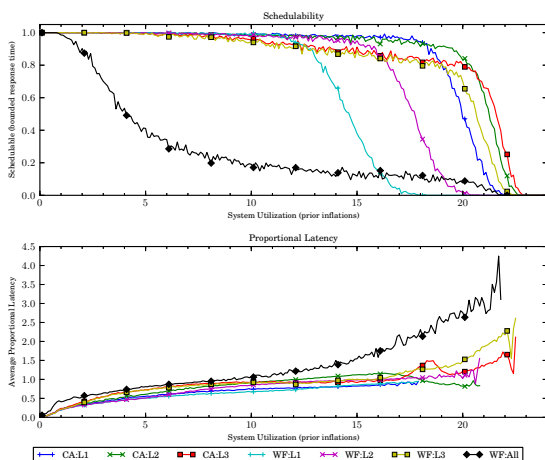


(a) Without polluter overheads.

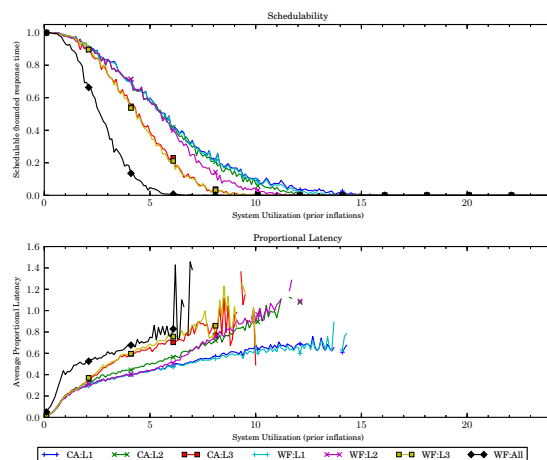


(b) With polluter overheads.

Figure 433: Results for *bimo-heavy* per-task utilization, *uni-moderate* period, *bimo-heavy-weight* EWSS, and *uni-short* height factor.

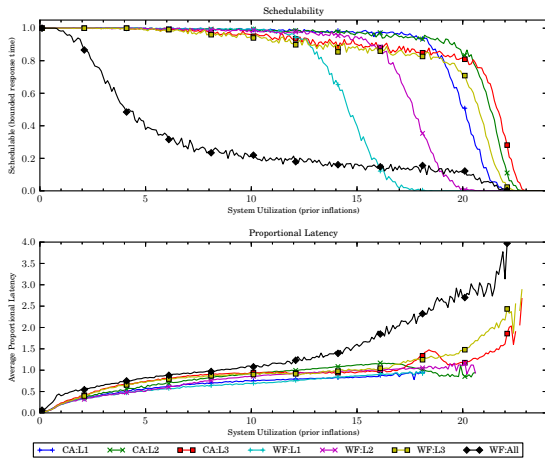


(a) Without polluter overheads.

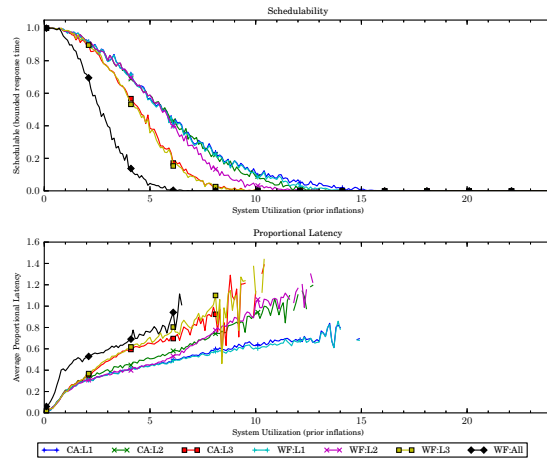


(b) With polluter overheads.

Figure 434: Results for *bimo-heavy* per-task utilization, *uni-moderate* period, *bimo-heavy-weight* EWSS, and *uni-medium* height factor.

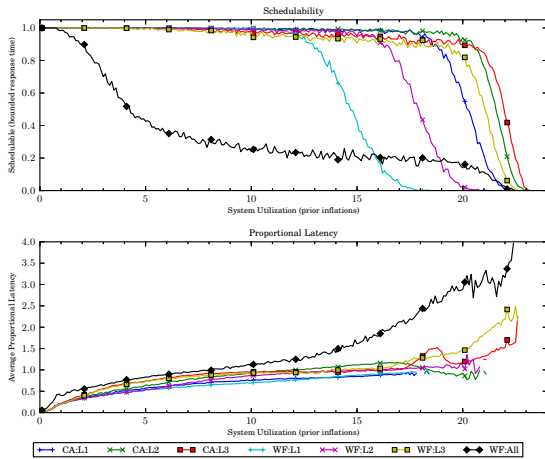


(a) Without polluter overheads.

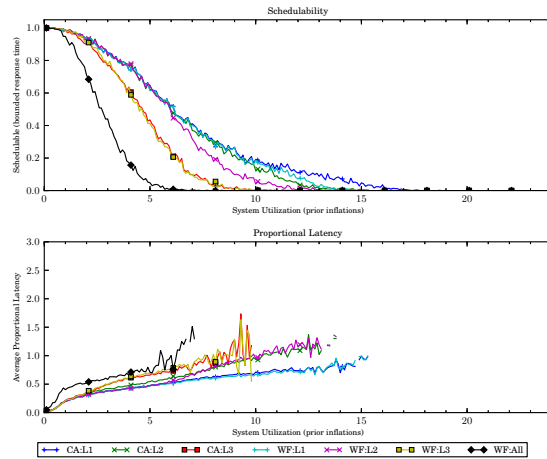


(b) With polluter overheads.

Figure 435: Results for *bimo-heavy* per-task utilization, *uni-moderate* period, *bimo-heavy-weight* EWSS, and *uni-tall* height factor.

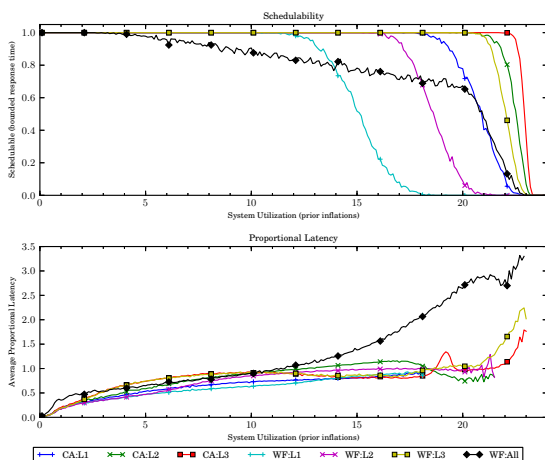


(a) Without polluter overheads.

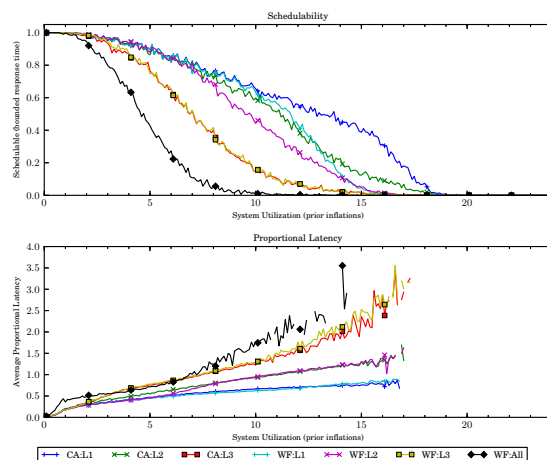


(b) With polluter overheads.

Figure 436: Results for *bimo-heavy* per-task utilization, *uni-moderate* period, *bimo-heavy-weight* EWSS, and *pipeline* height factor.

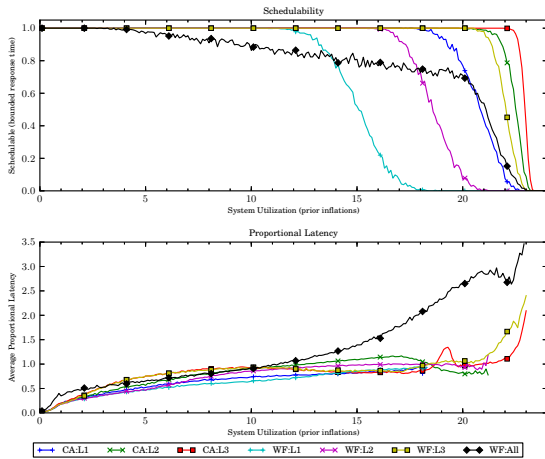


(a) Without polluter overheads.

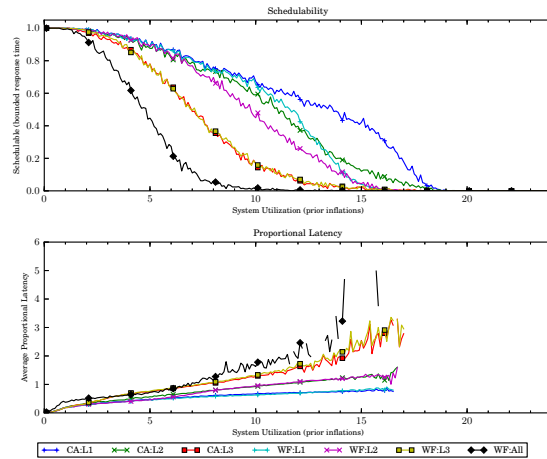


(b) With polluter overheads.

Figure 437: Results for *bimo-heavy* per-task utilization, *uni-long* period, *bimo-heavy-weight* EWSS, and *uni-short* height factor.

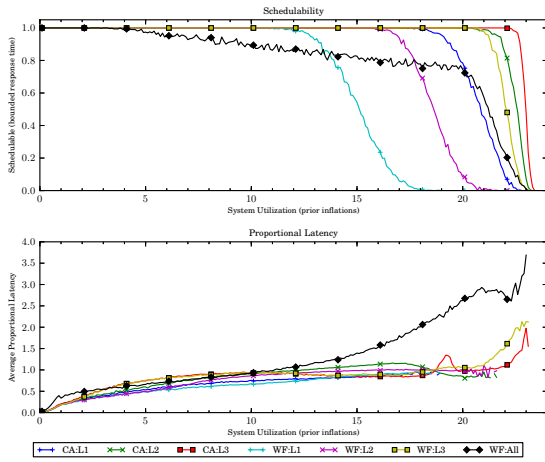


(a) Without polluter overheads.

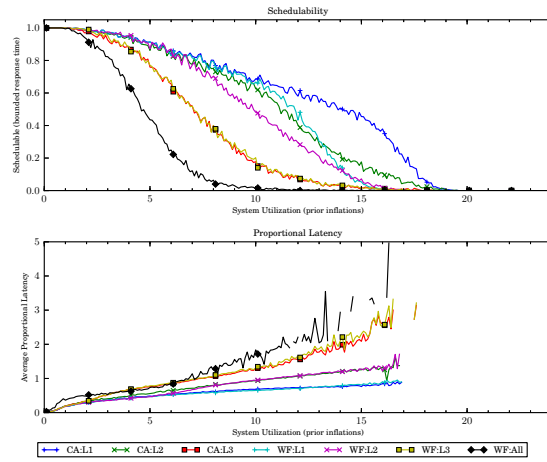


(b) With polluter overheads.

Figure 438: Results for *bimo-heavy* per-task utilization, *uni-long* period, *bimo-heavy-weight* EWSS, and *uni-medium* height factor.

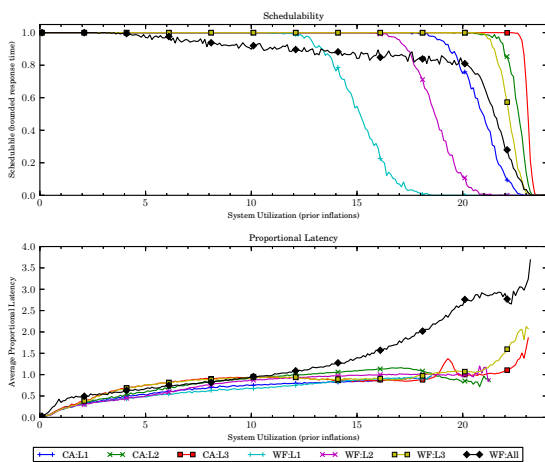


(a) Without polluter overheads.

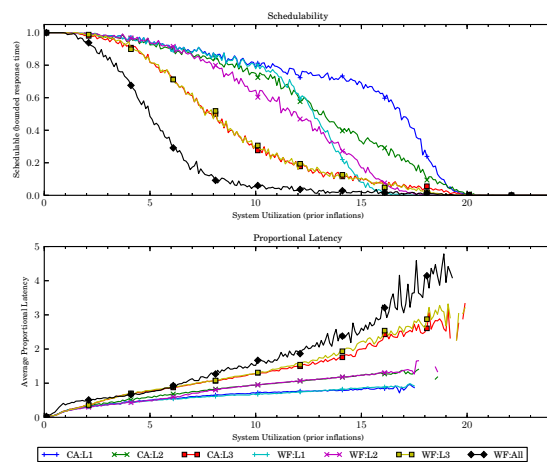


(b) With polluter overheads.

Figure 439: Results for *bimo-heavy* per-task utilization, *uni-long* period, *bimo-heavy-weight* EWSS, and *uni-tall* height factor.



(a) Without polluter overheads.



(b) With polluter overheads.

Figure 440: Results for *bimo-heavy* per-task utilization, *uni-long* period, *bimo-heavy-weight* EWSS, and *pipeline* height factor.